Plasma Assisted Decontamination of Biological and Chemical Agents

Edited by
Selçuk Güçeri
Alexander Fridman

🐎 Springer

NATO
OTAN

*This publication
is supported by:*

The NATO **Science** for **Peace**
and **Security** Programme

Plasma Assisted Decontamination of Biological and Chemical Agents

NATO Science for Peace and Security Series

This Series presents the results of scientific meetings supported under the NATO Programme: Science for Peace and Security (SPS).

The NATO SPS Programme supports meetings in the following Key Priority areas: (1) Defence Against Terrorism; (2) Countering other Threats to Security and (3) NATO, Partner and Mediterranean Dialogue Country Priorities. The types of meeting supported are generally "Advanced Study Institutes" and "Advanced Research Workshops". The NATO SPS Series collects together the results of these meetings. The meetings are co-organized by scientists from NATO countries and scientists from NATO's "Partner" or "Mediterranean Dialogue" countries. The observations and recommendations made at the meetings, as well as the contents of the volumes in the Series, reflect those of participants and contributors only; they should not necessarily be regarded as reflecting NATO views or policy.

Advanced Study Institutes (ASI) are high-level tutorial courses intended to convey the latest developments in a subject to an advanced-level audience

Advanced Research Workshops (ARW) are expert meetings where an intense but informal exchange of views at the frontiers of a subject aims at identifying directions for future action

Following a transformation of the programme in 2006 the Series has been re-named and re-organised. Recent volumes on topics not related to security, which result from meetings supported under the programme earlier, may be found in the NATO Science Series.

The Series is published by IOS Press, Amsterdam, and Springer, Dordrecht, in conjunction with the NATO Public Diplomacy Division.

Sub-Series

A.	Chemistry and Biology	Springer
B.	Physics and Biophysics	Springer
C.	Environmental Security	Springer
D.	Information and Communication Security	IOS Press
E.	Human and Societal Dynamics	IOS Press

http://www.nato.int/science
http://www.springer.com
http://www.iospress.nl

Series A: Chemistry and Biology

Plasma Assisted Decontamination of Biological and Chemical Agents

edited by

Selçuk Güçeri

Drexel University,
Philadelphia, PA, U.S.A.

and

Alexander Fridman

Drexel University,
Philadelphia, PA, U.S.A.

Assistant Editors:

Katie Gibson
Christine Haas

Drexel University,
Philadelphia, PA, U.S.A.

Printed on acid-free paper

CONTENTS

PREFACE

Within the past decade, increasing numbers of scientists and engineers have utilized plasma biology to effectively decontaminate chemical and biological agents. Today, plasma decontamination is applied in the sterilization of various surfaces including: medical instruments; spacecrafts; high volume air and water streams; industrial exhausts; and living tissues of animals and humans. As a result, this field of study has become a rapidly expanding area of modern science and engineering that possesses limitless potential for large scale applications in plasma decontamination and plasma medicine. Currently, scientists and engineers from around the globe are working together to develop new and broadly applicable plasma technologies in order to create solutions for evolving societal challenges.

Consequently, a group of leading plasma decontamination researchers, scientists, and students gathered in Çeşme-İzmir, Turkey in September 2007 for a ten-day institute under the sponsorship of the NATO-Advanced Study Institute (ASI). The meeting brought together scientists from basic and applied research areas from both NATO and partner countries to initiate further interactions aimed at translating basic research achievements into engineering applications. Additionally, the NATO-ASI *Plasma Assisted Decontamination of Chemical and Biological Agents* served as a forum for advanced teaching and learning, and facilitated discussions about research developments in the emerging field of plasma decontamination.

The NATO-ASI focused on four major areas relating to plasma decontamination: (1) Developing a fundamental understanding of plasma interaction with living tissue/cells; (2) Developing a fundamental understanding of molecular disintegration under cold plasma exposure; (3) Disseminating information to accelerate scientific developments in plasma decontamination with regard to bio-terrorism and terror-related incidences that involve contamination of air and water surfaces; (4) Fostering discussions and developments relating to global issues, including maintenance of clean water supplies and improved healthcare. The discussions regarding these topical, highly interdisciplinary, areas allowed leading researchers and students in plasma biology to discuss and advance new developments and effective solutions.

This text is categorized into four major aspects of modern plasma decontamination: (1) plasma bio-decontamination, including disinfection and sterilization of various surfaces, water and air streams; (2) plasma decontamination of chemical agents, including cleaning of air, water and industrial exhaust gases from different pollutants, especially volatile organic compounds (VOC); (3) plasma treatment of living tissue, including diverse subjects of plasma medicine from skin sterilization to tissue engineering; (4) major electric discharges applied for the plasma-assisted decontamination of chemical and biological agents.

This text is a compilation of manuscripts, presentations and contributions, which were presented during the ten-day NATO-ASI on Plasma Decontamination in Çeşme-İzmir, Turkey in September 2007. The proceedings within this text provide a fundamental introduction to virtually all aspects of modern plasma assisted decontamination of chemical and biological agents, as well as the most recent technological achievements in the scientific field. This volume, in addition to plasma text books such as *Plasma Physics and Engineering* (Fridman et al. 2004), *Industrial Plasma Engineering, Vol. 2, Applications for Non-Thermal Plasma Processing* (Roth 2008), and *Plasma Chemistry* (Fridman 2008) provides a complimentary and comprehensive overview of research activities in plasma biology.
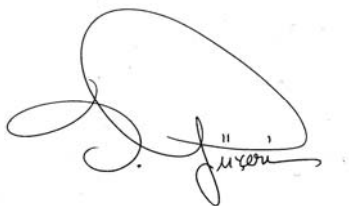
Selçuk Güçeri   Alexander Fridman
Philadelphia, January 2008

LIST OF CONTRIBUTORS

Name	Address
Dmitry Medvedev	Kurchatov Institute, Konionkova St. 14, app. 75 Moscow, 127560 – Russia
Siarhei Zhdanok	A.V. Luikov Heat & Mass Transfer Institute, 15, P. Brovka Street, 220072 – Belarus
Jen-Shih Chang	McMaster University, NRB118 Hamilton, L8S 4MI, Ontario – Canada
Jean-Marie Cormier	GREMI – University d'Orleans, 14 Rue d'Issoudun BP 6744, 45067 Orleans Cedex 2 – France
Pietro Favia	University of Bari, Department of Chemistry, Via Orabona 4 – 70126 Bari – Italy
Djoomart Otorbaev	Kyrgyz Russian Slavonic University, Chui Prospect 265A, Apartment 12, Bishkek 720071 – Kyrgyz Republic
Eva Stoffels	Eindhoven University of Technology, Biomedical Engineering, PO Box 513 5600 MB Eindhoven – The Netherlands
Alexander Fridman	Drexel University, College of Engineering, 3141 Chestnut Street, LeBow 239, Philadelphia, PA 19104 – USA
Alexander Gutsol	Drexel University, College of Engineering, 3141 Chestnut Street, LeBow 239, Philadelphia, PA 19104 – USA
Ahmed Khacef	GREMI – University d'Orleans, 14 Rue d'Issoudun BP 6744, 45067 Orleans Cedex 2 – France

Ronny Brandeburg   INP Greifswald, Institute of Low Temp. Plasma
                            Physics, Felix-Hausdorff,
                            17489 Greifswald,
                            Germany

Raymond Boxman   Tel Aviv University, Engineering,
                            PO Box 39040, Tel Aviv 69978,
                            Israel

Kazimir Karimov   Institute of Physics – Nat'l Academy,
                            Chui Prosp., 265-A, 720071,
                            Bishkek,
                            Kyrgzy Republic

Elena Filimonova   Institute for High Temp. – Russian Academy,
                            IVTAN, Izhorskaya, 13/19,
                            125412, Moscow,
                            Russia

Valery Gostev   Petrozavodsk State University, 185910,
                            33 Lenin Street, Petrozavodsk,
                            Russia

Natalie Medvedeva   Quinta LTD, 127224, Shirokaia Street,
                            21, ap. 107, Moscow,
                            Russia

Igor Alexeff   University of Tennessee, Electrical
                            Engineering, 315 Ferris Hall,
                            Middle Drive,
                            Knoxville, TN 37996,
                            USA

Halim Ayan   Drexel University, 3141 Chestnut Street,
                            LeBow 239,
                            Philadelphia, PA 19104,
                            USA

Moogega Cooper   Drexel University, 3141 Chestnut Street,
                            LeBow 239,
                            Philadelphia, PA 19104,
                            USA

Bakhtier Farouk   Drexel University, 3141 Chestnut Street,
                            LeBow 239,
                            Philadelphia, PA 19104,
                            USA

Greg Fridman	Drexel University, 3141 Chestnut Street, LeBow 239, Philadelphia, PA 19104, USA
Gennady Friedman	Drexel University, ECE Department, 3120-40 Market Street, Philadelphia, PA 19104, USA
Vladmir Genis	Drexel University, 3141 Chestnut Street, LeBow 239, Philadelphia, PA 19104, USA
Eda Yildirim	Drexel University, 3141 Chestnut Street, LeBow 239, Philadelphia, PA 19104, USA
David Staack	Drexel University, 3141 Chestnut Street, LeBow 239, Philadelphia, PA 19104, USA
A. Khacef	GREMI-Polytech'Orleans, 14 rue d'Issoudun, BP 6744, 45067 Orléans, France
Sameer Kalghatgi	Drexel University, 3141 Chestnut Street, Bossone Suite 312, Philadelphia, PA 19104, USA

1. PLASMA FOR BIO-DECONTAMINATION

BIOLOGICAL DECONTAMINATION USING AN ATMOSPHERIC PRESSURE RESISTIVE BARRIER PLASMA DISCHARGE

I. ALEXEFF, A. BALASUNDARAM, E. P. PRADEEP, N. KARNAM, AND N. R. PULASANI
University of Tennessee, Knoxville TN 37996-2100 USA
(email: arunb@utk.edu, alexeff@utk.edu)

Abstract: The following paper discusses the observations of the surface plasma treatment conducted on *Escherichia coli*, *Pseudomonas fluorescens (5RL)*, and Wild type standard *Lambdaphage*. The tests were aimed to determine the sterilization efficiency of the dc steady state atmospheric pressure with a water cooled resistive barrier discharge apparatus. The results achieved were encouraging and 100% decontamination was observed within the first ten minutes of plasma exposure. The decontamination efficiency was however raised significantly through the introduction of hydrogen peroxide in tandem with the plasma treatment. The combination resulted in a 100% kill rate of *E. coli* in under a minute and *Lambdaphage* in less than five minutes. Further tests involving electrostatic filters and nitrogen gas were conducted to isolate and probe the effects of ozone and charged ingredients in the decontamination process. Some interesting preliminary plasma treatment test data were also obtained on spores (*Bacillus stearothermophilus*).

1. Introduction

Plasma sterilization techniques rely on a combination of factors such as Ozone, UV photons and activated/charged species (O and OH radicals). Atmospheric non-thermal plasma discharges in particular are inexpensive and do not necessitate specific operational expertise. More importantly it is safe in contrast to toxic chemicals and atmospheric pressure-temperature operations tend to preserve the integrity of the desired instrument to be sterilized [1,2].

Hydrogen Peroxide has been particularly found to be an effective sterilization agent against micro-organisms including bacterial spores, vegetative bacteria and viruses [3–6]. It is known that aqueous Hydrogen Peroxide has been in use for well over a century, but the vaporized form has not been exploited to its full

particularly in healthcare settings [7]. The scheme of pairing hydrogen peroxide effects, plasma sterilization, ultrasound waves and UV irradiation techniques has been considered in the past [8,9,10,11]. This however has led us to analyze the combinatorial effect of non thermal atmospheric plasma discharge with Hydrogen Peroxide vapors on microbial inactivation. The paper documents the test results of the biological inactivation studies conducted on *Pseudomonas fluorescens (5RL)*, wild type standard *Lambdaphage* and *Escherichia coli*. The experiments conducted also tests for the effect of vaporized Hydrogen Peroxide in a non thermal atmospheric plasma discharge.

2. Plasma Discharge Apparatus

The plasma discharge apparatus generates significantly large volumes of non equilibrium resistive barrier plasma discharge at atmospheric pressure. The plasma is generated between two planar electrodes using direct current power source (30 kV, 10 mA) or with a low frequency alternative current (120 V, 60 Hz) fed through a neon-sign step-up transformer (Output voltage – 15 kV across secondary terminals at 60 mA). Figure 1 illustrates the experimental design set up of the plasma reactor consisting of two electrodes – a bottom and a top electrode which usually rests on a highly resistive wetted unglazed ceramic barrier (20 x 20 x 1 cm). The ceramic is cooled and rendered conductive by using either water or hydrogen peroxide (30%), while ensuring no contact with the test plates (inoculated agar plates). The working medium in the plasma reactor is air and traces of water vapour/hydrogen peroxide. The resistive barrier (ceramic tile) with a resistance of 1 M Ohm prevents the diffuse discharge from contracting into an arc. A non conducting frame separates the two electrodes creating an air gap of 0.25 in. and allowing for the placement of test plates during plasma treatment. The plasma sterilizer has an upper plastic containment wherein the electrode arrangement is housed in the upper section of plastic containment and the lower
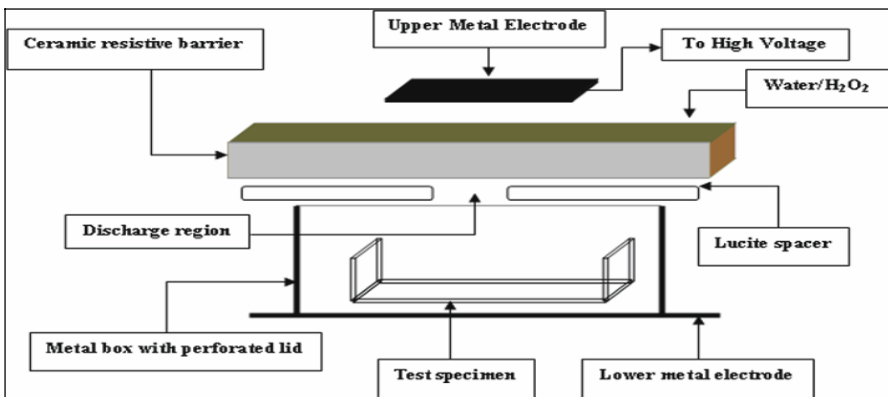
Figure 1. Schematics of the prototype sterilizer

compartment of the containment houses the high voltage circuitry as shown in Fig. 2. The upper compartment also houses a rotary blower to circulate the generated ozone and other plasma produced species during a plasma discharge. A filamentary discharge with air or a diffuse discharge with Helium gas can be achieved by applying high voltage between the two electrodes. Figure 3 depicts a plasma reactor that can typically generate up to 1,800 cc of He plasma. Microwave attenuation experiments conducted on the apparatus by Magesh Thiyagarajan et al. revealed an electron density of $10^{11}/cm^3$ with a microwave transmitter frequency of 2.5 GHz in helium atmosphere [11].
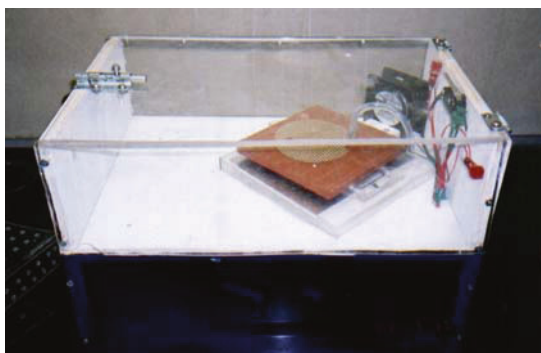
Figure 2. The direct current steady state atmospheric pressure plasma discharge apparatus
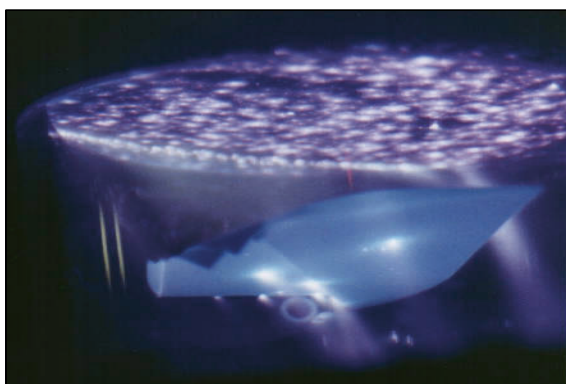
Figure 3. Helium plasma

Three spectra were taken from the high pressure discharge using an Ocean Optics USB2000 spectrometer along with background measurements. The resulting background corrected spectra are given in Figs. 4–6. Several helium lines are easily observed in these data. Three lines are of particular interest for plasma studies because they can be used for temperature and density determinations.
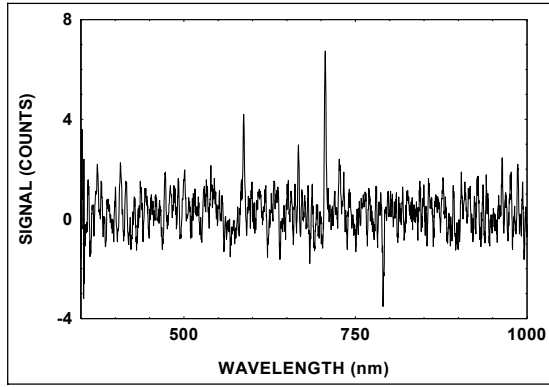
Figure 4. First spectra
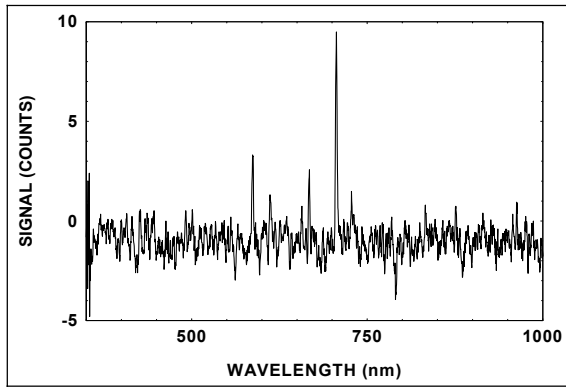
Figure 5. Second spectra
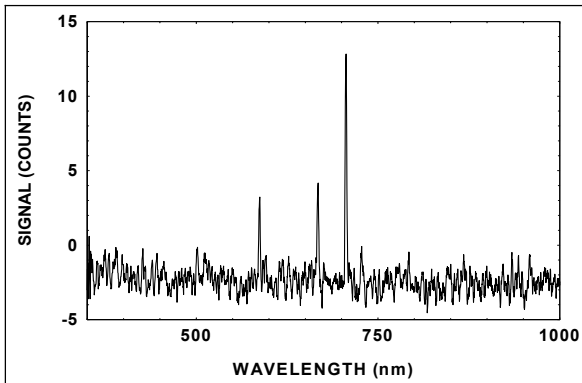
Figure 6. Third spectra

These lines are at 668, 706 and 728 nm. The ratio of intensities from 728 and 706 are used for temperature estimates and the ratio of intensities from 668 and 728 are used for density estimates. This technique has been applied for edge or diverter measurements in thermonuclear fusion devices where the electron temperature and density is low. For example, using plots from B. Schweer et al. [12], the estimates of temperature and density from the data shown in Figs. 4–6 is summarized in Table 1. Because the signals are all small the results will have some variation. With the data from Fig. 3 having the largest signal, it will probably represent the most accurate estimate. The intensities are determined by fitting a curve to the data around the expected wavelength for each line. Such fitting is illustrated in Figs. 7–9 for the three line fits from the data in Fig. 6. Because the light intensity is small the individual pixel readings have large variations due to the single count variations of the analog to digital conversions. This was reduced by averaging 10 scans for each spectrum and fitting around 25 pixels for each line shape. The fits are based on a least squares of a Gaussian with a three parameter fit: (a) the offset; (b) the line intensity; and (c) the line center. Note that two fits were tried for the line at 728 nm, the weakest of the three lines. This was to illustrate the sensitivity of the fit to different background selections and the results summarized in Table 1 reflect the average of these fits.

TABLE 1. The estimates of temperature and density for the data shown on Fig. [4–6].

Table	668 Intensity	706 Intensity	728 Intensity	Te(eV)	ne(cm^{-3})
Fig. 1	3.04	6.95	2.02	5	1×10^{11}
Fig. 2	3.60	10.09	1.565	4	5×10^{11}
Fig. 3	6.71	15.81	2.35	5	7×10^{11}
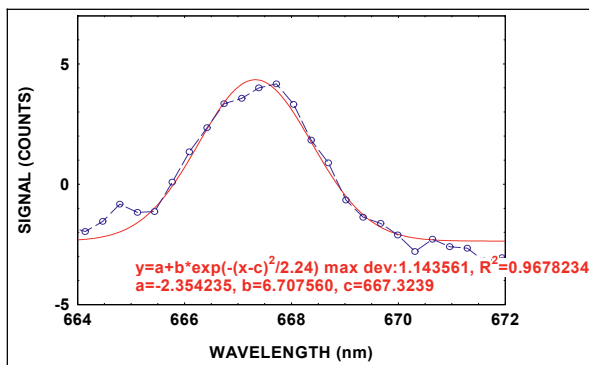
Figure 7. Line fit for 668 using the data on Fig. 6
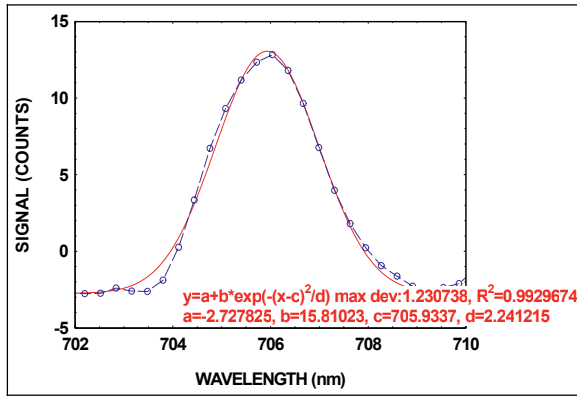
Figure 8. Line fit for 706 using the data on Fig. 6
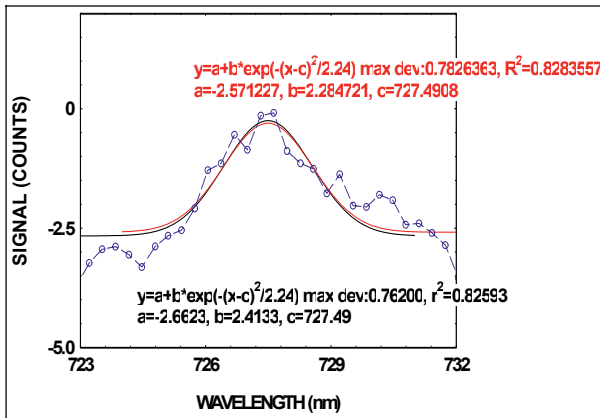
Figure 9. Line for 728 using the data on Fig. 6
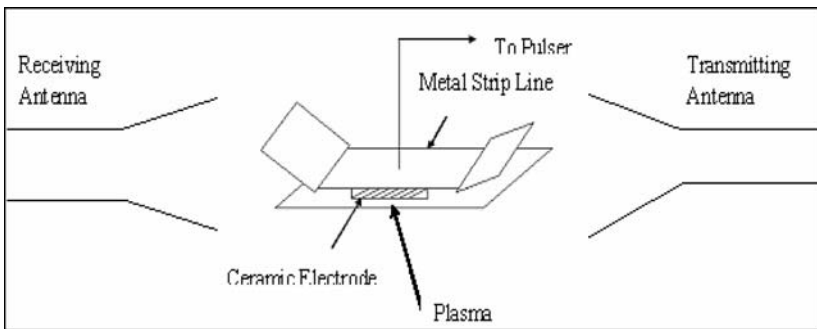
Figure 10. Schematics of a strip line configuration setup for microwave attenuation experiment

We have succeeded in measuring the free electron density generated in atmospheric pressure air and have generated $5 \times 10^{11}/cm^3$ in a pulsed discharge. The steady state free electron density extrapolates to $10^{11}/cm^3$. Microwave phase shifts do not occur, as the electron-gas atom collision rate is much higher than the applied frequency. However the electron-gas atom collisions do occur, which damp the microwave signal. Since the plasma layer is about 0.5 cm, the damping of microwaves traversing this layer is small, and difficult to observe. Thus our approach converted the plasma interaction region into a parallel-plate line configuration, with a 0.5 cm gap. The schematics are indicated on Fig. 10 And the construction of the apparatus is shown by Fig. 11. Waves of arbitrarily long wavelength propagate in such a system, just as they propagate in a coaxial cable of small diameter. This increases our wave plasma interaction distance from 0.5 to 15 cm, causing strong attenuation. A pulsed power supply was used to observe the plasma microwave attenuation, which clearly showed plasma absent and plasma present microwave signals. In addition, the pulse provided about five times the normally available operating current, causing increased plasma density and microwave attenuation. Under these conditions of operation we obtained 50% attenuation of the microwave signal. The upper trace indicated in Fig. 12 shows the Pulsed current (downward – 50 mA peak) and the lower trace in Fig. 12 indicates the Microwave attenuation pulse (full signal downward) on a time scale of 10 μs per large division. Extrapolating to the usual operating discharge current, we obtain a free electron density of $10^{11}/cm^3$. The microwave attenuation only lasted for about 30 μs. The electrons must attach to air molecules, creating negative ions. These negative ions form negative-positive ion plasma, which persists for a long time and can be detected at large distances from the ionization region. A common error in this work is in assuming that when free electrons disappear, all plasma is gone. It can be detected "with electric probes" at large distances.

Figure 11. Photograph of microwave attenuation
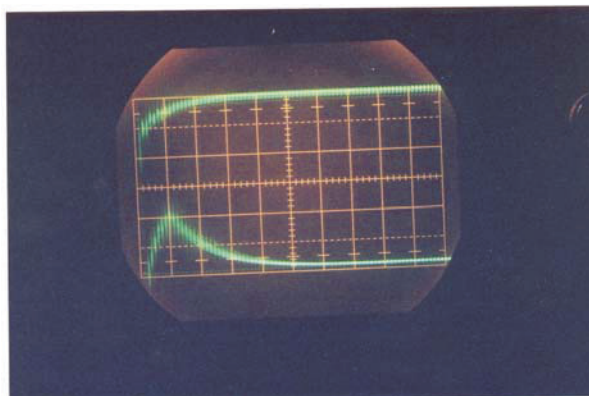
Figure 12. Oscillation graph depicting pulsed current and microwave attenuation. Upper trace is pulsed current (downward – 50 mA peak). Lower trace is attenuation (full signal downward). Time scale – 10 μs per large division

3. Methods and Materials

A. Cell culture – Escherichia coli

Frozen stocks of *E. coli* were cultured in 100 ml of LB (Luria Bertani growth medium) for 4–6 h at 37°C in an incubator equipped with a shaker. The strain of choice was a genetically engineered strain with GFP (Green Fluorescent Protein). The GFP allows for improved analysis of microscopic samples of plasma treated bacterial cells.

B. Cell culture – Pseudomonas fluorescens *5RL*

Frozen stocks of *P. fluorescens 5RL* were cultured in 100 ml of LB (Luria Bertani growth medium) supplemented with 100 μl of Tetracycline for 12–16 h at 28°C in an incubator equipped with a shaker. The *5RL* is also a genetically modified strain with a tetracycline resistant gene and a bioluminescence plasmid which causes gives out a bluish green light in the visible spectrum (495 nm) on contact to specified chemical targets (Naphthalene and Sodium Salycylate). The strain was particularly preferred for experimentation to address the "viable but non cultivable cells" issue.

C. Cell culture – Lambdaphage *(plate lysate preparation to isolate Lambda phage)*

E. coli (*XL1 Blue*) was used as the bacterial host for the *Lambdaphage*. Frozen stocks *E. coli* are thawed and suspended in LB medium substituted with maltose and MgSO$_4$. The mixture is then incubated for 10–12 h at 37°C. A fresh culture of an *E. coli* host strain (XL1Blue) is started by inoculating a single colony into 5 ml of LB medium supplemented with 50 μl of 20% maltose and 50 μl of 1 M MgSO$_4$. The mixture is shaken overnight at 37°C. A single phage of plaque from a master stock on an agar plate was eluted and expelled into 1 ml of SM buffer. The

solution containing the phage was then incubated for an hour at room temperature. About 60–100 µl of elute was mixed with 100 µl of a fresh overnight culture of the bacterial host (XL1Blue) and incubated at 37°C for 20 min. To that mixture 2.5 ml of melted LB top agarose was mixed gently and then poured onto an LB agar plate. After the top agarose had hardened, the plates were inverted and incubated at 37°C for 6 h or until the plaques had become confluent. The top agarose from the agar plate was scrapped after adding 2–3 ml of SM buffer. The resulting suspension was centrifuged (8,000–10,000 xg for 10 min) and then incubated at room temperature for 30 min, periodically shaking the tube. The *Lambdaphage* was then isolated from the supernatant solution.

D. Cell culture – Spores (Bacillus stearothermophilus)

A frozen stock of spores was maintained on trypticase soy broth with dextrose, incubated at a 60°C for 2–7 days. The purity of the spore culture and percentage of sporulated cells were regularly verified using a microscope and stain tests. After sufficient sporulation was achieved, the supernatant was resuspended in physiological saline and rewashed and centrifuged for plasma treatment tests.

E. Plasma exposure test protocol – E. coli and Pseudomonas Fluorescens *(5RL)*

E. coli and *Pseudomonas Fluorescens (5RL)* exposure samples for the bacterial decontamination experiments were prepared by inoculating 100 µl of cell suspension containing approximately 10^8 cells per ml in the growth medium onto LB-agarose plates. The concentrated cell suspension was diluted (1 to 10 serial dilution) such that it yielded about 100–150 colony forming units (CFU's) after an overnight incubation, to facilitate manual counting. Each experimental run involved the preparation of triplicate samples of inoculated agar plates (petri dishes) followed by a plasma exposure with varying time intervals. The configuration of specimen plates is shown in Fig. 1. The plates are then allowed to age overnight in an incubator alongside with the untreated plates (control plates). The *E. coli* cells on the control plates were provided the exact same growth conditions and temperature as the treated plates. The survival curves are then evaluated by obtaining a post incubation CFU count in each case. The temperature variations inside the discharge chamber and on the surface of the test specimens (inoculated agar plates) were monitored using a radiation thermometer before the and immediately after the discharge. The change in the temperature was within 2–4°C of the room temperature, thus rendering it insignificant in the context of contributing to the kill rate of microbes.

F. Plasma treatment protocol for Lambdaphage *experiments*

Test specimens were prepared for the phage experiments by inoculating the agar plates with 50 µl of the solution containing the isolated phage. The plates were then exposed to the plasma discharge similar to the bacterial decontamination experiments. All plates including the untreated control plates were then inoculated with a mixture containing 100 µl and 2.5 ml of melted top agarose. The mixture was allowed to cool until the top agarose hardened. The *XL1 Blue* is added specifically after the phage was exposed to plasma, to shield the bacterial host

from the sterilization effects of the plasma discharge. The separation provides the treated and untreated bacteriophage samples a healthy bacterial host thus allowing to isolate and analyze the effect on plasma discharge on phages. The plates were then incubated overnight at 37°C. The survival curves are then evaluated by obtaining a post incubation PFU (Plaque Forming Unit) count in each case. The measured temperature variations were within a 2–4°C (from room temperature).

4.   Discussion

A. Discharge parameters

All bacterial and bacteriophage samples mentioned in sections IV (B–E) were exposed to an atmospheric pressure plasma discharge with a specific power of 100 W, in a gas medium of air and residue from water. The residue is from hydrogen peroxide in experiments where the water cooled ceramic resistive barrier is replaced with a hydrogen peroxide cooled barrier electrode, elaborated in section V. The discharge products (charged ions, ozone and residue from water/H_2O_2) typically reach the surface of the specimen through diffusion, with the exception of nitrogen run tests detailed in section IV D where a rotary blower is employed. The specimen plates are usually placed directly below the region of discharge as in Fig. 1 during plasma exposure. The electrostatic filter tests (section IV E) for presence of charged ions, the petri dish is away from the discharge region owing to high voltage circuit constraints. The specimen plates particularly in tests with business envelopes test as described in section IV C were enclosed in glazed envelopes as opposing to samples in open inoculated agar plates in all other experiments.

B. Inactivation of Escherichia coli

Figure 13 illustrates the survival curves for *E. coli* subjected to a non thermal plasma discharge with a specific power of 100 W. The samples were exposed to plasma in medium consisting air and ionized residue from water. The experiment
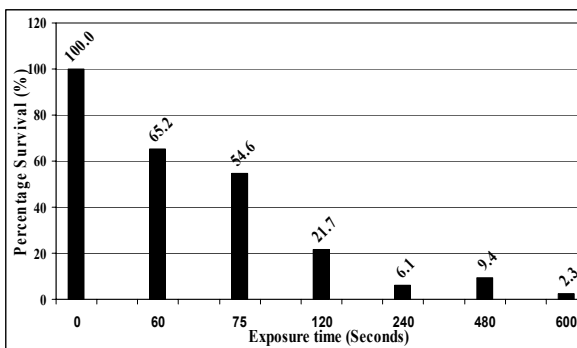
Figure 13. Survival characteristics of *Escherichia coli* on LB plates (Luria Bertani growth medium)

relied on plain diffusion of ozone and other species (positive and negative ions) produced by plasma, onto the samples and did not use a forced draft system. The percentage ratio of the viable *E. coli* CFU (Colony Forming Unit) count on the treated sample (T) to that on the untreated sample (To) is plotted against the exposure time along the horizontal axis. Each data point on the Fig. 13 represents the mean value of three exposures. The experiments also included negative controls to monitor any external decontamination in the inoculation plates (medium plates).

The decrease in the number of viable *E. coli* colonies in excess of 97% was achieved in 600 s. There was a noticeable increase in the survival rate for the 480 s exposure test, as opposed to the general deceasing survival rate with increasing exposure time periods. The possible explanation to the observation at this point could be attributed to growth of *E. coli* on inoculated plates before the plasma treatment.

C. E. coli *tests with business envelopes*

Figure 14 shows the kill curves for plasma treatment of *E. coli* placed within sealed and glazed business envelopes. The test involved exposing the microbes in sealed envelopes to simulate an environment wherein the apparatus could be used to decontaminate postal mail and media. Even under such experimental conditions similar levels of kill rate could be achieved.
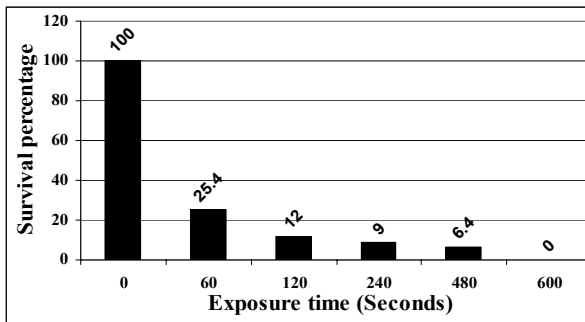
Figure 14. Survival characteristics of *Escherichia coli* on LB plates within sealed business envelopes without hydrogen peroxide

D. Plasma exposure tests with nitrogen gas

The primary motivation for exposure tests with nitrogen gas in the sterilizer chamber was to mask the effect of ozone as a decontamination agent and observe the change in the sterilization rate. All other experimental parameters were maintained consistent with previous test runs and in addition the sterilization chamber was flushed with nitrogen at 10 l/min during the plasma discharge to remove traces of oxygen (ozone) compounds. The gas inflow was monitored using an oxygen flow meter. Figure 15 depicts the results of the survival percentage of *E. coli*, which are consistent with earlier observations of the plasma exposure tests without nitrogen gas. Thus the results hint at the possibility of existence of additional sterilization agents other than the ozone that could play a critical role in the sterilization process.
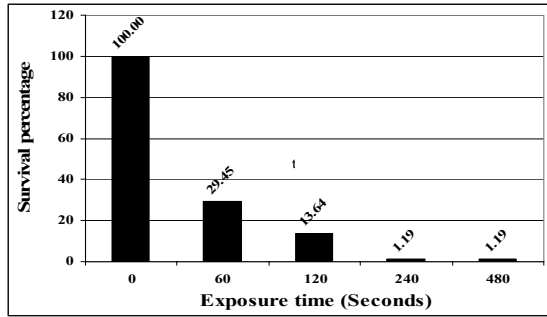
Figure 15. Kill curves of *Escherichia coli* with the sterilizer chamber flushed with nitrogen gas without the presence of hydrogen peroxide

E. Test for charged species in the discharge

This particular test involving electrostatic filters was designed to test for the presence of activated ingredients (charged ions) and attain insights on its role in the sterilization process. The filters were composed of two superimposed wire meshes placed over the petri dish. To activate the filter, the two meshes were charged to +/–400 V, which causes absorption of charged particles passing between them. The petri dish (agar plates) containing the inoculated samples in this experiment were placed to the side of the discharge region on the left shown in Fig. 1, away from the high voltage circuit due to the presence of the filter circuit (metal). A blower in the right corner blows discharge products over the petri dish. The production of activated ingredients during the plasma discharge is believed to be significant. The test run included plasma exposure with activated and de-activated filters. The higher rate of survival in the case of activated filters shown in Fig. 16 signify the presence and contribution of charged ions.
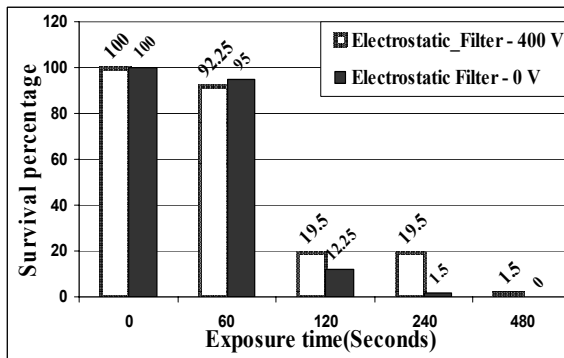
Figure 16. Plasma exposure test kill curves of *E. coli* with a electrostatic filter to remove activated ingredients

F. Bioluminescence tests with P. fluorescens *5RL*

The plasma exposure tests to determine the effective kill rate of the sterilizer were conducted by inoculating LB pour plates with microbes. The results of such experiments thus depended on the capability to be cultured on a medium plate. To address the case of viable but non culturable cells, inactivation studies were conducted on a genetically engineered bioluminescent bioreporter [13]. The bioluminescence could be induced artificially by sodium salycylate and the response could be measured with the Wallac (Liquid Scintillation counter). Thus the functional response of the plasma treated microbes could be monitored without the need to plate them on pour plates. The results are shown on Fig. 17, which contains the bioluminescence counts per second plotted on the vertical axis against the time on the horizontal axis. The samples treated for 6 min did not record any peak luminescence values above the background, compared to the untreated samples which had a varying response over the 24 h period. The inactivation effect was significant given the fact that plasma had acted on a volume as opposed to a thin layer of cells in earlier tests. The plasma discharge system was found to be comparatively less effective when the samples consisted of liquid broth, and thus ideally suited for surface decontamination.
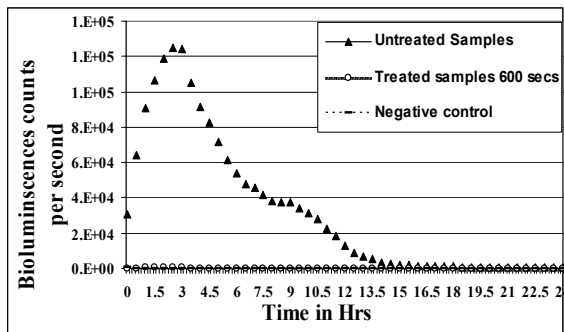
Figure 17. Bioluminescence response of plasma treated *P. fluorescencs 5RL*

5. Improved Decontamination Using H_2O_2

All the previous test runs were carried out using a resistive barrier electrode wetted with water to cool it and make it conductive. To improve the sterilization efficiency, the water was replaced with a 30% solution of Hydrogen Peroxide. During the experiment caution was observed to avoid any direct contact of aqueous H_2O_2 with the inoculation plates containing the microbes (specimen). The vapors of hydrogen peroxide eventually mixed with air diffused into the test samples. Control plates in this experiment were stored in the sterilizer chamber along with the ceramic barrier wetted with the hydrogen peroxide (no discharge) to maintain the consistency in treated plates. The results of synergy of the sterilization agent (H_2O_2) with the plasma discharge system are shown in

Fig. 18. In addition to these tests control plates were exposed to hydrogen per-oxide environment in the absence of the plasma discharge. Fig. 19 shows the plasma exposure test results with hydrogen peroxide, wherein the concentration of the microbes were increased successively by a factor of 10 for every exposure interval. The ceramic barrier was however mildly heated using an incandescent lamp to mimic the 2–4°C rise in temperature during a plasma discharge. The results of control plate tests are provided in Fig. 20 distinctly illustrates the effectiveness of hydrogen peroxide in conjunction with the plasma discharge. It also eliminates the hypothetical situation wherein the sterilization effect of hydrogen peroxide primarily drives the microbial kill rate. The sterilization of *E. coli* samples was achieved well under a minute of the exposure period. The results of the effect of plasma exposure and hydrogen peroxide on bacteriophages are indicated in Fig. 21. Preliminary test results of the effect of plasma treatment on spores (*Bacillus stearothermophilus*) are illustrated in Fig. 22. Pilot studies reveal that spores as opposed to *E. coli* could be eliminated in shorter exposure intervals. In case of phages a decontamination rate in excess of 98% could be observed in about 4 min of exposure. The pairing of hydrogen peroxide though works well, the exact proportion of the air-H_2O_2 mixtures contributing to higher kill rates are unknown at this point.
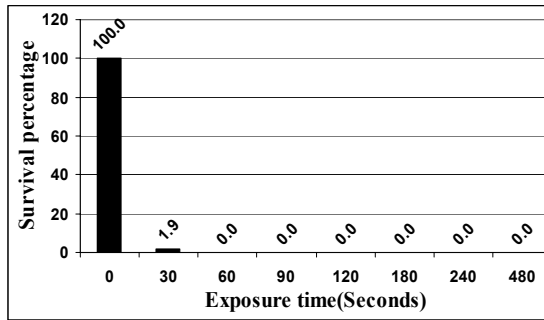
Figure 18. Plasma exposure test kill curves of *E. coli* curves in a hydrogen peroxide (30%) plasma discharge
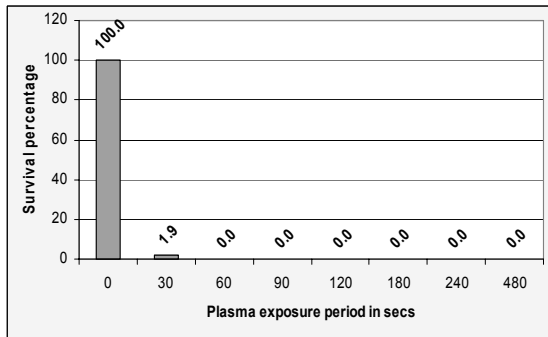
Figure 19. Plasma exposure test kill curves of *E. coli* curves in a hydrogen peroxide (30%) plasma discharge with increasing concentration of microbes by a factor of 10
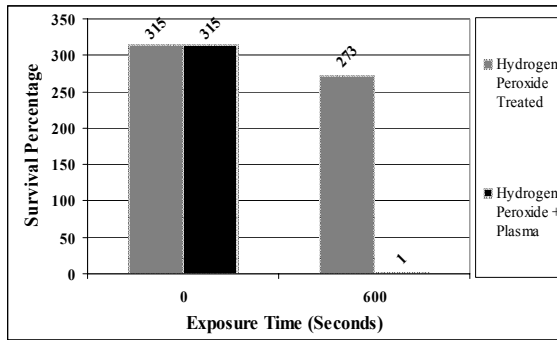
Figure 20. Plasma exposure test kill curves of *E. coli* plates for isolated effects of hydrogen peroxide
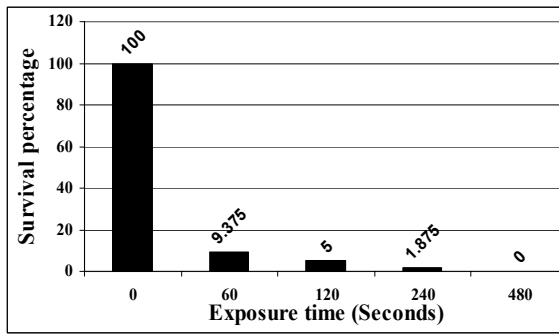
Figure 21. Plasma exposure test kill curves of wild type standard *Lambdaphage* in a hydrogen peroxide (30%) plasma discharge
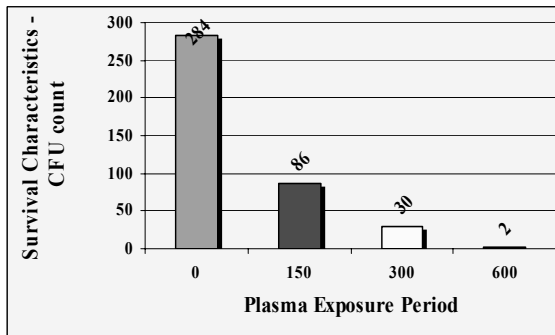
Figure 22. Preliminary plasma exposure test results demonstrating the survival count of spores (*Bacillus stearothermophilus*) in a hydrogen peroxide (30%) plasma discharge. The three sets of data were taken from different parts of the discharge, with that of Fig. 3 from the intense region of the cathode glow

Conclusion

The atmospheric pressure plasma apparatus was tested on *E. coli*, *Pseudomonas Fluorescens (5RL)*, *Lambdaphage* and spores (*Bacillus stearothermophilus)*. The results in essence depict a high efficacy of the sterilizer in realizing comprehensive decontamination against both bacterial strains and bacteriophages. Particularly the Tests with nitrogen gas instead of air, and with an electric filter demonstrate that sterilization occurs by processes in addition to ozone and other interaction products of oxygen. Rapid sterilization was achieved when the surface plasma treatment was combined with the hydrogen peroxide vapor diffusion process. Thus the versatility (dual power mode AC/DC), ease of operation, portability, rigid construction and high efficiency opens up a wide gamut of application.

Acknowledgment

References

[1]   Michel Moisan, Jean Barbeau, Marie-Charlotte Crevier, Jacques Pelletier, Nicolas Philip, and Bachir Saoudi (2002). "Plasma sterilization: Methods and mechanisms." *Pure and Applied Chemistry* **74**(3): 349–358.

[2]   Mounir Laroussi, Igor Alexeff, and Weng L. Kang (2000). "Biological decontamination by nonthermal plasmas." *IEEE Transactions on Plasma Science* **28**(1): 184–188.

[3]   Kokubo, M., Inoue, T., and Akers, J. (1998). "Resistance of common environmental spores of the genus Bacillus to vapor hydrogen peroxide." *PDA Journal of Pharmaceutical Science and Technology* **52**(5): 228–231.

[4]   French, G. L., Otter, J. A., Shannon, K. P., Adams, N. M. T., Watling, D., and Parks, M. J. (2003). "Tackling contamination of the hospital environment by methicillin-resistant *Staphylococcus aureus* (MRSA): A comparison between conventional terminal cleaning and hydrogen peroxide vapour decontamination." *Journal of Hospital Infection* **57**(1): 31–37.

[5]   McDonnell, G., Grignol, G., and Antloga, K. (2002). "Vapour-phase hydrogen peroxide decontamination of food contact surfaces." *Dairy, Food, Environment and Sanitation* **22**: 868–873.

[6]   Heckert, R. A., Best, M., Jordan, L. T., Dulac, G. C., Eddington, D. L., and Sterritt, W.G. (1997). "Efficacy of vaporized hydrogen peroxide against exotic animal viruses." *Applied and Environmental Microbiology* **63**: 16–18.

[7]   Klapes, N. A. and Vesley, D. (1989). "Vapor-phase hydrogen peroxide as a surface decontaminant and sterilant." *Applied and Environmental Microbiology* **56**(2): 503–506.

[8]   Bayliss, C. E. and Waites, W. M. (1979). "The combined effect on hydrogen peroxide and ultraviolet irradiation on bacterial spores." *Journal of Applied Bacteriology* **47**: 263–269.

[9]   Waites, W. M., Harding, S. E., Fowler, D. R., Jones, S. H., Shaw, D., and Martiin, M. (1988). "The destruction of spores of Bacillus subtillis by the combined effects of hydrogen peroxide and ultraviolet light." *Applied Microbiology* **7**: 139–140.

[10] Hofmann, J. O., Knoll, M., Durr, M., Schmitt, B., and Lipp, M. B. (2005). "Comparison of low temperature hydrogen peroxide gas sterilization for endoscopes using various sterrad models." *Journal of Hospital Infection* **59**: 280–285.

[11] Magesh Thiyagarajan, Igor Alexeff, Sriram Parameswaran, and Stephen Beebe (2005). "Atmospheric pressure resistive barrier cold plasma for biological decontamination." *Journal of Plasma Science* **33**(2): 322–323.

[12] Schweer, B., Mank, G., Pospieszczyka, A., Brosda, B., Pohlmeyer, B., Bauer Walter, H. W. L., Jackson Gary, L., and Porter Gary, D. (1992). "Electron temperature and electron density profiles measured with a thermal He-beam in the plasma boundary of TEXTOR." *Journal of Nuclear materials* **196–198**: 174–178.

[13] King, J. M. H. (1990). "Rapid sensitive bioluminescent reporter technology for napthalene exposure and biodegradation." *Science* **249**: 778–781.

PLASMA FOR AIR AND WATER STERILIZATION

A. GUTSOL[1], N. D. VAZE[2], K. P. ARJUNAN[2],
M. J. GALLAGHER, JR.[1], Y. YANG[1], J. ZHU[1],
V. N. VASILETS[1], AND A. FRIDMAN[1]
[1]*Department of Mechanical Engineering and Mechanics, College
of Engineering, Drexel University, Philadelphia, PA 19104 USA*
[2]*School of Biomedical Engineering, Science, and Health Systems,
Drexel University, Philadelphia, PA 19104 USA*

Abstract: This chapter describes the research efforts of Drexel Plasma Institute (DPI) in the area of plasma-based air and water sterilization. Motivation of this research is presented as well as the methods for selection of parameters for the experimental systems. Experimentally obtained results for air sterilization demonstrate that the direct influence of plasma charged particles on airborne bacteria in combination with active chemical substances generated by plasma is the probable reason for high sterilization efficiency of the Dielectric Barrier Grating Discharge (DBGD). Energy input on the level of 13 kJ/m^3 is enough to reach a 5-log reduction of viable *E. coli* bacteria. Experimentally reached D-value (the dosage required for a 90% reduction of the number of viable microorganisms) for *E. coli* bacteria deactivation in water using spark discharge is very low, about 125 kJ/m^3, and UV-radiation is the most plausible sterilization factor in this case. A new seminumerical model is proposed for initial phase of electrical breakdown in water.

Keywords: Dielectric barrier discharges, spark discharge, air sterilization, water sterilization, breakdown in liquid

1. Motivation

A low concentration of pathogenic microorganisms in air and water is a necessary condition of good health. As the world population and population density in major cities continues to grow, it becomes increasingly difficult to maintain high standards of air and water purity. There are some well known industrial technologies for water sterilization that are widely used in developed countries. Though these technologies have some drawbacks and limitations, they have been proven reliable in providing clean water for many people. Unfortunately in many poor and developing countries, the situation with water cleanness is very far from acceptable. The World Health Organization estimates that 900 million people each year suffer from diseases spread

by contaminated water. According to the World Bank, more than 2 million people, who are mostly children, die every year from health-related causes linked to the use of polluted water. In 2002, an estimated 1.1 billion people were unable to acquire safe drinking water [1].

Air sterilization technologies are not as well developed though there are several approaches that are used, for example, ultra-violet (UV) irradiation in hospital environments. The need for air sterilization in closed volume environments like aircrafts, space stations, or submarines always exists and became also important for all large buildings given the Anthrax bio-terrorism events that occurred in Washington, DC in 2001. Bioterrorism threats also exist for water sources, though to date no such incident has occurred. Financial support provided by the National Bioterrorism Civilian Medical Response Center (CIMERC) [2] has allowed the Drexel Plasma Institute to start research in the areas of air and water sterilization.

Why is plasma interesting for air and water sterilization? First of all, plasma has been used for many years as a remote source of the well known active agents, UV radiation and ozone, that can be transported over short distances for sterilization of air and water. It is an idea to use plasma for direct sterilization in hope of creating a synergistic sterilization effect by combining these transportable agents with other energetic and chemically aggressive agents that exist only within plasma and can not be transported (e.g. electrons, ions, short-living chemical radicals, excited molecules, VUV photons). Secondly, plasma has been investigated as a universal sterilization agent for a long time (see, for example, reviews [3,4]). Mostly these have been surface sterilization experiments, though some studies have been focused on sterilization in water [5–7].

In research devoted to sterilization of high volume streams of water and air that are typical for water supply and ventilation, the key issue that should be considered is economics. This issue for plasma technologies is formulated as a requirement of effective treatment with low energy consumption per unit of volume of air or water. Energy cost and sterilization efficacy are the figures of merit that define applicability of plasmas for air and water sterilization. Also it is rather obvious that the application of any special gases for plasma generation (helium, argon, etc.) can not be justified for economically viable method of air or water sterilization. Though it looks like all this is not so important for the case of bioterrorism emergency response, it is difficult to expect fast implementation of a technology if it does not have application in everyday life. Nevertheless, even rather energy expensive sterilization technology can find application for bio-defense if it has low capital cost and can exist for an unlimited time in a waiting mode. These arguments were considered when we started development of our plasma approaches for water and air sterilization.

The plasma discharge in water that we use for water sterilization and some other applications is under investigation by many research groups, but our analysis showed that all these groups do not have a satisfactory model for the initial phase of the discharge. This forced us to develop a new semi-numerical model that explains fast growth and branching of the gaseous discharge channel.

2. Air Sterilization

As experimental results of our research on air sterilization using non-equilibrium plasma are presented in some publications [8,9], here we will consider selection of the parameters of the experimental system because it can be interesting for other researchers in this area. In the development of our bioaerosol decontamination facility, named the Pathogen Detection and Remediation Facility (PDRF), we started with the literature analysis that showed that there were very few publications related to air flow sterilization using plasma [11–13]. The few publications that were found were devoted to combination of plasma with high-efficiency particulate-air (HEPA) filters to trap microorganisms on the surface of the filter and generate plasma to destroy them. Using this method, air sterilization using plasma is converted to the well-known task of surface sterilization. The major drawbacks of HEPA filters are that they cause significant pressure losses in heating, ventilation, and air conditioning (HVAC) systems and require regular replacement, giving rise to higher energy and maintenance costs. Therefore we designed the PDRF system to perform air stream sterilization using plasma without filters.

As there were no results in plasma deactivation of microorganisms 'in flight,' we decided to make a modular system that can work with different types of discharges, that can also provide low energy input and low pressure drop with rather uniform treatment. Additional requirements of scalability and relatively low capital costs were also taken into consideration. Based on these requirements, three types of discharges were selected for tests in the following order from the least to the most expensive (in capital costs): Dielectric Barrier Discharge in the form of grating (DBGD, Fig. 1) that consists of a thin plane of wires with equally spaced air gaps of 1.5 mm; plasma disc formed by gliding discharge rotation in magnetic field (Fig. 2) that was initially developed for combustion enhancement study [14]; and pulsed corona (Fig. 3) that was initially developed for VOC abatement [15]. All these discharge systems were specially designed to have very low resistance for air flow.
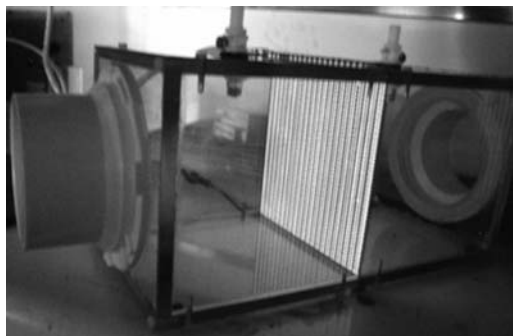
Figure 1. Dielectric Barrier Grating Discharge (DBGD) in the plasma-sampling module of the Pathogen Detection and Remediation Facility (PDRF)
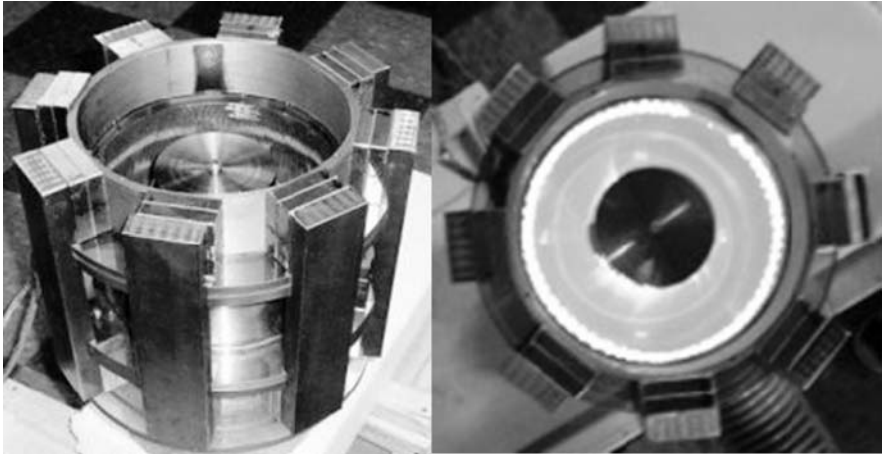
Figure 2. System for gliding discharge rotation in magnetic field and plasma disc developed in this system
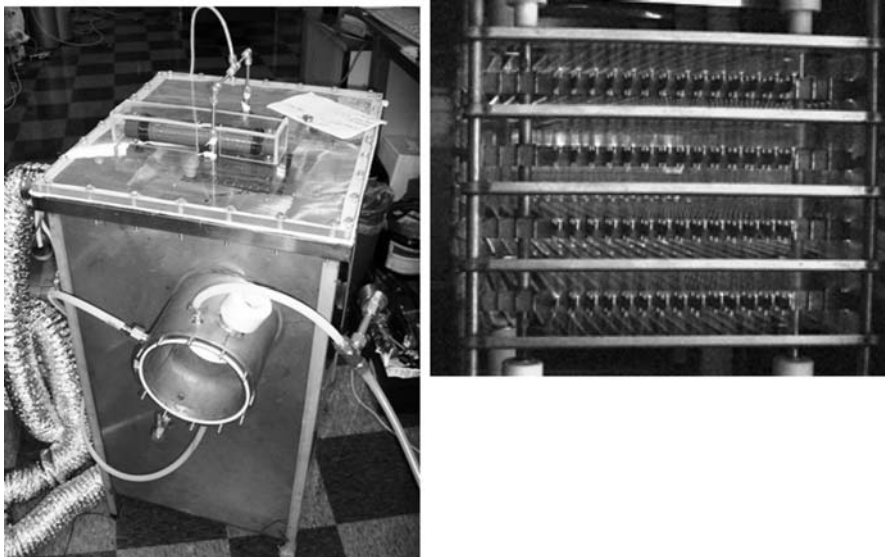
Figure 3. Pulsed corona unit and its electrode system with plasma discharge

To ensure system scalability we decided to have discharges with dimensions typical for HVAC systems. Also, typical indoor air has rather low and variable concentration of microorganisms of different kinds. Therefore it is clear that it is necessary to contaminate air with high concentrations of microorganisms for sterilization experiments. Most pure microbiological cultures are stored usually in the form of suspensions, and the typical concentration of microorganisms in a water-based suspension is $\leq 10^7$ CFU/ml (CFU – colony forming unit) if

suspension is still behaves as liquid. For reliable measurement of microorganism concentration by the conventional plating method a sample should contain at least 100 CFU. Our goal was to demonstrate at least 3-log reduction in viable microorganism concentration (in one or several stages of plasma treatment), therefore number of microorganisms in a sample before plasma treatment should be at least 10^5. Also, the PDRF should be at least quasi-sealed to prevent room contamination from leakage and it should operate at atmospheric pressure to imitate HVAC system and to avoid multiple technical difficulties. This means that the system pressure should not be significantly changed during sampling procedure. Also, the sampling procedure should not significantly change the total number of microorganisms in the PDRF. All this means that total initial number of microorganisms should be at least 10^7 CFU; therefore, during microorganism aerosolization, it is necessary to spray at least 1 ml of the water based suspension into the PDRF. Most of microorganisms are very sensitive to humidity and can not survive desiccation. On the other hand experiments with spores were included in the program, and sterilization of spores in dry and humid conditions can be very different. Therefore aerosol injection and evaporation should not result in significant humidity change, so humidity change due to evaporation of 1 ml of water should not give humidity increase larger than 10% (relative humidity – RH). Taking into account that 100% RH at room conditions corresponds to about 3 kPa of water vapor partial pressure, it is easy to come to conclusion that the PDRF volume should be at least 0.3 m^3.

Several different types of air sampling methods were investigated including filtration and liquid impingement. Air sampling that should collect about 1% of the total number of microorganisms can also collect about 0.01 ml of liquid in the case of operation with microorganisms that require high humidity. This amount of liquid can create a water film on a micro-porous filter requiring high pressure to overcome if the filter is used for sampling. Therefore we were forced to reject this option and to choose liquid impingement as the air sampling method. This method also minimizes desiccation stress and allows for the direct deposition of the microorganisms into growth media. Figure 4 presents a schematic and Fig. 5 presents a picture of PDRF.

The PDRF was designed as a plug flow reactor, i.e., air flow inside the system is turbulent so that radial variation of the bacterial concentration in the airflow is minimized. The system has a total volume of 0.25 m^3. The system has an injection inlet with attached Collison nebulizer for bioaerosol generation and two air sampling ports connected to a vacuum air sampling system. The PDRF also includes a large volume barrel that contains a series of aluminum baffle plates and a variable speed centrifugal blower motor that drives the air through the plasma treatment chamber. A rather high air flow rate (on the level of 25 l/s in most of experiments) was selected for the PDRF to imitate a typical HVAC system from the standpoint of volumetric as well as linear gas velocity. Taking into account that an office ventilation system should provide 5 l/s of air per person, the PDRF imitates a ventilation duct for an office with 5 people. The system recirculation time, i.e., the time for one bioaerosol particle to make one complete revolution

through the system, is approximately 10 s. Electrical heaters are installed in the large barrel of the PDRF for sterilization of the system by temperature between experiments.
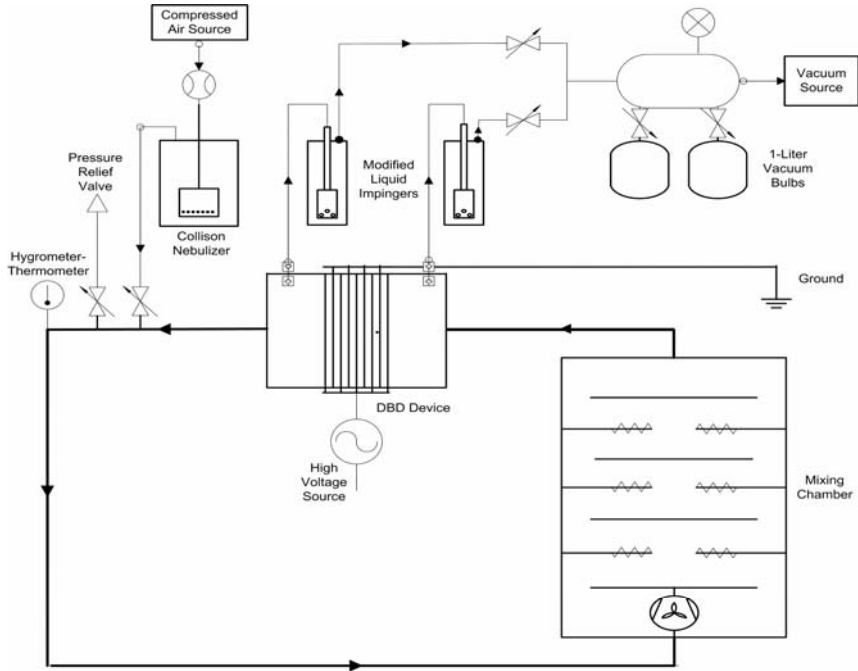
Figure 4. Schematic of the Pathogen Detection and Remediation Facility (PDRF) with DBGD

Sampling ports are located on both sides of a plasma unit and close to the electrodes. This configuration allows separation of the decontamination effect due to direct plasma exposure from the remote exposure of ozone and other long-lived chemical species that can interact with bio-aerosols downstream of the discharge. Each set of two air samples measures the change in viability of microorganisms on a "per pass" basis through the discharge. For each of the subsequent sets of air samples, the sample taken "before plasma" can give a measurement of the change in viability due to the effect of residual ozone from the previous "after plasma" sample. The liquid impingers used for air sampling operate by drawing a sample of air through an inlet tube submerged in a solution, thereby causing the air stream to strike the liquid bed trapping aerosols in the solution through forces of inertia [16]. Commonly used liquid impingers have too small critical orifice that does not allow a relatively large sample (at least 1 L) to be taken in a short time (about 1 s), which should be much shorter than the recirculation time (10 s). To accommodate a high air sampling rate, the AGI-30 impingers were modified by replacing the standard critical orifices with hollow metal tips with several jet ports. The overall efficiency of the injection-sampling system for *E. coli* was in the range of 6% ± 3%.

The overall efficiency was calculated as the ratio between the number of CFUs in a collected control sample and the number of bacteria calculated from the volume of nebulized suspension and volume of the air passed through the impinger.
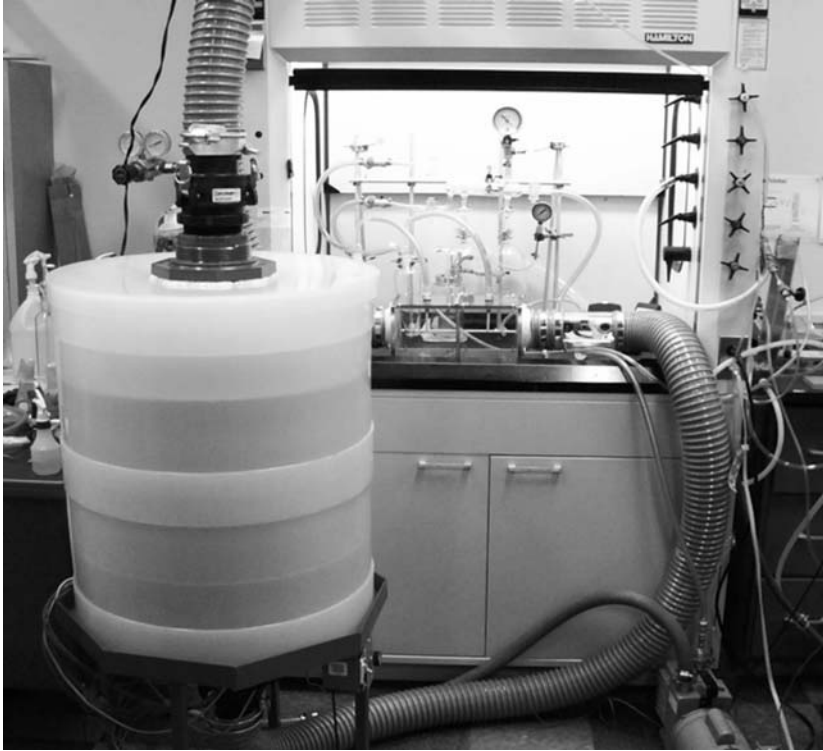
Figure 5. Picture of the Pathogen Detection and Remediation Facility (PDRF) with DBGD

As experiments using DBGD demonstrated unexpectedly good results (see below), this discharge is the only one used so far for the plasma process sterilization study. The DBGD is powered using quasi-pulsed power supply that delivers large voltage pulses with following damped oscillations when no current spikes are observed. Oscillograms indicate that the duration of one high voltage pulse period is approximately 600 µs and the maximum peak-to-peak voltage is 28 kV. Also, the discharge operates in a non-homogeneous streamer mode [17]. The average power of the discharge over one pulse period is approximately 330 W that is distributed over the whole grating area of 214.5 cm^2 (total minimal cross-section area for air flow through DBGD is 91.5 cm^2).

The culture test results from multiple replicate trials of *E. coli* bioaerosol treatment using DBGD in the PDRF system are shown in Fig. 6. Control experiments indicate negligible change in the surviving fraction of *E. coli* over the total experimental period. Plasma treatment results in an approximate 1.5-log reduction (97%) in the surviving fraction of *E. coli* just in 1 pass through DBGD,

which corresponds to an approximate 1 ms treatment time. A second decrease in the surviving fraction of *E. coli* between samples 2 & 3 occurs in the time between plasma treatments. In this second decline, the number of culturable bacteria decreased by an additional 99.95% (3.5 logs). Additional samples taken did not reveal any culturable bacteria; therefore those experimental points were omitted from Fig. 6.
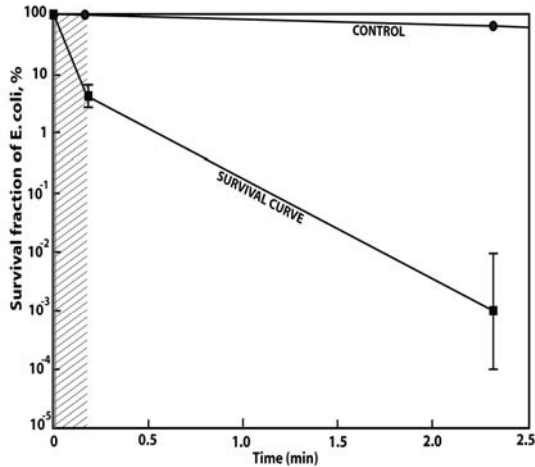
Figure 6. Survival curve for DBD-treated *E. coli* bioaerosol. The plasma treatment time is 10 s (the grey shaded area) that corresponds to the recirculation time of PDRF, so all bioaerosol particles make one pass through the discharge. Residence time of particles in the plasma zone is approximately 1 ms

Flow cytometry was employed to detect the presence *E. coli* in each air sample taken during experiments [8,9]. Where colony counting techniques are limited to detecting only culturable (i.e. visibly growing) bacteria, flow cytometry is capable of detecting the physical presence of bacteria in a sample regardless of culturability. Flow cytometry analysis [8,9] indicates that the total number of bacteria (both active & inactive) remains almost constant; therefore, the DBGD device is not acting as an electrostatic precipitator and the concentration of bioaerosol particles remains undisturbed for the duration of each experiment. Flow cytometry results also showed that outer membranes of *E. coli* bacteria were not damaged with up to three passes through the DBGD plasma.

Numerical analysis was made to investigate the reasons of the high efficiency of DBGD treatment [9]. It was shown that no single well-studied component of plasma, namely UV radiation, OH radicals, and ozone, can be solely responsible for the initial 97% reduction in culturability. UV radiation intensity from the discharge in the UVC spectral region was measured to be approximately 30 $\mu W/cm^2$ (measurements were performed using International Light IL1700, SED220 photodiode). A steady state concentration of ozone of 28 ppm was measured in the PDRF system after 10 s of DBGD operation. The concentration of OH radicals in

the PDRF system was estimated to be on the level of 10^{14} cm^{-3}. Subsequent remote exposure of *E. coli* to residual ozone in the two minutes following direct plasma treatment also can not explain the additional 3.5-log reduction without the assumption that the bacteria experienced significant stress in plasma causing their resistively to ozone to be significantly reduced. Taking into account these results together with the results of comparing direct and indirect plasma treatment effects on bacteria [18], it is possible to make a conclusion that the direct influence of plasma charge particles on *E. coli* bacteria in combination with active chemical substances generated by plasma is the probable reason for high sterilization efficiency of DBGD.

3. Water Sterilization

Our approach to the plasma sterilization of water was to some extent similar to our approach to air sterilization. We again started with analysis of applicability of different discharge systems. Literature analysis (see [6]) and economical estimations showed that it was worth while to compare three types of discharges: gliding arc over the water surface, and two pulsed discharges in the water volume: so-called 'corona' and spark discharge. Significant preliminary work was done by the first senior design project team (SDT-1, [19]) involved in this activity. This team collected literature data and made first experiments using these thee types of discharges (Figs. 7–9). They modified the small gliding discharge system with rotation in magnetic field [14] so that the water stream covers the surface of the outer tubular electrode (Fig. 7).
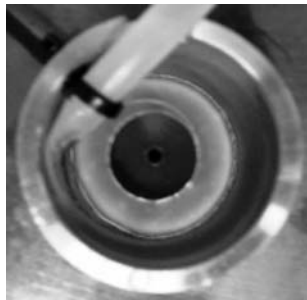
Figure 7. Plasma disc and water stream in the system for gliding discharge rotation in magnetic field

SDT-1 also developed a pulsed water discharge system using a pulsed power supply developed for the pulsed corona discharge (Fig. 3). If the distance between high voltage and grounded electrodes was large enough (in our case more than 5 cm), the discharge does not cover the whole gap between electrodes and a so-called 'corona' discharge (Fig. 8) forms in water. 'Corona' or 'streamer' discharge in water is a type of electro-hydraulic discharges [6] that is very much different from the discharges in gas phase with the same names.
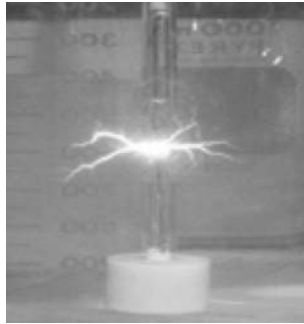
Figure 8. Electro-hydraulic corona discharge in water

If the distance between electrodes is short enough (in our case less than 2.4 cm), the discharge covers the whole gap and forms very bright spark (Fig. 9) creating a strong shock wave that can easily make a hole in a plastic jar.

Figure 9. Electro-hydraulic spark discharge in water

A preliminary study showed that spark discharge has much higher efficiency than gliding discharge over the water surface, or corona discharge in water. Later we also compared efficiency of the spark discharge with an intermediate corona-spark discharge (that was generated in our case when electrode gap was in the range of 2.4–5 cm), and found that the spark discharge is more efficient. Moreover, we found that the shorter distance, the higher sterilization efficiency of the spark discharge. Therefore the latest experiments were done with the shortest distance that we can keep more or less constant in conditions of strong shock waves – 5 mm. The results of these experiments are presented in Fig. 10.

The current version of the system for water treatment by spark discharge includes a container filled with water, a point-to-plane electrode system, a high voltage power supply that charges a capacitor bank, and an uncontrolled spark gap switch that connects the high voltage electrode and the capacitor bank. The high-voltage electrode (anode) is made from an insulated stainless steel wire (diameter of 0.175 mm) with an open tip. A grounded stainless steel container acts as the cathode. The experiments were conducted with a discharge having the following

parameters: peak-to-peak voltage 25 kV, peak-to-peak current 400 A, pulse duration 1.8 μs and energy per pulse 2 J.
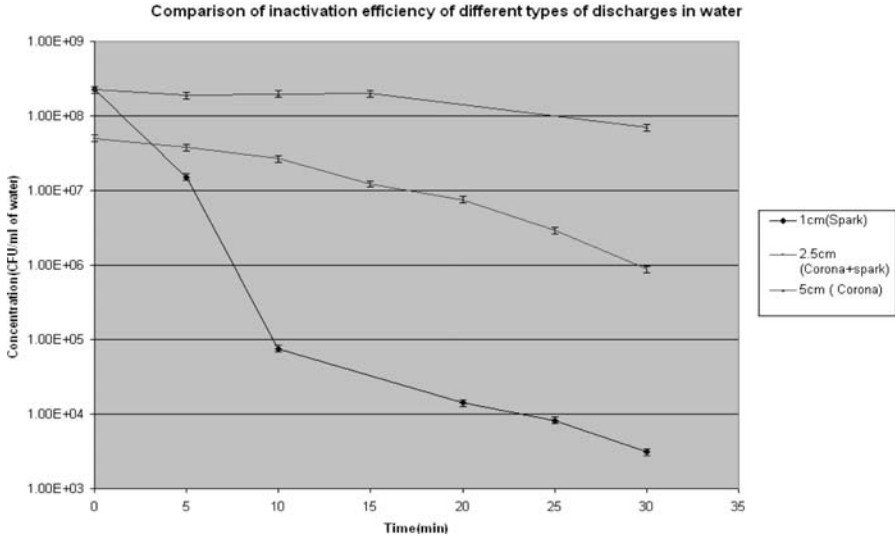
Figure 10. Comparison of the sterilization efficiency of different electro-hydraulic discharges

A non-pathogenic strain of *E. coli* bacterium, K12, was used in all sterilization experiments. Bacteria in the stationary phase was centrifuged, washed and diluted to different concentrations of 10^8, 10^7, 10^6, 10^5 and 10^4 CFU/ml using sterile water. Water contaminated with *E. coli* was then treated using a pulsed spark plasma discharge. Samples of treated water were taken after certain number of pulses or certain time interval (if the experiment was run for a relatively long time with constant frequency of pulses). The inactivation efficiency was assessed by using a plate counting method.

A study of the bacteria concentration influence on sterilization efficiency reveled very strong dependence (Fig. 11): it is much more difficult to inactivate bacteria in high concentrated opaque suspensions. The general trend shows that the D-value (the dosage required for a 90% reduction of the number of viable microorganisms) decreased with a decrease in initial bacterial concentration. For a relatively low initial concentration of 10^4 CFU/ml of water, a very low D-value of 125 J/L was obtained.

The different factors considered by many researchers to be responsible for the microbiocidal action of pulsed discharges in water include the production of active chemical species (ozone, hydrogen peroxide, hydroxyl and superoxide free radicals), nanoparticles [20] generated as a result of electrode deterioration, UV and VUV radiation, and shock waves [7]. The shock waves also help in mixing the treated water and in destruction of bacterial colonies thus facilitating the delivery of reactive agents to all parts of the treatment system. We did not yet make direct

measurements of these factors but, by comparing our results with the work done by other researchers [7], it is possible to conclude that the major sterilization factor in our case is UV radiation, which may be in synergy with active chemical substances generated by plasma.
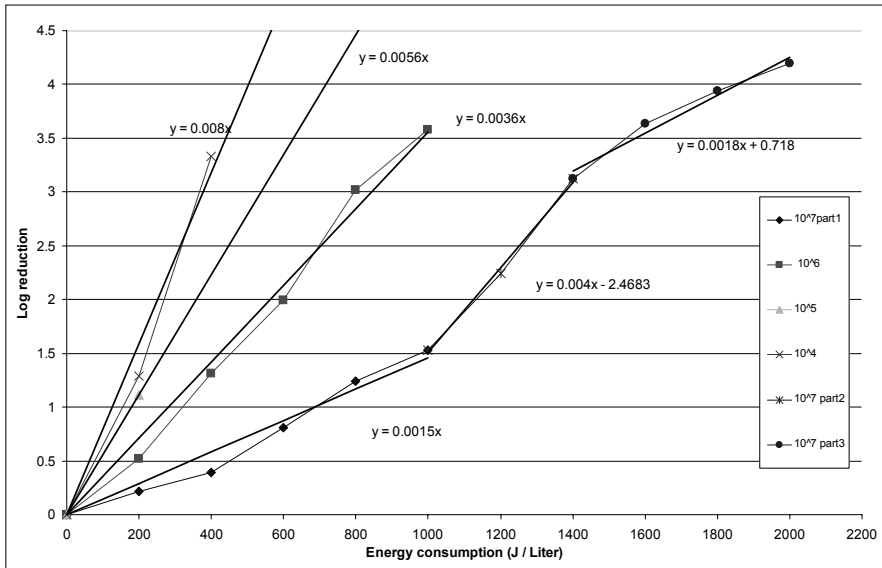
Figure 11. E. coli deactivation efficiency by spark discharge in water depending on power input and on initial concentration of bacteria

It is necessary to emphasize that the obtained D-value of 125 J/L at low bacterial concentration (which is nevertheless much higher than typical in natural water sources) make this approach very much attractive for commercialization. Our second senior design team (SDT-2 [21]) demonstrated that this technology can be used, for example, for additional sterilization of drinking water in office environment (Fig. 12). SDT-2 made a fully automated system that can be connected to a water line, and has the following operational logics controlled by a Programmable Logic Controller: (1) Inlet solenoid valve is open and tap water goes into the discharge chamber to the level controlled by a level sensor; (2) All solenoid valves are closed, a magnetic stirrer mixes water in the discharge chamber, a high voltage power supply with the help of a spark gap switch generates a series of pulses that cause spark discharges in the discharge chamber, the programmable logic controller counts the number of pulses and stops operation of the power supply when the energy input into the discharge chamber corresponds to the specified value (200 J/L, for example); (3) Solenoid valve in the bottom of the discharge system is open and water flows through an additional carbon filter (for absorbtion chemical components generated in plasma and particles formed due to the electrode deterioration) into the vessel for the treated water. This vessel is connected to the valve of the commercial chiller enclosure, so the treated water can be used by the office personnel; and (4) A

level sensor in the vessel for the treated water measures the water level, and if it is lower than conventional 'full' level the Programmable Logic Controller starts the whole procedure from the beginning. If the vessel for the treated water is full, everything is stopped.
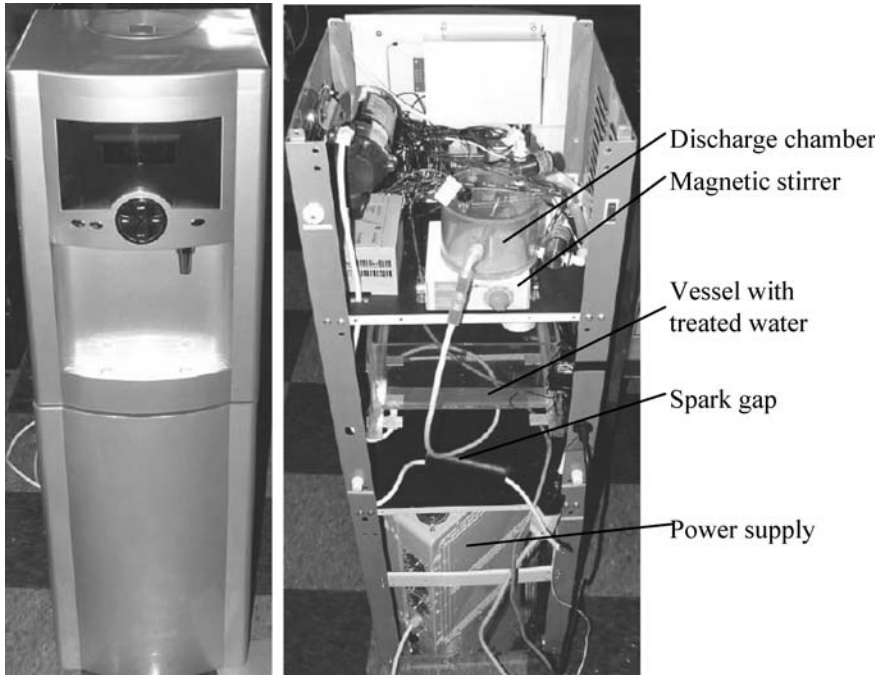
Figure 12. Prototype of the spark discharge based water sterilizer for office use in a water cooler enclosure, front and inside views

A specially developed power supply and sound insulation materials (e.g. Acoustiblok©) in combination with a smart design allowed for development of a compact and quite fully operational system. Indeed, this system is rather far from a real commercial prototype, which would require many additional experiments and approvals, but it demonstrates commercial potential of water spark technology.

4. Mechanism of Electric Breakdown Formation in Water

The successful application and development of any technology requires good understanding of the key physical effects that take place in a process. Plasma discharge in water that is used for water sterilization and other applications is under investigation by many research groups (see review [22]), but our analysis has shown that there is no satisfactory model to describe the initial phase of the discharge. It was shown [23] that the discharge channel formation starts in the first nanoseconds after application of the high voltage pulse. The thermal model of

channel formation [24] looks the most reasonable and it assumes extremely high initial concentration of electrons (in the order of 10^{18} cm^{-3}) in a micro-bubble on the surface of a high voltage electrode. Such a high electron density means very exotic conditions on the electrode surface that can ensure extremely high current density due to field emission. Physical intuition says that heating is not probably the best explanation of channel formation at the initial stage of a discharge, though it is very difficult to arrange an experiment that can characterize properties of a very small discharge in water in such a short time frame.

In our semi-numerical model, we assume the existence of micro-bubbles on the surface of the high voltage electrode. The size of these bubbles as well as pressure inside them can be influenced by the external pressure and preliminary water degassing. Indeed, such procedures change breakdown voltage and kinetics [25]. The application of high voltage results in plasma formation inside the micro-bubble (a sub-nanosecond process). The high mobility of electrons makes the whole bubble surface equipotential (Fig. 13a). Due to the strong electric field at the tip of the electrode, the opposite wall of the bubble is pushed to expand the bubble and form the major channel filament (Fig. 13b).

At the initial moment of high voltage application, the following forces act on the bubble surface: electrostatic expansion force opposes to combination of the hydrostatic pressure and the compressing surface tension force. It is possible to find the electrostatic pressure in the radial and axial direction:

$$E_r \sigma = \varepsilon_{water} \frac{\Phi_0^2}{r_0^2 [\ln(R/r_0)]^2}$$

$$E_z \sigma = -\varepsilon_{water} \frac{\Phi_0^2}{r_0^2}$$

where E_r and E_z are the electric field components in the radial and axial directions, respectively; σ is charge density on the surface of the filament; ε_{water} is the permittivity of water; Φ_0 is electrode potential; r_0 is the radius of the filament; and R is the radius where the electric field can be regarded as zero. Since $R \gg r_0$, it is obvious that the electrostatic pressure in the axial direction is much higher than that at the radial direction.
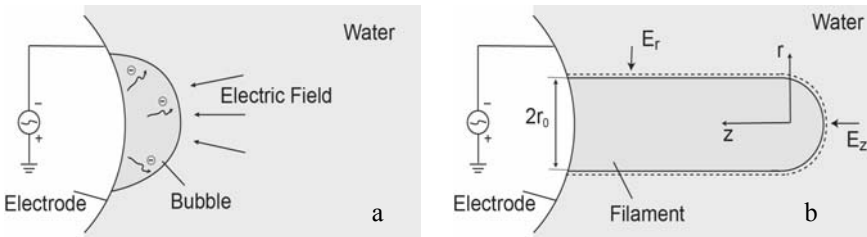
Figure 13. (a) – Initial bubble at the moment of high voltage application; (b) – bubble elongation and gaseous plasma filament formation due to interaction of electrical forces with surface tension and external pressure forces

Electrostatic expansion force is proportional to $(r)^{-2}$ while surface tension compression force is proportional to $(r)^{-1}$, therefore at some radius these two forces can balance each other. If we assume the force balance between electrostatic pressure, surface tension, and ambient pressure in the radial direction, it is clear that the filament will be pushed to grow in the axial direction because of the much larger amplitude of electrostatic pressure.

To determine the growth rate in the axial direction, it is assumed that the filament is a long, slender object with gradually reduced radius. Such a needle-like shape allows fast propagation in water, as the hydrodynamic pressure against growth is proportional to the tangent of angle of attack, which is small in this case. If to assume the force balance at the axial direction, the maximum growth rate of the filament can be described by the following equation:

$$v_0 = \frac{\Phi}{r_0}\sqrt{\frac{2\varepsilon_{water}}{\rho \tan \alpha}} \approx \frac{\Phi_0}{r_0}\sqrt{\frac{2\varepsilon_{water}L}{\rho r_0}}$$

where ρ is the density of water, and L is the length of the filament. At the initiation state of a typical breakdown of water, the radius of the filament is on the order of 1 μ and the length is about 1 mm. As shown in Fig. 14, the relation between growth rate and applied voltage can be calculated, which is in good agreement with experiment results [23] (about 3 km/s at 12 kV).
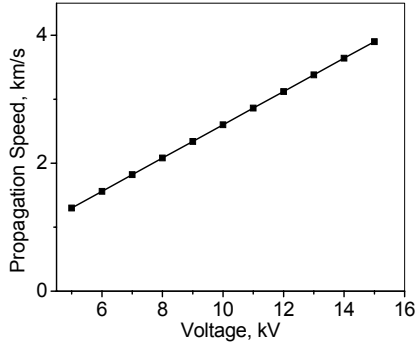
Figure 14. Calculated propagation speed of filament during breakdown of water

Below we briefly present the local linear stability analysis of axisymmetric perturbations to a plasma-filled filament that is based on the method used in [26]. As an initial assumption, a small wave-like disturbance occurs at the surface of cylindrical bubble with initial radius r_0, as shown in Fig. 15. The peak-to-peak amplitude and wave number of the disturbance is h and k, respectively and H is the depth of wave influence [27].
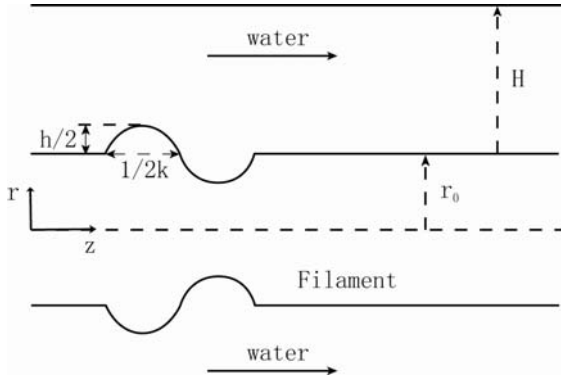
Figure 15. Schematic diagram of disturbance at the surface of filament

Using the classic instability analysis, the surface radius can be written as

$$r = r_0 + \frac{h}{2}\exp(ikz + iwt)$$

where w is the growth rate of the disturbance. When competition among electric pressure, surface tension and hydrodynamic pressure is considered, it is possible to show that

$$\rho w^2 = (\gamma - \frac{\varepsilon_{water}\Phi_0^2}{2r_0})(k^2 - \frac{1}{r_0^2})k$$

where γ is the surface tension coefficient of water. Since the difference between static pressure due to surface tension at the crest is less than that at the trough, it is possible to conclude that $1/k \ll r_0$, and the second factor in the equation above will always be positive. So when the voltage exceeds some critical value, which depends on the filament size, w^2 will be negative and the disturbance becomes unstable. Physically it means channel branching. When the radius goes to infinity, the equation reduces to $\rho w^2 = \gamma k^3$, which is the formula for a conventional capillary wave.

Conclusions

Our research and development efforts in the areas of plasma-based air and water sterilization show that dielectric barrier grating discharge is very promising for air flow disinfection and sterilization, and the technology based on spark discharge in water is very promising for water disinfection and sterilization. Energy consumption in the case of air sterilization (6-Log reduction in concentration of viable microorganisms) can be as low as 10–20 kJ/m^3 in the case of *E. coli* bacteria. Sterilization or even deactivation of air containing spores might require higher energy consumption or some technological modification. The D-value for

deactivation of *E. coli* in water can be on the order of 100 J/L for reasonable concentrations. Deactivation of other microorganisms may require different values of energy consumption.

A semi-numerical model was developed for explanation of the initial phase of electrical breakdown in water. This model is based on the assumptions about existence of micro-bubbles on an electrode surface, formation of plasma inside a bubble immediately after pulsed voltage application, then bubble elongation and branching because of the imbalance of electrical and surface tension forces in the points with high curvature. Numerical estimations made using this model are in good agreement with published experimental data. Linear analysis also shows that the instability of the Rayleigh-Taylor type develops in the plasma-gaseous channel surface points with high curvature.

Acknowledgment

References

[1]   United Nations. World Assessment Program 2005.

[2]   http://www.cimerc.org/

[3]   M. Laroussi, "Nonthermal decontamination of biological media by atmospheric-pressure plasmas: review, analysis, and prospects", IEEE Transactions on Plasma Science, Vol. 30(4), pp. 1409–1415, 2002.

[4]   M. Laroussi, "Low temperature plasma-based sterilization: Overview and state-of-art", Plasma Processes and Polymers, Vol. 2, pp. 391–400, 2005.

[5]   M. Sato, T. Ohgiyama, and J. S. Clements, "Formation of chemical species and their effects on microorganisms using a pulsed high voltage discharge in water", IEEE Transactions on Industry Applications, Vol. 32(1), pp. 106–112, 1996.

[6]   B. R. Locke, M. Sato, P. Sunka, M. R. Hoffmann, and J. S. Chang, "Electrohydraulic discharge and nonthermal plasma for water treatment", Industrial and Engineering Chemistry Research, Vol. 45, pp. 882–905, 2006.

[7]   A. M. Anpilov, E. M. Barkhudarov, N. Christofi, V. A. Kop'ev, I. A. Kossyi, M. I. Taktakishvili, and Y. Zadiraka, "Pulsed high voltage electric discharge disinfection of microbially contaminated liquids", Letters in Applied Microbiology, Vol. 35, pp. 90–94, 2002.

[8]   N. Vaze, M. Gallagher Jr., V. N. Vasilets, S. Anandan, A. Gutsol, and A. Fridman, "Air sterilization using non thermal plasma", 18th International Symposium on Plasma Chemistry, Kyoto, Japan, August 26–31, 2007: Abstracts and Full-Paper CD, p. 675 and paper 00320.pdf.

[9]   M. Gallagher, N. Vaze, S. Gangoli, V. N. Vasilets, A. Gutsol, T. N. Milovanova, S. Anandan, D. Murasko, and A. Fridman, "Rapid inactivation of airborne bacteria using atmospheric pressure Dielectric Barrier Grating Discharge", IEEE Transactions on Plasma Science, Vol. 35, pp. 1501–1510, 2007.

[10] M. Gallagher, G. Friedman, A. Gutsol, and A. Fridman, "Non-Thermal Plasma Application in Air Sterilization", 17th International Symposium on Plasma Chemistry, Toronto, Canada, August 7–12, 2005: Abstracts and Full-Paper CD, pp. 1056–1057 and 729.pdf.

[11] R. B. Gadri et al., "Sterilization and plasma processing of room temperature surfaces with one atmosphere uniform glow discharge plasma (OAUGDP)", Surface and Coatings Technology, Vol. 131(1), pp. 528–542, September 2000.

[12] K. Kelly-Wintenberg et al., "Air filter sterilization using a one atmosphere uniform glow discharge plasma (the volfilter)", IEEE Transactions on Plasma Science, Vol. 28(1), pp. 64–71, February 2000.

[13] R. Jaisinghani, "Bactericidal properties of electrically enhanced HEPA filtration and a bioburden case study", presented at the InterPhex Conf., New York, April 20–22, 1999.

[14] S. Gangoli, A. Gutsol, and A. Fridman, "Rotating Non-Equilibrium Gliding Arc Plasma Disc for Enhancement in Ignition and Combustion of Hydrocarbon Fuels", 17th International Symposium on Plasma Chemistry, Toronto, Canada, August 7–12, 2005: Abstracts and Full-Paper CD, pp. 1042–1043 and ISPC-ID778.pdf.

[15] M. G. Sobacchi, A. V. Saveliev, L. A. Kennedy, E. Lock, A. Fridman, A. Gutsol, A. Desai, G. Tak, K. Gutsol, S. Korobtsev, V. Shiryaevsky, D. Medvedev, and V. Abolentsev, "Pulsed Corona Plasma Technology for Treating VOC Emissions from Pulp Mills", 2004. TAPPI Paper Summit, Spring Technical and International Environmental Conference, May 3–5, 2004, Atlanta, GA, USA, Electronic Proceedings, PS04169.pdf.

[16] J. H. Perry, Chemical Engineers' Handbook, 2nd ed. New York: McGraw-Hill, 1941.

[17] A. Chirokov, A. Gutsol, and A. Fridman, "Atmospheric pressure plasma of dielectric barrier discharges", Pure and Applied Chemistry, Vol. 77(2), pp. 487–495, 2005.

[18] G. Fridman, A. D. Brooks, M. Balasubramanian, A. Fridman, A. Gutsol, V. N. Vasilets, H. Ayan, and G. Friedman, "Comparison of direct and indirect effects of non-thermal atmospheric pressure plasma on bacteria", Plasma Processes and Polymers, Vol. 4(4), pp. 370–375, 2007.

[19] Christopher A. Campbell, Frank Snyder, Vincent Szarko, Erik Yelk, and Jesse Zonolini, "Water Treatment Using Plasma technology", Final report of the Senior Design Project Team, Drexel University, Department of Mechanical Engineering and Mechanics, Philadelphia, 2006.

[20] V. A. Kolikov, V. E. Kurochkin, L. K. Panina, A. F. Rutberg, F. G. Rutberg, V. N. Snetov, and A. Yu. Stogov, "Prolonged microbial resistance of water treated by a pulsed electrical discharge", ISSN 1063–7842, Technical Physics, Vol. 52(2), pp. 263–270, 2007.

[21] Brian McNiff, Daniel Hanna, Kyle Malinowski, Michael Ryan, and Timothy Dietz, "Biological Decontamination of Water by Plasma Treatment", Final report of the Senior Design Project Team, Drexel University, Department of Mechanical Engineering and Mechanics, Philadelphia, 2007.

[22] Jen-Shih Chang, "Recent development of plasma pollution control technology: a critical review", Science and Technology of Advanced Materials, Vol. 2, pp. 571–576, 2001.

[23] W. An, K. Baumung, and H. Bluhm, "Investigation of Pulsed Corona Discharges in Water by Fast Imaging Diagnostics", presented at 32nd International Conference on Plasma Science Conference, Monterey, CA, June 20–23, 2005.

[24] P. K. Watson, "Electrostatic and hydrodynamic effect in the electric breakdown of liquid dielectrics", IEEE Transactions on Electrical Insulation, Vol. 20, pp. 395–399, 1980.

[25] S. M. Korobeynikov and Yu. N. Sinikh, "Bubbles and Breakdown of Liquid Dielectrics", 1998 IEEE International Symposium on Electrical Insulation, Arlington, Virginia, USA, June 7–10, 1998.

[26] Kern E. Kenyon, "Capillary waves understood by an elementary method", Journal of Oceanography, Vol. 54, p. 343, 1997.

[27] Kern E. Kenyon, "On the depth of wave influence", Journal of Physical Oceanography, Vol. 13, p. 1968, 1983.

PULSED SUBMERGED ARC PLASMA DISINFECTION
OF WATER: BACTERIOLOGICAL RESULTS
AND AN EXPLORATION OF POSSIBLE MECHANISMS

R. L. BOXMAN[1], N. PARKANSKY[1], H. MAMANE[2],
M. MEIROVITZ[1], Y. ORKABI[1], T. HALPERIN[4], D. COHEN[3],
N. ORR[3,4], E. GIDALEVICH[1], B. ALTERKOP[1],
AND S. CHESKIS[5]
[1]Tel Aviv University, Electrical Discharge and Plasma Lab
[2]Tel Aviv University, School of Mechanical Engineering
[3]Tel Aviv University, Faculty of Medicine [1]and Center for the Study of Bioterrorism
[4]Israel Defense Force, Center for Infectious Disease Research
[5]Tel Aviv University, School of Chemistry

Abstract: The pulsed submerged arc is a high-current electrical discharge between two electrodes in a liquid, in which the electrical current is conducted via a plasma bubble consisting of vaporized and partially ionized liquid and electrode material. The submerged arc discharge has the potential to kill harmful pathogens by a combination of several mechanisms. In this preliminary investigation, the ability of the pulsed arc to sterilize water was tested, hydroxyl radical (OH·) production and the radiation spectrum were measured, and shock wave production was estimated.

Vessels containing 50 ml of tap water were inoculated with 10^2–10^4/ml of *E. coli* TG-1 bacteria. A repetitively pulsed submerged discharge was then applied to the inoculated water. The discharge was sustained between pairs of either silver or graphite electrodes, which periodically contacted each other, and then separated, at a frequency of 100 Hz. With each separation, a 20 μs, 50 mJ arc discharge was ignited in the inoculated water sample. Samples were thus treated for times ranging from 5 s to 10 min. Samples of arc treated and control liquids were plated, incubated, and the bacterial colonies were counted. Colonization was observed only in the control samples, from which the bacterial concentrations reported above were determined. No colonies were observed in any of the discharge-treated samples, i.e. even at the minimum 5 s treatment time tested in these experiments, and thus the survival rate after even the shortest arc treatment tested was $<5 \times 10^{-4}$.

The radiation spectrum showed broadened strong H line radiation at 656 nm and broad bands of emission throughout the visible and extending into the ultra-violet region. OH·radical production was measured by a modified Nash technique,

and found to be 5×10^{-10} moles per pulse. Theoretical models indicate that the plasma and adjacent water experience a short duration pressure pulse reaching a peak of 10^{11} Pa. It is likely that some combination of radiation, radical induced chemical damage, and sonification is responsible for the observed bacterial inactivation.

1. Introduction

Plasma disinfection of water has been investigated as an alternative to conventional chlorination, and other advanced disinfection treatments such as ozonation and ultra-violet (UV) irradiation. A wide variety of plasma techniques have been considered. These techniques vary in how the plasma is generated (i.e. type of electrical discharge), and how the plasma is applied to the water. The types of discharges include the corona, glow, barrier, and arc, and they differ one from the other largely in the electron generation mechanism at the cathode. The plasma may be located far from the water, and reaction products convected to the water surface, in the air adjacent to the water surface, and submerged within the water. The submerged discharge, sometimes referred to as an electrohydraulic discharge, has the potential advantage that all of the radiation and active species produced by the plasma will be applied within the water, i.e. without convection or geometrical losses.

The electrohydraulic discharges include high voltage submerged coronas and high current submerged arcs. In the latter, high current passes through a plasma bubble comprised of ionized water vapor. This discharge has the potential to kill or inactivate harmful pathogens by a combination of several physical processes: (1) vaporization of pathogens directly within the discharge, (2) heating of the fluid adjacent to the plasma bubble, (4) bombardment by energetic particles, (4) sonification by shock waves produced by the discharge in the water, (5) radiation, particularly in the UV, (6) damage from chemical species (e.g. radicals) produced by the discharge and introduced into the water, and (7) interaction with nano-particles produced by the discharge. Possibly several of the above mechanisms work together synergistically [1]. Shockwave intensity is related to the discharge energy, and is also a function of the discharge circuit, pulse duration, water conductivity, electrode size, gap, distance and reactor configuration [2,3,4,5]. Submerged corona discharges can oxidatively degrade organic substances mainly through ultraviolet photolysis, but additional effects of electrohydraulic cavitation and supercritical water oxidation have been observed [2]. Gilliland and Spec [6,7] found that high voltage discharge treatment was effective in inactivating at least

99% of the vegetative cells of *E. coli*, *Enterococcus faecalis, Micrococcus radio-durans, Bacillus subtilis,* and its spores. Holland et al. used an electrohydraulic discharge with a total energy release of 0.12 kJ/L per pulse and reported that a lethal UV radiation flux of 10^4 μW-s/cm^2 was required to cause a 1-log (90%) reduction of micro-organisms [8]. Pulsed corona discharges in liquids have been shown to reduce low concentrations of chemical substances (e.g. Phenol) in water [9,10] and are now being used to decontaminate water from biological organisms. Abou-Ghazala et al. developed a wire-to-plate electrode pulsed corona discharge that produced a 1-log reduction of *E. coli* with a discharge energy density of 3 kJ/L [11]. Similarly, experiments with *B. subtilis* in the vegetative state yielded an energy efficiency of 10 kJ/L to reduce viable concentrations by 90% and there was no inactivation effect on *B. subtilis* in spore form. Recently B. R. Locke et al. [12] and J.-S. Chang et al. [13] published extensive reviews of submerged discharge water treatment techniques.

     All of the previous investigations of submerged discharge disinfection used high voltage to initiate the discharge, and the arcs generally used very high currents, e.g. kA's. The effectiveness and mechanisms of low voltage, low energy pulses in disinfecting water have not heretofore been investigated. The objective of this research was to preliminarily asses the effectiveness and mechanisms of low voltage, low energy submerged pulsed arcs for disinfecting water. Low voltage techniques are easier and less expensive to implement than high voltage pulses, and thus have the potential for encouraging industrial implementation. In this paper some preliminary bacteriological experiments, as well as preliminary measurements of photon and OH· production, will be reported.

2.   Water Disinfection – Bacteriological Experiment

Experiments [14] were conducted on tap water inoculated with 2.2 x 10^2 and 2.2 x 10^4 bacteria per ml of *E. coli TG1* bacteria. A repetitively pulsed submerged arc discharge was applied to the inoculated water. The discharge was sustained between graphite electrodes, submerged in a 50 ml inoculated water sample, which periodically contacted each other, and then separated, at a frequency of 100 Hz. With each contact, a 15 μF capacitor charged to 80 V was discharged. A 20 μs arc discharge was ignited in the inoculated water sample when the electrodes were separated. Of the 48 mJ stored in the capacitor, an energy of E = ∫V(t)I(t)dt≈36 mJ was dissipated in the discharge, where V and I are the discharge voltage and current respectively. Samples were thus treated for times of 60, 30, 10, and 5 s. Samples of 100 μl from the discharge-treated and control liquids were then plated onto Trypticase soy agar plates, and incubated at 37 C overnight. The bacterial colonies were then counted.

Colonization was observed only in the control samples, from which the bacterial concentrations reported above were determined. *No colonies were observed in any of the discharge-treated samples.*

Thus, within experimental sensitivity ($<\sim 5 \times 10^{-4}$ survival rate), *even the shortest treatment time was totally effective in disabling the target bacteria.* In this case, the total discharge time (= total treatment $\times$ pulse duration $\times$ repetition frequency) was 0.01 s. This result indicates that the submerged discharge is effective in disabling bacteria, and that possibly weaker discharge parameters (less energy per pulse, shorter treatment time) may also be sufficiently effective. The energy expenditure in this case was 0.5 J/ml, which would heat the water a mere 0.2 C, suggesting that the killing mechanism is not thermal. Given that the minimum treatment time proved to be totally effective, it is clearly desirable to conduct further tests, with less energetic pulses and less treatment time, to determine threshold effective values.

A mathematical model was postulated to describe the bacterial killing process, based on a model assumption that during each pulse, a bacterium may be randomly located within a spherical region having volume V_k surrounding the discharge in which there is unity inactivation probability and that outside this region the inactivation probability is negligible. Thus if the total number of bacteria N_0, comprising N_L live and N_D dead bacteria is constant, then

$$N_0 = N_L(t) + N_D(t) = N_L(0)$$

$$\frac{dN_L}{dt} = -\frac{dN_D}{dt} = -f\frac{N_L V_k}{V_t}$$

$$\ln(N_L(t)/N_0) = -\frac{fV_k}{V_t}t$$

where t is time, f is the pulse frequency and V_t is the total volume processed. Given that $N_L(5\text{ s})/N_0 < 5 \times 10^{-4}$, the kill radius may be estimated as $R_k > 5.7$ mm.

3. Radiation Spectrum

The radiation spectra from single arc pulses were measured qualitatively using a USB2000 (Ocean Optics Inc.) spectrophotometer. The optics were constructed with glass components, which had limited UV transmission. The spectra, shown in Figure 1, have an intense broadened line centered at the 656.28 nm H line, and broad bands extending to the optical transmission limit of the optics around 300 nm. Possibly more intense and shorter wavelength UV radiation is attenuated by the optics.
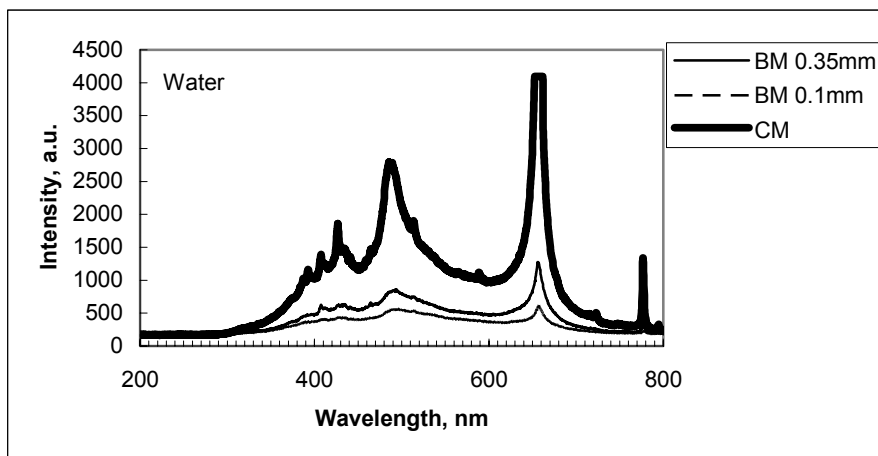
Figure 1. Emission spectra from submerged arc discharges. CM – contact mode, with arc parameters used in the bacteriological study. BM – break-down mode, where the arc was initiated by high-voltage breakdown, with a gap between the electrodes as indicated

4. OH· Radical Production Rate Measurement

Hydroxyl radicals were indirectly determined by the modified Nash method [15,16]. A repetitively pulsed submerged arc discharge was applied to water containing methanol (CH_3OH) buffered at pH 7. The methanol molecules act as scavengers of OH radicals, quickly reacting through a series of chemical reactions, to form formaldehyde (CH_2O). After arcing, a reagent consisting of a neutral solution of acetylacetone and ammonium salt (heated to 50°C for 10 min) was added to the treated water. The formaldehyde molecules react with the reagent to form 3,5-Diacetyl-1,4-dihydrolutidin (DDL). The DDL concentration was then determined by measuring optical absorption in the water solution at 412 nm. The reaction chain is summarized below:

$$CH_3OH + OH\bullet \rightarrow CH_2OH\bullet + H_2O$$
$$CH_2OH\bullet + O_2 \rightarrow O_2CH_2OH$$
$$O_2CH_2OH \rightarrow O_2^- + H^+ + CH_2O$$
$$CH_2O + reagent \rightarrow DDL$$
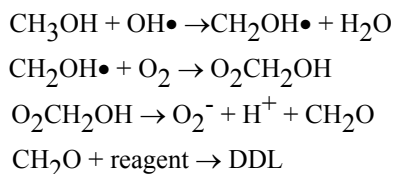
Pulsed submerged electrical arcs with capacitor charge energies of 7, 23, and 48 mJ were applied between graphite electrodes submerged in the water solution at a pulse repetition rate of f = 100 Hz for times of 3–30 s. The DDL
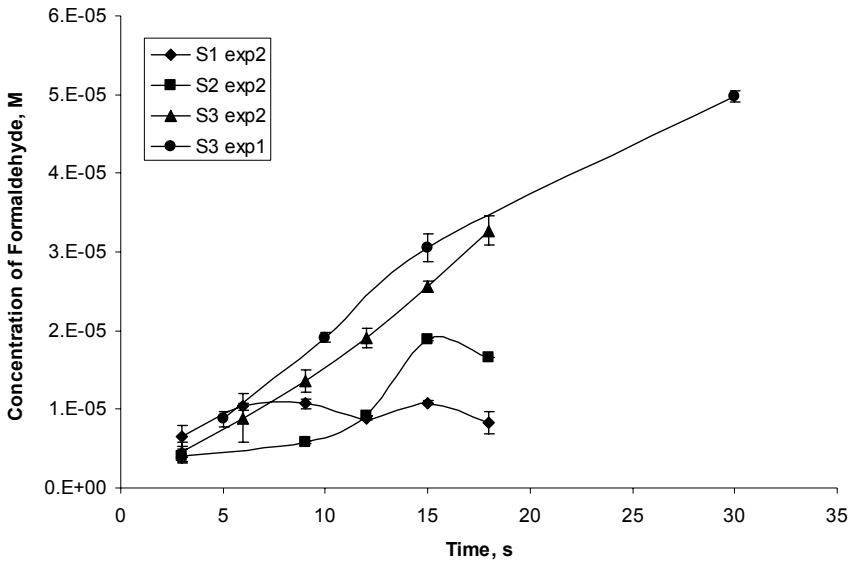
Figure 2. Derived concentration of Formaldehyde as a function of pulsed submerged arc treatment time. S1, S2, and S3 refer to different arc conditions, specifically 7, 23, and 48 mJ capacitor charge energy, respectively
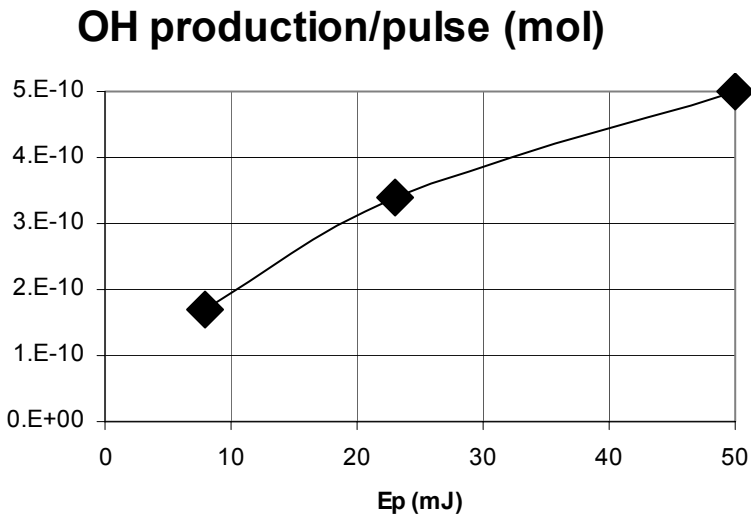
Figure 3. OH radical production per pulse

concentration, and hence the equivalent formaldehyde concentration, as a function of treatment time for various discharge energies is shown in Figure 2. It may be seen that the concentration generally increased with time, and in the case of the S3 conditions (48 mJ capacitor energy) the increase is approximately linear. Given that one molecule of DDL or formaldehyde represents the production of one OH·

radical, the radical production per pulse may be calculated as $\dfrac{\Delta C}{\Delta t}\dfrac{V_t}{f}$, where

ΔC is the increase in concentration. The radical production per pulse is shown in Figure 3. It may be seen that the production per pulse increased with pulse energy, reaching a value of 5×10^{-10} moles per pulse under the conditions used in the bacteriological experiment.

5. Pressure Wave Estimation

Various plasma parameters, including the plasma pressure, were estimated using a model presented by Gidalevich [17,18]. The model assumes that after the discharge is initiated, the plasma is a uniform column of radius R. R, and the various plasma parameters, vary with time. The plasma/water boundary was modeled as an arbitrary discontinuity. Initial conditions were chosen by trial and error, such that the calculated voltage and current are reasonable approximations of experimentally measured values.

It was found that depending on the choice of parameters, the plasma expands in time. Because of the inertia of the water, the expansion velocity is always less than the speed of sound in the plasma. This facilitates homogenizing the temperature in the plasma column, as demanded by the model assumption. However the plasma expansion velocity may either be sub-sonic or trans-sonic with respect to the speed of sound in water. If the plasma expansion velocity is faster than the speed of sound in the water, a shock wave is formed, and a region of compressed, high pressure water is formed around the plasma column. A schematic graph of the density, and a shock wave in water, is shown in Figure 4. Graphs of various plasma parameters as a function of time, including the velocity of plasma expansion are presented in Figure 5, for the case of an 8 A arc, which corresponds to an initial radius of $\sim 10^{-5}$ m and an initial temperature of $\sim 10^4$ K. It may be seen that an exceedingly high pressure ($\sim 10^{11}$ Pa) and temperature ($\sim 10^6$ K) pulse is generated in the plasma, for a short time (~ 5 ns).
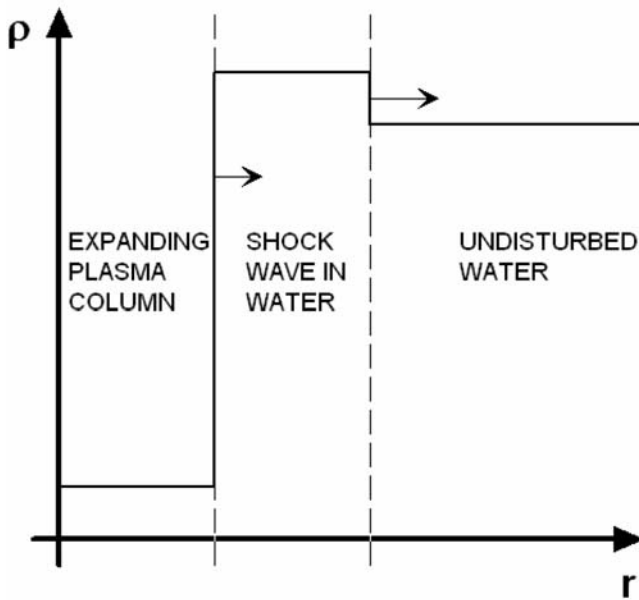
Figure 4. Schematic diagram of plasma column expansion and shock wave in water, showing the density ρ as a function of r
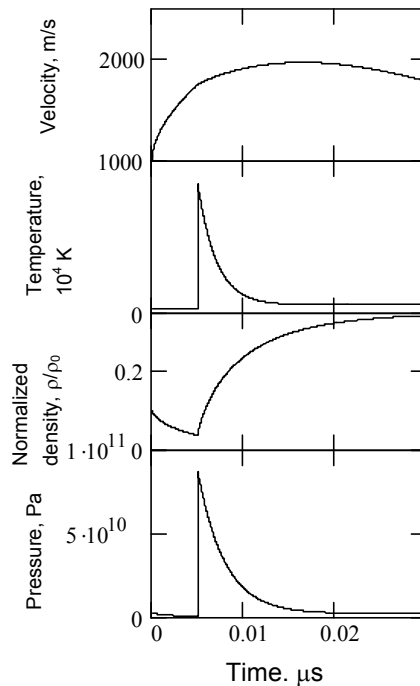
Figure 5. Variation with time of the plasma front velocity, plasma temperature, plasma density (normalized to the water density) and plasma pressure

6. Discussion and Conclusions

The bacteriological experiments show that the low voltage pulsed submerged arc is effective in inactivating at least *E. coli* bacteria. The use of a low voltage technique facilitates industrialization, in particular for low volume and portable applications. The spectral radiation and OH· experiments and the pressure wave estimation show that bactericidal agents, UV, OH·, and high pressure waves, are produced by this discharge. However further work is required to determine the range of pathogens which can be inactivated by this discharge, and the optimal parameters and required dosages for each. Furthermore, additional research is required to determine quantitatively which bactericidal agent, or combination of agents, is responsible for the inactivation in each case.

References

[1]   M. Moisan, J. Barbeau, M-C. Crevier, J. Pelletier, N. Philip, and B. Saoudi "Plasma sterilization. Methods and mechanisms". Pure Appl. Chem. 74:349–358 (2002).

[2]   P. Sunka, V. Babicky, M. Clupek, P. Lukes, M. Simek, J. Schmidt, and M. Cernak, "Generation of chemically active species by electrical discharges in water". Plasma Sources Sci. Technol. 8:258–265 (1999).

[3]   H.Y. Lee, H.S. Uhm, and H.N. Choi, "Underwater discharge and cell destruction by shockwaves," J. Korean Phys. Soc. 42:S880–S884 Suppl. S (Feb 2003).

[4]   M. Sato, T. Ohgiyama, and J.S. Clements, "Formation of chemical species and their effects on microorganisms using a pulsed high-voltage discharge in water". IEEE Trans. Ind. Appl. 32 (1):106–112 (Jan–Feb 1996).

[5]   A.M. Anpilov, E.M. Barkhudarov, and Y.B. Bark, "Electric discharge in water as a source of UV radiation, ozone and hydrogen peroxide". J. Phys. D-Appl. Phys., 34 (6):993–999 (Mar 2001).

[6]   S.E. Gilliland and M.L. Speck, "Inactivation of microorganisms by electrohydraulic shock". Appl. Microbiol. 15(5):1031–1037 (1967).

[7]   S.E. Gilliland and M.L. Speck, "Mechanism of the bactericidal action produced by electrohydraulic shock". Appl. Microbiol. 15(5):1038–1044 (1967).

[8]   R.V. Holland, P.W. Board, and K.C. Richardson, "Sterilization by electrohydraulic discharges". Biotechnol. Bioeng". XIV:459–472 (1972).

[9]   A.A. Joshi, B.R. Locke, P. Arce, and W.C. Finney, "Formation of hydroxyl radicals, hydrogen peroxide and aqueous electrons by pulsed streamer corona discharge in aqueous solution". J. Hazard. Mater. 41:3–30 (1995).

[10] B. Sun, M. Sato, and J.S. Clements, "Use of pulsed high-voltage discharge for removal of compounds in aqueous solution". J. Appl. Phys. 32:1908–1915 (1999).

[11] A. Abou-Ghazala, S. Katsuki, K.H. Schoenbach, F.C. Dobbs, and K.R. Moreira, "Bacterial decontamination of water by means of pulsed-corona discharges". IEEE Trans. Plasma Sci. 30:4 (2002).

[12] B.R. Locke, M. Sato, P. Sunka, M.R. Hoffmann, and J.-S. Chang, "Electrohydraulic discharge and nonthermal plasma for water treatment". Ind. Eng. Chem. Res. 45:882–905 (2006).

[13] J.-S. Chang, S. Dickson, Y. Guo, K. Urashima, and M.B. Emelko, "Electrohydraulic discharge direct plasma water treatment processes", in *Advanced Plasma Technology*, Wiley-VCD, ed. R. D'Agostino and P. Favia, 2008.

[14] N. Parkansky, Y. Orkabi, T. Halperin, D. Cohen, N. and Orr, R. Boxman, "Submerged arc plasma disinfection of water". The First Mid-East Conference on Ultraviolet Technologies, Tel Aviv, Israel (Nov 20–22, 2005).

[15] G.V. Buxton, C.L. Greenstock, W.P. Helman, and A.B. Ross, "Critical review of rate constants for reactions of hydrated electrons, hydrogen atoms and hydroxyl radicals (OH/O-) in aqueous solution". JPCRD 17(2):513–886 (1988).

[16] T. Nash "The colorimetric estimation of formaldehyde by means of the Hantzsch Reaction". Biochem. J., 55:416–421 (1953).

[17] E. Gidalevich, R.L. Boxman, and S. Goldsmith, "Hydrodynamical effects on liquids subjected to pulsed low cyrrent arc discharges". J. Phys. D: Appl. Phys. 37:1509–1514 (2004).

[18] E. Gidalevich and R.L. Boxman, "Sub- and supersonic expansion of an arc channel in liquid". J. Phys. D: Appl. Phys. 39:652–659 (2006).

ANTIMICROBIAL TREATMENT OF HEAT SENSITIVE PRODUCTS BY ATMOSPHERIC PRESSURE PLASMA SOURCES

R. BRANDENBURG, U. KROHMANN, M. STIEBER,
K. -D. WELTMANN, T. V. WOEDTKE, AND J. EHLBECK
INP Greifswald (Leibniz-Institute for Plasma Science and Technology), Germany; email: brandenburg@inp-greifswald.de

Abstract: The technological potential of non-thermal plasmas for the antimicrobial treatment of heat sensitive materials is well known. Despite a multitude of scientific activities with considerable progress within the last years the realization of industrial plasma-based decontamination or sterilization technology remains a great challenge. The aim of the work presented in this contribution is to demonstrate the applicability of plasma-based processes for the antimicrobial treatment on selected, heat sensitive products. The idea is to use modular and selective plasma sources. These plasma sources are driven at atmospheric pressure due to its technological advantages (avoidance of vacuum devices and batch processing). According to the specific requirements given by the product different plasma sources, namely rf-driven plasma jets, microwave-driven air plasmas are used.

Keywords: Plasma jet, microwave plasma, sterilization, decontamination, non-thermal plasma

1. Introduction

Within in the last two decades a growing attention on the application of plasmas in life science and environmental issues has been obtained. Decontamination of sensitive goods is one of the fields [1–4]. Decontamination includes antimicrobial treatment which is defined as "killing or inactivation of micro organisms (MO) with the purpose to reduce infections". Thus antimicrobial treatment is a collective term for "disinfection", "sterilization" and "aseptic" as well as "antiseptic". All these terms have different definitions, all basically referred to the inactivation of MO. But indeed the inactivation of pyrogens, fungi, viruses and prions is of relevance, too. Although there are some commercial plasma-assisted or plasmas-based sterilization systems available (e.g. TipCharger by CerionX; Sterrad by ASP [5,6]), the realisation of industrial plasma-based decontamination or sterilization technologies remains a great challenge up to now. One of the reasons for this

situation is the fact that an antimicrobial treatment process needs to consider all properties of the product to be treated as well as the requirements of the complete procedure, e.g. the reprocessing of a medical instrument. Furthermore studying and comparing the literature one notice that the antimicrobial effect is very specific in many respects. The efficiency is affected by:

- Plasma parameters and components
- Specific lethality of test MO on each single component of plasma
- Preparation of the samples (e.g. sample, humidity, placement of MO)
- Specifications of micro-biological test procedures etc.

The aim of the activities described in this contribution is to demonstrate the applicability of direct plasma processes for the antimicrobial treatment on certain selected, heat sensitive products. The idea is to use modular and selective plasma sources, which are driven at atmospheric pressure due to its technological advantages compared to low-pressure processes, e.g. the avoidance of vacuum devices and batch processing. According to the specific requirements different plasma sources are used:

- RF-driven plasma jets in argon for the outer surface treatment of catheters for intracardial electrophysiological studies
- Microwave-driven self-propagating air plasma for the inner treatment of hollow packaging for pharmaceutical products, namely PET-bottles

With both plasma sources different micro-biological tests are performed. An important point of the activities described is to test the plasma treatment on real products under practically relevant conditions. It shall be demonstrated that the level of practicability can be reached. Furthermore problems and additional basic questions which must be answered on the way to an industrial sterilization or decontamination process shall be carried out.

2. RF-plasma Jets for Treatment of Medical Products

The particular products chosen in this work for demonstrating the applicability of direct plasma treatment for decontamination on medical products are catheters for minimal invasive intracardial electrophysiological studies. Such a catheter is a partly isolated wire electrode (about 1 m long) connected with a hand piece. Only the wire electrode is inserted into heart ventricles via the blood vessels. These catheters do not contain any inner cavities. Thus only the outer surface of the instrument may be contaminated and consequently has to be treated. The RF-driven plasma jet in argon (see Fig. 1), has already been described detailed elsewhere [7,8]. This plasma jets have a compact design and can be miniaturized down to a diameter of about 0.5 mm. Thus the plasma jets are predestined for a modularisation and can be adapted to nearly any complex 3-dimensional structure, such as given by the catheters. The plasma jet is non-thermal and thus the heating

of the treated surface is moderate. Additional, a single jet is able to penetrate even in narrow gaps, which can exist on the instruments.
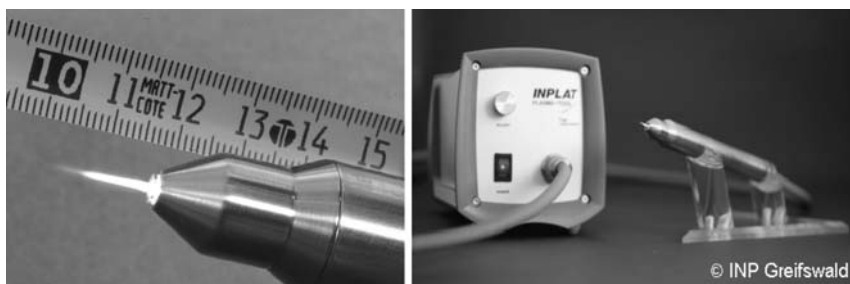
Figure 1. RF-driven plasma jet in miniaturized version (left) and as a handheld device (right)

2.1. STUDY OF THE ANTIMICROBIAL EFFICIENCY BY SINGLE PLASMA JETS

To investigate the effect of single plasma jets on micro organism, test strips made of plastic are inoculated punctually and treated by the plasma. A special plasma jet (so-called APPJ-1; Atmospheric Pressure Plasma Jet) is used for the antimicrobial treatment of punctually contaminated strips in order to treat the whole contaminated area. In this case moving the plasma source is not necessary and thus the treatment time is well defined. Therefore jet consists of a nozzle having an inner diameter of about 7 mm at the outlet and a centered needle electrode (see Fig. 2). The nozzle is made of ceramics. The argon gas (purity 5.0) flows through the nozzle and the RF-voltage (f = 27.12 MHz) is coupled to the needle electrode via a matching network.
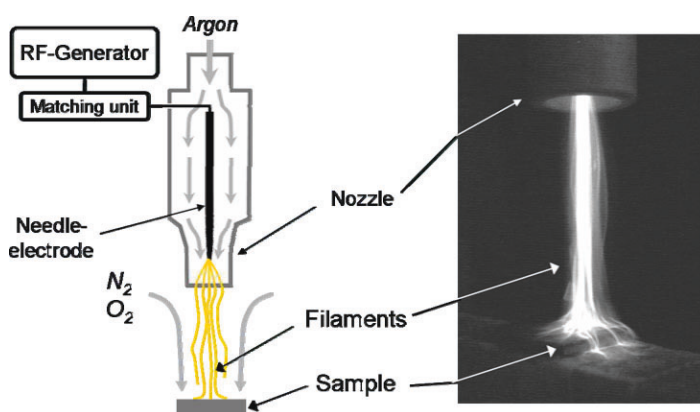
Figure 2. Plasma jet (APPJ-1) for antimicrobial treatment of punctually inoculated test trips (left – sketch of the plasma jet device; right – short exposure time photos showing the filamentary nature of the plasma)

Filamentary plasma consisting of many individual discharge channels is generated by the plasma jet device. These channels start from the tip of the needle electrode inside the nozzle and expand into the surrounding air outside (see short exposure time photo in Fig. 2), since the substrate serves as a kind of grounded electrode due to the effect of stray capacitances. In this configuration the plasma jet has a length of about 25 mm measured from the nozzle outlet and a diameter of about 8 mm on the substrate for the conditions being considered (power 20 W, gas flow 20 slm, distance from the nozzle outlet about 20 mm). Along the pathway to the sample a gradual mixing of the expanding argon gas with the surrounding air and thus the production of reactive oxygen species (O, OH, O_2^*) as well as plasma-chemical products (NO, O_3) takes place [9].

The test strips (usually made of PE; size 8 x 32 mm) are inoculated punctually (so-called spot contamination; diameter of the area: 4–5 mm) with 25 μL of a use-dilution suspension of vegetative bacteria (Escherichia coli) or endospores (Bacillus atrophaeus), respectively, and dried under aseptic conditions (laminar flow) for at least 1 h. The mean contamination rate is $2 \ 10^6$ cfu/strip for Bac. atrophaeus spore strips and $6 \ 10^5$ cfu/strip for E. coli strips.[1] Thus the initial density of MO is about $1 \ 10^7$ MO cm^{-2} for Bac. atrophaeus spore strips and $3 \ 10^6$ MO cm^{-2} for E. coli strips. This values are at least one order of magnitude higher than usually studied in antimicrobial plasma treatment experiments [4]. TEM-photos of the contaminated area show that the MO are arranged in several layers on the sample (see Fig. 3).
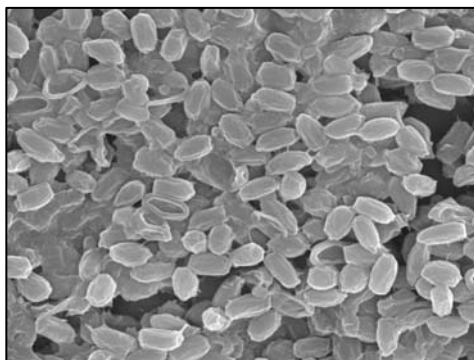
Figure 3. TEM-photo of Bacillus atrophaeus spores on PE test strips (before treatment). A spore of Bac. atroph. is about 1 μm long

To study the effect of the dose of the plasma the treatment time is varied. The recovery of MO after plasma treatment is investigated by an established procedure [10,11]. Briefly, plasma treated test strips are transferred into sterilized test tubes containing 10 mL sterile sodium chloride solution 0.9% with 0.1% Tween 80 as well as 10 sterile glass spheres, each, and agitated for 20 min on a shaking machine. Based on a dilution series using 100 μL of the resulting MO suspension,

---

[1] cfu – colony forming units; n – number of objects

the number of colony forming units per test strip (cfu/strip) is estimated by the surface-spread plate count method (performed on CASO agar or Mac Conkey agar) according to the European Pharmacopoeia 5.0 [12]. Although it is not common to give detection limits of the MO recovery after plasma treatment in literature, it is necessary in our opinion. For the method mentioned above the detection limit is 10^2 cfu/strip. The results for the treatment with APPJ-1 (argon gas flow 20 slm; power 20 W; voltage applied to the needle electrode 1 kV$_{pp}$; distance between sample and nozzle outlet 20 mm) are shown in the Figs. 4 and 5.
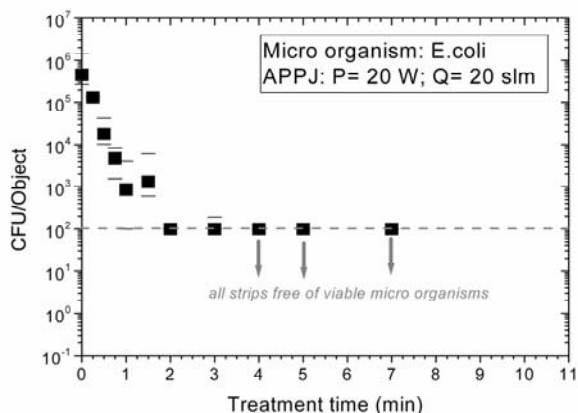
Figure 4. Median number (n = 6) of surviving MO after APPJ-1 treatment of E. coli (error bars: spread between minimum and maximum values, dashed line: detection limit) [9]

Plasma jet treatment of B. atrophaeus spores and E. coli on PE-strips results in an increasing time-dependent reduction. Because of the detection limit of MO recovery, this is the maximum reduction that can be proven experimentally if no surviving MO are detected after treatment. However, even if test strips without viable spores are found after a certain time of treatment, surviving MO can still be detected on some strips. That means that within the treatment time tested here, a maximum lethal effect of plasma treatment (i.e. all strips are free of viable spores) is not reached. For vegetative bacteria E. coli after plasma jet treatment of 240 s all test strips are free of viable counts.

It was shown in a previous work that the lethal effect of the plasma is based on a direct interaction of the plasma with the MO [9]. The separated effects of the plasma components (UV-radiation and moderate heating) are not able to explain the antimicrobial effect. Thus, a coaction of excited reactive species (OH and O radicals) generated in the plasma, partially assisted by (V)UV radiation (NO$_\gamma$-emission, Ar$_2$*-excimer emission [13]), ions, heat and low-molecular chemical products (NO, O$_3$) can be assumed.
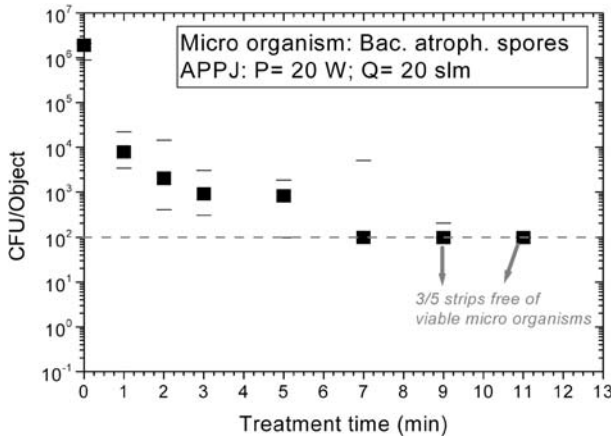
Figure 5. Median number (n = 6) of surviving MO after APPJ-1 treatment of B. atrophaeus spores (error bars: spread between minimum and maximum values, dashed line: detection limit 100 cfu/strip) [9]

The impedance matching of APPJ-1 has been found to be sensitive on stray capacitances through the surrounding. Thus by moving the jet along a catheter or another complex work piece it will be unstable. To overcome this problem an additional grounded ring electrode is placed at the nozzle outlet (so-called APPJ-2; see Fig. 6). Even in this configuration the plasma is filamentary. Inside the nozzle discharge channels propagates to the wall. However discharge channels outside the nozzle are observed too, since the surrounding and the sample acts like a third electrode due to stray capacitances. Furthermore the plasma is significantly shortened (about 8 mm without sample). Thus less reactive oxygen species and plasma-chemical products will be formed due to the reduced mixing of the expanding argon gas with the surrounding air.
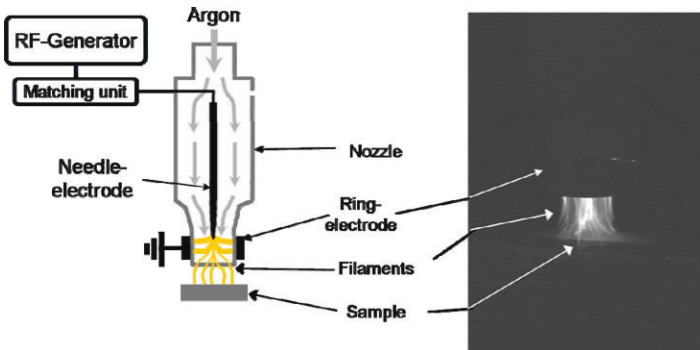
Figure 6. APPJ-2 – Argon plasma jet with additional grounded ring-electrode

The procedure for MO recovery tests is somewhat modified for longer treatment times, i.e. when a low residual contamination can be expected and thus the sensitivity of the method needs to be improved. Therefore the resulting MO suspension is filtered through a membrane which is incubated on an agar plate for at least 24 h. The detection limit of this method is 1 cfu/object. Additionally Staphylococcus aureus vegetative MO are used. These bacteria have a higher practical relevance than E. coli. Some results of antimicrobial treatment by the APPJ-2 are shown in Fig. 7.

A similar effect of the direct plasma treatment by APPJ-2 than by APPJ-1 is observed. Both vegetative bacteria (E. coli and Staph. aur.) show a comparable lethality on the plasma treatment. However APPJ-2 seems to be less effective than APP-1. For example for E. coli after 4 min of treatment with APPJ-1 the detection limit of 100 cfu/object is reached (compare Fig. 4). Using APPJ-2 this value is reached after 7 min. This difference can be understood by taking into account the reduced production of reactive oxygen species and chemical compounds as well as the lower energy input on the contaminated area by using APPJ-2. Furthermore the initial contamination can hardly be controlled in our procedure and thus, it is slightly different for both experiments. This may have an influence on the reduction of MO, too.
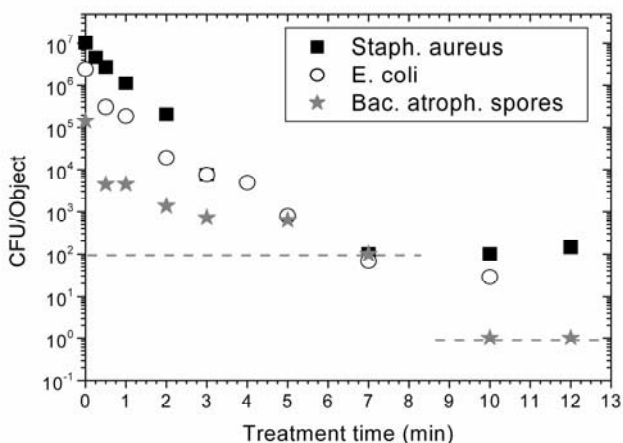
Figure 7. Median number (n = 5) of surviving MO after APPJ-2 treatment (dashed lines: corresponding detection limits)

2.2. TREATMENT OF CATHETERS BY PLASMA JET MODULES

To treat complete catheters with plasma the catheter is fixed in horizontal direction and a plasma module is moved along the catheter (see Figs. 8 and 9).
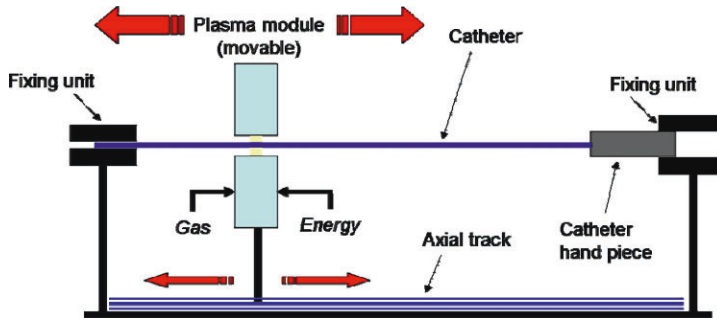
Figure 8. Principle of plasma treatment of catheters by means of plasma jets
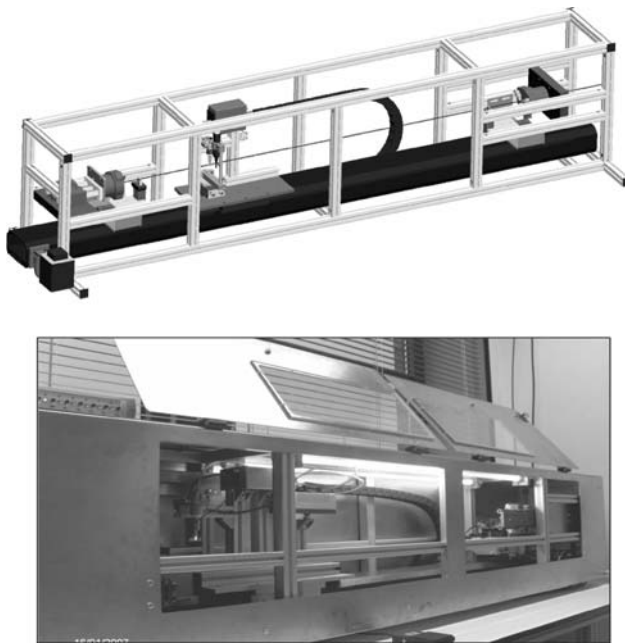
Figure 9. Device for the plasma treatment of catheters

Different modules are developed (see Fig. 10). Ring-modules consist of four or eight single plasma jets arranged as a ring around the work piece (Fig. 10, left). In another case the jet nozzle is equipped with a "T-type" adapter made of glass (Fig. 10, left). The plasma is generated inside the glass adapter, while the catheter is guided via the apertures at both sides of the vertical part. In both cases the plasma covers the outer surface of the catheters more or less completely.

To investigate the efficiency of antimicrobial plasma treatment by means of plasma jets on catheters they are divided in six sections (6 cm long). Each section

is contaminated with a suspension of vegetative bacteria (Staphylococcus aureus). The first five sections of the catheter are treated with the plasma module (1 or 2 cycles). The sixth section is not treated and used to determine the initial contamination (control). The results after a treatment using the "T-type" jet module (10 W, 20 slm argon with and without air admixture of 0.25 vol.%) are shown in Fig. 11.
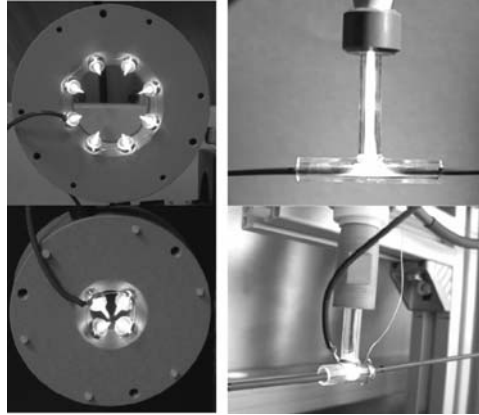
Figure 10. Plasma jet modules for the treatment of catheters. Ring-modules (left) and "T-type" jet (right)
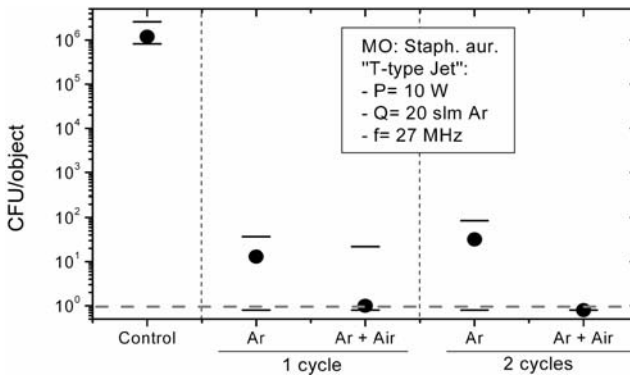
Figure 11. Median number (n = 5) of surviving MO (Staph. aureus) after treatment with "T-type" plasma jet module (10 W, 20 slm Ar) on catheter parts (error bars: spread between minimum and maximum values). Dashed gray line: detection limit 1 cfu/object

A reliable reduction of MO between four and six orders of magnitude on the catheter sections is shown in Fig. 11. On some catheter sections no viable MO are found after plasma treatment, i.e. the minimum values are at the detection limit for all conditions. But on some objects there are still survivors, thus the maximum values and the median values (data points) are somewhat higher. The spread

between minimum and maximum values decreases if air is admixed to the argon gas. In this case three or more objects of five are free of viable MO, thus the median is at the detection limit. This tendency may be explained by a higher number of reactive oxygen species due to the air admixture. These results demonstrate that the findings of the treatment of plastic strips can principally be transferred to the processing on real medical products. However the plasma process needs further improvement of stability and reliability. Furthermore other MO needs to be tested, too.

3. Treatment of Hollow Packaging by Means of Microwave Air Plasmas

The realisation of an antimicrobial treatment process of hollow packaging for pharmaceutical products, namely PET-bottles has quite different demands than the decontamination of medical products. In particular, the process is needed to be very fast in order to be implemented in an in-line filling procedure. The use of expensive inert gases, e.g. helium is also not desired. Therefore a self-propagating microwave-driven discharge in usual air at atmospheric pressure has been developed. The basic scheme of the plasma source is given in Fig. 12.
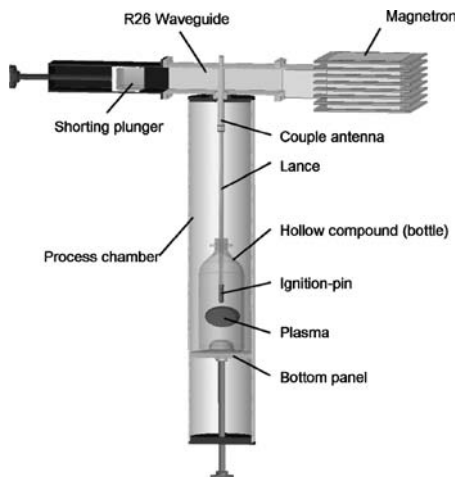
Figure 12. Device for the treatment of bottles by means of propagating microwave-driven air plasma

In principle, the device consists of a waveguide structure which serves as the process chamber and an ignition device which is mounted on a moveable lance [14]. The microwave radiation is generated by a magnetron (frequency 2.45 GHz; power up to 1.7 kW) and is coupled to the waveguide via a coupling antenna. The alignment of the magnetron frequency to the process chamber geometry is performed via a moveable shorting plunger. The bottle or another packaging is

placed in the center of the process chamber, the lance with the ignition device is driven into the bottle and after applying the microwave field the plasma is ignited in their bottom region. Driven by convection and interaction of the plasma with the microwave field the plasma propagates upwards through the bottle (see Fig. 13). After the ignition of the plasma the lance is moved to its home position, thus the plasma is allowed to move freely to the neck of the bottle. The device is well suited to treat all kinds of hollow compartments. In these studies standard 200 ml-bottles made of PET, and used as packaging for pharmaceutical products are treated.
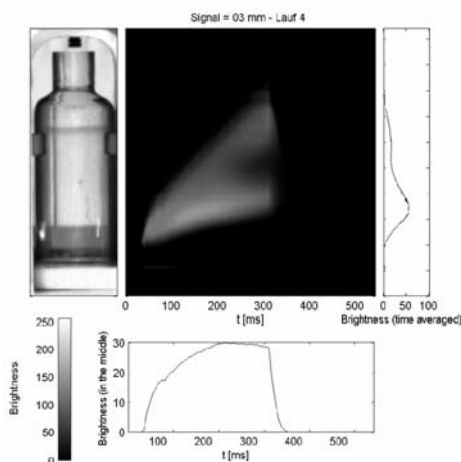
Figure 13. Visualisation of single plasma run in a bottle made of quartz glass

For microbiological tests MO containing dilution (E. coli, Staph. aureus or Aspergillus niger) is sprayed into the plastic bottles and dried under aseptic conditions. Contaminated PET-bottles are treated by the plasma three times, while each plasma cycle is about 550 ms long and characterized by a dissipated energy of about 300 J/cycle. After the plasma treatment the bottle is agitated and the resulting suspension is analyzed by membrane filtration as describe before. The results are summarized in the Table 1.

TABLE 1. Results after treating contaminated bottles with propagating microwave-driven air plasma

MO	Max. reduction of MO (log-steps)
Escherichia coli	6.8
Aspergillus niger	5.1
Staphylococcus auraeus	6.7

Depending on the MO 5 to about 7 orders of magnitude of reduction of micro organisms are observed. Note that the total plasma-on time is about 1.5 s only. Therefore, indeed with respect to further needed improvements, the device shows the suitability for the use in an in-line aseptic filling procedure. But for further advances more detailed experiments concerning the plasma composition, the antimicrobial activity and the reproducibility are necessary.

Conclusions

Two different plasma sources (plasma jet and microwave propagating discharge) for the antimicrobial treatment of heat sensitive goods were presented. The design of the plasma sources considers the properties of the product as well as the requirements on the desired treatment process. These are as different as the plasma sources themselves. The application of plasma jets in the special reprocessing of expensive medical products, namely catheters was shown. For PET bottle decontamination a low cost application for in-line treatment with high process rates by means of microwave-driven air plasmas was investigated. In principle both plasma sources have been demonstrated to reach the demands of a reliable decontamination on real products, but needs further improvements concerning process stability and applicability.

Nevertheless, a detailed understanding of the plasmas and the interaction of the plasma with the micro organisms as well as the drawback to its confinement is required in order to success in the development of stable industrial processes.

Acknowledgment

References

[1] Moisan, M.; Barbeau, J.; Crevier, M. C.; Pelletier, J.; Philip, N.; Saoudi, B.: Plasma sterilization: Methods mechanisms. *Pure and Applied Chemistry* 74 (2002) 3, 349–358

[2] Lerouge, S.; Tabrizian, M.; Wertheimer, M. R.; Marchand, R.; Yahia, L.: Safety of plasma-based sterilization: Surface modifications of polymeric medical devices

induced by Sterrad((R)) and Plazlyte (TM) processes. *Bio-Medical Materials and Engineering* 12 (2002) 1, 3–13

[3]   Laroussi, M.: Low temperature plasma-based sterilization: Overview and state-of-the-art. *Plasma Processes and Polymers* 2 (2005) 5, 391–400

[4]   Boudam, M. K.; Moisan, M.; Saoudi, B.; Popovici, C.; Gherardi, N.; Massines, F.: Bacterial spore inactivation by atmospheric-pressure plasmas in the presence or absence of UV photons as obtained with the same gas mixture. *Journal of Physics D-Applied Physics* 39 (2006) 16, 3494–3507

[5]   ASP Advanced Sterilization Products[(R)] a Johnson & Johnson company: *STERRAD systems[(R)]*: *http://www.sterrad.com/Products_&_Services/STERRAD/* consulted on 08 Sept. 2007

[6]   CerionX[(TM)]: *The TipCharger™ System*: *http://www.cerionx.com/TC_landing.php*, consulted on 28 March 2007

[7]   Foest, R.; Kindel, E.; Lange, H.; Ohl, A.; Stieber, M.; Weltmann, K. D.: RF capillary jet – a tool for localized surface treatment. *Contributions to Plasma Physics* 47 (2007) 1–2, 119–128

[8]   Foest, R.; Kindel, E.; Ohl, A.; Stieber, M.; Weltmann, K. D.: Non-thermal atmospheric pressure discharges for surface modification. *Plasma Physics and Controlled Fusion* 47 (2005), B525–B536

[9]   Brandenburg, R.; Ehlbeck, J.; Stieber, M.; von Woedtke, T.; Zeymer, J.; Schluter, O.; Weltmann, K. D.: Antimicrobial treatment of heat sensitive materials by means of atmospheric pressure rf-driven plasma jet. *Contributions to Plasma Physics* 47 (2007) 1–2, 72–79

[10] Sugimoto E. E.; Raasch A. J.; Ehioba R. M. *Journal of Applied Bacteriology* 80 (1996), 147–152

[11] Pfeiffer, M. *Pharm. Ind.* 59 (1997), 890–894

[12] *2.6.12. Microbiological examination of non-sterile products (total viable aerobic count), 5.1.2 Biological indicators of sterilization*: Ph. Eur. 5.0 – European Pharmacopeia. vol. 5, 2005

[13] Foest, R.; Bindemann, T.; Brandenburg, R.; Kindel, E.; Lange, H.; Stieber, M.; Weltmann, K.-D.: On the vacuum ultraviolet radiation of a miniaturized non-thermal atmospheric Pressure plasma jet. *Plasma Processes and Polymers* 4 (2007) S1, S460–S464

[14] Ehlbeck, J.; Ohl, A.; Maass, M.; Krohmann, U.; Neumann, T.: Moving atmospheric microwave plasma for surface and volume treatment. *Surface & Coatings Technology* 174 (2003), 493–497

COLD PLASMA – A POWERFUL AGENT
FOR BIOLOGICAL APPLICATIONS

V. A. GOSTEV[1], V. S. IGNAKHIN[1], E. K. POPOVA[2],
AND O. A. OSTASHKOV[2]
*[1]Petrozavodsk State University. Lenin street, 33, 185910,
Petrozavodsk, Russia*
[2]Scientific and technical co-operative "Resonance"

Abstract: This work represents the results of cold plasma processing of *St. epidermidis* bacteria, living measles virus vaccine culture and fish spawn. The obtained results shows that the cold plasma has strong bactericidal and virus inactivating effect. A series of experiments on fish spawn has revealed that the cold plasma treatment has a number of positive effects on its development. A possibility of absolute suppression of spawn dermatomycosis by means of plasma treatment has been experimentally proved.

Keywords: Cold plasma, inactivation, bacteria, viruses, fungi, plasma stimulation

1. Introduction

Plasma is a unique complex medium which contains charged species, active radicals and photons etc. Due to wide spectrum of phenomena which occur while these components interact with biological objects it is widely adopted in the biological and medical areas [1–3]. Depending on thermal capacity of the plasma flow there can be various calorific effects in tissues during the direct contact. It is known that if the temperature of plasma is about 40°C no irreversible changes of biological tissues caused by plasma treatment are observed [1,2]. In this connection sources of cold plasma at atmospheric pressure are of great interest. Cold plasmas allow to accomplishing "soft" nondestructive affection on biological tissues with strong bactericidal and stimulation effects. Recent years have brought much progress in developing cold plasma sources [3,4].

Future trends of using cold plasma are connected with solving the following problems:

- Investigation of plasma radiation and of corpuscular flows influence on different cells and their components
- Examination of biochemical reactions in cells and tissues under plasma influence

- Investigation of possibilities of medical treatment of various pathological processes with plasma
- Investigation of plasma influence mechanism and of plasma characteristics
- Optimization of plasma influence rate and revealing the range of plasma parameters with the best medical and biological effect

2. Experimental Device

A number of plasma devices that able to generate cold plasma have been developed in the Petrozavodsk State University. One of them is a generator of cold plasma at atmospheric pressure (GCPAP) which produces plasma with the average mass temperature of 30–40ºC by using atmospheric air and noble gases as working substances [4,5]. Similar GCPAP was used in the presented work as a source of cold plasma, but with water as a working substance. The GCPAP (Fig. 1) consists of coaxial cathode and needle-like anode which is fixed in dielectric capillary. Photos of the GCPAP are shown in Fig. 2.
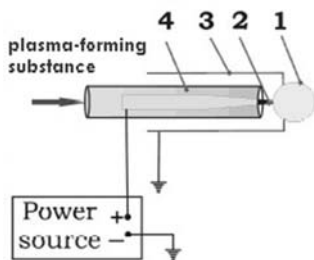
Figure 1. Scheme of the experimental device. 1 – cold plasma, 2 – needle-like anode, 3 – cathode, 4 – insulating capillary
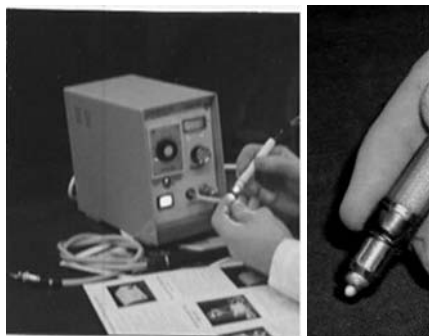
Figure 2. Photos of the GCPAP

Consumption of water is 25–50 ml/h. The GCPAP is powered by 220 V circuit. Consumable power is 20 W. The power density of plasma flow is 0,4–0,8 W/cm^2 when its diameter is 3–5 mm and its length is 5–8 mm.

The flow of plasma generated contains electrons, ions, excited atoms of hydrogen and oxygen, and excited molecules of water. It is of special interest that active molecular singlet oxygen presents in the flow in quite high concentration. Cold plasma is a source of electromagnetic waves in UV, visible and infrared ranges. The power of radiation has been estimated to be in the order of order hundreds and tens mW in UV-visible range and in red-infrared ranges, correspondingly. A corpuscular flow of plasma radiation can be absorbed, reflected, diffused and re-emanated by the tissue. There is a wide variety of processes of interaction between plasma and molecules – dissociation, electronic, oscillatory and rotary excitation. The influence of these processes on bacteria can be both selective and thermal.

3. Cold Plasma in Biological Experiments

3.1. BACTERICIDAL ACTION

We have carried out *in vitro* investigation of cold plasma effect on *St. epidermidis* culture containing $3 \cdot 10^9$ colony formative units (CFU) per 1 ml. Two different experiments have been conducted [6].

In the first experiment liquid containing staphylococcus culture was passed through the GCPAP as working substance. The results have proved strong bactericidal effect of cold plasma. Cold plasma treatment results in total disinfection at rate of processing of 10^{-2} ml/s.

In the second experiment 10 ml of staphylococcus culture suspension was treated in Petri dish in contact with plasma. The results obtained have shown that 100% inactivation of the whole volume occurs after 5 min treatment (Fig. 3).
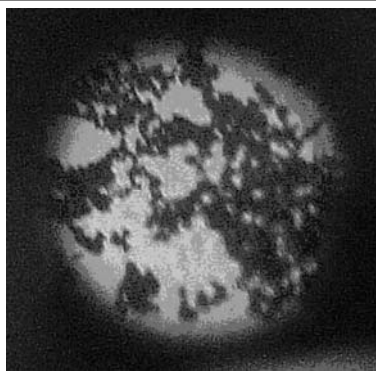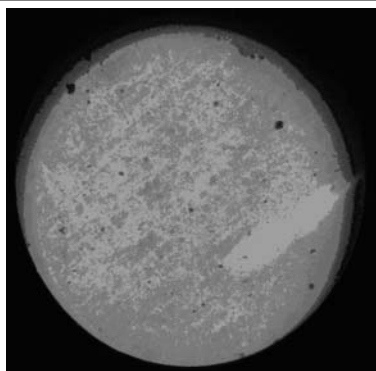
Before plasma treatment   After plasma treatment

Figure 3. Cold plasma affection on staphylococcus culture

3.2.   INACTIVATING EFFECT ON VIRUSES

We have carried out *in vitro* investigation [7] of plasma affection on live culture of measles virus vaccine on the cell line a-41, which were treated with cold plasma. The treatment duration variated from 30 s to 5 min. We have processed open surface of upright placed glass dish with liquid containing live cultures of measles virus vaccine. The edge of plasma contacted with the liquid surface. The dose of the treatment was determined by the equation:

$$D_{tr} = P \cdot t / V \tag{1}$$

where D_{tr} – is the dose of the treatment by volume, joule per milliliter; P – is the power of a plasma flow, watt; V – is a fluid volume, milliliters; t – is the duration of the treatment, seconds.

The carried out investigations have shown direct relation of cold plasma inactivating action with total treatment dose (Fig. 4).
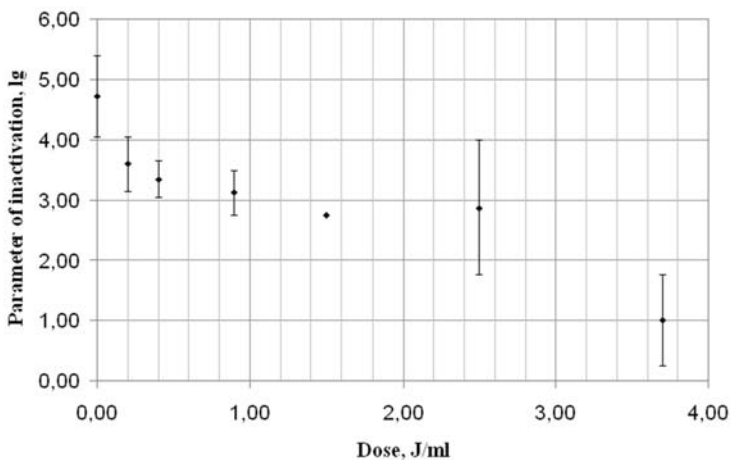
Figure 4. Inactivating effect of cold plasma

3.3.   INFLUENCE ON FISH SPAWN

Chemical energy of cold plasma is enormous. It makes possible to apply the device for stimulation of fish spawn. We have carried out a series of experiments aimed at investigation of cold plasma influence on perch (*Perca fluviatilis*) spawn development at contact affection.

The first experiment diameter of spawn berries, dimensions of hatched out larvae and survival rate have been investigated depending on the time of the treatment (5, 15, 30, 60 s). Non-treated eggs were used as control. The number of incubated spawn berries amounted to 200 in each variant. Plasma treatments were conducted at the stage of eyed egg (the beginning of eye pigmentation). The data on the egg diameter are given in Table 1.

TABLE 1. Diameter of perch eggs treated by cold plasma at the stage of eyed egg

Treatment duration, s	0 (Control)	5	15	30	60
Mean diameter, mm					
$x_{cp} \pm \Delta_{Xcp}$	2.59 ± 0.12	2,79 ± 0.09	2.77 ± 0.06	2.89 ± 0.06	3.23 ± 0.04
Min	2.2	2.5	2.6	2.6	3.1
Max	3.0	3.1	3.0	3.0	3.4

Eggs treated for 60 s were significantly larger compared to those in control variant. Eggs were very regular and their diameter deviations were slight. The larvae had hatched out completely 5 days later in the variant "30 s". Those in others experimental groups were hatching out during the 5th day after the experiment. Isolated instances began to occur in the control for the 5th day. The control larvae had hatched out by the 6th day.

Recently hatched larvae were larger in treated by plasma experimental groups of fish compared to those in the control. Variability of body length of the larvae in the control group is slightly bigger (Table 2).

TABLE 2. Body length of perch larvae after cold plasma treatment

Treatment duration, s	0 (Control)	5	15	30	60
Mean body length, mm					
$x_{cp} \pm \Delta_{Xcp}$	6.21 ± 0.06	6.52 ± 0.04	6.52 ± 0.07	6.41 ± 0.05	6.45 ± 0.03
Min	5.9	6.3	6.3	6.2	6.3
Max	6.5	6.7	6.8	6.7	6.6

Survival rate of perch embryos depends on the dose interval (Fig. 5).
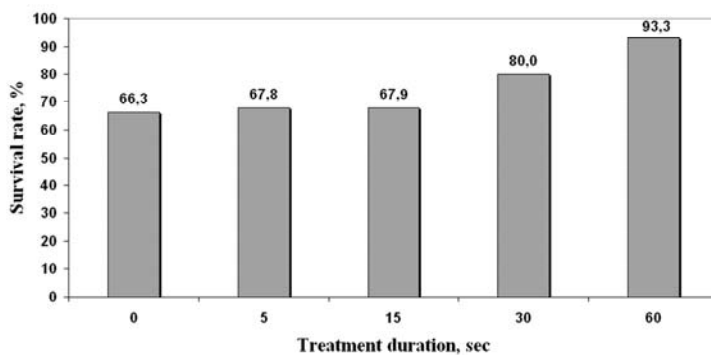
Figure 5. Dependence of survival rate of perch embryos on the duration of plasma treatment

The second experiment on perch spawn was conducted at the stage of blastodisk division. The same expositions were used. The total number of incubated spawn berries amounted to 120 in each variant. On the second day after treatment eggs had almost the same diameters with the exception of those treated for 30 s (Table 3).

TABLE 3. Diameter of perch eggs treated by cold plasma at the stage of blastodisk division

Treatment duration, s	0 (Control group)	5	15	30	60
Mean diameter					
$x_{cp} \pm \Delta_{xcp}$	2.39 ± 0.03	2.41 ± 0.03	2.30 ± 0.06	2.21 ± 0.01	2.31 ± 0.01

Three-day embryos in the control group were at the developmental stage of the beginning of tail bud growth. At this age the embryos treated by cold plasma for 60 s were active and pigmentation of eyes began.

In the control group hatching began on the 4th day after treatment, but mass hatching occurred only on the 8th day. In the treated by plasma experimental groups hatching begun simultaneously on the 7th day after fertilization. Data on the survival rate of perch embryos treated by cold plasma are given in Fig. 6.
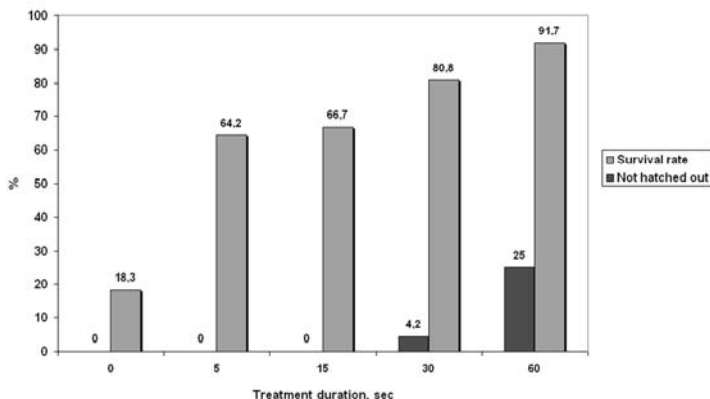
Figure 6. Survival rate of perch embryos treated by cold plasma at the stage of blastodisk division

Body length of recently hatched larvae was larger when eggs had been treated by plasma for 60 s compared to those in the control group. Standard deviations of larvae length were smaller in the groups treated by cold plasma compared to those in the control group (Table 4).

TABLE 4. Body length of perch larvae treated by cold plasma at the stage of blastodisk division

Treatment duration, s	0 (Control group)	5	15	30	60
Mean body length, mm $x_{cp} \pm S_{Xcp}$	5.7 ± 0.1	6.15 ± 0.04	5.83 ± 0.03	5.82 ± 0.03	6.25 ± 0.03
Min		5.1	6.0	5.7	5.7	6.0
Max		6.2	6.3	6.0	6.0	6.4

Thus, 60 s treatment of fish spawn by cold plasma revealed some positive effects, such as increase of the survival rate, synchronism in the development, increase in larvae body length.

3.4. TREATMENT OF SPAWN DERMATOMYCOSIS

These results gave us ground to assume that cold plasma can be used for treatment of spawn infected by *Saprolegnia* ("cotton mould") infection. This dermatomycosis causes serious damage to fish-farming. In this connection an extremely important task is to find active biological factors and agents which can stimulate the development of the host and suppress the fungus at the same time.

In the experiments we used artificially inseminated spawn of *Cyprinidiae* fishes, such as roach *Rutilus rutilus* (L.), bream *Ambramis brama* (L.) and bleak *Albumis albumis* (L.). Spawn samples were taken at different stages of development and had different damage rate.

Experiment 1: Roach Rutilus rutilus (L.)

Incubation of eggs was carried out in the presence of large number of *Saprolegnia* spores. A clod of unfertilized spawn was placed into an aquarium together with fertilized spawn. Hyphae of the fungus developed rapidly on the unfertilized spawn. Three days later all eggs were divided into five groups (100–200 eggs in each group), treated by plasma and placed into glass beakers. Treatment duration was 30, 60, 90 and 120 s for the 1st, 2nd, 3rd and 4th groups, correspondingly. Non-treated eggs were used as control group. Two replications were used. At the time of plasma treatment, embryos already occupied 2/3 of eggs, eye buds were visible and body segments appeared.

As a result the spawn treated by plasma for 30 s gave the greatest yield of larvae and *Saprolegnia* infection was prevented. The average yield of larvae was 44.7%, which is 2.1 times higher compared to the yield in 60 s treatment group and 4.2 times higher compared to that in control group (Fig. 7). Longer than 30 s effects of plasma have resulted in death of *Saprolegnia* spores, but also destruction of eggs.
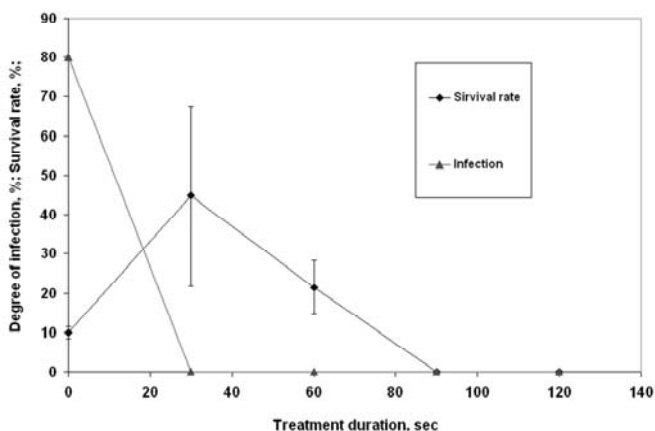
Figure 7. Survival rate of perch embryos and degree of *Saprolegnia* infection after the treatment by cold plasma. Experiment 1

Experiment 2: Bream Abramis brama (L.)

Clods containing 100–150 eggs were taken from the mass of artificially inseminated spawn and placed into Petri dishes with small amounts of water. The embryos were in the stage of body segmentation. Plasma treatment duration was 30, 60, 90, 120 s. Non-treated eggs were used as control. Two replications were used.

On the second day all spawn in the control group was infected by actively developing *Saprolegnia* fungus and lost. In the dishes treated by plasma for 30 and 60 s all *Saprolegnia* hyphae and spores died before affecting spawn. Thus, spawn was not affected and on the 7th day gave yield of normally developed larvae. The longer plasma influence (90 and 120 s) had negative effect both on fungus and eggs, which capsules were ruptured.

This experiment confirmed the results obtained in the experiment 1 and proved that the treatment of spawn by cold (super-cooled) plasma during 30 s prevents dermatomycosis infection without causing spawn destruction.

Experiments 3, 4: Bleak Alburnus alburnus (L.)

In the third experiment clods of infected by *Saprolegnia* spawn were put into Petri dishes with small amounts of water. The treatment duration was 5, 10, 15 and 20 s. Non-treated eggs were used as control. After the treatment by plasma the number of infected eggs did not increase while in the control dish the infection gradually spread. By the 5th day all control eggs were infected (Fig. 8).
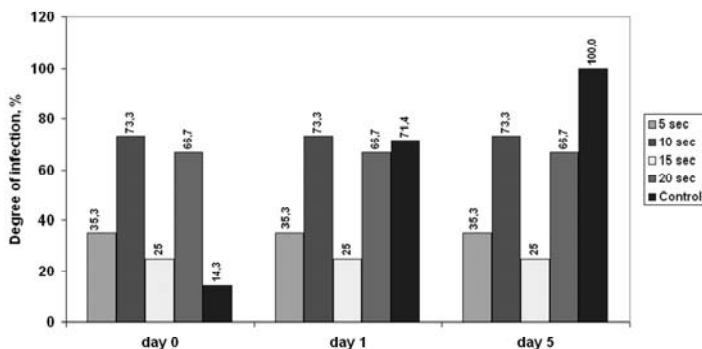
Figure 8. Saprolegnia infection spreading on the spawn of bream immediately before (day 0), one day later (day 1) and at the end of the 5th day (day 5) after plasma treatment of different duration. Experiment 3

In the experiment 4 water was added to spawn after plasma treatment. The treatment duration was the same as in experiment 3. The obtained results (Fig. 9) gave ground to conclude that different treatment techniques have different effects on vital functions of *Saprolegnia* fungus. Thus, in case of 5 and 10 s treatment in the absence of water development of *Saprolegnia* hyphae continues, though it is slightly suppressed.
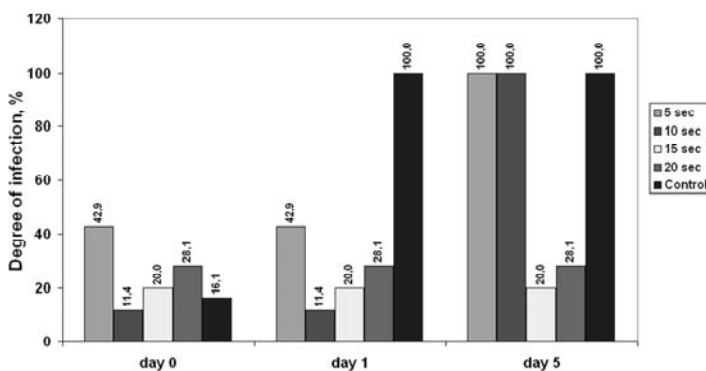
Figure 9. Saprolegnia infection spreading on the spawn of bream immediately before (day 0), one day later (day 1) and at the end of the 5th day (day 5) after plasma treatment of different duration. Experiment 4

3.5. POSSIBILITY OF USING DISTILLED WATER PASSED
THROUGH COLD PLASMA AS A REMEDY FOR THERAPY
OF FISH DERMATOMYCOSIS

One of the physical-chemical properties of cold plasma is presence of considerable amount of active singlet oxygen. In the distilled water passed through the plasma its concentration rises from 6.6 up to 12.0 mg/l, but it drops almost to initial value in 24 h. Scheme of the device for obtaining activated water is presented in Fig. 10.
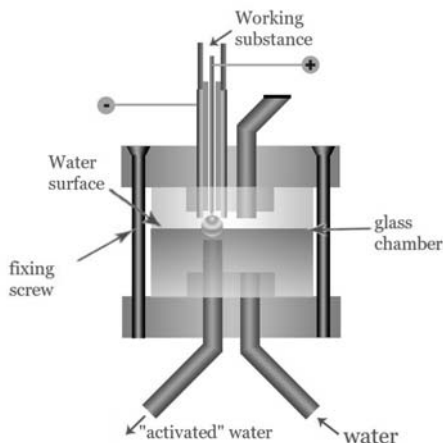
Figure 10. Scheme of the device for obtaining activated water

An attempt has been made in order to apply distilled water passed through cold plasma as an anti-dermatomycosis remedy. The experiments have been carried out on impregnated spawn of perch and bleak.

Experiment 5: Roach Rutilus rutilus (L.)

Incubated roach spawn was at the stage of the beginning of eye pigmentation. The total number of eggs was 200 in each experimental group. Some eggs were infected by *Saprolegnia*. Activated water was added to distilled water at ratios 500:0, 250:250, 150:350, 50:450 and 0:500 (control).

Twelve hours after the incubation yolk in the eggs placed into activated water coagulated, the embryos were destroyed and many capsules were ruptured. The same situation was observed in the groups placed into 50% and 43% mixtures. The spawn in 11% solution normally developed and the number of *Saprolegnia* hyphae did not increase, but all the embryos at the time of control group hatching out. In the control 80% hatched out, but 20% was infected by *Saprolegnia*. Thus, water passed through plasma as well as its mixture with distilled water at ratios from 1:1 to 1:9 has been found to be destructive both for fungus and spawn.

Experiment 6: Bleak Alburnus alburnus (L.)

The aim of the experiment was to investigate the effect of low concentrations of activated water on *Saprolegnia* infection development and spawn itself. Bleak spawn at the stage of division (large cell morula) was fertilized and in 4 h after fertilization placed into glass vessels. There were 120–150 eggs in each vessel. Activated by cold plasma water was added to distilled water at ratios 4:396, 20:380, 40:360 and 0:500 (control).

Four days later all control spawn was infected by *Saprolegnia* and lost. 40% and 25% eggs have hatched out in the variants 4:396 and 20:380, correspondingly (Fig. 11). Development of the infection was suppressed in the experimental groups treated by activated water.
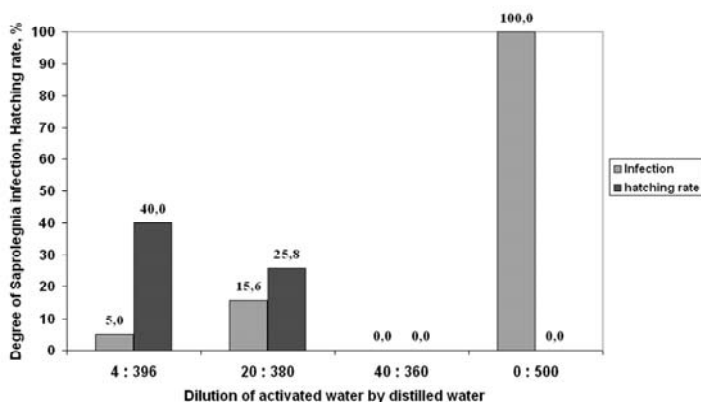
Figure 11. Saprolegnia infection spreading and hatching rate on the 4th day after the treatment of bleak spawn by activated by super-cooled plasma water in different proportions. Experiment 6

3.6. TREATMENT OF SEEDS

In addition a series of qualitative experiments aimed at investigation of cold plasma influence on soybean has been conducted. The obtained results are presented in Table 5. 100% of soybean seeds treated by super-cooled plasma have germinated, while in the control group the germination rate was only 50%.

TABLE 5. Germination rate of soy-bean seeds

	Specific dose, J/seed	Number of planted seeds	Number of come up seeds
Experiment	4.5	180	180
Control	–	180	91

Conclusions

The obtained results show that:

- Cold plasma has strong bactericidal and virus inactivating effects when contact treatment is applied.
- Treatment of fish spawn by cold plasma revealed some positive effects, such as increase of the survival rate, synchronism in the development, increase in larvae body length.
- Absolute suppression of spawn Saprolegnia infection is possible by means of plasma and activated by plasma water.
- Cold plasma treatment of soybean seeds increases germination rate.

  Therefore, cold plasma can be used for:

- Bactericidal processing of liquids.
- Enhancing fish reproduction especially under extreme conditions (low oxygen content in water, absence of running water etc.) and also for Saprolegnia infection control.
- Presowing treatment of plant seeds for improving germination rate.
- Disinfection of medical instruments and bandaging material.

Acknowledgments

References

[1] Tuchin V.V. Interaction of laser radiation with tissues. Laser physics. 3rd fascicle. St. Petersburg. Russian center of laser physics. 1992. pp. 87–108. (in Russian)
[2] Tuchin V.V., Shubochkin L.P. Lasers applications in ophthalmology. First part. Interaction of visual radiation with eye tissues. "Reviews on electronic techniques. 11th series. Laser techniques and optical electronics." Moscow. Central scientific research institute "Electronics". 1984. 2nd fascicle (1037). (in Russian)
[3] Stoffels E. "Tissue processing" with atmospheric plasmas.//Contributions to plasma physics." 47, No. 1–2, 40–48. 2007. pp. 40–48.
[4] Gostev V., Dobrynin D. Medical microplasmatron Proceeding 3rd International Workshop on Microplasmas. c.108, May 9–11.Greifswald, Germany, 2006. p. 201.

[5] Gostev V.A., Tikhomirov A.A., Ignakhin V.S., Sysun V.I. Generator of air-plasma flow for biological and medical applications. V International Conference Plasma Physics and Plasma Technology, Minsk, Belarus, 2006. Vol. II. pp. 791–794.

[6] Misyn F., Besedin E., Gostev V., Komkova O. Experimental studying of bactericidal action of cold plasma (in Russian).//Diagnostics and treatment of infectious diseases. Petrozavodsk. 2000. pp. 40–41. http://medicine.onego.ru/prakt/p0305_a.shtml

[7] Tischenko M.S., Surovceva T.A., Gostev V.A. Low temperature plasma utilization as remedy for influence on agents of virus infections (in Russian).//Diagnostics and treatment of infectious diseases. Petrozavodsk. 2000. pp. 41–42 http://medicine.onego.ru/prakt/inf/inf16_a.shtml

PRELIMINARY EVALUATION OF LOW POWER PULSED CORONA DISCHARGE FOR CHARACTERIZATION OF LIQUIDS

D. STAACK[1], A. GUTSOL[1], G. FRIEDMAN[2], AND A. FRIDMAN[1]

[1]*Department of Mechanical Engineering and Mechanics, Drexel University, Philadelphia, PA, USA*
[2]*Department of Electrical and Computer Engineering, Drexel University, Philadelphia, PA, USA*

Abstract: A low power pulsed corona discharge has been created in liquid media. The corona is generated at the ~1 μm sharp tip of a tungsten wire submerged in the liquid. The voltage pulse of about 15 kV applied to the tip is generated using spark gaps in air resulting in a rise time of ~300 V/ns. During this voltage pulse a small bubble and light emission is visible from the wire tip. The color of light emission depends on the liquid media. Optical emission spectroscopy is used to analyze the light emitted by the discharge. Due to the small size the plasma electron density is several orders of magnitude lower than for larger scale pulsed coronas and may remain non-thermal. Tested liquids include tap water and aqueous salt solutions. The light emission is unique to the constituents of the liquid in which the discharge is created. These preliminary results indicated that this corona in liquid may be a unique tool for the diagnostics of liquids such as species and contaminant detection.

Keywords: Pulsed corona, microplasma, non-thermal plasma, optical emission spectroscopy, plasma in liquids, electrohydraulic discharge, breakdown spectroscopy, water contamination detection

1. Introduction

Plasma discharges within liquid water have been studied for several years due to their importance for many environmental, chemical and biological applications [1]. Since water is conductive, high voltage pulsed discharge systems are used. Generally two types of transient discharges are used: (1) pulsed corona and (2) pulsed spark. Steady-state arc discharges can also be formed in a gas bubble within the liquid but in initial phases are similar to the pulsed spark. The corona systems operate at ~1 J/pulse where as the sparks typically have energies of ~1

kJ/pulse. These systems generate sound and shock waves, bubbles, visible and UV radiation, radicals and reactive species to various degrees depending on the discharge conditions. These processes resulting from the discharge are used in a wide variety of applications including the production of UV radiation and radicals for biological decontamination, the degradation of organic and inorganic compounds for drinking water and waste water treatment, and the generation of shock waves for rock fragmentation and surgery [1].

The breakdown of the liquid and formation of plasma discharges in liquids is a complex process which currently is only partially understood. Several theories for the method of breakdown are available in the literature [2] but no single comprehensive quantitative model exists. In their initial phases (<1 μs) sparks and coronas may develop similarly through non-thermal plasma mechanisms. In water electrons cannot attain sufficient energy to ionize or multiply within the liquid phase since the water has many inelastic scattering mechanisms and essentially $\alpha = 0$, where α is the Townsend ionization coefficient. Most theories assume that the plasma propagates through a low density region or bubble where $\alpha > 0$ and electron avalanches can occur. This bubble is thought to be preexisting or formed by heating of the water (through various mechanisms). The bubble expands through vaporization pressures and electro-hydrodynamic forces at the bubble liquid interface eventually forming a streamer structure (for coronas) or connecting to a second electrode (in the case of a spark). It is currently unresolved if the plasma inside of the growing bubble is thermal or non-thermal or what the dominant mechanism of bubble expansion is [3].

In this study we utilize a variation of the corona type discharge wherein the power level of the discharge (~10 mJ/pulse) is significantly less than that typically studied. This is done by using a 1 μm sharp electrode which reduces the necessary voltage to initiate the discharge and reduces the current into the liquid. The reduction in the discharge power significantly reduces thermally associated effects. A bubble is seen to form during the voltage pulse though the mechanism of formation is not clear. Images of the discharges and emission spectroscopy indicate that the discharge should be able characterize liquids similar to results from laser breakdown spectroscopy [4]. Described herein are: the voltage waveforms and images characterizing the discharge; the use of emission spectra to diagnose several liquids; and comparison to other corona discharge systems.

2.   Experimental Setup

A schematic of the experimental setup and the electrical circuit used to generate the discharge is shown in Fig. 1. A pulsed power supply was constructed using a spark gap as is common for pulsed corona configurations [5]. A DC power supply is connected to a *RC* circuit which charges the capacitor until the voltage is sufficient to cause breakdown across the primary spark gap, S1. The length of S1 is adjustable with a micropositioner and determines the voltage applied to the electrode. Wire lengths to the electrode and high voltage probe were

approximately the same length (15 cm) to have similar voltage rise times. A Pearsons model 2,877 current transformer was used to estimate the current on the electrode lead. The voltages and currents measured by the probe may not precisely be that experienced by the electrode due to complications regarding the high frequency of the pulses and displacement currents. The R, C, and power supply voltage, V_{ps}, determine the repetition rate of the discharge which was between 1 and 30 Hz.
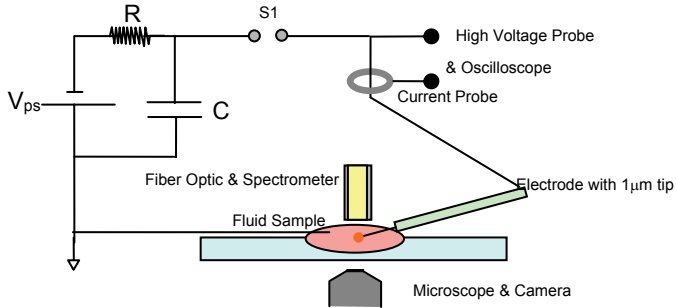
Figure 1. Schematic of discharge circuit and experimental setup

The electrode tip was manufactured by electrolytically etching [6] a ~70 µm tungsten wire to a tip radius of ~1 µm. The fluid sample is held in a microscope well slide and the tip of the wire is inserted into the fluid. Tested liquids include tap water and simple aqueous solutions of NaCl. A grounding wire is also placed in the fluid at a relatively far distance from the electrode tip (>5 mm), as such the discharge always operates as a corona or 'incomplete' discharge. The discharge is visualized using a microscope and digital camera. An optical fiber is also inserted into the liquid at a distance of ~3 mm from the discharge. Light collected by the fiber is connected to a Princeton Instruments TriVista spectrometer system and PI-MAX CCD camera. The CCD camera is triggered by an output from the oscilloscope such that the light collection is synchronized with the initial voltage rise on the electrode.

3.   Results and Discussions

3.1.   VOLTAGE-CURRENT MEASUREMENTS

Figure 2 shows the voltage and current waveforms measured for the corona discharge. The primary spark gap gives a voltage rise of about 300 V/ns. In this case a voltage spike of 15 kV was applied. In the initial part of the pulse a plasma discharge is created at the tip of the electrode. In the remainder of the pulse the voltage is dissipated through the electrolyte liquid at a current of about 4 mA causing electrolysis and bubble formation along the tungsten wire. Light emission, as indicated by the emission spectra, is only visible during the initial application of

the voltage pulse. Considering a 15 kV voltage, a ~2 μs light emission duration, and a measured peak current of 0.4 A the energy in the plasma per pulse is less than 10 mJ. The actual discharge power is likely even less than this considering the measured current includes displacement currents.
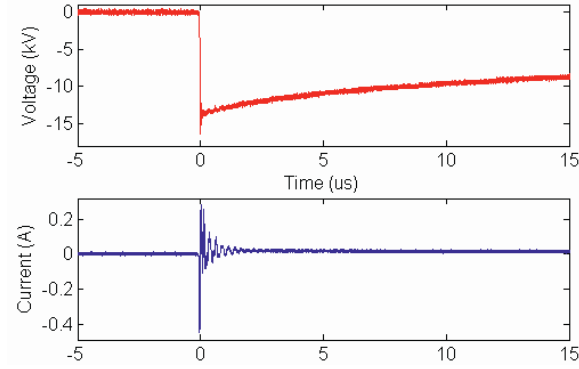
Figure 2. Measured voltage and current on the electrode

The creation of the plasma discharge is characterized by visible light emission from the tip of the wire and only occurs above a certain applied electric field. The voltage required is dependant on the sharpness of the tip and high electric field near the sharp tip inducing breakdown. Addition effects especially fluid motion are apparent due to the electro-hydrodynamic forces generated near the high field gradients at the probe tip. The corona discharge could operate repeatable over several thousand pulses. If the power was significantly increased the electrode tip could become visibly less sharp and the voltage for breakdown corresponding increases.

3.2. DISCHARGE VISUALIZATION

Figure 3 are several images of the corona discharge in liquid during operation. The tungsten wire shank is 76 μm is diameter and is visible coming from the lower left of the image in Figs. 3a, d, and f. Figure 3b shows a magnified view of the sharp tip prior to discharge operation. In the case of a discharge in Philadelphia tap water the light emitted by the discharge was violet/pinkish in color and was significantly dimmer than for a discharge in NaCl salt water for the same voltage conditions. The salt water discharge was orange with the color corresponding with the Na line transition at 588 nm. The salt water discharge was sufficiently bright to compete with ambient light sources as shown in Fig. 3f. The discharges were 10–20 μm in diameter and increase in size with increasing voltage. Bubbles formed along the wire shank due to electrolysis as seen in Fig. 3d and f and were accelerated toward the probe tip during the voltage pulses due to electro-hydrodynamic forces [7].
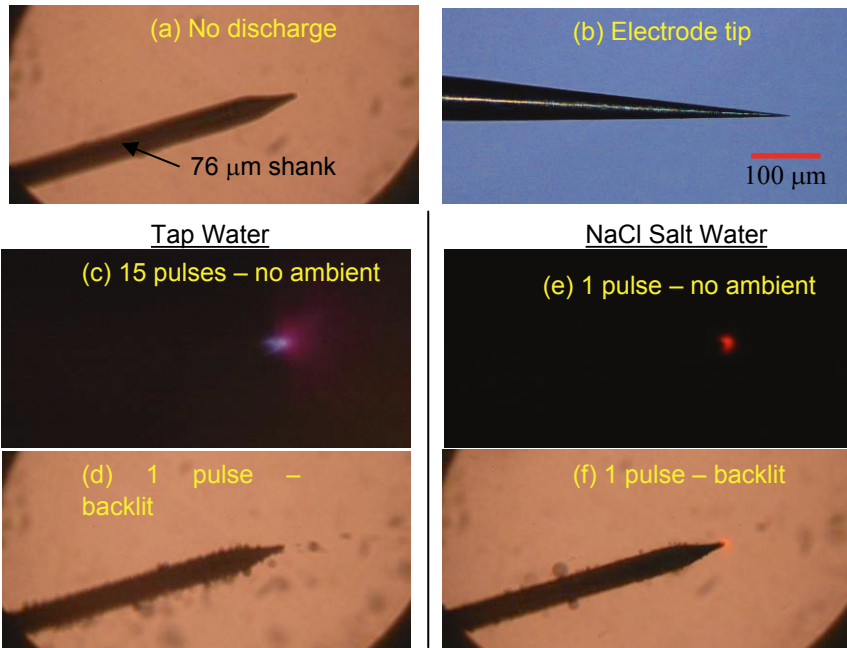
Figure 3. Images of the (a) unpowered electrode and (b) magnified tip. Low power corona discharges in tap water collecting light from (c) 15 pulses without external lighting and (d) 1 pulse with back lighting. Discharge in NaCl salt water from (e) 1 pulses without external lighting and (f) 1 pulse with back lighting (f)

3.3. EMISSION SPECTROSCOPY

The light emitted by the discharge is dependant upon the liquid tested. Figure 4 shows the emission spectra from tap water and NaCl salt water. The peaks are due to the emission of atomic Na, H and O. H and O arise from decomposition of the water during the discharge. Na occurs as a trace quantity in tap water, and is more strongly present when intentionally added in the NaCl solution. The strongest sodium emission is due to transition from the first electronic state to the ground state ($2p^63p \rightarrow 2p^63s$, 2.1 $\rightarrow$ 0 eV) and occurs as a doublet at 588.995 nm and 589.592 nm. A weaker sodium line is due to a grouping of lines around 819 nm corresponding to transition from the second electronic state to the first electronic state ($2p63d \rightarrow 2p63p$, 3.62 $\rightarrow$ 2.1 eV). The strong hydrogen line is due to the common Balmer alpha line at 656 nm ($3d \rightarrow 2p$, 12.09 $\rightarrow$ 10.2 eV). Atomic oxygen transition are visible at 777.3 nm ($2s^22p^3(^4S°)3p \rightarrow 2s^22p^3(^4S°)3s$, 10.74 $\rightarrow$ 9.15 eV) and 844.6 nm ($2s^22p^3(^4S°)3p \rightarrow 2s^22p^3(^4S°)3s$ 10.99 $\rightarrow$ 9.52 eV).
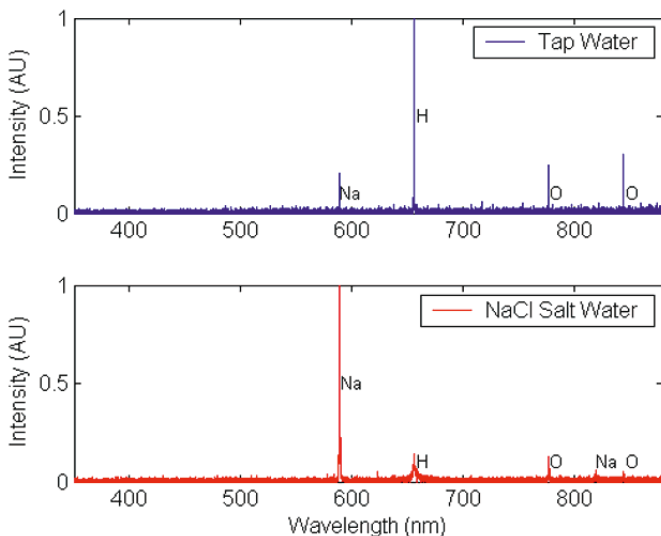
Figure 4. Emission spectra from the low power pulsed corona discharge in (a) tap water, (b) NaCl salt water

The emission spectra shown in Fig. 4 clearly indicate the ions present in the solution. In comparing the tap water and salt water samples we see that the sodium concentration is higher in the salt water as expected. The change in the relative Na/H peak height of the tap water and salt water solutions (0.2 and 7.2 respectively) indicate that this spectroscopic method may be useful for quantitatively determining concentrations of ions present in the aqueous solution.

Significant differences in the spectra are also seen when larger millimeter-tiped electrodes and higher voltages are used. In such a situation the currents and powers are much larger ~1 J/pulse similar to those traditionally used for water decontamination. Figure 5 shows the spectra attained from a ~1 J/pulse corona in water. Here the H Balmer series α and β lines and atomic O lines are observable. Comparing Fig. 5 to Fig. 4a both for tap water we see a significant difference in the broadening of the line shape for high power pulses. Such Lorentzian type line broadening is typically due to collisional interaction of the atom during the light emission. The most dominant form of collisional broadening for our conditions is stark broadening which is due to the interaction of the emitting atom with free electrons. Based upon the changes in the energy of the atom during collision with electrons the line is broadened. The degree of line broadening can be related to the electron density in the plasma discharge [8]. Using the H_α line width the electron density from Stark broadening in the high energy pulsed corona is $n_e \sim 10^{18}$ cm^{-3}; for the low power corona we reach the limit of the spectrometer resolution but a limit of $n_e < 10^{16}$ cm^{-3} can be determine. The significantly lower electron density in the case of the low power corona discharge allows for more spectral features to be seen. The Na lines present in Fig. 4a are not present in the

higher power corona discharge (Fig. 5) due to the overwhelming and broad hydrogen lines. Due to less overlap and broadening of the lines the lower power corona discharge has the unique opportunity to measure trace species present.
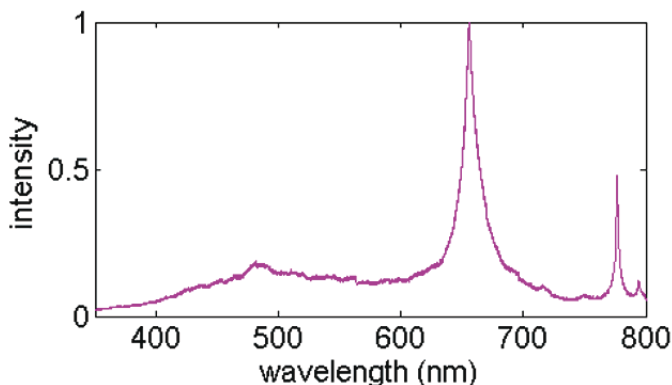
Figure 5. Emission spectra of a high energy pulsed corona in tap water

Conclusion

Pulsed corona discharges in water of approximately 10 mJ/pulse, several orders of magnitude weaker than typically studied, have been created by using a wire with a sharp ~1 μm tip as the electrode. For rapid rise time pulses, 15 kV in 50 ns, light emission from a volume approximately 20 μm in size is visible. Ionic species present in the liquid can be identified from the spectra and the intensity depends on their concentration. The observed spectrum consists of atomic Na, H, and O lines for low power corona discharge in salt water. The H_α line shape can be used to estimate the electron density which is $<10^{16}$ for a 10 mJ/pulse corona. In comparison the electron density is $\sim 10^{18}$ cm^{-3} for a 1 J/pulse corona. In the low power pulsed corona discharges in liquid spectroscopic observations of lower electron density and thus decreased line broadening due to the stark effect allows for the clear identification of species present in the liquid.

References

[1] B.R. Locke, M. Sato, P. Sunka, M.R. Hoffmann, and J.-S. Chang, "Electrohydraulic discharge and nonthermal plasma for water treatment", Ind. Eng. Chem. Res., 2006, Vol. 45, pp. 882–905.
[2] H.M. Jones and E.E. Kunhardt, "The influence of pressure and conductivity on the pulsed breakdown of water", IEEE Trans. Dielectr. Electr. Insul. Magn., 1994, Vol. 1, p. 1016.
[3] Y. Yang, J. Zhu, Y. Cho, A. Gutsol, and A. Fridman, "Model for Development of Electric Breakdown in Liquids and Stability Analysis", in Plasma Assisted Decontamination of Biological and Chemical Agents, (Ed) S. Güçeri and V. Smirnov, Springer, New York, 2008.

[4]   J. Ben Ahmed, N. Terzi, Z. Ben Lakhdar, and G. Taied, "Temporal characterization of a plasma produced by interaction of laser pulses with water solutions", Laser Chem., 2002, Vol. 20 (2–4), pp. 111–122.
[5]   J. Mankowski, "A review of short pulse generator technology", IEEE Trans. Plasma Sci., 2000, Vol. 28 (1), pp. 102–108.
[6]   Allan J. Melmed, "The art, science and other aspects of making sharp tips", J. Vac. Sci. Technol. B 1991, Vol. 9 (2), pp. 601–608.
[7]   D.A. Saville, "Electrohydrodynamics: The Taylor-Melcher Leaky Dielectric Model", Annu. Rev. Fluid Mech., 1997, Vol. 29, pp. 27–64.
[8]   A. Descoeudres, C. Hollenstein, R. Demellayer, and G. Walder, "Optical emission spectroscopy of electrical discharge machining plasma", J. Mat. Proc. Technol., 2004, Vol. 149, pp. 184–190.

CONCURRENT TREATMENT OF CHEMICAL AND BIOLOGICAL CONTAMINANTS IN WATER BY A PULSED ARC ELECTROHYDRAULIC DISCHARGE

J. S. CHANG AND K. URASHIMA
McIARS, McMaster University, Hamilton, Ontario, L8S 4M1
Canada

Abstract: Pulsed Arc Electrohydraulic Discharge (PAED) is one of the advanced oxidation and reduction technology for drinking and waste water treatments for multi-chemical pollutants and inactivation of biological contaminants. Water treatment in past was conducted by the remote plasma process such as ozone processes, where active species was generated by barrier discharge plasmas and injected into water. UV and electron beam processes were called indirect plasma method, where UV lights or electrons were generated under reduce gas pressure plasma and injected to water through windows. Electrohydraulic discharge (ED) is a direct plasma technology that has the ability to treat a wide range of aqueous contaminants within a single unit process, since it combines the both radical and UV processes. Among different ED techniques, the pulsed corona (PCED) deal with low current/high voltage and pulsed power (PPED) deal with high current/high voltage process. Pulsed arc electrohydraulic discharge (PAED) injects energy directly into an aqueous solution through a plasma channel formed by a high-current/high-voltage electrical discharge between two submersed electrodes. High frequency pulse spark electrohydraulic discharge characteristics are in between PCED and PAED. The process involves pulsed arc discharges within the water to be treated in order to initiate a variety of physical and chemical processes, including: UV irradiation, radical reactions, electron processes, ionic reactions, thermal dissociation, and pressure waves. In this work, a review of current on-going activity for PAED, PCED, HF PSED and PPED will be critically summarized, and recent PAED results will be introduced.

Keywords: Pulsed arc, electrohydraulics discharge, biological contaminants, chemical contaminants, inactivation, thermal plasma

1. Introduction

The application of plasma technologies for the treatment of drinking and waste water is not new. Three categories of plasma treatment technologies exist, including:

remote, indirect, and direct plasma methods. Remote plasma technologies involve plasma generation in a location away from the water to be treated, e.g. ozone generated by barrier discharge non-thermal plasmas (Chang 2001; Locke et al. 2005). Indirect plasma technologies generate plasma near to, but through the window, the water to be treated, e.g. UV generated in reduced pressure glow discharges or barrier discharges (Chang 2001; Locke et al. 2005), or electron beam generated in high vacuum and injected from Ti window (Chang 2001; Locke et al. 2005). More recently, direct plasma technologies (i.e., electrohydraulic discharge) have been developed that generate plasma directly within the water to be treated thereby increasing treatment efficiency (Chang 2001; Chang et al. 2002). Four types of electrohydraulic discharge systems, pulsed corona (PCED), pulsed arc (PAED), high frequency pulsed spark (HF PSED), and pulsed power (PPED) electrohydraulic discharges have been employed in numerous environmental applications (Chang 2001), including the removal of foreign objects (e.g., rust, biofilm, zebra mussels) (Kunitomo et al. 2003), disinfection (Sato et al. 1996; Emelko et al. 2003, 2004, 2006), chemical oxidation (Sun et al. 1999, 2000; Sato et al. 2000; Sharma 1993), and the decontamination of sludges (Warren et al. 1996a, b).

PAED may provide many benefits to the drinking and waste water industry as an additional tool in the multi-barrier approach to drinking and waste water treatment. PAED may have the ability to treat a wider range of contaminants concurrently than those of other conventional and emerging technologies (e.g., various classes of chemical contaminants and microbial contaminants); moreover, it is likely that PAED will be able to treat many of these contaminants concurrently due to the large range of physical and chemical reaction mechanisms generated by the process. Karpel Vel Leitner et al. (2001, 2006) observed both oxidation and reduction reactions induced by the PAED process when treating acids, atrazine etc. in water. Urashima et al. (2004), using PAED to treat ammonia compounds in water and chemical kinetics, observed both the oxidation and reduction as well as photolysis. Angeloni et al. (2007) treated MTBE by PAED and proposed oxidation may play a major role in the process based on ozone, hydrogen para-oxide and photo catalytic reactions.

This work will compare the characteristics of the pulsed corona, pulsed arc and pulsed power electrohydraulic discharge systems, discuss the treatment mechanisms generated by electrohydraulic discharge technologies, the application of these technologies to concurrent water treatment of chemical and biological contaminants in water by a PAED technique.

2.   Characteristics of Electrohydraulic Discharge Systems

The types of electrohydraulic discharge systems differ in several operational characteristics, as summarized in Table 1, due to their different configurations as well as the different amounts of energy injected into each type of system. The PCED system employs discharges in the range of 1 J/pulse, while the PAED and PPED systems use discharges in the range of 1 kJ/pulse and larger. The pulsed corona system operates at a frequency of 10^2 to 10^3 Hz with the peak current below 100 A and the voltage rise occurring on the order of nanoseconds. A

streamer-like corona is generated within the liquid to be treated, weak shock waves are formed, and a moderate number of bubbles are observed Teslenko et al. 1995). This system also generates weak UV radiation (Hoffman 1997) and forms radicals and reactive species in the narrow region near the discharge electrodes.

TABLE 1. Characteristics of electrohydraulic discharge systems

Property	Pulsed corona (PCED)	Pulsed arc (PAED)	Pulsed power (PPED)	Pulsed spark (PSED)
Operating frequency [Hz]	10^2–10^3	10^{-2}–10^2	10^{-3}–10^1	10^3–10^4
Current [A]	10^1–10^2	10^3–10^4	10^2–10^5	10^2–10^3
Voltage [V]	10^4–10^6	10^3–10^4	10^5–10^7	10^3–10^4
Voltage rise [s]	10^{-7}–10^{-9}	10^{-5}–10^{-6}	10^{-7}–10^{-9}	10^{-6}–10^{-8}
Pressure wave generation	Weak	Strong	Strong	Moderate
UV generation	Weak	Strong	Moderate	Weak

PAED employs the rapid discharge of stored electrical charge across a pair of submerged electrodes to generate electrohydraulic discharges forming a local plasma region. The PAED system operates at a frequency of 10^{-2}–10^2 Hz with the peak current above 10^3 A and the voltage rise occurring on the order of microseconds (Robinson 1973). An arc channel generates strong shock waves with a cavitation zone (Martin 1958) containing plasma bubbles (Robinson et al. 1973) and transient supercritical water conditions (Ben'Kovskii et al. 1974). This system generates strong UV radiation and high radical densities, which have been observed to be short-lived in the cavitation zone (Hoeben et al. 2000). Pulsed spark electrohydraulic discharge (PSED) system characteristics are similar to those of PCED, with a few characteristics falling between those of PCED and PAED. More recently, RF-bipolar PSED system was developed for inactivation of *E. coli* (Takeda et al. 2007).

The PPED system operates at a frequency of 10^{-3} to 10^1 Hz with the peak current in the range of 10^2–10^5 A (Willberg et al. 1996). The voltage rise occurs on the order of nanoseconds. This type of system generates strong shock waves and some moderate UV radiation.

3. Treatment Mechanisms Generated by Pulsed Arc Electrohydraulic Discharge

Conventional water treatment technologies can be broadly classified into three categories: biological, chemical and physical processes. However, many water systems are difficult to treat target compounds such as organics, such as MTBE, phenols, TCE, TCA, NDMA, etc., and pathogens, such as *Cryptosporidium*, viruses, etc. To be effectively removed from drinking water supplies, many of these recalcitrant compounds require specialized, and often target specific treatment technologies. Applying a multiple treatment technology can be quite

costly, especially for small plants and systems. In order to meet the challenges presented by continuously emerging contaminants and increasingly stringent regulations, new and promising treatment technologies, such as electrohydraulic discharge, must be developed (Chang et al. 2007a).

Depending on the technology, the treatment mechanisms generated by plasma technologies include (1) high electric fields; (2) radical reactions (e.g., ozone, hydrogen peroxide); (3) UV irradiation; (4) thermal reactions; (5) pressure waves; (6) electronic and ionic reactions; and (7) electromagnetic pulses (EMP) (Chang et al. 2007). In general, both electron and ion densities are proportional to the discharge current, while UV intensity, radical densities and the strength of the pressure waves generated are proportional to the discharge power. Direct plasma electrohydraulic discharge technologies have the potential to be more efficient than either indirect or remote plasma technologies as they capitalize, to some degree, on all of these mechanisms due to the direct application (Chang et al. 2007a, b). Figure 1 shows the treatment mechanisms initiated by PAED (Chang et al. 1998).
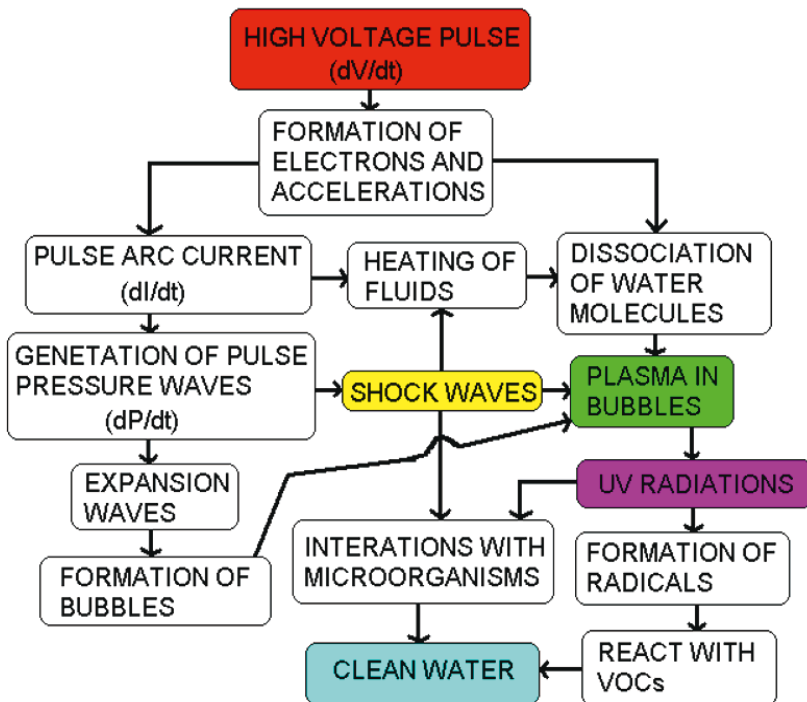
(b) Pulse arc

Figure 1. Water treatment mechanisms initiated by PAED. (After Chang et al. 1998)

A typical PAED reactor is shown in Fig. 2, where eccentric position of discharge electrode normally is optimized for better pressure wave generation. Typical discharge and pressure waveforms generated by PAED reactor are shown in

Figs. 3 and 4, respectively, where the results clearly support the treatment mechanism as proposed in Fig. 1. Typical PAED optical emission spectrum observed is shown in Fig. 5, where UV-A, UV-B, as well as UV-C, were observed.
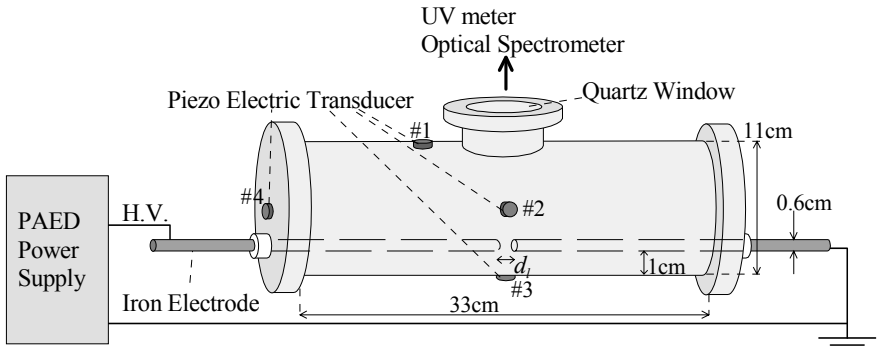
Figure 2. Schematics of typical PAED reactor (Yamatake et al. 2007)
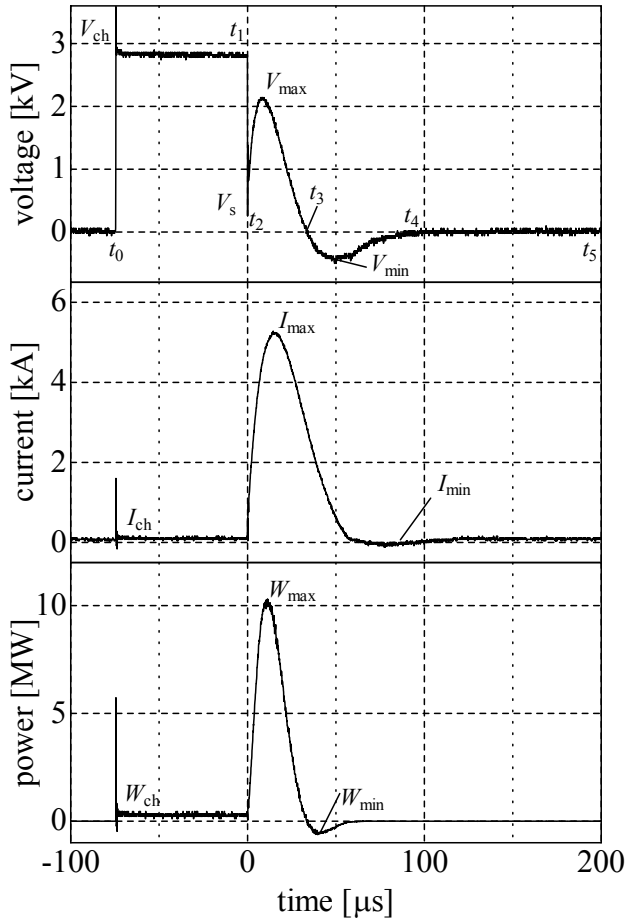
Figure 3. Typical PAED voltage, current and power waveforms (Yamatake et al. 2005)
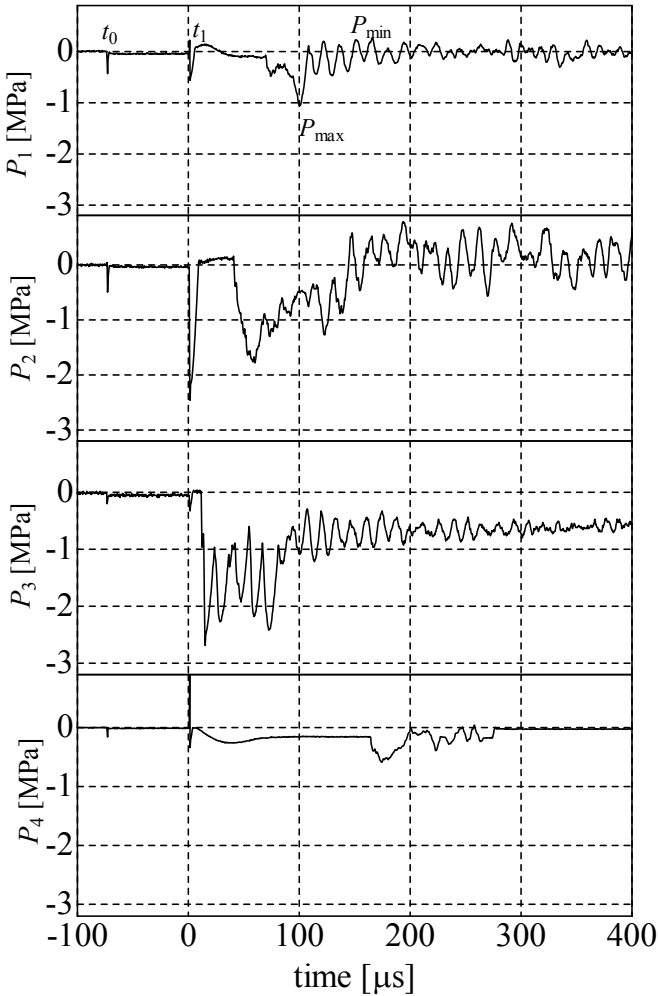
Figure 4. Typical PAED pressure wave (Yamatake et al. 2005)

Since electrohydraulic discharge systems do exploit all of the treatment mechanisms generated by the plasma reaction, both chemical and physical, these technologies have the ability to effectively treat a range of contaminants broader than that of other conventional and emerging technologies. Preliminary research has indicated that PAED offers advantages over indirect plasma methods in that it can provide comparable or superior treatment of microorganisms, algae, volatile organics, nitrogenous municipal waste compounds, and some inorganics; these results are qualitatively summarized in Table 2 (Chang 2001). Moreover, these benefits are available concurrently from one technology as opposed to a series of treatment technologies.
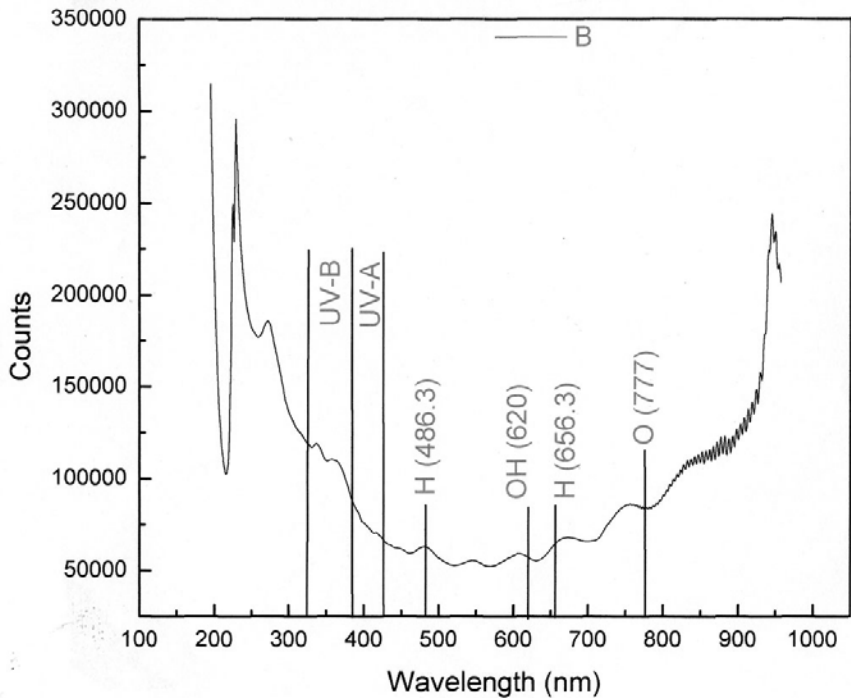
Figure 5. Typical PAED optical emission spectrum (Chang et al. 2007)

TABLE 2. Comparison of plasma and conventional water treatment processes (Chang 2001)

Target compounds	Cl/ClO$_2$	Ozone	Electron Beam	PCED	PAED	UV-C
Microorganisms	Adequate	Good	Adequate	Good	Good	Good
Algae	None	Partial	None	Partial	Good	Adequate
Urine components	Adequate	Good	Good	Good	Good	None
VOCs	None	Adequate	Good	Good	Adequate	None
Inorganics	None	Partial	Partial	Adequate	Adequate	None

4. Treatment of Chemical Contaminants by Pulsed Arc Electrohydraulic Discharge

Several studies have demonstrated that electrohydraulic discharge can effectively treat aqueous chemical contaminants such as atrazine, paraquinone, 4-chlorophenol, 3,4 dichloroanaline, phenol, dyes, urine compounds, MTBE, and 2,4,6-trinitrotoluene, as reviewed by Chang et al. (2007). Several investigations employing pulsed streamer corona discharge (PCED) have been conducted (Locke et al. 2005), however, it has been observed that organic compound treatment by

PCED requires the addition of activated carbon, a photocatalyst, or the superimposition of glow corona above the liquid surface (Locke et al. 2006). Willberg et al. (1996) investigated the removal of 4-chlorophenol [4-CP], 3,4-dichloroanaline [3,4-DCA] and 2,4,6-trinitrotoluene [TNT] by PPED. Lang et al. (1998) investigated the kinetics of TNT removal by PPED as a function of aqueous phase ozone concentration, pH, discharge energy, and water gap distance.

Karpel Vel Leitner et al. (2006) identified various reaction mechanisms initiated by PAED by treating various molecules with known degradation pathways. They employed both maleic and fumaric acids, which are known to photoisomerize by UV radiation, to confirm the presence of UV radiation in PAED systems. Approximately 35% of the maleate and fumarate ions removed in their experiments were converted to fumarate and maleate ions respectively. It was therefore concluded that PAED does induce photochemical reactions, but that photolysis is not the only phenomenon responsible for the abatement of these molecules. Karpel Vel Leitner et al. also treated solutions of nitrate ions to demonstrate reduction reactions. They observed that 75–86% of the nitrate ions removed were converted to nitrites, and concluded that reducing species played a significant role in the transformation, as photolysis alone could not account for the observed nitrite production. Karpel Vel Leitner et al. investigated the presence of oxidizing species on aqueous solutions of hydroquinone. Although the hydroquinone was oxidized, the study was not able to identify the mechanism responsible for the oxidation reaction.

Karpel Vel Leitner et al. (2006) investigated the effect of various additives, initial concentration, and operating conditions on the degradation of atrazine by PAED. Several additives were considered, including bicarbonate, dihydrogen-phosphate, and hydrogen peroxide; PAED alone, with no additives, constituted the reference case. The hydrogen peroxide had no significant effect on degradation of atrazine by PAED, and that both bicarbonate and dihydrogenphosphate addition inhibited the removal of atrazine by PAED.

Angeloni et al. (2007) investigated the effects of initial solution pH, charging voltage, detention time (i.e., cumulative input energy) and water-arc-electrode gapon the removal of methyl-tert butyl ether (MTBE) from an aqueous solution by PAED. The experimental investigation indicated that the initial solution pH did not have a significant effect on MTBE removal; however the MTBE decom-position increased with increasing charging voltage and increasing detention times. MTBE decomposition decreased with increasing water-arc gap distances; this was attributed to the fact that PAED discharges weaken with increasing water-arc gap distances. UV photolysis was not considered to be a mechanism of MTBE decomposition. No significant liquid MTBE decomposition by-products were observed as ozone or hydrogen para-oxide treatments.

5.   Disinfection of Pathogenic Contaminants by PAED

The relative ease of disinfection of *E. coli*, as compared to protozoan pathogens such as *Cryptosporidium parvum*, is commonly studied. *E. coli* disinfection has been achieved with several treatment technologies, including UV irradiation. Many strains of *E. coli* have demonstrated an ability to repair after irradiation with low- and medium-pressure UV. *E. coli* inactivation by electrohydraulic discharge was reported by Ching et al. (2001), who employed PPED. Emelko et al. (2002, 2004, 2006) investigated the disinfection of *E. coli*, *B. subtilis* and MS-2 suspension by PAED with 0.3 kJ/pulse at 2.2 kV and a water gap of 1 mm. Figure 6 shows the $\log_{10}$ inactivation of *E. coli* cells, MS-2 and *B. subtilis* in PBS as a function of the cumulative power input per liter of solution treated. This result clearly indicates average *E. coli*, MS-2 and *B. subtilis* inactivation. The pattern of *E. coli* inactivation observed by Emelko et al. (2006) is similar to that observed by Ching et al. (2001) (PPED), in that the rate of inactivation is initially high, and decreases as the cumulative power input increases.
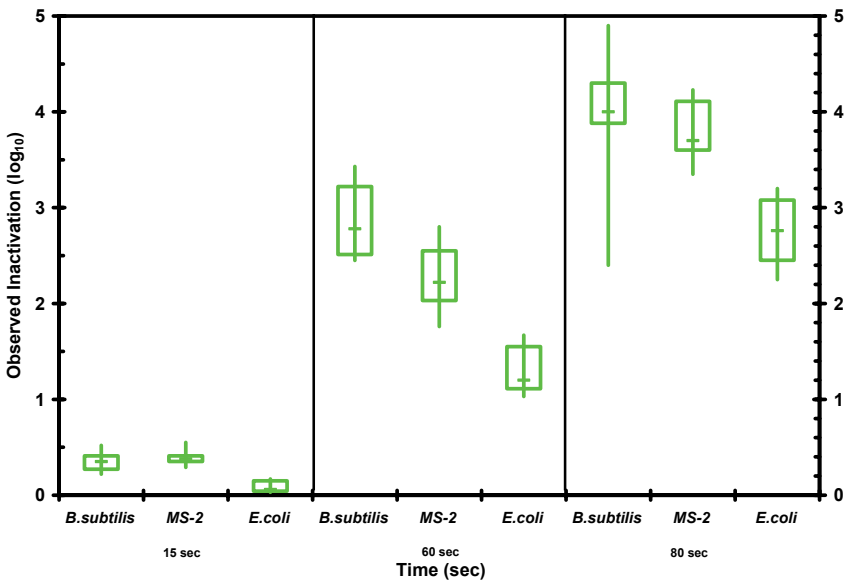
Figure 6. Box and whisker plots of *E. coli*, MS-2 and *B. subtilis* (suspended in 0.01 M PBS) inactivation by PAED. V = 2.2 kV, E = 0.3 kJ/pulse, pH 7.4, water gap = 1 mm. (After Emelko et al., 2006)

6.   Concluding Remarks

This work conducted a review of the application of direct plasma electrohydraulic discharge technologies to the removal/inactivation of chemical and microbial contaminants in water. The pulsed arc electrohydraulic discharge technologies,

PAED, generate a range of treatment mechanisms, both chemical and mechanical, suitable for removing/inactivating both chemical and microbial contaminants. The results of bench-scale PAED experiments show the potential to treat these contaminants as effectively, and more economically, than conventional treatment technologies. The optimization of the reactor for a range of operating conditions, a more complete understanding of the reactions initiated by PAED, potential additives and catalysts to the reactions initiated, hazardous by-product formation, and the economics as compared to more conventional treatment technologies are required to be investigated.

Acknowledgement

References

Angeloni DM, Dickson SE, Emelko MB, Chang, JS (2007) Jpn J Appl Phys 45:8290–8293
Ben'Kovskii VG, Golubnichii PI, Maslennikov SI (1974) Phys Acoust 20:20
Chang JS (2001) Sci Technol Adv Mat 2:571–576
Chang JS, Looy PC, Urashima K, Bryden AD, Yoshimura K (1998) Proc. Asia-Pacific AOT Workshop, pp. 148–158
Chang JS, Urashima K, Uchida Y, Kaneda T (2002) Research Report of Tokyo Denki University – Tokyo. Denki Daigaku Kogaku Kenku J 50:1–12
Chang JS, Dickson SE, Guo Y, Urashima K, Emelko MB (2007a) Electrohydraulic Discharge Direct Plasma Water Treatment Processes. In: d'Agostino R (ed) Advanced Plasma Technology, Wiley-VCH Verlag
Chang JS, Ukai H, Ono S, Sato, M, Teii S, Liu, Ting (2007b) Int. J. Plasma Envir. Sci. & Tech.,1 (2),130–134
Ching WK, Colussi AJ, Sun HJ, Nealson H, Hoffmann MR (2001) Environ Sci Technol 35:20:4139–4144
Emelko MB, Dickson SE, Chang JS (2003) Proc. AWWA Water Quality Technology Conference, Pittsburgh, PA: AWWA
Emelko MB, Dickson SE, Chang JS, Lee L (2004). Proc. AWWA Water Quality Technology Conference, San Antonio, TX: AWWA
Emelko MB, Dickson SE, Chang JS, Lee L (2006) AP-GORT Meeting, Dalian, China
Hoeben WFLM, van Veldhuizen, EM, Rutgers, WR, Kroesen, GMW (2000) J Phys D: Appl Phys 32: L133
Hoffman MR (1997) Proc. 2nd Int Environ Appl Adv Oxid Tech, EPRI Report CR-107581

Karpel Vel Leitner N, Urashima K, Bryden A, Ramot H, Touchard G, Chang JS (2001) Proc. 3rd Int Symp Non-Thermal Plasmas, April 23–27. Chang JS, Kim J (eds.), Kimm Press, Tajun, Korea

Karpel Vel Leitner N, Syoen G, Romat H, Urashima K, Chang JS (2006) Water Research 39:4705–4714

Kunitomo S, Obo T (2003) Proc. 14th IEEE Int. Pulse Power Conf. M. Giesselman M, Neuber A (eds.) IEEE-NPSS

Lang PS, Ching WK, Willberg DM, Hoffmann MR (1998) Environ Sci Technol 32(20):3142–3148

Locke BR, Sato M, Sunka P, Hoffman MR, Chang JS (2005) Ind Eng Chem Res 45: 882–905

Martin EA (1958) J Appl Phys 31:255

Robinson JW (1973) J Appl Phys 44:76

Robinson JW, Ham M, Balaster AN (1973) J Appl Phys 44:72–75

Sato M, Ohgiyama T, Clements JS (1996) IEEE Trans Indust Appl 32:106–112

Sato M, Yamada Y, Sugiarto AT (2000) Trans Inst Fluid Flow Machine 107:95

Sharma AK, Locke BR, Arce P, Finney WC (1993) J Hazard Waste and Hazard Mater 10:209–219

Sun B, Sato M, Clements JS (1999) J Phys D: Appl Phys 32:1

Sun B, Sato M, Clements JS (2000) Environ Sci Technol 34:509

Takeda T, Baroch P, Ishizaki T, Saito N, Ohta M, Takai O (2007) Int Symp Plasma Chem (ISPC-18) Abstract. Book, p. 733

Teslenko VS, Zhukov AJ, Mitrofanov VV (1995) Lett ZhTF 21:20–26

Urashima K., Chang JS, Uchida Y (2004) Proc. ISNTP-4, pp. 93–97

Warren D, Russel J, Siddon T (1996a) Proc. AOT-3, Cincinnati, Oct. 27–29

Warren D, Russel J, Siddon T (1996b) Presentation of 3rd Int Conf on Adv Oxidation Tech, Cincinnati, Oct. 27–29

Willberg DM, Lang PS, Hochemer RH, Kratel A, Hoffmann MR (1996) Environ Sci Technol 30(8):2526–2534

Yamatake A, Angeloni DM, Dickson SE, Emelko MB, Yasuoka K, Chang JS (2007) Jpn J Appl Phys 45:8298–8301

Yamatake A, Angeloni DM, Dickson SE, Emelko MB, Yasuoka K, Chang JS (2005) Proc. APSPT-2005 Meeting

2. PLASMA FOR CHEMICAL DECONTAMINATION

MULTI-POLLUTANT GAS REMOVAL CHARACTERISTICS OF CORONA DISCHARGE RADICAL SHOWER-CATALYST HYBRID SYSTEM FOR TREATMENT OF JET ENGINE TEST CELL FLUE GASES

K. URASHIMA AND J. S. CHANG
McIARS and Department of Engineering Physics, McMaster University, Hamilton, Ontario, Canada

Abstract: Acid gas removal experiments carried out in a large bench scale and semi-pilot scale corona radical shower-catalyst hybrid system are reviewed. The results show that both the removal efficiencies of NO and SO_2 increase with increasing applied power. It is also shown that injection of NH_3 or CH_4 radical in flue gas have an enhancement of reduction effect on NO removal, where the part of the NO is converted only to NO_2 but not to ammonium nitrate aerosol particles or reductions to N_2 and H_2O. The effect of heating of catalyst is significant with CH_4 injections without catalyst heating for NO_x and SO_2 removals. However, SO_2 removal efficiently is degraded by catalyst heating. In this work, a large scale laboratory study, semi-pilot scale tests in real jet engine test cell and economic evaluation were reviewed.

NO_x and SO_x are air pollutants of concern and the major cause of acid rain. Many NO_x and SO_x conversion techniques such as wet scrubber, selective catalytic reactor, sorbent injection, low NO_x burner, etc., have been used. More recently, non-thermal plasma techniques have been used in commercial plants, however, the energy efficiency of the non-thermal plasma reactors have not yet been optimized. For example, the electron beam, barrier discharge and pulsed corona reactors, i.e. direct plasma treatments of flue gases, may lose input energy to activate unwanted components of flue gases such as CO_2, N_2, etc. Hence, the corona discharge radical injection techniques have been developed (Okhubo et al. 1996; Park et al. 1997; Chang et al. 1998). In the corona discharge radical injection techniques, NH_3 or CH_4 mixture with Ar, N_2 or dry air wire injected to flue gas via corona discharge, hence NH_x, CH_y, N_x^*, and O_y^* (x = 1 or 2, y = 1, 2 or 3) radicals were more selectively produced with an optimum energy loss to the flue gas main component molecules, On the other hand, the treatment of an engine combustion flue gas by non-thermal plasmas have been investigated by many researchers, where the most of works based on the direct plasma oxidation of NO to NO_2 (Hoard and Balmer 1997) and reduction of NO_2 by a catalyst (Penetrante et al. 1997; Hackam and Akiyama 2000). However, no simultaneous removal of NO_x

and SO_2 from engine flue gas was attempted by a non-thermal plasma reactor (Hoard and Balmer 1997; Higashi et al. 1992; Hammer et al. 1999). In this work, an experimental investigation has been conducted to remove NO_x and SO_2 from low concentration of simulated combustion flue gases by corona discharge radical shower-catalyst hybrid system.

Keywords: Jet engine test cell, radical shower, corona discharge, plasma-catalyst, multi-pollutants

1. Jet Engine Test Cell Flue Gas Environments

A typical time evolution of the NO concentrations ("NO_{in}" in the figure) in the exhaust gas from a jet engine test cell (JETC) during an Air Force "Acceptance Test" (Haythornthwaite et al. 1997a, b; Spicer et al. 1992) is pulse operating mode with 20 to 30 minute period. The NO concentration is quite time-varying, because a load condition on the engine is not held for more than several minutes in the test. The exhaust gas from jet engines is diluted with the air in a JETC by as much as 20 times in order to cool down the gas and to dissipate a portion of the kinetic energy. The NO_x concentration at the exit of JETC is, therefore, low and 36 ppm at maximum. The exhaust gas flow rates from a JETC are also time-varying correspondingly, and reach as high as 6.80×10^6 m^3/h at maximum. The exhaust gas temperature is lowered by dilution and is somewhere between the ambient temperature and 100°C. The NO_x removal system for a JETC must be able to handle such a high flow rate with low temperature and follow their large and rapid time evolutions.

The typical emissions from JETCs (Spicer et al. 1992) are as follows:

Emission	Amount [ton/year]
Particulates	26.721
PM^{-10}	4.454
SO_x	30.712
NO_x	113.010
HC	100.450
CO	156.335

The data were taken at Tinker Jet Engine Test Cells 112 in 1995, where 3,414,836 gallons of JP-5 Fuel were used in the year (Haythornthwaite et al. 1997a, b). Air toxic emissions are included in HC (hydrocarbon). The main VOCs (volatile organic compounds) are acetaldehyde (4.65%WT) and formaldehyde (15.01%WT).

By fixing the NO_x concentration to 36 ppm of NO, the volume concentrations of the other gas components are as follows:

Species	Concentration [ppm]	notes
SO_x	4.59	SO_2 base
NO_x	36.00	NO base
HC	60.00	CH_4 base
	(32.00	CH_2O base)
CO	53.36	

The concentrations of CO_2, H_2O and O_2 in the exhaust gas from JETC are not available in literatures. We may assume these values approach the ones of those in the air because of the high dilution with the ambient air.

The other important aspect is the sensitivity of the engines to backpressure so that the pressure drop in the NO_x removal system must be low enough not to interfere with the engines.

2.   Laboratory Experimental Apparatus

The experimental apparatus is shown in Fig. 1. In the present simulated flue gas which is contents NO, SO_2, air and toluene, toluene has been used as hydrocarbon. The concentration ratio between NO-SO_2 and air-NH_3 or air-CH_4 is fixed at 1 mole ratio; then NO, SO_2 and Toluene initial concentration were fixed at 10, 5 and 30 ppm, respectively. NO, NO_2 and SO_2 concentrations were measured by a Green Line gas analyzer and the trace by-products are determined by Fourier Transform Infra-Red spectroscopy (FTIR). The aerosol particles generated by the acid gases and CH_4 related plasma processes were collected by the electrostatic precipitator operated at 19 kV dc downstream of the reactor. The size of the reactor is ($10 \times 30 \times 100$ cm) and three radical injectors were placed in series. The corona radical shower electrode used a 6 mm o.d. tube equipped with 28 hollow electrodes (1.2 mm i.d./1.5 mm o.d.). Additional gas consisting of an air-NH_3 or air-CH_4 mixture was injected from these hollow electrodes to the reactor via the corona discharge generated by a positive dc high voltage at the edge of the hollow electrodes. Catalyst (Pd + Pd/Rd, TENNECO, No. 15147) was placed 20 cm downstream of corona shower reactor and electrically heated by heating tapes.

3. Mechanism of Corona Discharge Radical Injection for SO$_2$ and NO$_x$ Removal Processes

The addition of NH$_3$ or CH$_4$ in a flue gas significantly reduces NO formations and NO$_x$ reductions in an energetic electron induced plasma in hollow electrode exists due to the dissociation of CH$_4$ and H$_2$O to NH, NH$_2$, OH and H. Chang (1989), Ohkubo et al. (1996) analyzed that the following reduction and oxidation reactions will be playing an important role in the NO$_x$ removal processes:

$$NO + NH_2 \rightarrow H_2O + N_2; \qquad k = 2.1 \times 10^{-11} \text{ [cm}^3\text{/s]} \qquad (1)$$

$$NO + NH \rightarrow N_2 + OH; \qquad k = 4.7 \times 10^{-11} \text{ [cm}^3\text{/s]} \qquad (2)$$

$$NO + OH + N_2 \rightarrow HNO_2 + N_2; \qquad k = 6.7 \times 10^{-31} \text{ [cm}^6\text{/s]} \qquad (3)$$

$$NO + H + H \rightarrow HNO + H; \qquad k = 3.5 \times 10^{-32} \text{ [cm}^6\text{/s]} \qquad (4)$$

$$NO_2 + H \rightarrow OH + NO; \qquad k = 1.1 \times 10^{-10} \text{ [cm}^3\text{/s]} \qquad (5)$$

$$NO_2 + OH + N_2 \rightarrow HNO_3 + N_2; \qquad k = 2.6 \times 10^{-30} \text{ [cm}^6\text{/s]} \qquad (6)$$

$$NO + N^* \rightarrow N_2 + O \qquad (7)$$

$$NO_2 + N^* \rightarrow N_2 + O \qquad (8)$$

where N* is the excited state nitrogen. Among the above reactions, oxidation reactions (3), (4) and (6) will become to form ammonium nitrate aerosol particles [13–15] as follows:

$$HNO_3 \text{ (g)} + NH3 \text{ (g)} \rightarrow NH_4 NO_3 \text{ (S)} \qquad (9)$$

For the SO$_2$ removal processes, radicals generated by corona discharges mainly action as oxidation processes as follows (Chang and Masuda 1988):

$$O + SO_2 + M \rightarrow SO_3 + M; k = 8.2 \times 10^{-32} \text{ [cm}^6\text{/s]} \qquad (10)$$

$$SO_3 + H_2O \rightarrow H_2SO_4 \qquad (11)$$

$$H_2SO_4(g) + 2NH_3 \text{ (g)} \rightarrow (NH_4)_2 SO_4 \text{ (s)} \qquad (12)$$
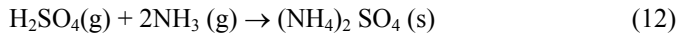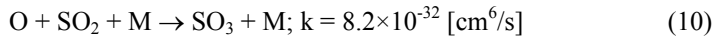
Hence, ammonium sulphate aerosol particles will be generated.

A detailed kinetic mechanism of methane (natural gas) reburning has been proposed by Glarborg et al. (1986), Miller and Boman (1991), and Kilpinen et al. (1992). All of these models proposed that methane radicals CH$_x$ produced by the reburning zone heat will react with N, O and H to form NH and NH$_2$ radicals via H$_x$N$_y$C$_z$O$_m$ (x, y, z, m = 0 or 1). Hence, these ammonia radicals can be reduced NO$_x$ via reactions (1) to (8). In an energetic electron induced plasma, various ionic and electronic processes (Chang et al. 1991; Vercammen et al. 1997; Urashima and Chang 2000) will generate these methane radicals instead of thermal processes in reburning as follows:

(i)   Direct electron impact dissociation

$$CH_4 + e \rightarrow CH_3 + H + e \qquad (13)$$
$$\rightarrow CH_2 + H_2 + e$$
$$\rightarrow CH + H_2 + H + e$$
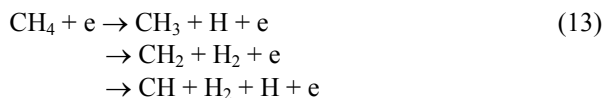
(ii)   Electron impact ionization/dissociative recombination

$$CH_4 + e \rightarrow CH_x^+ + H_y + 2e \text{ (x = 0–4, y = 0–2)} \qquad \rightarrow H^+ + CH_3 + 2e \quad (14)$$
$$CH_x^+ + e \text{ or } X^- \rightarrow CH_z + ZH \text{ (x = 0–3)} \qquad\qquad\qquad (15)$$
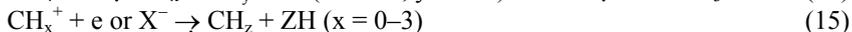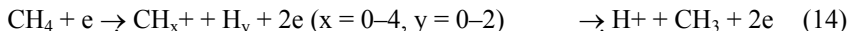
where X^- is the all negative ions and Y is the dissociative recombination by-products.

(iii)   Ion-molecule reaction/dissociative recombination

$$Z^+ + CH4 \rightarrow CH_x^+ + ZH \text{ (x = 0–3)}$$
$$X^- + CH_4 \rightarrow CH_m^+ + xH \text{ (m = 0–3)}$$
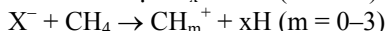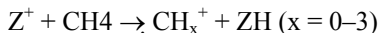
where Z^+ is the all positive ions. Based on above analyses, the methane radical injection is similar to ammonia radical injection SO_2 and NO_x removal processes.

4.   Experimental Results for Laboratory Study

4.1.   COMPARISON OF RADICAL INJECTION GASES

Acid gas (NO_x, NO and SO_2) removal efficiency as a function of corona shower system applied power for NH_3 or CH_4 radical injection, and gas temperature at catalyst exist $T_g = 293$ K are shown in Figs. 2 and 3 for downstream of the catalyst. Figure 3 shows that acid gas removal efficiencies increase with increasing applied power, 100% of NO removal and up to 40% of SO_2 and 54% of NO_x can be removed by the non-thermal plasma system with NH_3 radical injections at room temperature. Figure 3 also shows that NO reduction rate is increasing with increasing applied power but no reduction rate observed for SO_2. By comparing with Figs. 2 and 3, the NO concentration is decreasing up to 15 W both NH_3 and CH_4 injection case, however, low NO_x reduction rate observed at NH_3 injection than CH_4 injection case. For SO_2 treatment, no reduction rate observed with CH_4 injection.

The catalyst even operated at room temperatures that can significantly enhance SO_2 and NO_x removal due to the NH_x radical generated by the corona shower reactor with NH_3 injections (Kanazawa et al. 1997) as has been observed by various investigators using pulsed corona or barrier discharge non-thermal plasma reactor (Oda and Shimizu 1999; Kim et al. 1999). For NO_x removal, the role of catalyst is mainly NO_2 catalytic reductions and maybe adsorption/surface reaction and/or catalytic reactions for SO_2 and SO_3.

Figure 3 shows that NO removal efficiency can reach up to 100% with NH_3 injection due to the heterogeneous reactions at the surface of ammonium sulphate aerosol particles collected by an electrostatic precipitator (Chang et al. 1991; Kanazawa et al. 1998); however, no significant NO_x removal efficiency is improved. By comparison with NO_x removal with NH_3 or CH_4 injections, NH_3 injection shows much higher (up to 62%) NO_x removal efficiency than that of CH_4 injections due to the more effective generation of NH_x radicals and aerosol particles (Urashima et al. 1999a, b, 2007).

4.2. EFFECT OF CATALYST HEATING

The effect of heating catalyst on the acid gas removal characteristics is shown in Fig. 4, where the gas temperature observed at the exit of catalyst is T_g = 339 K. The NO_x and SO_2 removal rate increased with increasing applied power and up to 100% of NO and 67% of SO_2 reduced.

By comparison between Figs. 3 and 4, the effect of heating catalyst (monitored by catalyst exist gas temperatures) shows high SO_2 removal rate CH_4 injection. However, NO_x removal efficiency is no too much difference with and without heating of catalyst. It maybe caused of adsorption capability of ceramic catalyst under higher temperature. Maximum NO_x removal efficiency is almost the same for NH_3 or CH_4 injections but SO_2 removal with NH_3 injections is much higher compared with CH_4 injections.

The energy efficiency of the process is calculated based on the energy yield (x g of NO_x or SO_2 are removed by 1 kWh of electrical energy input) and the specific energy density (electrical energy input (W) to the flue gas per gas flow rate Nm^3/h). Here, 1 $[Wh/m^3]$ is corresponding to 3.6 [J/L]. Approximately 45 g of SO_2 and 20 g of NO_x were removed by 1 kWh of energy input in the present system without heating catalyst.

5. Concluding Remarks for Laboratory Study

In this work, an experimental investigation has been conducted to remove low concentration of NO_x and SO_2 from combustion flue gases with Toluene by corona discharge methane radical shower-catalyst hybrid system. An experimental investigation has been conducted to remove acid gases from stationary engine flue gas and the following concluding remarks are obtained: (1) NO, NO_x and SO_2 removal efficiencies increase with increasing applied power; (2) High NO reduction rate observed with NH_3 injection at room temperature, however, NO_x reduction rate is lower more than with CH_4 injection; and (3) SO_2 reduction rate increased with heating of catalyst at CH_4 injection.

6. Semi-Pilot Experimental Apparatus

6.1. EXPERIMENTAL SET-UP FOR SEMI-PILOT TEST

The experimental apparatus is shown in Fig. 5. The semi-pilot plant were consist of three part, exhaust gas from engine, gas treatment apparatus (corona radical shower-catalyst hybrid system) as shown in Fig. 6 and gas sampling part. The corona radical shower electrode was a 4 mm o.d. tube equipped with 56 hollow electrodes (1 mm i.d./1.5 mm o.d.) as shown in Fig. 7.

Additional gas consisting of an air-NH_3 mixture was injected through these hollow electrodes to the reactor via the corona discharge generated by a positive dc high voltage at the edge of the hollow electrodes. The applied voltage for

corona radical injection is 22–28 kV and injected ammonia concentration ratio for NO and SO_2 are from 0.5 to 1 mol ratio. Two parallel channels of tree way catalytic converters limited test loop flow rate optimum at 75 Nm^3/h. The exhaust gas from JETC was carried to the reactor trailer through about 23 m of insulated, plastic-lined, air-handling ductwork. NO, NO_2 and SO_2 concentrations and the trace by-products were determined by Fourier Transform Infrared spectroscopy (FTIR). The catalyst is placed downstream of the corona shower reactor.

6.2. EXPERIMENTAL CONDITION

In stationary engine flue gas treatment, the combustion flue gas is normally diluted with air for cooling down to room temperature. Figures 8 and 9 show gaseous pollutants (NO_x, CO, VOC) concentrations and particulate matter concentration respectively for JETC exhaust fuel gas as a function of engine exhaust temperature.

The part of exhaust gas from JETC, the flow rate between 28.68–152.52 Nm^3/h was exhaust for the present test. The initial main gas condition and the calculated annual emission inventory volume are shown in Table 1. The data were taken at JETCs, where 3,414,836 gallons of JP-5 Fuel were used in the year (Spicer et al. 1992). Air toxic emissions are included in HC (hydrocarbon). The main VOCs (volatile organic compounds) are acetaldehyde (4.65%WT) and formaldehyde (15.01%WT). Means of calculating inventories for air pollutants arising from such sources have been formulated and documented.

TABLE 1. Typical exhaust gas composition from JETC (Spicer et al. 1992)

	NO	NO_2	N_2O	SO_2	CO	VOC
ppm	~7	~1	~0.5	~5	55	60
	N_2, O_2, CO_2, H_2O			Carbon soot		
Vol.	Rest			~800 $\mu g/m^3$		

7. Experimental Results for Semi-Pilot Tests

7.1. CURRENT-VOLTAGE CHARACTERISTICS

The time averaged current-voltage characteristics at gas temperature 25°C and 75°C are shown in Fig. 10. The time averaged current or power increases with increasing applied dc voltage. The result indicated that the corona discharge on-set around 22 kV and the maximum current was up to 24 mA before on-set of spark discharge.

7.2. POLLUTANT GAS REMOVAL EFFICIENCY

Acid gas (NO_x, NO_y and SO_2) removal efficiency as a function of gas flow rate is shown in Fig. 11. Figure 11 shows that NO and SO_x removal efficiencies are

100% up to gas flow rate of 110 Nm^3/h, and NO_x and NO_y removal efficiencies slightly decrease with increasing gas flow rate up to 75 Nm^3/h where limitation of the present apparatus capacity. The gas flow rate significantly influenced NO_x and NO_y removal efficiencies due to the residence time of NH_x radical generated by the corona shower reactor with NH_3 injection (Chang et al. 1996). For NO_x removal, the role of catalyst was mainly NO_2 catalytic reductions and maybe adsorption and/or catalytic reactions for SO_2 and SO_3. Figure 11 also shows that the NO_x and NO_y can be removed up to 81 and 46%, respectively, up to flue gas flow rate of 75 Nm^3/h, i.e. the present design limits of corona shower-catalyst hybrid system. Detail by-products analyses also show that the parts of hydro-carbon were oxidised and the unwanted by-products such as CO and aldehyde formed are below 5 and 0.5 ppm, respectively. However, no significant discharge generated ozone (<0.2 ppm) and slip ammonia (below detection limit: BDL) were observed at downstream of corona shower-catalyst hybrid system.

7.3. ENERGY EFFICIENCY

Energy efficiency of acid gas treatments was indicated by the energy yield of NO_x or SO_x pollutants, where the energy yield was defined by [g (NO_x or SO_x)] removed by [1 kWh] of electric power inputs. The experimental results in Fig. 11 shows that the maximum of 1.9 NO_x and 11.7 g/kWh SO_2 energy efficiency can be obtained by the specific energy density of 3.6 and 1.7 Wh/m^3, respectively.

Detail particulate nitrate and sulphate contents collected at upstream and downstream of corona radical shower-catalyst system are compared in Table 2. Table 2 shows that clearly that the corona radical shower-catalyst system not only reduces acid gas but also the part of acid gas converted by oxidation processes to form ion-induced particle formations (Chang et al. 1991; Park et al. 1999).

TABLE 2. Particle acid residue analysis results (Rosocha et al. 2001)

Reactor	Nitrate		Sulphate	
	(μg)	(μg/cm^2)	(μg)	(μg/cm^2)
Inlet	4286	18.32	42.3	0.18
Outlet	17441	63.89	67.7	0.25
Wipe	35415	68.11	112.0	0.22

8. Economic Model

The computer code to predict scale-up and economic evaluation of several eligible non-thermal plasma processes for air pollution control was developed for a com-mercial power plant (Urashima et al. 2003). The data obtained from pilot-plant tests are input with general data to provide information for the conceptual design of scaled-up commercial plants. Economic evaluations are needed not only for the

selection of the best-matched technology for the operating facility, but also for providing guidance for future R&D on those technologies and to provide guidance to the users on viable, alternative NTP air-pollution control technologies. For the JETC applications, the SUENTP (Simulation of scale-up and economic evaluation of non-thermal plasma) Code (Urashima et al. 2003) was modified to evaluate, electron beam, pulsed corona, corona radical shower, wet-scrubber-SCR (Selective Catalytic Reduction) and SCR-electrostatic precipitator, i.e. the SUENTP-J Code (Rosocha et al. 2001). For an input data, the pulsed corona pilot tests results of Haythornthwaite et al. (1997a, b) was used without considered additional wet scrubber costs for NO to NO_2 conversion, and the electron beam pilot tests of Chang et al. (1996) for low density NO_x and SO_2 removals were used. The calculated total annual costs (a) and specific costs (b) for NO removal [\$/ton NO] as a function of JETC flue gas rate is shown in Fig. 12 for various control systems. The conventional SCR requires the gas heating and hence the costs increase with increasing flue gas flue rate. However, the specific costs of NO removal decrease with increasing flue gas flow rate for NTP system, since the system can be operated at ambient temperature. The total annua cost of corona shower process was almost the same as a pulsed corona system was shown in Fig. 12. However, pulsed corona case doesn't include wet scrubber, therefore it's easy to expect that the corona radical shower case was most economic technologies.

Conclusion

An experimental investigation has been conducted to remove acid gases from stationary engine flue gas and the following concluding remarks are obtained. The experimental results show that: (1) SO_2 and NO removals of 100% were obtained up to Q_f = 130 and 110 Nm^3/h, respectively; (2) the maximum NO_x and NO_y removals achieved were 81% and 46% respectively; (3) No significant ozone (<0.2 ppm) and ammonia (BDL) slips were observed; (4) Trace amounts of unwanted by-products such as CO (<5 ppm), aldehyde (<0.5 ppm), etc. were observed; and (5) The maximum 1.9 g/kWh of NO_x removal energy efficiency was obtained at a specific energy density of 3.6 Wh/m^3 while the maximum 11.7 g/kWh SO_2 removal energy efficiency was obtained at 1.9 Wh/m^3. Based on the pilot tests and economic evaluation plasma-catalyst-particulate trap system can be used in JETC system pollution control effectively and economically.

Acknowledgement

References

Chang JS (1989) J Aerosol Sci 20:1087–1090

Chang JS, Masuda S (1988) Conf Record of IEEE Ind Appl Soc 1988 Meeting 1645–1653

Chang, JS, Lawless PA, Yamamoto T (1991) IEEE Trans Plasma Sci 19:1151–1166

Chang JS, Kohno H, He W, Berezin AA, Looy PC, Iijima K, Honda S, Matsumoto Y, Shibuya A (1994) Acta Physica UC 35:5967

Chang JS, Looy PC, Aoki S, Kageyama Y, Okamoto K, Maezawa A (1996) Electron beam corona discharge radical shower injection hybrid systems for reduction of low density NOx from air stream. AOTs-3:39

Chang JS, Urashima K, Arqulla M, Ito T (1998) Comb Sci and Tech 133:31–47

Glarborg P, Miller JA, Kee RJ (1986) Combust Flame 65:177–202

Hackam R, Akiyama H (2000) IEEE Trans PEI 7:654–683

Hammer T, Broer S, Kishimoto T (1999) J Adv Oxid Tech 4:368–374

Haythornthwaite SM, Durham MD, Rugg D, Wander JD (1997a) Application of pulse-corona-induced plasma to jet engine test cells. Presented at the Air & Waste Management Association's 90th Annual Meeting & Exhibition, June 8–13, 1997, Toronto, Ontario, Canada

Haythornthwaite S, Anderson G, Durham M (1997b) NOx control from gas turbines by corona discharge. Presented at the Workshop on Applications of Electrostatics for Control of Gas Phase Air Pollutants, Aug. 22, 1997, Cincinnati, Ohio, USA

Higashi M, Uchida S, Suzuki N, Fujii K (1992) IEEE Trans Plasma Sci 20:1–12

Hoard JW, Lou Balmer M (1997) J Adv Oxid Tech 4:417–423

Kanazawa S, Chang JS, Round GF, Sheng G, Ohkubo T, Nomoto Y, Adachi T (1997) J Electrost 40&41:651–656

Kanazawa S, Chang JS, Round GF, Sheng G, Ohkubo T, Nomoto Y, Adachi T (1998) Comb Sci & Tech 133:93–105

Kilpinen P, Glarborg P, Hupa M (1992) Ind Eng Chem Res 31:147–1490

Kim H, Tsunoda K, Katsura S, Mizuno A (1999) IEEE Trans IAS 35: 1306–1310

Miller JA, Boman CT (1991) Int J Chem Kinetics 23:289–313

Oda T, Shimizu K (1999) J Adv Oxid Tech 4:352–357

Ohkubo T, Kanazawa S, Nomoto Y, Chang JS, Adachi T (1996) IEEE Trans Ind Appl 20:1058–1062

Park JY, Tomicic I, Round GF, Chang JS (1999) J Phys D: Appl Phys 32:1006–1011

Park JY, Urashima K, Chang JS, Kanazawa S, Ito T (1997) J Aerosol Sci 28:S399–S400

Penetrante BM, Bardsley JN, Hsiao MC (1997) Jpn J Appl Phys 36:5007–5017

Rosocha LA, Chang JS, Snyder HR, Urashima K, Miziolek AW (2001) Proc 3rd Int Symp Non-Thermal Plasma Pollut Control Tech: 105–110

Spicer CW, Holdre MW, Smith DL, Miller SE, Smith RN, D.P. Hughes DP (1992) Chemical composition of exhaust aircraft turbine engines. J Eng Gas Turbines and Power 144:111–117

Urashima K, Chang JS (2000) IEEE Trans DEI 7:602–614

Urashima K, Kim SJ, Chang JS (2003) J Adv Oxid Tech 6:123–131

Urashima K, Chang JS (2007) 2007 Tahiti Symp Non-Thermal Plasma and Electrost 36–40

Urashima K, Tong X, Chang JS, Miziolek A, Rosocha LA (1999a) SAE 99FL-258

Urashima K, Tong X, Miziolek A, Rosocha LA, Chang JS (1999b) Proc AOT-4

Vercammen KL, Berezin AA, Lox F, Chang JS (1997) Destruction of volatile organic compounds by non-thermal plasmas: a critical review. J Adv Oxid Tech 2:312–329

PULSED CORONA PLASMA PILOT PLANT FOR VOC ABATEMENT IN INDUSTRIAL STREAMS

A. FRIDMAN AND A. GUTSOL
Department of Mechanical Engineering and Mechanics, College of Engineering, Drexel University, Philadelphia, PA 19104 USA

Abstract: A pulsed corona plasma-based mobile pilot plant was developed for demonstration of the emerging technology for volatile organic compounds (VOC) abatement in industrial streams of paper and wood industry. Pilot plant development was sponsored by the U.S. Department of Energy (DOE) Office of Industrial Technologies in the framework of the Forest Products program. The heterogeneous pulsed corona discharge was chosen as the best non-equilibrium plasma approach for control of the vent emissions from Brownstock Washers in paper industry, and the pilot plant was initially designed for demonstration on this kind of vent stream. Later it was modified for possibility of operation in the wood industry where water discharge is prohibited. The technology base of the pilot plant, as well as history of its development and the results obtained during testing are presented in this paper. For VOCs of interest to the paper and wood industry, (methanol, acetone, dimethyl sulfide and α-pinene), high removal efficiencies were obtained with power consumptions competitive with the present technologies for the VOCs control.

Keywords: Pilot plant, plasma technology, pulsed corona, heterogeneous corona, VOC control, air cleaning

1. Prehistory and Motivation

There are many individual air pollutants and their classes that cause public and regulation concerns, for instance heavy metal vapors (Hg, Cd), NO_x, SO_x, soot and other particulates, ozone, CO_2, H_2S, Volatile Organic Compounds (VOCs), etc. A class of VOCs is a vaguely defined one, and the decision of whether or not a particular carbon-based substance belongs to this class depends mostly on legal regulations in a particular country. For simplicity and for the matter of this paper, any organic substance that has a measurable vapor pressure at room temperature can be considered as a VOC. So following this definition, almost all non-polymerized organic substances are VOCs. The most notorious VOCs are different kinds of mercaptans which have a very bed smell; the most dangerous VOCs are dioxins; and the most common are methanol, ethanol and acetone.

Almost all of these substances have some negative effect on the environment, and many technological processes (even those as simple as cooking food) produce some amount of VOCs as undesirable byproducts. In particular, the forest product and paper industries emit significant amounts of VOCs, and anyone can easily detect these emissions sensing their specific smells, for example, in the vicinity of a paper mill.

"Agenda 2020" of the DOE Office of Industrial Technologies, Forest Products program, set forth an agenda for the significant reduction of VOCs in the exhaust streams of paper and wood industry before the year 2020. Currently, there are very few VOC control options [1]: simple incineration that works well with high concentration streams, and more sophisticated thermal or catalyst based technologies for VOC oxidation in low concentration streams (recuperative or regenerative thermal oxidizers – RTOs). The major advantage of these oxidation based technologies is that they are not sensitive to a specific VOC. The major disadvantage is that they are energy intensive and expensive to build and operate. There are several emerging technologies like low-temperature catalytic oxidation, bio-filtration or bio-treatment, and low-temperature plasma oxidation. However, bio-treatment requires significant residence time which means very large size of appropriate facilities and catalysts have limited lifetimes and high operational costs.

In the research [2] sponsored by the National Council for Air and Stream Improvement (NCASI) it was shown that non-equilibrium plasma can be a base for development of the competitive technology for VOC control. Therefore in 2000, DOE Office of Industrial Technologies funded a project FWP 49885, "Experimental Assessment of Low-Temperature Plasma Technologies for Treating Volatile Organic Compound Emissions from Pulp Mills and Wood Products Plants." The goal of this project was to evaluate the applicability of various plasma technologies for VOC abatement in paper and wood industry. Based on the results presented in that report [18], four non-thermal plasma technologies were selected for testing: (1) dielectric packed bed corona discharge in the form of so-called Gas Phase Corona Reactor, GCPR, developed in the Pacific Northwest National Laboratory (PNNL); (2) electron beam discharge; (3) non-thermal gliding arc discharge; and (4) heterogeneous pulsed corona discharge. An appropriate team was gathered to run this project: PNNL was responsible for testing GCRP; University of Illinois at Chicago (UIC) was responsible for testing gliding arc (later they also run experiments with pulsed corona) and for the general project management; Ecos, Ltd, a spin-off of the Kurchatov Institute (Moscow, Russia) was responsible for testing the electron beam and heterogeneous pulsed corona discharge; Argonne National Laboratory (ANL) was responsible for interaction with industrial partner, Georgia Pacific, that was supposed to provide a place for testing of the technology to be selected.

2. Mechanism of Plasma Oxidation of VOCs and History of the Project

Gas phase hazardous organic wastes can be destroyed by oxidation to non-hazardous compounds, such as carbon dioxide and water. The most straightforward way of oxidizing organics is to use highly reactive species, i.e. reactants with a high oxidizing potential, such as OH, O, H, O_3, and H_2O_2. The hydroxyl radical is especially known to play an important role in oxidative purification and degradation of organic compounds [3]. In a combustion process, the efficiency of production and concentration of these free radicals and active species depend on the reaction temperature. In order to attain the required temperature, a considerable amount of energy must be spent for direct heating of the gas. To perform oxidation of VOCs in High Volume Low Concentration (HVLC) gas streams, some quantity of fuel must be added to promote effective combustion, since the concentration of organic material is not sufficient to sustain combustion by itself. To uniformly heat the whole gas stream by thermal plasma, a high amount of electric energy must be spent. Both these methods are inefficient in terms of production of active species [4].

Low-temperature non-equilibrium (non-thermal) plasma discharges represent an alternative approach for VOC removal. In non-thermal plasma most of the energy (up to 99.9% in some special cases) is directed into ionization [5], rather than into gas heating. Radicals, ions and other active species, which oxidize, reduce or decompose the pollutant molecules, are efficiently produced mainly via electron-impact dissociation, excitation and ionization of the background gas. This is in contrast to the mechanism involved in thermal incineration processes, which require heating the entire gas stream in order to destroy the pollutants. Non-equilibrium discharges have been tested for removal of a number of different toxic or environmentally hazardous compounds, such as SO_x, H_2S, VOCs, PAHs (Polycyclic Aromatic Hydrocarbons), heavy metals, and some others, like chemical warfare gases [6–12].

During the first year of the DOE funded research project, the team members studied the efficiency of different plasma systems in VOC removal from the simulated Brownstock Washer vent stream, which is typical for paper mills. The average composition and conditions of this stream are presented in Table 1.

TABLE 1. Estimated gas composition and process conditions for Brownstock Washer vent stream

Methanol	83 ppm
Acetone	3 ppm
α-pinene	209 ppm
Dimethyl sulfide	2 ppm
Humidity	100% RH
Temperature	317 K

Analysis of the results obtained during the first year of the project showed that the heterogeneous pulsed corona discharge looks like the best non-equilibrium plasma technology for control of VOCs in the HVLC vent emissions from Brownstock Washers. Laboratory experiments were carried out using installation with the average power below 20 W. For the compounds of interest (methanol, acetone, dimethylsulfide and α-pinene), high removal efficiencies were obtained with power levels competitive with RTO technologies [13]. More information about the research results obtained in the framework of the project and about the mechanisms of plasma cleaning can be found in [13,14]. These results and the willingness of the DOE to accelerate development of new technologies for VOC control allowed for initiation of an additional project with the goal of developing a trailer mounted pilot plant for testing in industrial conditions. The pilot plant (Fig. 1) initially was built for demonstration of heterogeneous pulsed corona plasma technology, and then it was modified for operation in the conditions of zero water discharge policy accepted by the wood product industry.

Figure 1. Picture of the Mobile Plasma Pilot Plant

It is worth while to describe the major challenges that appeared during the Pilot Plant design and manufacturing. The key idea that was suggested by our industrial partners was to make a mobile Pilot Plant, to allow for technology demonstrations at different industrial sites. Our experience showed that there are many drawbacks in this approach that were difficult to predict. The major challenge that appeared during the system design was the height limitation. The system in its initial technological approach contained two large volumes with water flows (see details below): a scrubber to remove particulates and soluble VOCs, and the heterogeneous corona reactor that required water mist motion downward. Creation of gravity fed uniform water flows in these two volumes requires either a significant height of the system, or an enormous number of water nozzles that are difficult to control. On the other hand, the total height of the Pilot Plant together with a trailer was limited by 4.115 m (13'6" – required height of

bridges in the USA road system). Significant efforts were spent to find a large (48' = 14.6 m) used trailer with a relatively low and flat deck that provide enough space for the Pilot Plant together with the appropriate analytical lab space (see Fig. 1). Funding limitations that always exist in R&D work did not allow purchase of a new or customized trailer.

Another immediate limitation that appeared was space restrictions that very often contradict safety requirements and service convenience. Pilot plant technicians were expected to work with high voltage equipment in limited space; expensive analytical equipment and high-voltage Pilot Plant equipment should be secured from the possibility of theft. All these contradictory requirements make the system design and integration process very complicated. Especially difficult is to make any modification or modernization of the system that is already built. For example, simple installation of oil-catching tanks under the oil-filled high-voltage transformers (requirement of industrial partner that appeared late) became a difficult engineering challenge.

A new round of problems appears when the progress comes to the issues where to storage the Pilot Plant and how to arrange maintenance and operational tests. Universities usually do not have secured space of this size. Later when the project leadership came to Drexel University, a special underground space with trailer access was found and renovated (Fig. 2) in the middle of the city of Philadelphia, and rent payments for this place are still collected from the project leaders.

Figure 2. Underground space with trailer access specially prepared for the Pilot Plant storage and maintenance

All these issues appeared to be solvable, and what later became a major problem was further cooperation with industry. As the Pilot Plant belongs to a university, an industrial partner should bear all kinds of liabilities when borrowing the plant for testing. As this plant is rather expensive, just one day of keeping it out of the storage space costs about \$1,000 in insurance alone. Even large companies usually do not have a budget for such expenses. Also, as a company did not participate in design of this plant, it is difficult to accept liabilities for all possible accidents that can happen during testing, and a university, as a non-profit organization, can not bear this kind of risk. Therefore these legal issues together with the issues related to Intellectual Properties (IP) moved negotiations about the field tests to a dead end. Because of internal re-organizational issues, the DOE lost interest in continuing the project, and therefore the Pilot Plant and the technology commercialization activity became the sole responsibility of Drexel University. Fortunately it was possible to arrange some tests on site and obtain results (included below) that raised interest of the companies in the environmental control industry; however, the commercialization process is moving very slow, and an opinion exists that the 'mobility' of the Pilot Plant played a rather negative role in the commercialization of the technology. The situation might be just opposite if the Pilot Plant belonged to a private company or to a National Laboratory with continuous and timely governmental support.

2. Pilot Plant Design and Parameters

The main part of the Pilot Plant, where the gas treatment process takes place, is the unified reaction chamber reaction chamber with complex inner structure that includes also a scrubber and a mist separator (Fig. 3). The chamber was designed and manufactured by Ecos, Ltd., and has the following dimensions (length-width-height): 2.9 m–1.3 m–2.56 m.

For maximum soluble dust and VOC removal, gas flow initially passes through a scrubber where the direction of the water motion is opposite to that of the gas stream. The scrubber volume is about 1 m^3 and the total water flow rate through 4 nozzles is about 0.5 m^3/h. The scrubber is filled with special low density high surface packed bed material. From the scrubber, the gas stream is directed to the pulsed corona chamber where plasma is combined with water spray. The direction of water droplet motion in this case is also opposite to the direction of gas stream. Compressed-air atomizers are used for spray formation (4 atomizers with total water flow rate about 0.5 m^3/h and compressed air flow rate about 20 SCFM – 40 m^3/h, air pressure 2 bars).

The pulse corona power system consists of 12 units (channels), and each of them includes a high-frequency converter with an intermediate frequency of 25 kHz on the base of field (IGBT) transistors, pulse high-voltage transformers, work capacitance and special high-voltage self-firing discharge gap for high voltage pulse formation on the corona electrodes. Discharge power is regulated by stepwise changing of the pulse repetition frequency in the range 20–100% (20%,

40%, 60%, 80%, and 100%). An additional method of the process regulation is gas flow rate control. Reduction of the flow rate means an increase of the residence time resulting in considerable increase of purification degree. In general, the pilot plant was designed to operate with a gas flow rate of 200–600 m³/h (100–300 SCFM). The main parameters of the corona discharge are the following: peak voltage is about 40 kV, pulse repetition frequency is up to 1 kHz, and pulse duration is of 200–250 ns. The structure of the pulsed corona discharge blocks (Fig. 4) consists of alternate rows of grounded and high-voltage electrodes. Such a structure provides transparency of the discharge volume for the water spray. Plasma discharge zone is formed by 12 corona blocks installed in three layers (Fig. 5). Total discharge volume is about 3.6 m³.The total consumed power of the corona unit was measure to be 8.5 kW.
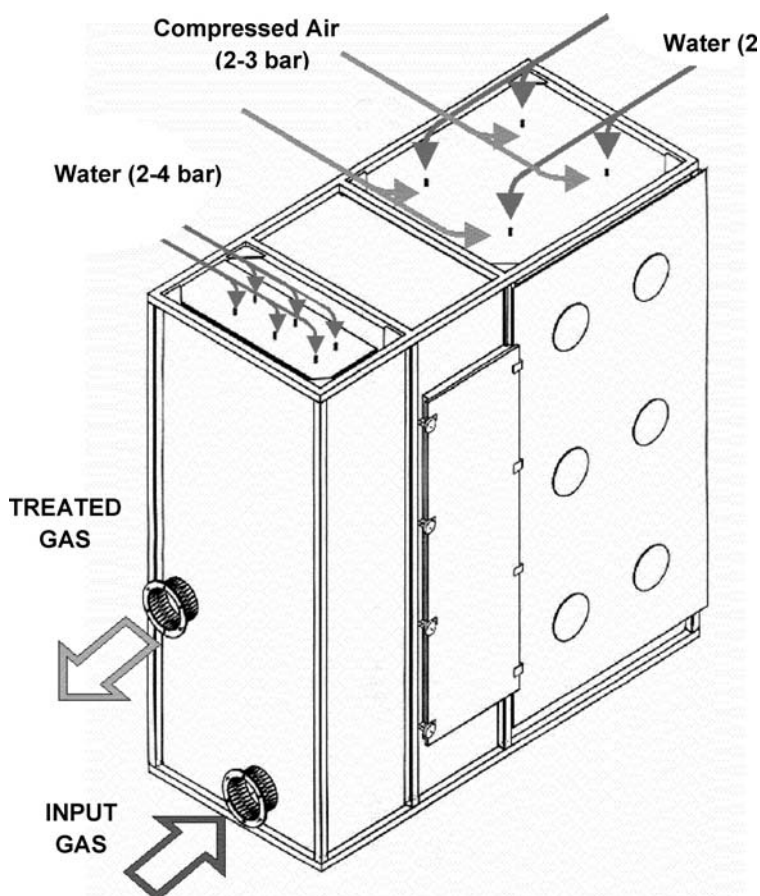
Figure 3. Heterogeneous pulsed corona plasma chamber (on the right, with circular windows) combined with a scrubber (in the left) and a mist separator (in the middle, with a service door)

Figure 4. Pulsed corona block electrode structure
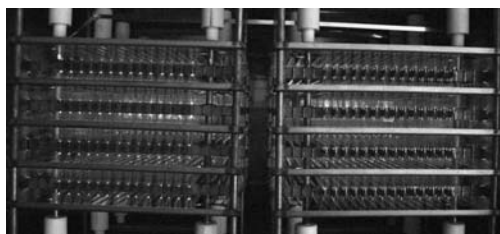
Figure 5. One layer of pulsed corona plasma inside the Pilot Plant

The last cleaning stage includes adsorption and oxidation of any remaining VOCs with a filter. The filter is formed by activated charcoal particles of 3 mm size in layers of 2 cm thickness. Total area of the layers is about 2 m^2. This filter allows for complete removal of any remaining VOCs, ozone and nitrogen oxides.

The pilot plant has three sampling ports after the three cleaning stages for precise analysis of the removal efficiency. In general, industrial wastewater could be used in the scrubber to remove soluble VOCs and products of the plasma-chemical destruction. Additionally clean water flow is necessary for cooling electronic equipment.

3. Pilot Plant Test Results

Figure 6 shows the effects of scrubber and plasma on removal and oxidation of methanol. It is possible to reach high level of Destruction and Removal Efficiency (DRE) (for example 98%, according to U.S. regulations for paper and wood industry) by two ways: increase plasma power, or combine low plasma power level with scrubbing. If scrubbing and subsequent wastewater treatment is acceptable (as in paper mills), the second approach looks much more economically feasible. If water discharge from scrubbers is not permitted (as in U.S. wood industry with zero water discharge policy), plasma treatment should be applied without preliminary scrubbing, or an additional closed loop water treatment system should be built to destroy any residual VOCs captured by the scrubbing system. Plasma treatment of methanol is relatively energy expensive process, even for low concentrations, because as it was shown earlier [13,14] the energy cost of one VOC molecule oxidation by plasma rises enormously with a decrease in VOC concentration. Our results are comparable to that obtained with small 20 W pulsed corona system [13,14]: the energy cost is about 300 eV per methanol molecule for 12 ppm initial concentration.
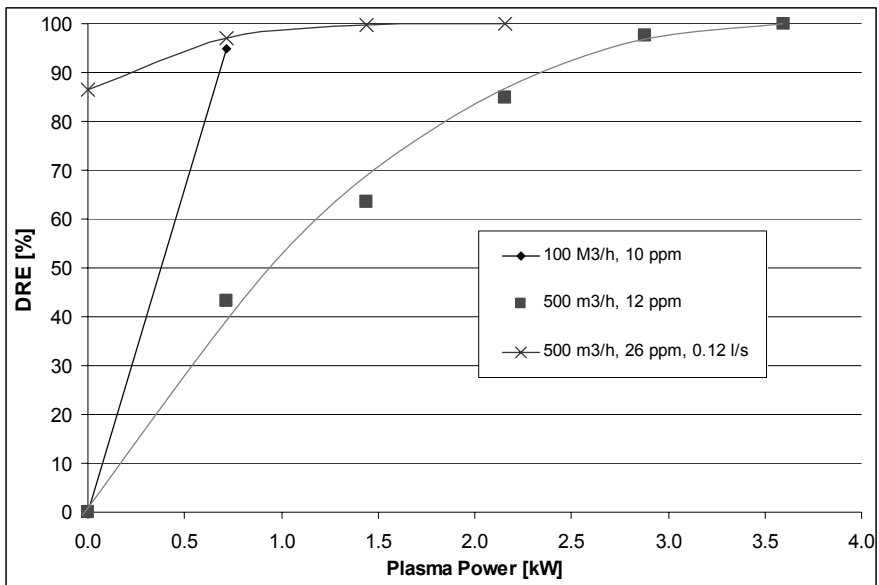
Figure 6. Methanol destruction and removal efficiency depending on plasma power with and without water scrubbing using 0.12 l/s of water flow rate (upper curve)

It is necessary to note that the major analytic tool in the Pilot Plant is a California Analytical Model 300HFID/MHFID Heated Hydrocarbon Analyzer, which is in contrast to the previous laboratory research [13,14] when gas chromatographs were used for measurement of the destruction and removal efficiency. The big difference is that chromatographs measures the concentration of a particular initial substance and some known by-products, while the Hydrocarbon Analyzer measures the total content of the carbon compounds that were not completely oxidized or removed from the stream. This change of analytical approach gave some interesting scientific results (see below).

Methanol oxidation (Fig. 6) in plasma occurs without formation of any by-products [13,14], so interpretation of these results is very simple. As it was demonstrated earlier [13,14], oxidation of dimethylsulfide (DMS, Fig. 7) in plasma occurs faster than oxidation of methanol, but is accompanied by formation of byproducts – methanol and acetone. It is possible to distinguish two parts on concentration curves in Fig. 7: the initial concentration of total hydrocarbons drops relatively fast (mostly DMS oxidation with energy cost about 200 eV per DMS molecule for 10 ppm initial concentration), and is followed by a much weaker dependence on power (compare with Fig. 6) that corresponds to oxidation of byproducts.
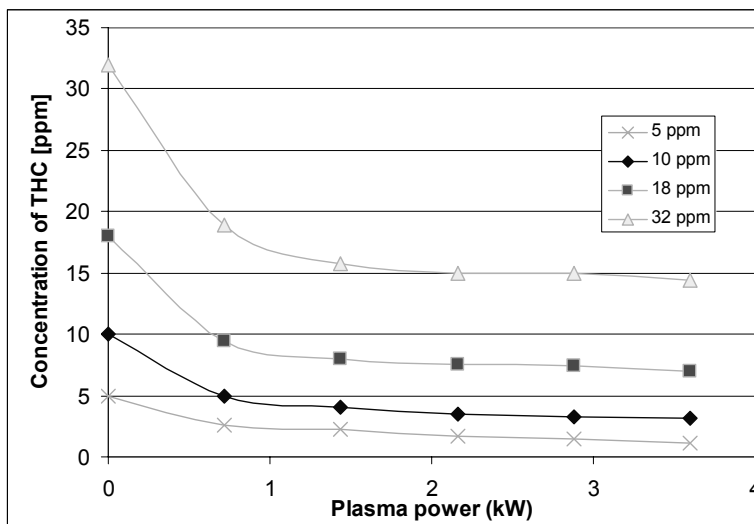
Figure 7. Dimethylsulfide oxidation in plasma: concentration of total hydrocarbons (THC) in 500 m^3/h air stream depending on plasma power

Alpha pinene ($C_{10}H_{16}$) processing in plasma has an even stronger influence of by-product formation (Figs. 8 and 9).
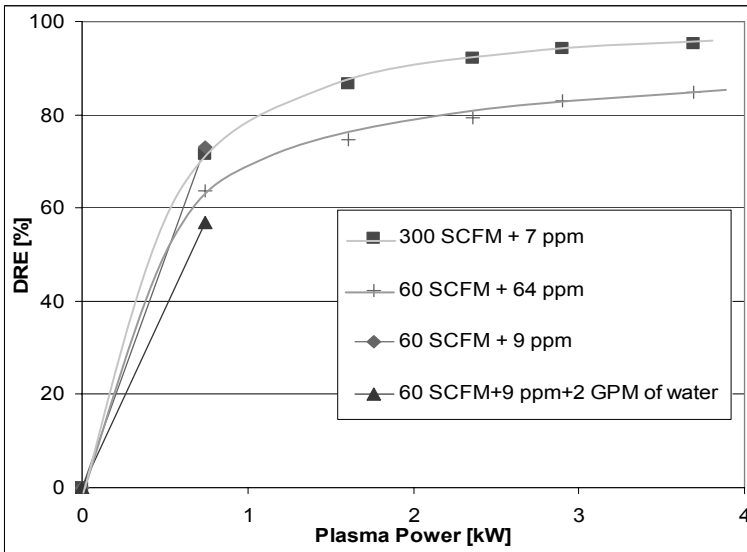
Figure 8. Destruction and Removal Efficiency for alpha-pinene depending on plasma power, air flow rate (60 SCFM = 100 m^3/h; 300 SCFM = 500 m^3/h), alpha-pinene concentration and use of water spray in the pulsed corona (2 GPM = 126 ml/s). Water spray in the corona reactor does not promote alpha-pinene elimination process. Energy cost is about 40 eV per alpha-pinene molecule for 64 ppm initial concentration, in a good agreement with the data obtained using 20 W pulsed corona [13, 4]
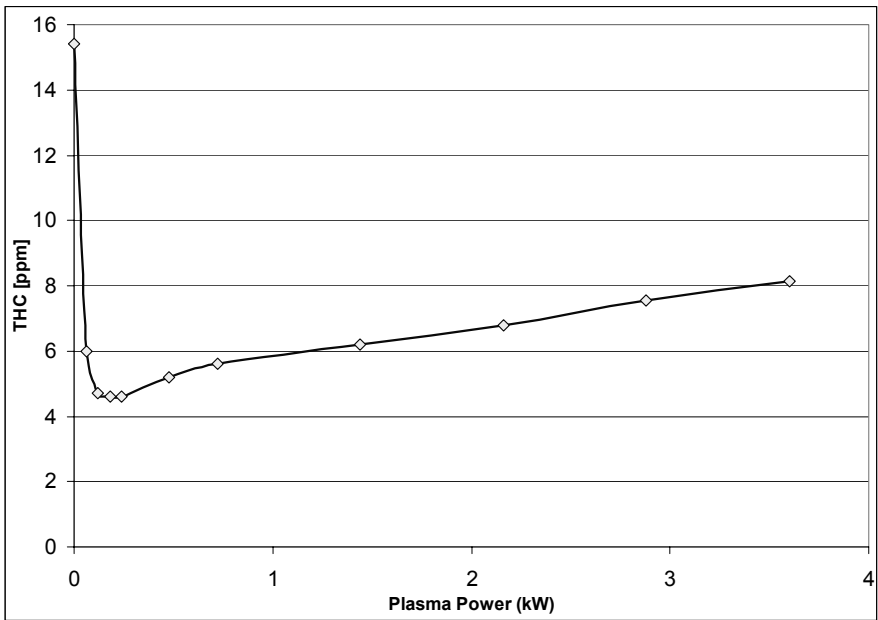
Figure 9. Alpha-pinene oxidation process accompanied by production of stable by-products. Air flow rate is 180 m^3/h

This influence is not so obvious (Fig. 8) at relatively high concentrations of alpha-pinene (note that 1 ppm of $C_{10}H_{16}$ approximately corresponds to 10 ppm of THC). Nevertheless, control of by-products using GS-MS (HP5890A gas chromatograph with HP5970 Mass Selective detector) revealed large-molecular byproducts (like $C_{25}H_{46}$) that contained cyclopentane rings in their molecular structure, which are difficult to decompose as these molecules can be considered as soot precursors. The strong influence of these by-products was found in experiments with a low concentration of alpha-pinene (Fig. 9).

This very specific picture points out that there are two very different mechanisms of alpha-pinene interaction with plasma products: oxidation by radicals that occurs without formation of stable by-products; and polymerization which is probably caused by ionization of organic molecules and results in formation of soot precursors. Direct electron ionization of the VOC admixture should have low probability because of low concentration of VOC; however, VOC molecules can be easily ionized because of charge transfer processes. Ionization of VOC molecule makes it very reactive, but the reaction pathway can be very much different in comparison with the normal oxidation process caused by radicals (O, OH, etc.). Other researchers [15,16] also emphasized correlation between low ionization potential of VOC molecules and their susceptibility to non-thermal plasma destruction.

An additional test was made that showed the difference in VOC removal in two cases: with and without influence of ionized species. This test was already made in a special installation that has a reduced size (it has just one corona block shown in Fig.4 as opposed to 12 which are in the Pilot Plant), so it can be used in a laboratory, but it still has the same electrode structure and treatment ability.

Experiments (Fig. 10) were arranged so that in some cases, flow of VOC (alpha pinene) was pre-mixed with air and treated by pulsed corona ('PT' – plasma treatment curves in the Fig. 10); in other cases the air flow was treated with plasma and immediately after that it was mixed with the flow of VOC ('RS'– radical stream curve in the Fig. 10). Sampling was arranged so that the residence time of VOC in the 'radical stream' was comparable with the residence time of the contaminated flow in the corona reactor for the case of plasma treatment. All experimental data in Fig. 10 were recalculated so that the amount of VOC is presented as a stream of a C_1 hydrocarbon mixed with the air flow. To get these data in concentration of THC (ppm), anyone can divide THC flow (in ml/s) by the air flow rate (in l/s). For example, 1 ml/s of THC in 16 l/s of air corresponds to $(1/16) \cdot 10^{-3} = 62.5$ ppm of THC, or about 6 ppm of alpha-pinene.

The results presented in Fig. 10 show that plasma treatment results in formation of stable products as the power increase above 300 W does not result in the reduction of THC concentration. On the contrary, an increase in power input into the radical stream results in about twice slower initial increase in DRE with power growth, but the THC concentration reduction is continuous in this case. This means that depending on the type of a dominant VOC, an optimal technological arrangement can be different even if the plasma type is pre-defined.
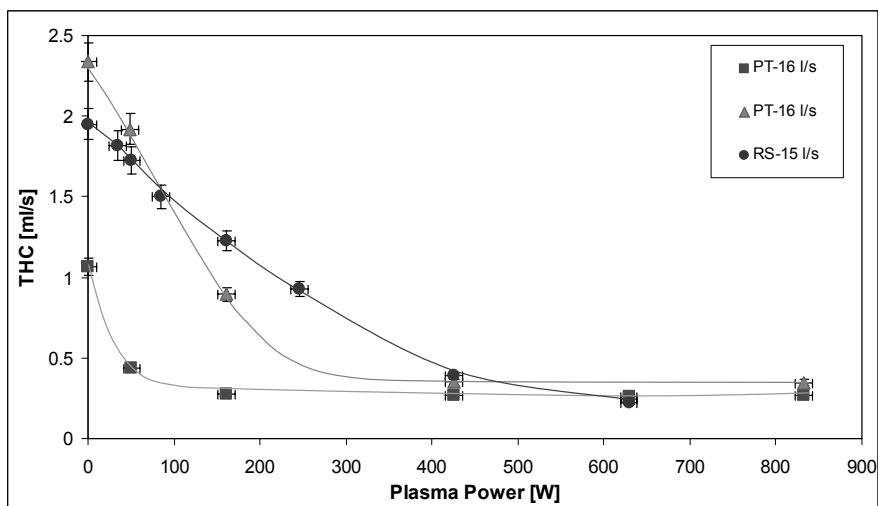
Figure 10. Alpha-pinene oxidation process accompanied by production of stable by-products in the case of plasma treatment ('PT' curves) and pure oxidation process in the case of treatment by radical stream ('RS' curve). Air flow rates are 15 or 16 l/s

4.   Application of the Pilot Plant as an Educational Laboratory

The pulsed corona Pilot Plant or Mobile Environmental Plasma Laboratory (Fig. 1) that was built to demonstrate the promising plasma technology for control of VOC emissions on paper mills is a valuable asset of Drexel University. To maximize use of this asset, the laboratory course AET 380 "Environmental Control Plasma Educational Laboratory" was developed in the Goodwin College of Professional Studies of Drexel University [17]. The primary goal of this laboratory course is to introduce students to the engineering principles of non-thermal plasma application for air cleaning from VOCs and other methods of VOC control and measurements, by combining hands-on laboratory experience with lectures. More details about this course can be found in the paper [17] published in this book.

References

[1]   Paur, H. R., "Removal of Volatile Hydrocarbons from Industrial Off-Gas. Non-Thermal Plasma Techniques for Pollution Control", eds. B. M. Penetrante and S. E. Schultheis, pp. 277–289. Berlin, Springer-Verlag, 1992.
[2]   Harkness, J. B. L. and Fridman, A. A., "The Technical and Economic Feasibility of Using Low-Temperature Plasma to Treat Gaseous Emissions from Pulp Mills and Wood Products Plants", NCASI Technical Bulletin No. 795, September 1999.

[3]   Sun, B., Sato, M., and Clements, J. S., "Use of Pulsed High-Voltage Discharge for Removal of Organic Compounds in Aqueous Solution", Journal of Applied Physics, **32**, pp. 1908–1915, 1999.

[4]   Rosocha, L. A. et al., "Treatment of Hazardous Organic Wastes Using Silent Discharge Plasmas", in Non-Thermal Plasma Techniques for Pollution Control, eds. B. M. Penetrante and S. E. Schultheis, pp. 281–311. Berlin, Springer-Verlag, 1992.

[5]   Fridman, A. and Rusanov, V., "Theoretical Basis of Non-Equilibrium Near Atmospheric Pressure Plasma Chemistry", Pure and Applied Chemistry, **66**, pp. 1267–1274, 1994.

[6]   Czernichowsky, A., Labbé, Ph., Laval, F., and Lesueur, H., "Plasma-Assisted Cleaning of Flue Gas from a Sooting Combustion", Emerging Technologies in Hazardous Waste Management V. American Chemical Society, pp. 144–153, 1994.

[7]   Penetrante, B. M. et al., "Non-Thermal Plasma Techniques for Abatement of Volatile Organic Compounds and Nitrogen Oxides", Preprint for the Workshop on Plasma Based Environmental technologies, Berlin, 1995.

[8]   Czernichowsky, A., Fridman, A., Chapelle, J., and Liventsov, V., "Gliding Arc as Non-Equilibrium High-Power Atmospheric Pressure Discharge", Preprint of the Russian Research Center "Kurchatov Institute", IAE-5892/6, Moscow, 1995.

[9]   Mutaf Yardimci, O., Saveliev, A. A., Fridman, A. A., and Kennedy, L. A., "Thermal and Nonn-Thermal Regimes of Gliding Arc Discharge in air Flow", Journal of Applied Physics, **87**, pp. 1632–1641, 2000.

[10] Penetrante, B. M., Bardsley, J. N., and Hsiao, M. C., "Kinetic Analysis of Non-Thermal Plasmas Used for Pollution Control", Japanese Journal of Applied Physics, **36**, pp. 5007–5017, 1997.

[11] Penetrante, B. M., Preface to "Non-Thermal Plasma Techniques for Pollution Control", eds. B. M. Penetrante and S. E. Schultheis, pp. 33–42, Heidelberg, Springer-Verlag, 1992.

[12] Dalaine, V., Cormier, J. M., and Lefaucheux, P., "A Gliding Discharge Applied to H_2S Destruction", Journal of Applied Physics, **83**, pp. 2435–2441, 1997.

[13] Sobacchi, M. G., Saveliev, A. V., Fridman, A. A., Gutsol, A. F., and Kennedy, L. A., "Experimental Assessment of Pulsed Corona Discharge for Treatment of VOC Emissions", Plasma Chemistry and Plasma Processing, **23**, No. 2, pp. 347–370, 2003.

[14] Sobacchi, M. G., Saveliev, A. V., Kennedy, L. A., Lock, E., Fridman, A., Gutsol, A., Desai, A., Tak, G., Gutsol, K., Korobtsev, S., Shiryaevsky, V., Medvedev, D., and Abolentsev, V., "Pulsed Corona Plasma Technology for Treating VOC Emissions from Pulp Mills" 2004 TAPPI Paper Summit, Spring Technical and International Environmental Conference, May 3–5, 2004, Atlanta, GA, USA, Electronic Proceedings, PS04169.pdf.

[15] Stacy L. Daniels, ""On the Ionization of Air for Removal of Noxious Effluvia" (Air Ionization of Indoor Environments for Control of Volatile and Particulate Contaminants With Nonthermal Plasmas Generated by Dielectric-Barrier Discharge)", IEEE Transactions on Plasma Science, **30**, pp. 1471–1481, 2002.

[16] A. Koutsospyros, S.-M. Yin, C. Christodoulatos, and K. Becker, "Destruction of Hydro-carbons in Non-Thermal, Ambient-Pressure, Capillary Discharge Plasmas", International Journal of Mass Spectrometry, **233**, pp. 305–315, 2004.

[17] Genis, V., Fridman, A., and Gutsol, A., "Use of Environmental Control Plasma Laboratory for Educational Purposes", in "Plasma Assisted Decontamination of Biological and Chemical Agents", eds. S. Güçeri and V. Smirnov, Springer, 2008.

DEGRADATION OF ORGANICS COMPOUNDS AND PRODUCTION OF ACTIVATED SPECIES IN DIELECTRIC BARRIER DISCHARGES AND GLIDARC REACTORS

J. M. CORMIER, O. AUBRY, AND A. KHACEF
GREMI – Polytech'Orleans, 14 rue d'Issoudun, BP 6744,
45067 Orléans Cedex 2, France

Abstract: Major sterilization mechanisms are related to atoms and radicals, charged particles, excited molecules, ozone, and UV radiation. The ROS (Reactive Oxygen Species) are well known as evildoers. These species are easily created in ambient air and water and they live long enough to reach the cell and attack the organic matter. Test molecules conversion in dry and wet air is studied using Dielectric Barrier Discharge (DBD) and Gliding Arc Reactors (GAR). The effects of temperature and energy deposition into the media on the active species production and then on the organics compounds degradation are presented for two non thermal plasma reactors: DBD and GAR. Main production species investigated are OH, O_3, NOx, CO and $C_xH_yO_z$ by-products. It is shown from experiment analysis that the reactive species production is quite different from one reactor to another. GAR and pulsed DBD are two chemical processing ways in which the temperature of heavy species in ionized gas is determinant. By reviewing the species production obtained from both reactors, a discussion is open about plasma decontamination.

Keywords: Non thermal plasma, glidarc, Dielectric Barrier Discharge (DBD), non thermal arc, active species, plasma depollution, sterilisation, decontamination

1. Introduction

Non-thermal atmospheric pressure plasma processing is one of the most effective technology for removal pollutants (nitrogen oxides NOx, sulfur oxides, volatile organic compounds VOCs) from flue gas [1–11] and syngas gas production from hydrocarbons and alcohols [12–15] at relatively low energetic costs. NTP that has a low gas temperature and a high electron temperature can be produced by a variety of electrical discharge methods (pulsed corona discharge, barrier discharge, and dc discharge, gliding arc) [16–22] or electron beam irradiation [1,23]. The energy supplied into the discharge is used preferentially to create free

electrons, which are then used to produce ionization and excitation of the gas mixture components. Gas phase radicals such as hydroxyl (OH), hydroperoxyl (HO$_2$) and oxygen atoms (O) were generated and were consumed in chemical reactions, part of them promoting the desired conversion of pollutants. In this last case, high electron energy is observed although the gas remaining at room temperature. In the case of non thermal arcs operating at low current intensity (I < 2 A), electron temperature is generally higher than 8,000 K and gas temperature smaller than 6,000 K. Non thermal behavior is quite different in this case because of a sufficient gas temperature able to ignite chemical reactions. Mechanisms in high voltage transient discharges (DBD, Corona) and non thermal arc discharges (Glidarc) lead the production of different species. Our main interest is the nature of these species as well as their properties for sterilisation, decontamination and medical applications.

2. The Gliding Discharge Plasma Reactor "Glidarc"

Gliding arc discharges had been presented previously [20–22]. The electrical system consists of two arcing horns and a DC high voltage power supply (Fig. 1).
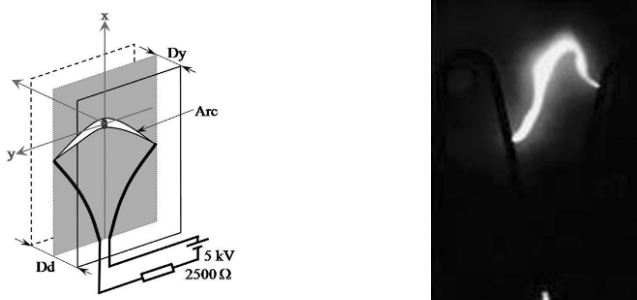
Figure 1. Schematic of gliding arc reactor and photography of the discharge

Through the inlet nozzle, the reacting gas flows and blows the arc. The vessel is built with two electrodes made of copper tubes. These tubes have a diameter of 8 mm and a length of 20 cm. Electrodes is gripped between two panes of glass. These panes are spaced of 1.2 cm and insulated the area between the electrodes. The arc characteristics (gas flow rate, electric field strength, power density), gas temperature, plasma radii-conduction and apparent, are given in Table 1. Direct current intensity is 0.9 and 1.7 A. Spectroscopic measurements show that electron temperature is in the range 10,000–12,000 K.

TABLE 1. Arc characteristics

Flow (Nm^3/h)	E (V/m)	E I (W/m)	T (K)	Conduction radius (mm)	Apparent radius (mm)
3	7,700	7,000	5,200	1.6	1.4
8	14,500	24,700	6,200	0.8	0.7

According to Cavvadias [4], the mechanisms for NO production at low temperature (T < 4,000 K) (ions are not taken into account) are given by the following chemical reactions

$$O_2 + M \underset{k_2}{\overset{k_1}{\Longleftrightarrow}} 2\ O + M \qquad\qquad O_2 + N \underset{k_8}{\overset{k_7}{\Longleftrightarrow}} NO + O$$

$$N_2 + M \underset{k_4}{\overset{k_3}{\Longleftrightarrow}} 2\ N + M \qquad\qquad N_2 + O_2 \underset{k_{10}}{\overset{k_9}{\Longleftrightarrow}} NO + O$$

$$O + N_2 \underset{k_6}{\overset{k_5}{\Longleftrightarrow}} NO + N \qquad\qquad NO + M \underset{k_{12}}{\overset{k_{11}}{\Longleftrightarrow}} N + O + M$$
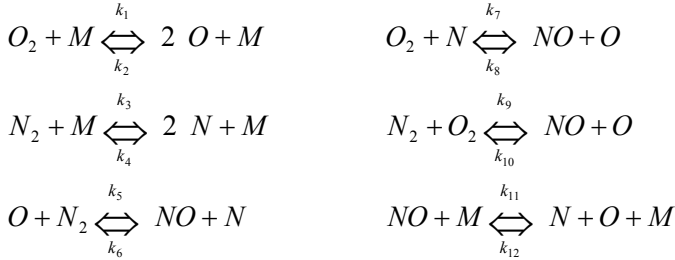
Solutions of the set of the coupled differential equations are given using "Chemical Workbench" code and kinetic constants were taken from NIST data base.

Let us consider a one dimensional air flow device with a hot region on which temperature is increasing from A to B and decreasing from B to C. The temperature profile is supposed to be calculated as a function of the distance: x (Fig. 2). The air molecules are flowing from A to D at a velocity v. A is corresponding to the input and D to the output. From A to D the air flow is submitted to heating and cooling. The transition time from hot region crossing is: $t_C - t_A = (x_C - x_A)/v$.
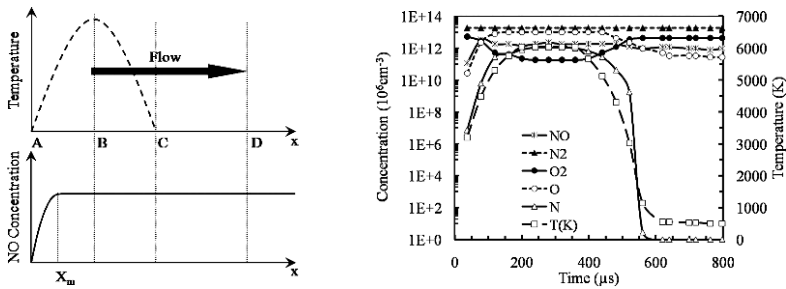
Figure 2. Schematic picture of NO formation and calculated concentration species for an axial temperature of 5,000 K

The NO concentration is increasing as the molecules are flowing in the heated zone and a maximum value of NO concentration is reached at a distance X_m which corresponds to a flowing duration time of $\delta t = t_A - t_{Xm}$. In a general case, X_m does not correspond to the maximum temperature because NO production is decreasing at high temperature. Solving kinetic equations of the above chemical reactions, NO concentration at the output of the device can be calculated. Simulations were carried out using temperature profiles and gas velocities obtained from the plasma string model. Example of results is given on Fig. 2. Calculation leads to 2,700

ppm and 500 ppm of NO for low rate of 3 Nm^3/h and 8 Nm^3/h, respectively. The measured NO concentrations are 3,000 ppm and 500 ppm respectively.

Analysis of NO production shows that NO production chemistry can be described by a quasi-thermal process. NO oxidation leads to NO_2 production. Measured N_2O concentration remains at low values (<1%) in all cases. Mains chemical effects after reaction with water lead to acids production (HNO_2, HNO_3).

3.   Rotating Discharge Plasma Reactor

The "rotating discharge" reactor (Fig. 3) operating at atmospheric pressure was powered with a 50 Hz high voltage step-up transformer, 220 V/10 kV, with leakage fluxes. The effect of leakage fluxes determines a reactance that produces a constant RMS value of the discharge current (100–200 mA). The reactor consists of a quartz tube in which a conical central electrode and a cylindrical external are laid out. The gas is injected into the reactor transversely with the axis of the system. The voltage applied to the electrodes can reach several tens of KV. The discharges are produced between the electrodes at the place where those are closest.
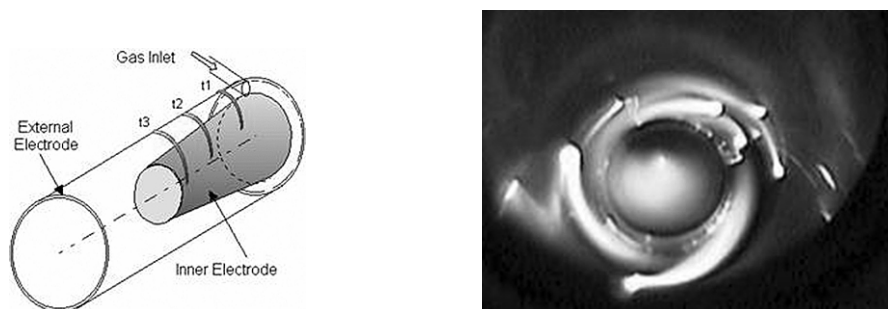
Figure 3. Rotating discharge reactor and photography of the rotating discharge

Experiments with "Rotarc" were performed at room temperature [10] using the following mixture: O_2 (10%) – NO (500 ppm) – C_3H_6 (500 ppm) and N_2 as balance at 1 atm. Output species are shown on Fig. 4.
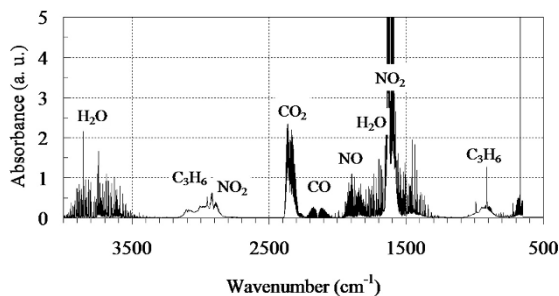
Figure 4. Typical FTIR spectrum (O_2 (10%) –NO (500 ppm) – C_3H_6 (500 ppm) – N_2 mixture)

Main detected products are CO, CO_2, NO, NO_2, and H_2O. Output species concentrations obtained after plasma processing were compared to those without plasma. Results are shown on the Table 2.

TABLE 2. Output concentration of mains products

Species	Plasma OFF	Plasma ON
NO	(539 ± 27) ppm	$(1,838 \pm 92)$ ppm
NO_2	(27 ± 5) ppm	(362 ± 18) ppm
NOx	(566 ± 28) ppm	$(2,200 \pm 110)$ ppm
CO	(10 ± 5) ppm	(98 ± 5) ppm
CO_2	(4 ± 2) ppm	(117 ± 5) ppm
C_3H_6	(508 ± 10) ppm	(438 ± 10) ppm

Results show the ability of rotating discharge for high values of NOx concentrations production in air. NOx repartition is NO (84%) and NO_2 (16%). NOx production in rotarc and Gliding discharge is similar and very effective because of temperature of the plasma gas column. As the 210 ppm of input atoms of carbon lead to CO (98 ppm) and CO_2 (117 ppm) carbon balance is satisfied. These results show that no other species are produced in the limits of the detection capacity of the FTIR. Physics and chemistry in rotating discharge and gliding arc reactor are similar.

4. Stationary Non Thermal Plasma "Statarc"

The plasma was created between two carbon electrodes with few mm gap spacing (Fig. 5) at atmospheric pressure. One may underline a typical feature of the plasma which is the difference between electron and gas temperature.
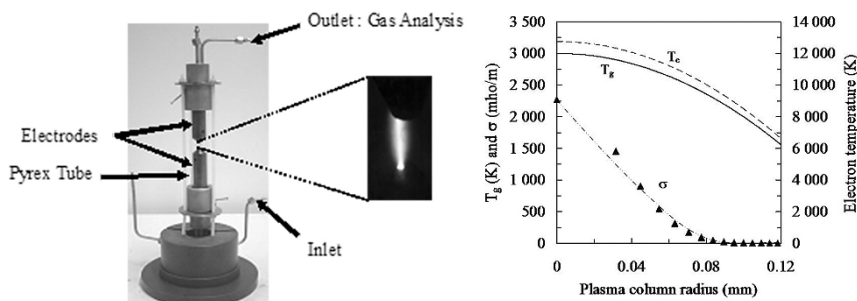
Figure 5. "Statarc" reactor photograph and plasma characteristics plasma column (case of N_2)

The device has been mainly tested for the conversion of methane in various mixtures (Steam and air). Typical results of conversion are shown in Fig. 6.
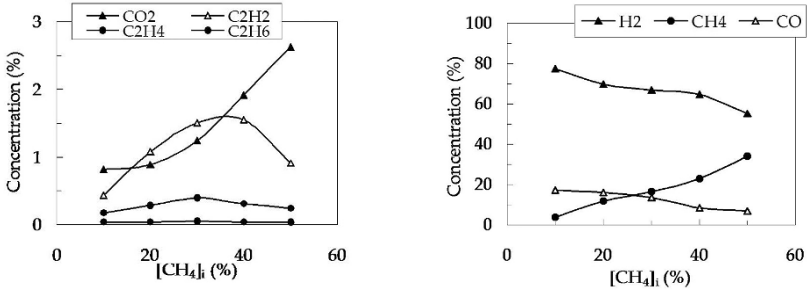
Figure 6. Exhaust gas composition *vs* inlet CH_4 concentration in a steam reforming plasma reactor

The plasma was modeled by FEMLAB software by using a simplified kinetic model. Plasma is supposed to be described by the following energy equation in which transport properties are polynomial fitted as function of plasma temperature.

$$\rho C_p \frac{\partial T}{\partial t} + \vec{\nabla}\left(-\lambda\vec{\nabla}T + \rho C_p T\vec{u}_s\right) = \sigma E^2$$

Kinetic is described by the following simplified equation in which rate constant is a function of temperature.

$$\vec{\nabla}\left(-D\vec{\nabla}y + y\vec{u}_s\right) = k\left(\left[CH_4\right]_0 - y\right)\left(\left[H_2O\right]_0 - y\right)$$

A Kinetic rate expression (k (T)) deduced from the fits obtained with results of GRI-3 mechanism is used. A picture of a discharge and CH_4 conversion map are shown on Fig. 7.
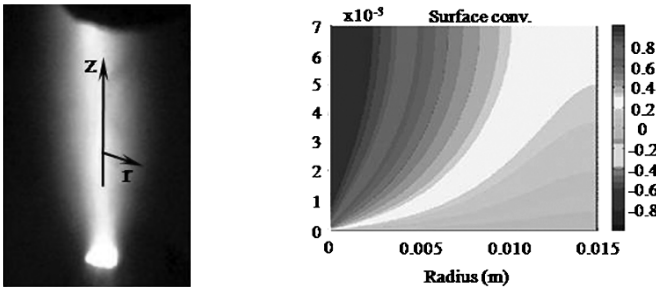
Figure 7. Photography of the plasma column and methane map conversion (calculated conversion rate: 40%, measured conversion rate: 48%)

Experimental and calculated conversions are compared. Taking into account roughly approximations in plasma modeling one may conclude in a useful first description given. "Statarc" studies show that a quasi-thermal analysis leads to results in good agreement with experiments. "Statarc" can be considered as elementary reactor in which main phenomena are similar that the ones involved in "Glidarc" and "Rotarc".

5. Non Thermal Arc Conclusion

"Glidarc", "Rotarc", and "Statarc" reactors involve similar physical and chemical processes, and basically non equilibrium plasma: electron temperature is higher than gas temperature. First chemical approach can be performed using simplified kinetics and plasma fluid model.

- Main species produced in air and CH_4-H_2O mixtures are NOx, CO, CO_2, C_2H_2, C_2H_6 and H_2.
- Oxidized high hydrocarbon species are observed at very low concentrations and not significant for such a plasma treatment.
- Others species can be produced in post discharge regions by reaction with added products.
- Because of output temperature higher than 200°C no ozone production is available from these devices.

6. Non-Thermal Plasma Study in VOCs' Treatment: Propane Conversion in a Pulsed DBD Reactor

Non-thermal atmospheric pressure plasma processing is being actively studied for removal of volatile organic compounds (VOCs') diluted in air (25–30). In spite of the well-established implementations, experimental and fundamental knowledge of chemical processes need to be improved, especially products analysis and mass balance.

Propane (C_3H_8) decomposition was investigated using a pulsed high voltage Dielectric Barrier Discharges (DBD) reactor in a wire to cylinder configuration. At room temperature, the propane removal efficiency and by-products production depends strongly on input energy density (E_d). Main carbon species produced are CO and CO_2. Others $C_xH_yO_z$ (formaldehyde, formic acid, …) species can be produced for the lowest energy density studied.

A temperature effect (up to 800 K) on propane conversion and species production was studied. Main results show that an increase of the temperature leads to an increase of the propane consumption (Fig. 8). High propane conversion rates are obtained for the lowest E_d at high gas temperature. As example, for $E_d = 100$ J.L^{-1}, C_3H_8 is entirely consumed at 800 K whereas only 50% are converted at 450 K.
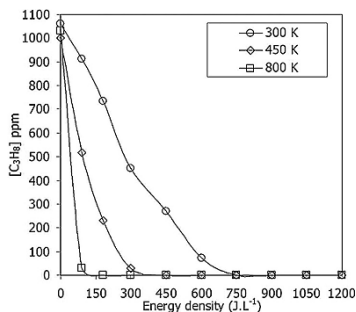
Figure 8. Outlet C_3H_8 concentration *vs* E_d for 300, 450 and 800 K (Charging voltage=5 kV)

Plasma plays a major role to initiate propane decomposition. Without plasma, no reactions are observed even for the highest temperature investigated. In terms of energetic cost for VOCs conversion, the gas temperature should be taken into account. Thermal energy, E_{th}, can be calculated. In comparison to 300 K, E_{th} contribution is about 120 and 220 $J.L^{-1}$ for 450 and 800 K, respectively. Temperature variation leads to a dramatic effect on the species produced. Increasing the temperature promotes CO_2 which becomes the main specie in the outlet gas (Fig. 9).
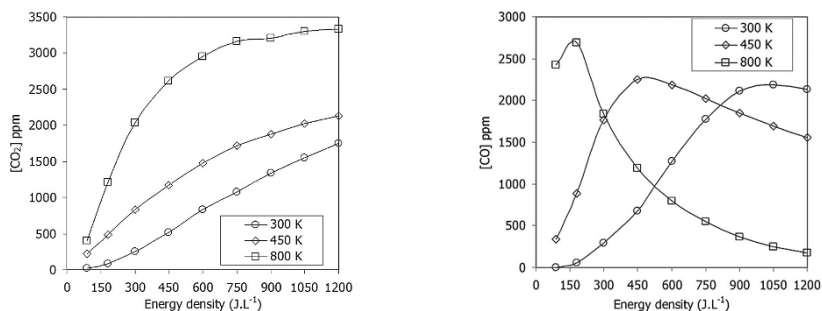
Figure 9. Outlet CO and CO_2 concentration *vs* input energy density for 300, 450 and 800 K

In Fig. 10 are reported measured carbon concentrations ([MC]) from non-consumed C_3H_8 and CO and CO_2 produced ([MC] = 3[C_3H_8] + [CO] + [CO_2]). Carbon deficit increases when gas temperature decreases. Input energy density range where carbon balance is not complete depends strongly on gas temperature. At room temperature, carbon deficit (ΔC) is observed in the range 50–900 $J.L^{-1}$ whereas at 450 K, the ΔC range is reduced to 50–400 $J.L^{-1}$. This means that the number or the concentration of non-measured carbon species increase. These species such as formaldehyde, acetaldehyde, formic acid, and others $C_xH_yO_z$ are observed experimentally but are not quantified in that study.

Ozone (O_3) production seems to be an important parameter to explain measured carbon profiles. Maximum carbon deficit measured can be linked to the maximum
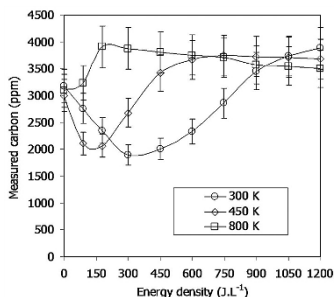
Figure 10. Measured carbon *vs* input energy density for different gas temperature

ozone concentration. In Fig. 11 are reported ozone concentrations as functions of input energy density for gas temperature up to 800 K. When O_3 concentration decreases, carbon deficit decreases and corresponds to the decrease of carbon species others than CO and CO_2. Oxidized hydrocarbons $C_xH_yO_z$ consumption could be enhanced with active species produced when ozone is destroyed or less produced when E_d or temperature increase. O-atoms are available to produce active species (OH. O_3, O) which react with by-products to produce CO and CO_2.
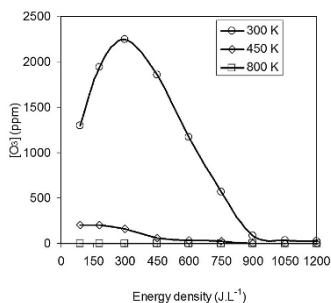
Figure 11. Ozone concentration *vs* input energy density for different gas temperature

Conclusions

Chemical mechanisms in high voltage transient discharges (DBD) and in non thermal arc discharges (gliding, rotating and stationary discharges) lead to high production of active species. Depending on the inlet and on the nature of the discharge, the main oxidized species could be ozone, carbon monoxide and dioxide, nitrogen oxides, and $C_xH_yO_z$ species such as aldehyde, formic acid, ...

NOx, CO, CO_2, H_2, C_2-hydrocarbons are produced in non thermal arcs devices: Glidarc, Rotarc and stationary glow discharge Statarc. Because of high reactor outlet temperature, no ozone production is observed. Conversion of high hydrocarbon is available by using these reactors.

It could be supposed that main effect for decontamination and sterilisation would be involved by the NO production. NO in interaction with water can leads to acid mixture able to attack the organic matter.

Ozone can be easily produced in dielectric barrier discharges (DBD). Also DBD is able to produce various oxidized species. Maximum of $C_xH_yO_z$ production is obtained at "medium" values of energy density in wet air conditions. Adjustment of DBD reactor dedicated to oxidized oxygen species must be taking into account in order to optimize the reactive species production.

References

[1] Penetrante BM and Schultheis SE (ed.) 1993 Non-thermal Plasma Techniques for Pollution Control (Part A and B) (New York: Springer-Verlag).
[2] Park JY, Tomicic I, Round GF, and Chang JS 1999 J. Phys. D: Appl. Phys. 32, pp. 1006–1011.
[3] Kim HH, Prieto G, Takashima K, Katsura S, and Mizuno A 2002 J. Electrostatics, 55, pp. 25–41.
[4] Urishima K and Chang JS 2000 IEEE Trans. Dielect. & Elect. Insul. 7, pp. 602–610.
[5] Van Veldhuizen EM, Zhou M, and Rutgers WR 1998 Plasma Chem. Plasma Process, 18, pp. 91–111.
[6] Sun W, Pashaie B, Dhali SK, and Honea FI 1996 J. Appl. Phys. 79, pp. 3438–3444.
[7] Khacef A, Cormier JM, and Pouvesle JM 2005 J. Adv. Oxid. Technol. 8(2), pp. 150–157.
[8] Khacef A, Cormier JM, and Pouvesle JM 2002 J. Phys. D: Appl. Phys. 35, pp. 1491–1498.
[9] Khacef A and Cormier JM 2006 J. Phys. D: Appl. Phys. 39, pp. 1078–1083.
[10] Khacef A, Pouvesle JM, and Cormier JM 2006 Eur.Phys. J.: Appl. Phys. 33, pp. 195–198.
[11] Gorce O, Jurado H, Thomas C, Djéga-Mariadassou G, Khacef A, Cormier JM, Pouvesle JM, Blanchard G, Calvo S, and Lendresse Y 2001 SAE paper N° 2001-01-3508.
[12] Ouni F, Khacef A, and Cormier JM 2006 J. Chem. Eng. and Technol. 29(5), pp. 604–609.
[13] El Ahmar E, Met C, Aubry O, Khacef A, and Cormier JM 2006 Chem. Eng. J. 116, pp. 13–18.
[14] Aubry O, Met C, Khacef A, and Cormier JM 2005 Chem. Eng. J. 106(3), pp. 241–247.
[15] Rusu I, Cormier JM, and Khacef A 2001 http://preprint.chemweb.com/ inorgchem/0106001
[16] Masuda S and Nakao H 1990 IEEE Trans. Ind. Appl. 26, pp. 374–383.
[17] Dhali SK and Sardja IJ 1991 Appl. Phys. 69, pp. 6319–6324.
[18] Penetrante BM, Hsiao MC, Bardsley JN, Merrit BT, Vogtlin GE, Wallman PH, Kuthi A, Burkhart CP, and Bayless JR 1996 Pure Appl. Chem. 68, pp. 1083–1087.
[19] Evans D, Rosocha LA, Anderson GK, Coogan JJ, and Kushner MJ 1993 J. Appl. Phys. 74, pp. 5378–5386.
[20] Lesueur H, Czernichowski A, and Chapelle A 1994 Int. J. Hydrogen Energy, 19, pp. 139–144.
[21] Richard F, Cormier J.-M, Pellerin S, and Chapelle J 1996 J. Appl. Phys. 79, pp. 2245–2250.
[22] Fridman A, Nester S, Kennedy LA, Saveliev A, and Yardimci OM 1999 Prog. Energy Comb. Sci. 25, pp. 221–231.
[23] Frank NW 1995 Radiat. Phys. Chem. 45, pp. 989–1002.
[24] Cavvadias S, PhD Thesis 1987 University Paris 6 (France).
[25] McAdams RJ 2001 J. Phys. D: Appl. Phys. 34, pp. 2810–2821.
[26] Chang CL, Bai H, and Lu SJ 2005 Plasma Chem. Plasma Process, 25(6), pp. 641–657.
[27] Motret O, Aubry O, Thuillier C, Lascaud M, Met M, and Cormier JM 2005 Proc. 17th Int. Symp. Plasma Chemistry, Toronto (Canada). pp. 1159–1160.
[28] Guo YF, Ye DQ, Chen KF, and Tian YF 2006 Plasma Chem. Plasma Process, 26, pp. 237–249.
[29] Kim HH 2004 Plasma Process Polym. 1, pp. 91–110.
[30] Blin-Simiand N, Jorand J, Belhadj-Miled Z, Pasquiers S, and Postel C 2006 Proc. 5th ISNTPT, Oleron Island (France).
[31] Jarrige J and Vervisch P 2006 J. Appl. Phys. 99, pp. 113303.1–113303.10.

MECHANISMS OF CONVERSION OF HEAVY HYDROCARBONS IN BIOGAS INITIATED BY PULSED CORONA DISCHARGES

V. A. BITYURIN, E. A. FILIMONOVA, AND G. V. NAIDIS
Institute for High Temperatures of Russian Academy of Sciences, Moscow, Russia

Abstract: The numerical results on naphthalene removal in biogas are presented and compared with experiment. Plasma-chemical processes in discharge and post discharge stages are considered. The self-consistent approach for modeling of cleaning process on the base of pulsed corona discharge is demonstrated.

1. Introduction

Several technologies for production of hydrogen-containing fuels from biomass have been elaborated. One of them is gasification, converting biomass to biogas with a typical composition of 15–21% H_2, 10–22% CO, 11–13% CO_2, 1–5% CH_4, the rest being N_2. The biogas contains a considerable amount (~10^3 ppm) of heavy hydrocarbons (tars), such as naphthalene, benzene, toluene and other, which condense in the downstream equipment leading to serious operational problems. In [1,2] a possibility of biogas purification from tar using pulsed (streamer) corona discharges has been demonstrated.

By now, information on the chemical kinetics of interaction of heavy hydrocarbons with active species of plasma (ions, radicals, excited molecules and atoms) is rather scarce. Decomposition of tar, most of all, toluene, has been experimentally investigated using several kinds of discharge and electron beam. The study has been conducted in air, pure N_2, and N_2 with addition of O_2 and H_2O [3–9].

The key role of exited molecular nitrogen, $N_2(A^3\Sigma)$, and exited nitrogen atom, $N(^2D)$, in the opening of hydrocarbon ring is discussed in the work [6]. They used the high pressure glow discharge and filamentary discharge of a streamer-to-spark transition type on removal of cyclohexanone. The IR spectra of the gas phase and solid products allowed authors to view some of the decomposition $C_6H_{10}O$ mechanisms and probable reaction pathways occurring in the discharge chamber.

The authors of work [8] on the base of analyses of measuring by Gas Chromatography coupled with a Mass Spectrometer concluded $N(^2D)$ atoms are not involved in macromolecules formation but react only with small molecules and radicals. They applied isotopic labelling method to experiments on toluene destruction by DBD at atmospheric pressure to identify the reaction pathways. From their point of view only electrons and O exited atoms in collisions with toluene break the cycle. However, this assumption about the role of O atoms is doubtful. They are quickly quenched by nitrogen molecules and their energy is too low to open the ring in comparison with $N_2(A^3\Sigma)$. The chromatograph analysis of C_7H_8 conversion by-products in pure N_2 in the work [7] is evidence of reaction toluene with nitrogen metastable states.

Addition of a few percent of O_2 to nitrogen improves the removal of toluene [5,7] and p-xylene [4], but with increase of O_2 concentration up to 20% the removal efficiency decreases and becomes lower than in pure N_2 and Ar [4,5]. Authors [4] explain the effect of O_2 content by change of electron energy distribution because of triggering of electron attachment reactions. Increasing oxygen content in the gas will limit electron density in DBD reactor, and reduce the power deposited into the plasma.

The hydroxyl is also an active component; its reactivity is 1–2 orders of magnitude higher than that of O radical. The influence of H_2O on removal of polycyclic aromatic hydrocarbons (PAH) has been experimentally investigated in DBD [4,7] and electron beam [3,9] systems. In general, the presence of water vapor, improves decomposition. The H_2O effect depends on a background composition and gas temperature. In the work [3] it is assumed that OH radical attack occurs first and the other ones follow this reaction because OH radical is the most efficient to decompose VOCs (volatile organic components). However, this conclusion is questionable because the constant rate of OH with PAH is 1 or 2 order of magnitude lower [10] than that with $N_2(A^3\Sigma)$ [11]. In the plasma hydroxyl is formed both by direct electron impact and in charge transfer reactions [9].

The comparative estimation of rates of electron impact p-xylene dissociation, ion-molecule interactions and radical attacks have been showed the most important role of electron impact is during the discharge stage, and radical mechanisms is at afterglow period, whereas the contribution of ions is negligible [4]. However, the concentration of PAH is 3–4 orders of magnitude lower than that one of main molecules. Electron will more likely collide with N_2 or O_2, than PAH.

The influence of temperature on PAH removal is able to have a non-monotone character [3], but usually the growth of temperature increases decomposition rate [2,4]. The temperature effect is related with a change of electron density, n_e, in agreement with the scaling law $n_e \sim N^2$; constant rates of reactions and residence time in reactor. The reduced electric field, E/N, weakly depends on temperatures.

The modeling of removal process of PAH is difficult task because of absence of many data for simulation of plasma-chemical kinetics at intermediate temperatures. The results of simplified modeling of removal process are presented for air by electron beam in [9] and for synthetic gas (no oxygen) by pulsed streamer discharge in [2]. The discharge phase and reactions with $N_2(A^3\Sigma)$ and $N(^2D)$ have

been not included in consideration [2,9]. Some information about constant rates of excited nitrogen atoms and molecules and OH radicals with hydrocarbons are reviewed in [10,11] and papers regarding to N_2-H_2 plasma decay and NO removal in N_2 and N_2 with CO, O_2 mixtures. The reaction mechanisms and rate constants with participation of PAN have been mainly developed for combustion problems and high temperature oxidation (T > 1,000 K) [12].

In the given work the physical-chemical processes in biogas are considered. To reveal the leading processes under the treatment of biogas by streamer discharges, the numerical simulation has been performed for conditions of experiments [1,2]. As noted above there is no simulation of streamer discharge in biogas. The first results of discharge stage modeling and removal of naphthalene have been published in [13,14]. The characteristic properties of the work are: (1) several gas compositions without O_2, (2) the gas temperature is close to 500 K; (3) simulation of positive streamer propagation in biogas; (4) consideration of primary plasma-chemical processes in discharge stage; (5) consideration of naphthalene removal, it is a one of the most stable component; (6) using the chemical kinetics code taking into account non-uniform distribution of components in discharge reactor; and (7) comparison with experimental results obtained at the pilot setup [1,2].

2. Simulation of Positive Streamer Propagation

The problem of simulation of the cleaning process includes description of two stages. The first, fast stage is generation of primary active species during streamer propagation. The second, slow stage is the chain of chemical transformations triggered by these species. The input parameters for the modeling of the second stage are *G*-values for generation of radicals, ions, excited molecules and atoms.

Streamer parameters are governed by the kinetic and transport properties of electrons and by the rate of photoionization: production of precursor electrons ahead of the streamer front at absorption of ionizing radiation emitted by the streamer head. Calculation of kinetic and transport coefficients in various mixtures of nitrogen with H_2, CO, CO_2 and H_2O (at high content of N_2), including biogas, shows that their values are close (in the range of electric fields relevant to streamer propagation) to those in air and in pure nitrogen (see Fig. 1). In our calculations of the EEDF the BOLSIG+ code [15] has been used.

As for the photoionization efficiency, in pure nitrogen it is about two orders of magnitude lower than in air; and the dependence on the distance from the source of radiation in N_2 being rather close to that in air [16]. A mechanism of photo-ionization in pure nitrogen and in its mixtures with gases other than oxygen (such as biogas) is not clear. In our simulations the value of photoionization efficiency in the considered mixtures is taken the same as in pure nitrogen. Additionally the absorption of ionizing photons by CO_2 molecules has been taken into account. The absorption coefficient was taken from [17]. Such approach results in the identity of streamer parameters in all the considered mixtures.
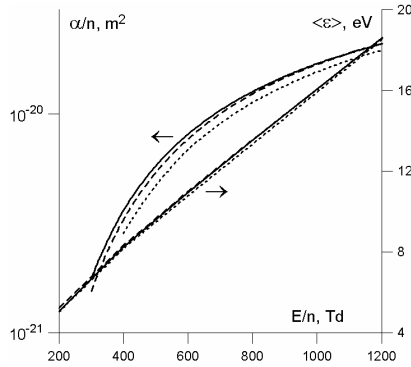
Figure 1. The ionization coefficient and mean energy of electrons versus *E/N*. Solid line is N_2: $CO : CO_2 : H_2 = 0.51 : 0.20 : 0.12 : 0.17$ mixture, dashed line is air, dotted line is N_2

It follows that the value G_j for the production of active particles of sort j at a given mixture composition may be evaluated by weighting of partial G-values as

$$G_j = \sum_i X_i G_{ij},$$

where X_i is the molar fraction of species of sort i, G_{ij} is the partial G-value for production of species j in the reaction of electrons with particles of sort i (normalized to the relative density of species i equal to unity). Note that in this approach the values G_{ij} are independent of mixture composition. They are governed by the reduced electric field in the streamer head, the latter being relatively weakly dependent on the external conditions (gas pressure and temperature, the applied voltage, the geometry of the discharge gap) [13]. The estimates for G_{ij} in the mixtures of N_2 with H_2, CO, CO_2, CH_4 and H_2O obtained on the basis of streamer simulations and analytical consideration are as follows:

$$G_{CH3,H} = 6, \quad G_H = 2.6, \quad G_{CO,O} = 0.5,$$
$$G_{OH} = 0.02, \quad G_{C,O} = 0.6, \quad G_N = 0.25,$$
$$G_{N(2D)} = 0.25, \quad G_{N2(A3\Sigma)} = 2.2, \quad G_e = 0.7.$$

Note that the G-value for $N_2(A^3\Sigma)$ is evaluated with account of cascade transitions both from both higher triplet and from singlet states. It is assumed that the dominating channel of nitrogen dissociation is $N_2 + e \rightarrow N(^4S) + N(^2D)$ [18].

Primary positive ions in a chain of fast ion-molecule reactions transform into more stable positive ions, reaction time of $\sim 10^{-9}$ s. The latter recombine with electrons, resulting in an additional (to direct dissociation) production of active particles. Detailed ion kinetics is not included in the presented model; it is assumed that the dominating stable ion is N_4^+ (in pure N_2 and its mixtures with H_2), H_2O^+ (in mixtures including H_2O) or CO_2^+ (in mixtures including CO_2). The dominating channels of dissociative recombination of these ions are assumed to be $N_4^+ + e \rightarrow N_2 + N_2(A^3\Sigma)$ [19] and $CO_2^+ + e \rightarrow CO + O(^1D)$, $H_2O^+ + e + M \rightarrow OH + H + M$, reaction time is $\sim 10^{-8}$–10^{-7} s.

In Table 1 the *G*-values are given in pure nitrogen, in the mixture 10% CO_2 + 90% N_2 and in biogas, estimated according the above relations. These *G*-values are used at the modeling of the second stage of the cleaning process.

TABLE 1. *G*-values in pure nitrogen (I), in 10% CO_2 + 90% N_2 mixture (II), and in biogas (III)

	I	II	III
H	–	–	0.5
C	–	–	0.12
$N_2(A^3\Sigma)$	2.9	2.0	1.1
N	0.25	0.22	0.12
$N(^2D)$	0.25	0.22	0.12
O	–	0.05	0.18
$O(^1D)$	–	0.7	0.7
CH_3	–	–	0.06

3.   Chemical Kinetics Modeling

Simulation of tar conversion in the reactor has been carried out using the approach and software RADICAL [20]. The model takes into account the specifics of energy input: the energy is released in narrow streamers channels, the species are distributed non-uniformly in space, and energy is deposited discretely during many pulses. The chemical transformations are simulated in the streamer trace spreading due to diffusion, with account of the change of the background-gas composition caused by preceding discharge pulses. The set of chemical kinetic processes included 350 elementary reactions involving 77 components. The reaction data were taken from many sources, indicated in [20,21]. The temperature effect on the removal process was considered similar to one in the work of [21].

A peculiarity of the reactor system [1,2], consisting of an active (discharge) zone and a 'dead' zone, is taken into account [14]. Gas is circulated in and out of the active zone in a recycle loop driven by a high-temperature fan.

For the modeling of chemical conversion in the mixture after streamer propagation, the knowledge of the number densities of active species in the streamer trail is required. As the number densities are proportional to the *G*-values, they can be easily estimated by comparison of corresponding *G*-values with the *G*-value for generation of electrons, $G_e \approx 0.7$, taking into account that the number density of electrons n_e in streamer channels in the considered gas mixtures is about 5×10^{14} δ^2 cm^{-3}, where δ is the ratio of the gas density to its normal value (corresponding to atmospheric pressure and room temperature).

4.   Results

In Fig. 2 the results are given of naphthalene removal depending on the specific energy input in pure N_2, and biogas 50% N_2 + 20% CO + 12% CO_2 + 17% H_2 + 1% CH_4. The experimental data [1] are also shown (various sets of symbols

correspond to various sets of experimental data obtained in similar conditions). The best removal is observed in pure N_2, where the leading reactions are:

$$N_2(A^3\Sigma) + C_{10}H_8 \rightarrow \text{products}, \quad k = 1.6 \cdot 10^{-10} \text{ cm}^3 \text{ s}^{-1} \tag{1}$$
$$N(^2D) + C_{10}H_8 \rightarrow \text{products}, \quad k = 3 \cdot 10^{-11} \text{ cm}^3 \text{ s}^{-1} \tag{2}$$
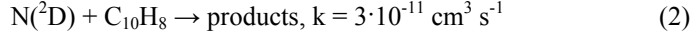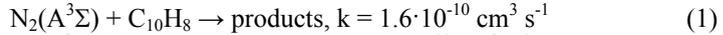
The rate constants for processes (1) and (2) were taken according to the data [11] for reaction of C_6H_6 with $N_2(A^3\Sigma)$, and for reactions of different hydrocarbons with $N(^2D)$, respectively (as the data for naphthalene are not available). In the reaction (2) atom H may be released [11]. Competitive process for $N_2(A^3\Sigma)$ removal is self-quenching:

$$N_2(A^3\Sigma) + N_2(A^3\Sigma) \rightarrow N_2 + N_2(A^3\Sigma), \tag{3}$$
$$k = 4 \cdot 10^{-10} \text{ cm}^3 \text{ s}^{-1}.$$
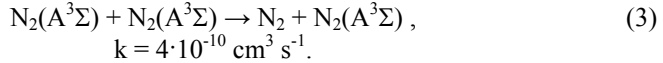
With decreasing of naphthalene concentration due to processes (1) and (2) the contribution of reaction (3) in the removal of $N_2(A^3\Sigma)$ increases.

When CO_2 is added to N_2, the G-value for $N_2(A^3\Sigma)$ becomes lower (see Table 1), so that the contribution of reaction (1) in the removal process diminishes, however the additional naphthalene removal becomes noticeable (though less effective), in reactions with O and H atoms [12,22]:
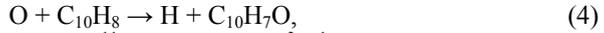
$$O + C_{10}H_8 \rightarrow H + C_{10}H_7O, \tag{4}$$
$$k = 2.32 \cdot 10^{-11} \exp(-902/T) \text{ cm}^3 \text{ s}^{-1},$$

$$H + C_{10}H_8 \rightarrow \text{products}, \tag{5}$$
$$k = 1.41 \cdot 10^{-9} \exp(-2570/T) \text{ cm}^3 \text{ s}^{-1}.$$

Atoms O appear both at the streamer stage and as the product of quenching of $O(^1D)$ and of the reactions with NO and $N_2(A^3\Sigma)$:

$$N_2 + O(^1D) \rightarrow O + N_2, \tag{6}$$
$$k = 1.8 \cdot 10^{-11} \exp(110/T) \text{ cm}^3 \text{ s}^{-1}, [20,21]$$
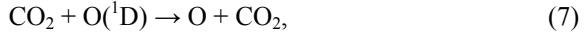
$$CO_2 + O(^1D) \rightarrow O + CO_2, \tag{7}$$
$$k = 7.4 \cdot 10^{-11} \exp(120/T) \text{ cm}^3 \text{ s}^{-1}, [20,21]$$

$$NO + N \rightarrow O + N_2, \tag{8}$$
$$k = 2.2 \cdot 10^{-11} \exp(160/T) \text{ cm}^3 \text{ s}^{-1}, [20,21]$$

$$CO_2 + N_2(A^3\Sigma) \rightarrow O + CO + N_2, \tag{9}$$
$$k = 2 \cdot 10^{-14} \text{ cm}^3 \text{ s}^{-1}, [11,21]$$
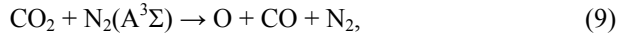
$$CO_2 + N \rightarrow CO + NO, \tag{10}$$
$$k = 3.2 \cdot 10^{-13} \exp(-1710/T) \text{ cm}^3 \text{ s}^{-1}, [20,21]$$

$$CO_2 + N(^2D) \rightarrow CO + NO, \tag{11}$$
$$k = 3.6 \cdot 10^{-13} \text{ cm}^3 \text{ s}^{-1}, [11].$$

At the biogas treatment, due to the presence of H_2 molecules in the incident mixture, the concentration of atoms H is higher than in the case of $CO_2:N_2$ mixture, and that the main process of naphthalene removal is reaction (5). The role of reaction (1) is decreasing also due to the fast quenching of $N_2(A^3\Sigma)$ by CO [11]:

$$CO + N_2(A^3\Sigma) \rightarrow N_2 + CO, \tag{12}$$
$$k = 3.8 \cdot 10^{-11} \exp(-940/T) \text{ cm}^3 \text{ s}^{-1}.$$
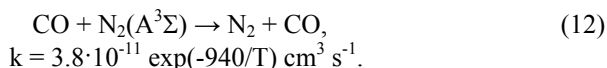
Because in the biogas the concentration of atoms H grows in comparison with the $CO_2{:}N_2$ mixture, the consumption of H in the reactions with CO, CHO, $C_{10}H_7O$ and other species increases without an advantage for naphthalene removal. On the other hand, NO reacts with NH producing O, OH and H radicals, so that the total number of these produced radicals is higher than the number of O atoms formed in reaction (8). Naphthalene removal by OH radical is important in the presence of H_2O in the gas primordially or at the end of removal process (last cycles), with production of water in the reactor.

In such a complex mixture as biogas there are many processes competitive to useful reaction (1). For this reason, naphthalene removal is notably worse than in pure N_2.

During the removal process, the balance of $C_{10}H_8$ in a streamer trace is mainly determined by the diffusion of $C_{10}H_8$ from outside of the trace in each pulse.
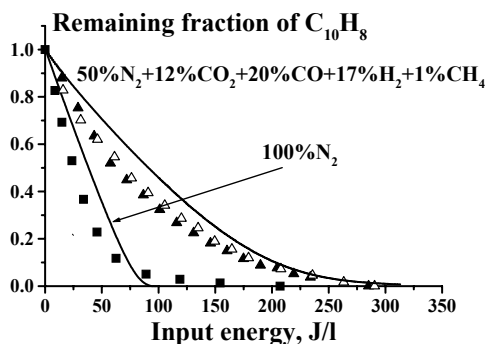
Figure 2. Naphthalene removal in pure N_2 and in gas mixture versus the specific energy input into the gas. Symbols are experiments [1], lines are calculations. T = 200°C

Conclusions

The results of simulation on naphthalene removal in biogas, pure nitrogen and mixtures of N_2 with CO, CO_2 and H_2 agree with the experimental data [1] rather well.

An original self-consistent approach for modeling of cleaning process on the base of pulsed corona discharge has been presented.

Plasma-chemical processes in discharge and post discharge stages were taken into consideration.

It has been found that the reaction of naphthalene with exited nitrogen molecules plays a key role in the removal process. Addition to nitrogen of such gases as CO, CO_2 and H_2 worsens the removal efficiency.

Acknowledgment

References

[1]   S.A. Nair, A.J.M. Pemen, K. Yan et al., Plasma Chem. Plasma Process. **23**, 665 (2003).
[2]   S.A. Nair, K. Yan, A.J.M. Pemen et al., Ind. Eng. Chem. Res. **44**, 1734 (2005).
[3]   J.-C. Kim, Radiation Phys. Chem. **65**, 429 (2002).
[4]   H.M. Lee and M.B. Chang, Plasma Chem. Plasma Proc. **23**, No 3, 541 (2003).
[5]   Z. Falkenstein, J. Appl. Phys. **85**, No 1, 525 (1999).
[6]   Z. Machala, M. Morvova, E. Marode, and I. Morva, J. Phys. D: Appl. Phys. **33**, 3198 (2000).
[7]   N. Blin-Simiand, F. Jorand, Z. Belhadj-Miled et al., In Proc. 5th Int. Symp. on Non-thermal Plasma Technology for Pollution Control and Sustainable Energy Development (ISNTPT-5), Oleron Island, France, June 19–23, 2006.
[8]   S. Ognier, L. Martin, and J. Amouroux, In Proc. ISPC 17, Toronto, Canada, August 7–12, 2005.
[9]   H. Nichipor, E. Dashouk, S. Yacko et al., Radiation Phys. Chem. **65,** 423 (2002).
[10] R. Atkinson and J. Arey, Chem. Rev. **103**, 4505 (2003).
[11] J.T. Herron, J. Phys. Chem. Ref. Data **28**, 453 (1999).
[12] H. Richter and J. Howard, http://web.mit.edu/anish/ www/mechanismsymp2002.doc
[13] G.V. Naidis, In Proc. XXVIIth ICPIG, Eindhoven, The Netherlands, July 18–22, 2005, Paper 18–454.
[14] V.A. Bityurin, E.A. Filimonova, R.A.B.P. Kerst et al., In Proc. XVI Int. Conf. on Gas Discharges and their Applications, Xi'an, China, September 11–15, 2006.
[15] G.J.M. Hagelaar and L.C. Pitchford, Plasma Sources Sci. Technol. **14**, 722 (2005); hhtp://www.codiciel.fr/plateforme/plasma/bolsig/bolsig.php
[16] G.W. Penney and G.T. Hummert, J. Appl. Phys. **41**, 572 (1970).
[17] G.R. Cook, P.H. Metzger, and M. Ogava, J. Chem. Phys. **44,** 2935 (1966).
[18] E.C. Zipf and R.W. McLaughlin, Planet. Space Sci. **26**, 449 (1978).
[19] Y.S. Cao and R. Johnsen, J. Chem. Phys. **95**, 7356 (1991)
[20] E.A. Filimonova, R.H. Amirov, H.T. Kim, and I.H. Park, J. Phys. D: Appl. Phys. **33**, 1716 **(**2000).
[21] E.A. Filimonova**,** Y. Kim, S.H. Hong, and Y.H. Song, J. Phys. D: Appl. Phys. **35**, 2795 (2002).
[22] NIST Chemical Kinetics Database on the Web, http://kinetics.nist.gov.

PLASMA METHODS FOR TOXIC WASTES PROCESSING

S. A. ZHDANOK AND A. L. MOSSE
Heat and Mass Transfer Institute, 15 P. Brovka Str., Minsk, 220072, Belarus

Abstract: Experimental study of thermal neutralization of some toxic chlorine and bromine industrial wastes, as well as of pesticides with a expired term of validity was carried out in the three-jet plasma reactor. Different physical-chemical methods were used for analysis of products of waste processing. It was shown that plasma technology provides effective processing of toxic wastes.

Keywords: Plasma, toxic wastes, plasma-chemical reactor, pesticides, hydrocarbons, destruction, vaporization, compounds

1. Introduction

Alternative to conventional low-temperature methods of toxic wastes incineration is their destruction in thermal plasma, which takes place at high temperature. Using arc and other plasmas delivering temperature of the order of 5,000 K makes possible to break down organic and inorganic compounds in plasma is highly effective even without oxygen. The other merit is the possibility of good mixing in plasma-chemical reactor, this is the important factor of wastes thermal processing. This process can be realized in the multi-jet plasma reactor, which provides good mixing of plasma with treated wastes [1,2]. The plasma reactor including three-jet mixing chamber with attached three plasma torches. The installation contains a system of raw material supply into the plasma reactor. A system of stub tube, vacuum pump and a set of evacuated flasks were used to extract exhaust gas for analysis. There were also units for power and water supply, for arc ignition and for control system of work parameters of the installation. The system works on the following principle: interaction between three intakes plasma jets and wastes produces in the mixing chamber a certain heterophase flow which then forms the reaction zone over the whole length of the reactor dust. The physical-chemical processes of wastes thermal destruction take course just in this reactor and separation of the power products takes place then in a hopper whereas gases are conveyed into special filter to remove ultra-dispersed fractions. Gases pass then through a lye scrubber and are exhausted into atmosphere by a fan.

2.   Processing and Destruction of Chloroorganic Wastes [3]

Decomposition (destruction) products of the real withdrawals were analyzed. The withdrawals were the mixture of the following products: trichloroethylene – 80%, nitrotoluene – 17%, nitrobenzoalcohol – 1.1%, nitrobenzaldehyde – 1.1%, carbon tetrachloride – 0.8%. Toxic connections were not established in the composition of exiting products.

All experimental investigations were made with a constant waste feed of 3.6 kg/h. The variation of the plasma air supply was connected with a corresponding change of the carbon-oxygen ratio in the plasma reactor. On the other side the increase of the plasma generator. Due to the realized air supply, the waste conversion took place in all cases in a reduction atmosphere. In agreement with the calculation of the thermodynamic equilibrium the analysis of the gas phase shows a complete conversion of the organic substance into carbon monoxide and hydrogen respectively carbon dioxide and stream. Each sample contained hydrogen chloride and hydrogen sulfide in small concentrations. Free chlorine was not be detected. The gaseous phase was analyzed by means of gas chromatography and the mass-spectrometer MAT 311 Varian.

In some cases the product gas contained a insignificant amount of soot which points out that locally a pyrolysis regime took place. The formation of soot could be stopped by supply secondary air at the end of the reactor. In all experiments in gas phase a small concentration of nitrogen oxides was found, although in the thermodynamic calculations it occurred only in oxygen atmosphere. This fact may be connected with the formation of the oxides in the plasma jet and the short reaction time prevented the decomposition.

3.   Processing and Destruction of Bromine Containing Waste [4]

Study was done with the solid free-flowing wastes containing bromide phenols with different proportions. Elemental analysis of the wastes was made by different methods before experiments. The average results obtained by different methods are: C = 30.03%; H_2 = 4.31%; Br = 50.32%; N_2 = 0.51%; S = 0.08%; O_2 = 14.75%. The previous thermal analysis was also used for bromide-phenol wastes, which was studied for content of water and mineral impurities.

Water solution of 2.5% bromine mass was prepared for the first run of bromine wastes. It was expedient for the sake of monitoring disperse solution feed into the plasma heat medium at the high concentration of material. The run of experiments with this solution was carried out at variation of power and material feeding rate. Consumed electric power ranged over 95–120 kW, plasma-forming gas flow rate accounted for 4.7 g/s, and material supply varied from 1.0 to 15.5 g/s. The degree of decomposition amended to 100% for all experiments of the run. Chemical analysis of exhausting gases for content of bromine and toxic components was made after every experiment. No toxic dioxin and oxide was detected.

Possibility to increase the efficiency of the process at the expense of the solution doping was investigated at the second run of experiments. Three experiments, with the 75% solution of wastes in a polar organic solvent were made for processing optimization. At this run, electric power varied from 80 to 110 kW, material rate ranged over 5.6–12.5 g/s and flow rate of the working gas was taken at the constant level 6.0 g/s. The complete decomposition was observed at the maximal material rate, but the incineration was incomplete and a lot of unoxidized carbon was settled out in the water-alkaline scrubber. Exhausting gases produced during the plasma-chemical processing of the wastes were analyzed for the content of dioxides and their analogues, carbon oxides and dioxides, as well as for concentration of bromine hydrogen. Mass-spectrometer Hewlett-Packard GC/MS 5890/5972 was used for analysis of dioxides applying EPA 8270 method with gas filtration through methanol and the subsequent examination of methanol solution. All experiments exhibit no dioxide. Content of CO was analyzed by mass-spectrometer MX-1320 with high resolution. The observed m/z 29 peak had intensity 0.8% that indicates the absent of CO in the gaseous phase. As to content of oxygen, it was found to be low in the first experimental run and negligible in the second one. On the other hand, the measurements demonstrated high concentration of nitrogen. Proportion of HBr in the produced gaseous mixture was measured by gravimetric chemical-analytical method with titration of HBr by silver nitride solution and subsequent analysis of silver bromide by mass-spectrometry. The concentration of HBr in the gaseous phase at normal conditions was determined both runs: for optimal experiment of the first run upstream from scrubber – 0.337 g/l and downstream of it – 0.143 g/l; for optimal experiment of the second run upstream from scrubber – 0.03 g/l and downstream of it – 0.015 g/l.

The component HBr can be considered as a useful desired product of such a wastes processing that can be used for pure bromine production. The experiments have shown that the yield of HBr in the first run applying water-emulsion feed of the wastes is about an order higher then in the second run when organic solvent was used and the plasma-chemical process proceeded at the excess of free carbon and deficient air. Bromine vaporization and reduction at the excess of H_2O according to the first variant is apparently the most efficient method of the wastes processing.

4. Processing and Destruction of Pesticides with a Expired Term of Validity

Investigations are carried out in different regimes of the work of plasma reactor for processing of two pesticides – isophene ($C_{14}H_{18}O_7N_2$) and concentrate of butyl ether of 2,4-dichlorphenoacetic acid ($C_4H_9CH_2COOC_6H_3Cl_2$), with expired term of validity.

Both these pesticides consist of 50–60% of base material (butyl ether and isophene) and 50–40% of the filler substances, which contains of kaolin, aerosol and silica gel. The detailed analysis of gases at the outlet of plasma reactor is

executed. The methods of chromato-mass-spectrometry and absorption spectroscopy in ultraviolet (UVR), visible and infrared (IR) wavelength range are used.

Absorption spectra in the UVR, visible and near IR wavelength range $(0.2 \le \lambda \le 3.,0 \; \mu m)$ were recorded with UV- Vis -NIR- spectrophotometer "Cary 500 Scan" of the firm "Varian" (USA), in such spectra in the distant IR area $(2.5 \le \lambda \le 25 \; \mu m)$ – were detected by Fourier spectrometer "IFS28" of the firm "Brucker" (Germany).

The analysis of the obtained spectrograms made it possible to establish that they weakly depend qualitatively on the type of the raw material used and are presented by three characteristic absorption bands:$\Delta\lambda = 0.2\frac{1}{4}0.25 \; \mu m$, $\Delta\lambda = 0.35\frac{1}{4}$ 0.,6 μm, and $\Delta\lambda = 2,5 \; \frac{1}{4} \; 25 \; \mu m$.

Because of the high optical density of mixture in the UVR region of the spectrum we could not interpret reliably the recorded maximums of absorption. They can be the diffuse absorption bands of hydrocarbons of the type of the benzaldehyde C_6H_5CHO of the propionaldegida C_2H_5CHO, benzene C_6H_6, formaldehyde CH_2O, acetaldehyde C_2H_4O, etc. with transitive into the intensive continuum.

The visible region of the spectrum is presented by the electron- vibrational-rotational absorption bands of molecules NO, NO_2, HNO_2, O_2, CO_2, C_2, AlO, AlH, HfO, CaO, FeO, CuO, CuH, CN, SiN, CH, CHO. However we could not identified a number of the maximums of absorption as well as in the spectrograms of UVR range.

In the absorption spectra in the IR region we discovered the bands CH_3-, CH_2-, CH- of the groups of hydrocarbons and NO_3 – group, bands CO_2, H_2O, N_2, NO_2, the traces of bands NO, bands of the condensed phase HNO_3, of the vapor phase H_2CO_3, the bands of the valence oscillation of the carbonyl group $C = O$, and also the weakly intensive bands of the deformation oscillations OH and CO.

Obtained data testify about the intensive thermal decomposition of pesticides in the plasma airflow, which is accompanied by oxidation and nitriding of the products of decomposition. Bands CH_3-, CH_2-, CH-, and $C = O$ groups are caused by the formation of the secondary hydrocarbons at the outlet of the plasma reactor in hardening zone. Formed simple oxides and nitrides are not highly toxic or carcinogenic substances and are not ecologically dangerous. Some of them can be separated, assembled and used further.

Chromato-mass-spectrometric analysis of emanated gases was performed for a determination of a type of produced hydrocarbons and their quantitative content in the outlet of plasma reactor. Chromato-mass-spectrometer "MM" of "Brucker" firm (Germany) was used, range of mass numbers was 28–400, resolving power R was ~ 10,000, threshold of detectability was ~ 1 ppb ($\sim 10^{-3}$).

Samples were taken after hardening zone with help of program pump SKS and were placed at two-layer absorb tubes of the firm "Dreger". Activated coal and tenaks were used as absorption substances. Duration of sample taking was 4 min, velocity of pumping (circulation rate) of samples trough sorbents was 300 l/min. Preliminary separation of mixture components was curried out at the capillary column. Quadrupole mass-analyzer was used as a mass-detector.

Produced products were identified by the comparison of complete mass-spectrum of analyzed substance or of its separate peaks with mass-spectra from the bank of standard substances. In order to increase statistic significance of the identification we used two methods of library search: a straight one, which provides computer comparison of analyzed spectrum with each library spectrum consequently, and a reverse method, which provides comparison of library spectra consequently with analyzed one.

For a calculation of every component concentration an evaluation of absorb substance mass and data of normalization of chromatometry results were used. Instrumental error of an evaluation of different substance contents in analyzed gases mixture was less 30–40%.

Results of tests in the experiments with isophene and butyl ether processing are presented in the tables. After butyl ether processing without hardening we found saturated, unsaturated and aromatic hydrocarbons, ordinary and complicated ethers, alcoholes, ketones, acids nitrogencontaining and chlorine-containing compounds in the products leaving plasma reactor.

4.1. RESULTS OF THE CHROMATO-MASS-SPECTROMETRIC ANALYSIS OF THE COMPOSITION OF WASTE GAS DURING THE PLASMA-CHEMICAL PROCESSING OF PESTICIDES

- Plasma-forming gas – technical air
- Average value of the specific enthalpy of plasma along the length of reactor H ~ 6,000 kJ/kg

TABLE 1. Pesticide on the basis of isophene $c_{14}h_{18}o_7n_2$

Designation of the substance	Chemical formula	Concentration in the waste gas flow, mg/l
		With the charge of raw material, with the hardening
Methyl nitrate,	CH_3NO_3	2.3
1,3 propandioldinitrat,	$C_3H_6N_2O_6$	
1,3 propenediol	$C_4H_6N_4O_{11}$	
3-heptanone	$C_7H_{14}O$	0.17
Isoamyl nitrite	$C_5H_{11}NO_2$	0.06
2-propyl-1-pentanol	$C_8H_{18}O$	0.59
3,5,5-trimethylhexanol	$C_9H_{20}O$	0.04
3,5-dimethyloctane	$C_{10}H_{22}$	0.04
Undecane	$C_{11}H_{24}$	0.09
2,2-dimethyl-3-hexanol	$C_8H_{18}O$	0.71

TABLE 2. Pesticide on the basis of R- butyl ether $C_4H_9CH_2COOC_6H_3CL_2$.

Designation of the substance	Chemical formula	Concentration in the waste gas flow, mg/l		
		With the charge of raw material, without the hardening	With the charge of raw material, with the hardening	Without the raw material, without the hardening
Methyl cellosolve	$C_3H_8O_2$	0.63	3.01	1.18
Diisopropyl ether	$C_6H_{10}O$	3.08	–	6.86
Heptanone, 3	$C_7H_{14}O$	0.44	–	–
Hexanol, 2-ethyl	$C_8H_{16}O$	1.64	–	–
Heptene 1/3	C_7H_{14}	2.24	5.1	–
Butylisocyanate	C_5H_9NO	2.61	–	–
2-nitrophenol	$C_6H_5NO_3$	0.78	–	–
Acetophenone	C_8H_8O	2.68	–	1.88
Benzoic acid	$C_7H_6O_2$	5.12	6.76	7.30
Benzophenone	$C_{13}H_{10}O$	0.91	3.29	4.03
Acetophenone, 8-chloro	C_8H_7ClO	4.35	–	6.13
Heptachlorepoxide	$C_{10}H_5Cl_7O$	3.28	–	–
Xylene	C_8H_{10}	–	0.15	–
Benzene trimethyl	C_9H_{12}	–	0.09	–
Undecane, dodecane, tridecane	$C_{11}H_{24}$, $C_{12}H_{26}$, $C_{13}H_{28}$	–	0.13	
Butanol, ethyl	$C_6H_{14}O$	–	–	2.92
Isobutylacetate	$C_6H_{12}O_2$	–	–	0.15

As Tables 1 and 2 show, a hardening changes significantly the composition of reactor off-gases. Chlorine- and nitrogen-containing compounds, as well as some substances which contain ether groups and aldehyde groups were not detected at the outlet of reactor. Benzol derivations appear instead of them. Absence of compounds with ether groups and aldehyde ones and content increasing of compounds of types of methylcellosolve and benzoic acid can be caused by processes of secondary oxidation in the zone of hardening.

Nitrogen-containing substances can be performed in the presence of hydrogen into nitroacid or nitrozoacid, that was proved by the spectroscopy analysis. Chlorine-containing compounds can be performed into chlorine salt at the base of calcium, copper and iron, presence of with was detected also by spectroscopy method.

References

[1] A. L. Mosse, I. S. Burov. Treatment of dispersed materials in plasma reactors. Nauka i tekhnika, Minsk (1980).

[2] A. L. Mosse. Plasmotrons, plasma reactors and plasma furnace for processing of toxic industrial wastes. R"99 Congress Proceeding, Published EMPA, Volume 2 (1999), pp. 104–109.

[3] A. Mosse, G. Kusnetzov, D. Hebecker. Conversion of liquid toxic waste by means of a plasma reactor. VDI Berichte Nr.1166 (1995), pp. 651–657.

[4] A. L. Mosse, A. N. Knak, E. M. Ermolaeva, L. I. Krasovskaya. Neutralization of toxic organic wastes in three-jet plasma reactor. 14th International Symposium on Plasma Chemistry, Prague, Volume 5 (1999), pp. 2483–2488.

ENVIRONMENTAL CONTROL PLASMA EDUCATIONAL LABORATORY

V. GENIS[1], A. FRIDMAN[2], AND A. GUTSOL[2]
[1]Goodwin College of Professional Studies, Drexel University, Philadelphia, 19104
[2]College of Engineering Drexel University, Philadelphia, Pennsylvania, 19104

Abstract: The primary goal of the Environmental Control Plasma Educational Laboratory is to introduce students to the engineering principles of non-thermal plasma application for air cleaning from Volatile Organic Compounds (VOC) and other methods of VOC control and measurements, by combining hands-on laboratory experience with lectures. Specifically, during the laboratory sessions, the students learn the engineering and physical principles of non-equilibrium plasma systems operation using the unique pulsed corona system of the Drexel Plasma Institute Environmental Laboratory, carry out experiments on plasma cleaning of VOC contaminated air, measure dependence of Destruction and Removal Efficiency (DRE) of particular VOC on plasma power and other system parameters, and calculate the energy cost of VOC removal. In addition, the students are able to determine the air flow rate and VOC concentration in air stream before the treatment, after the scrubber, after the pulsed corona, and after the mist separator. Efficiency of VOC control by scrubbing is also discussed in details. The work in the laboratory enhances the fundamentals taught in the classroom sessions. Another goal of this laboratory course is to improve the students' data gathering and communication skills. Therefore, a concise written report clearly describing all conclusions and comments is required within 7 days after completion of the laboratory session, upon which the students become familiar with basic VOC control techniques, gain hands-on experience with scrubbing and low-temperature plasma equipment, and are able to demonstrate the basic principles of low temperature plasma cleaning.

Keywords: Applied engineering technology, volatile organic compounds, destruction and removal efficiency, and pulsed corona

1.   Introduction

Drexel University's Goodwin College offers a B.S. degree in Applied Engineering Technology (AET) since 2002. The program content provides an integrated educational experience directed toward developing the ability to apply the fundamental knowledge gained in the Goodwin College to the solution of practical problems in the engineering technology field. The AET program is based on a cyclic model of the relationship between knowledge production and improvement of practice and clearly distinguishes itself from traditional engineering programs in the following ways:

- It forms the bridge between the engineer/scientist and the technical and/or production workforce.
- The curriculum places emphasis on the application of theory rather than on derivations and proofs.
- The majority of courses are fully integrated with training and laboratory experience, extensive use of software and industrial case studies.
- Faculty members with extensive industrial and academic experience support the program.

   The goals of Drexel's Applied Engineering Technology program are:

- ➢ To become a sustainable provider of graduates with terminal 2- and 4-year degrees.
- ➢ To become a national model for the delivery of high-quality, affordable, technically-oriented education by focusing on student-centered learning and the integration of hands-on laboratory and industry-based experiences.
- ➢ To create a flexible curriculum that is responsive to the workplace and which incorporates advances and the best practices in science and technology.
- ➢ To provide students with a strong foundation of engineering practices and stimulate students' interest by using a problem-solving approach in state-of-the-art laboratories.
- ➢ To provide students with leadership, management, and communication skills, as well as an understanding of professional ethics, which will serve as a foundation for future development and success in their careers.

   To achieve these goals, Goodwin College of Professional Studies is in the process of expanding and upgrading its educational facilities within the Applied Engineering Technology Program. These facilities will allow all AET students to be involved in the educational, research, and training process and also will alleviate the shortage of trained specialists in applied electrical, mechanical, and industrial technology. Key factors in the development process include creation of the educational laboratories that can significantly contribute to the development of technologically literate students and workforce that could be in great demand not only in the tri state area but also nationwide [1–3]. Several state-of-the-art

laboratory and project-based courses were developed and one of them, such as Environmental Control Plasma Educational Laboratory is described in this paper.

2.   Course Development

The objective of this project was to implement the material developed at the Drexel Plasma Institute for undergraduate AET students and expand it to a course with a problem-based learning approach to non-thermal plasma application for air cleaning from Volatile Organic Compounds (VOC) through real-life problems. Such educational laboratories are non-existent in our geographic area and would be welcomed by the working community (Fig. 1). The establishment of a state-of-the-art laboratory for air cleaning purposes allows Drexel and its community college partners to develop training options for technicians located in the region's key industries. After completion of all laboratory sessions, the students become familiar with basic VOC control techniques, gain hands-on experience with scrubbing and low-temperature plasma equipment, and are able to demonstrate the basic principles of low temperature plasma cleaning [4–6]. The work in the laboratory enhanced the fundamentals taught in the classroom sessions. The purpose of this project is not to develop new techniques in air cleaning, but to expose students to existing techniques by introducing them to the equipment and methods that could be used in real-world industrial applications.

During the past 3 years, Environmental Control Plasma Educational Laboratory course was developed and offered at the undergraduate level for the Applied Engineering Technology students. This is a hands-on, two-credit course (within the frame of Drexel's quarter system).

The course exposed students to basic applications of non-thermal plasma for air cleaning from Volatile Organic Compounds (VOC) and other methods of VOC control and measurements. Lecture time with students allowed for the introduction of topics included in the laboratory experience. The industrial case studies in laboratory environment enhance the fundamentals taught in the classroom sessions.

Figure 1. Mobile environmental control plasma educational laboratory

The course syllabus, which was developed by the faculty of the Drexel Plasma Institute in collaboration with the faculty of the Goodwin College, describing all laboratory procedures, requirements, objectives, and outcomes is presented below.

Drexel University
Goodwin College of Professional Studies

Course: MHT 295, Environmental Control Plasma Laboratory.
Term:
Credits: 2

Course Description:

This laboratory course introduces students to the engineering principles of non-thermal plasma application for air cleaning from Volatile Organic Compounds (VOC) and other methods of VOC control and measurements, by combining hands on laboratory experience with lectures. Specifically, the students will learn the engineering and physical principles of non-equilibrium plasma systems operation using the example of the unique pulsed corona system of the Drexel Plasma Institute Environmental Laboratory, will carry out experiments on plasma cleaning of VOC contaminated air, will measure dependence of Destruction and Removal Efficiency (DRE) of particular VOC on plasma power and other system parameters, will calculate the energy cost of VOC removal. The work in the laboratory will enhance the fundamentals taught in the classroom sessions.

Course Objectives:

The main objective of this laboratory course is to introduce students to fundamentals of Volatile Organic Compounds (VOC) control and to demonstrate the basic principles of non-thermal plasma application to air cleaning. Another objective of the course is to improve students' communication skills. Therefore, a lab report, clearly describing all conclusions and comments will be required within 7 days after completion of the laboratory session.

Prerequisites: CHEM 111 and CHEM 113.
Required Text: 1. Class-notes.
                 2. Alexander Fridman & Lawrence A. Kennedy, Plasma Physics and Engineering, Taylor & Francis, 2004.

Course Schedule:
Location:
Instructor: Dr. A. Gutsol
                 Tel.:
                 E-Mail:

Teaching assistant: To be assign.
Course outcomes: After completion of this course the students:

- Will become familiar with basic VOC control techniques.
- Will gain hands-on experience with scrubbing and low-temperature plasma equipment.
- Will be able to demonstrate the basic principles of low temperature plasma cleaning.
- Will be able to determine:

    1. Air flow rate
    2. VOC concentration in air stream

        ❖ before treatment
        ❖ after scrubber
        ❖ after pulsed corona
        ❖ after mist separator
    3. Plasma system power
    4. DRE (destruction and removal efficiency)
    5. Dependence of DRE on plasma power
    6. Plasma energy cost of particular VOC removal
    7. Efficiency of VOC control by scrubbing

Date	Week	Instructor	Topic
xxxx	1	AG	Basic principles of VOC control in air (lecture). (Hess Lab)
xxxx	2	AG	Basic principles of low temperature plasma and its application to VOC control (lecture and demonstrations).
xxxx	3	AG	Familiarization with the Drexel Plasma Institute Environmental Laboratory.
xxxx	4	AG	Measurements of plasma power, air and water flows.
xxxx	5	AG	Admixing and concentration measurements of VOC.
xxxx	6	AG	Experimental data and their analysis (lecture), Group discussion.
xxxx	7	AG	Measurements of dependence of insoluble VOC concentration on air flow and Plasma Power.
xxxx	8	AG	Measurements of dependence of soluble VOC concentration on water flow and Plasma Power.
xxxx	9	AG	Group discussions of the collected experimental data and their analysis.
xxxx	10	AG	Final presentation.

Experimental work: Each laboratory will be conducted in groups of 6 students.

Evaluations: Each student will be graded weekly. Class participation 10%, Laboratory reports – 60%, Final presentation – 30%.

The syllabus also clearly states the course policies, including Americans with Disability Act, Academic Honesty Policy, Student Responsibilities, Course Drop Policy, Course Withdrawal Policy, and Financial Obligations.

3.   Sample Projects

This is a two-credit course consisting of a lecture and a laboratory each week. Laboratory sessions were organized around current developments in the field of plasma applications for air cleaning from VOC. Students worked as teams to research the problem, develop possible approaches to solving the problem, and structure possible solutions. During the laboratory sessions, students were introduced to tools, methodologies, and techniques that could be useful for solving the problem. Finally, students carried out experiments they have designed and described the results of the experiments in individual reports for each lab. After completion of all laboratory sessions, each team was responsible for writing a final report that summarized the current state in the area, described the experimental techniques utilized, discussed the expected outcomes, provided data of the actual outcomes, and explained the reasons for the departures between the expected and the actual results. The team analyzed the data, described conclusions and suggested possible ways for improving the accuracy of their experiments. The team then presented their findings to the class as a whole.

The experiments described below were carried out using the Mobile Environmental Control Plasma Educational Laboratory according the following block diagram (Fig. 2):

During the laboratory procedures, the students were able to determine the air flow rate and VOC concentration in air stream before the treatment, after the scrubber, after the pulsed corona, and after the mist separator (see Fig. 2). 100 ppp of the admixture of methanol was used as a soluble VOC. The bubbling small air flow was applied to this admixture through the special bottle with ethanol that was kept under constant known temperature. As a result, the small flow was saturated with methanol vapor and mixed with the main flow. Data of the flow rates for both streams and the temperature of the bottle allow calculating initial methanol concentration with required accuracy. Calculated concentration was then compared with the measured during the experiments. Gas Chromatograph with Mass-Spectrometer (GC-MS) was used for the measurements of VOC concentration and analysis of the products. The hydrocarbon analyzer was used for the measurements of the total amount of VOCs (initial and by-products). Evaluation of DRE efficiency of soluble VOC by scrubbing only, by plasma treatment only, and by plasma treatment in combination with scrubbing was determined and discussed in details. The results of the measurements are presented in Fig. 3.

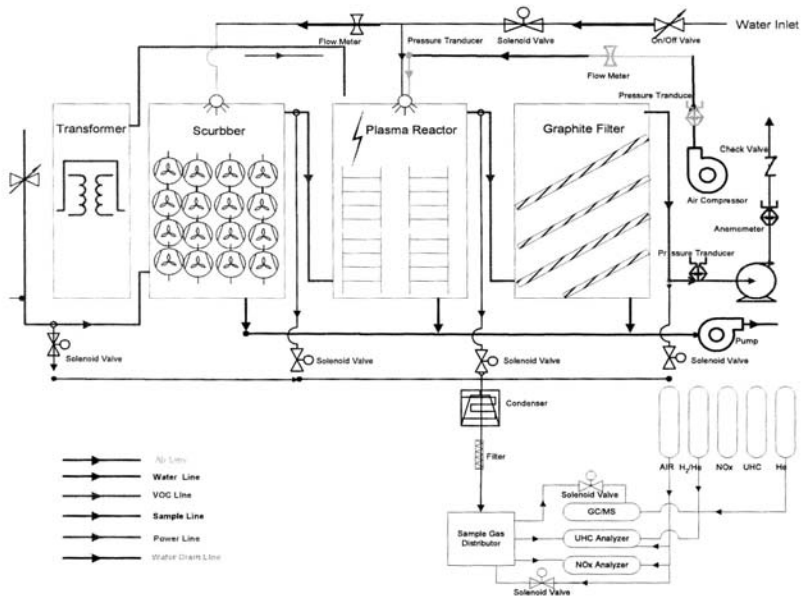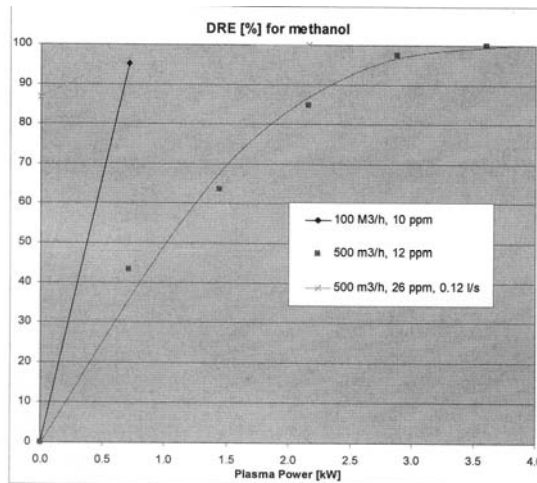*Figure 2.* Block diagram of the pulsed corona pilot plant

Figure 3. Measurements results during the laboratory procedures

Similar procedures for admixing of insoluble VOCs, such as alpha-pinene and dimethyl-sulfide, were applied. DRE for insoluble VOCs was evaluated for both dry and wet pulsed corona. During the wet pulsed corona discharge, the soluble by-products were removed by the water spray [5,6].

4.   Summary

MHT 295, Environmental Control Plasma Laboratory course was offered to AET students since 2003. The faculty of the Drexel Plasma Institute in collaboration with the faculty of the Goodwin College developed the experiments based on the real-world industrial problems. The authentic problems were presented to the Goodwin's faculty responsible for the final phrasing of the given task, such that the description of the task, including the objective of the project, its motivation, and the expected deliverables are clear and understood by the students. During the laboratory sessions, the students learned the engineering and physical principles of non-equilibrium plasma systems operation using the unique pulsed corona system of the Drexel Plasma Institute Environmental Laboratory. Students carried out experiments on plasma cleaning of VOC contaminated air, measured dependence of Destruction and Removal Efficiency (DRE) of particular VOC on plasma power and other system parameters, and calculated the energy cost of VOC removal. The work in the laboratory complemented the fundamentals taught in the classroom sessions. The students were able to determine the air flow rate and VOC concentration in air stream before the treatment, after the scrubber, after the pulsed corona, and after the mist separator. Efficiency of VOC control by scrubbing was also discussed in details. An important objective of this laboratory course was to improve the students' knowledge of data gathering, the identification of sources leading to erroneous measurements, and proficiency in communication skills. Therefore, a concise written report clearly describing all conclusions and comments was required within 7 days after completion of each laboratory session. Students worked in teams on projects drawn from several areas of technological interest. The simulation of plasma applications used by companies in industry was implemented in the course.

References

[1]   Felder, R. M. and Brent, R. The intellectual development of science and engineering students. Part 2: Teaching to Promote Growth. Journal of Engineering Education. Vol. 93, No. 4, 2004, p. 279.

[2]   Workforce 2002: Measuring what matters. The Reinvestment Fund. October 2002.

[3]   Pennsylvania Economy League's Report, *Building a World-Class Technical Workforce*. Report #686.

[4]   Alexander Fridman & Lawrence A. Kennedy, "Plasma Physics and Engineering", Taylor & Francis, New York, 2004.

[5]   Mario G. Sobacchi, Alexei V. Saveliev, Fridman, A. A., Gutsol, A. F., and Lawrence A. Kennedy, "Experimental Assessment of Pulsed Corona Discharge for Treatment of VOC Emissions", Plasma Chemistry and Plasma Processing, Vol. 23, No. 2, 2003, pp. 347–370.

[6]   Sobacchi, M. G., Saveliev A. V., Kennedy, L. A., Lock, E., Fridman, A., Gutsol, A., Desai, A., Tak, G., Gutsol, K., Korobtsev, S., Shiryaevsky, V., Medvedev, D., and Abolentsev, V. "Pulsed Corona Plasma Technology for Treating VOC Emissions from Pulp Mills" 2004 TAPPI Paper Summit, Spring Technical and International Environmental Conference, May 3–5, 2004, Atlanta, GA, USA, Electronic Proceedings, PS04169.pdf.

3. PLASMA DECONTAMINATION IN MEDICINE

COLD PLASMA TREATMENT OF *IN VITRO* DENTAL PLAQUE

S. K. FILOCHE[1], C. H. SISSONS[1], R. E. J. SLADEK[2], AND E. STOFFELS[2]

[1]*Dental Research Group, Department of Pathology and Molecular Medicine, Wellington School of Medicine and Health Sciences, University of Otago, New Zealand*
[2]*Department of Biomedical Engineering, Eindhoven University of Technology, Eindhoven, The Netherlands*

Abstract: We investigated the effects of a non-thermal atmospheric plasma (plasma needle) and chlorhexidine digluconate (CHX) on the growth of human oral bacteria. We used the microplate biofilm microcosm (MBM) model to replicate dental plaque; the antimicrobials were tested on 1 old biofilms. After treatment, the growth of the biofilms was studied by taking photographs. The differential effect of the treatments among the species was analyzed by the DNA-DNA checkerboard technique. Furthermore, the biofilms were placed in fixative and observed under transmission electron microscope (TEM).

The results show a complex response of MBM to plasma and CHX treatments. TEM images show that bacteria are physically damaged; DNA-DNA checkerboard analyses show that some species were significantly suppressed, while others were increased by plasma and CHX treatments. Photographs show that the only the chlorhexidine treatment visually changed the structure of the biofilm.

Keywords: Cold atmospheric plasma, dental caries, *in vitro* dental plaque

1. Introduction

Dental plaque is a complex oral biofilm made up of hundreds of oral bacteria organized in communities. These bacterial communities are embedded in an exopolysaccharidic matrix with a com plex architectural structure. Bacteria in these communities can cause diseases such as dental caries and periodontitis, but they also play an important role in oral health.

Mechanical removal of dental plaque by efficient oral hygiene can almost completely prevent caries. Other approaches to prevent caries are fissure sealants, antimicrobial agents, fluoride, and dietary sugar substitutes (e.g. xylitol). Cavities will form if the caries prevention is not sufficient.

Preparation of cavities prior to filling is done by removing necrotic, infected and non-remineralizable tissue by means of mechanical drilling or laser techniques. In both methods heating takes place, and in mechanical drilling vibrations are induced. Heating and vibrations are usually painful for the patient. Moreover, these methods are often too destructive: an excess of healthy tissue must be removed to ensure that the cavity is free of bacteria. In addition, the remaining tooth structure is weakened and prone to fractures.

An alternative painless and tissue-saving method to manage caries is plasma treatment [1]. Plasma is a gaseous medium that contains short-living active particles such as reactive oxygen species, ROS [2]. When applied in moderate amounts, plasma can inactivate bacteria without heating and damage to the living tissue. Antimicrobial properties of plasmas have been described in literature [3–5]; the effects of plasma treatment on living animal cells have been also studied [6]. In our approach a non-thermal atmospheric micro-plasma, the plasma needle [1] is used. The principle of plasma treatment is the deactivation of dental bacteria by the active plasma species, in a painless, non-contact and non-destructive way.

The plasma needle was tested on *Escherichia coli* and *Streptococcus mutans* bacteria grown on agar dishes [7,8] and *Streptococcus mutans* biofilms [9]. The plasma needle treatment killed *E. coli* and *S. mutans* bacteria grown on agar plates and stopped the re-growth of the *S. mutans* grown in biofilms. It should be noted that these studies were primarily concerned with single-species cultures and biofilms. However, the antimicrobial effect of the plasma needle treatment should be studied on more complex, and thus more realistic bacterial samples.

To predict the antimicrobial susceptibility of bacteria grown in oral biofilm, complex model systems have been developed. In these models dental plaque biofilms can be replicated and studied *in vitro*. Several of these artificial dental plaque model systems are described by Sissons et al. [10]. These include the growth-rate-controlled biofilm fermenters (GRBF), constant-depth film fermenters (CDFF), chemostat-based systems, and most recently the artificial mouth model systems (MAM). In the artificial mouth model system, multi-plaque microcosms can be grown. A microcosm is defined as "a laboratory subset of the natural system from which it originates but from which it also evolves". The microcosms used in the artificial mouth model system by Sissons et al. contain hundreds of species of bacteria and are nowadays the closest laboratory approach to plaque in the human mouth. This model is labor-intensive and requires specialist equipment. However, the plaque biofilms that are generated appear to reflect the complexity, diversity and heterogeneity of *in vivo* plaques [11].

In this paper we use an easily reproducible model to replicate dental plaque, the microplate biofilm microcosm (MBM) model. This MBM model is used to test the susceptibility to antimicrobial agents. The MBM model is relatively simple to prepare, maintain and analyze. The advantage of the model is that it allows for the short-term and efficient exposure of the biofilm to antimicrobials. In the MBM experiments the differential effect of the treatments among the species was analyzed by the DNA-DNA checkerboard technique [12]. Checkerboard DNA-DNA hybridization (CKB) is a technique which gives a simultaneous and quantitative analysis of up to 28 plaque samples against 40 key microbial species, blanks and standards on a quare nylon membrane.

Plasma treatment of biofilms was studied in relation to food safety [13], but there was hitherto no information on plasma deactivation of complex dental biofilms. To check the bactericidal effectiveness of the plasma, microcosm microplate biofilms were grown and treated by the plasma needle. The effect of the plasma needle treatment was compared with that of chlorhexidine digluconate mouthwash. Photographs and transmission electron microscopy (TEM) images of treated biofilms were taken. We also investigated the composition of the biofilms by checkerboard DNA-DNA hybridization technique. Furthermore, in the MBM experiments we studied the effect of the sucrose concentration on the biofilm behaviour.

2.   Materials and Methods

2.1.   THE PLASMA NEEDLE APPARATUS

The plasma needle used in the present study (Figure 1), consisted of a tungsten wire (0.3 mm diameter with a sharp tip, confined in a Perspex tube (4 mm inner diameter). Because the voltage needed to ignite the plasma in helium is lower than in pure air, the plasma was sustained in a helium-air mixture. The Perspex tube was filled with helium (ZG Helium, Purity > 99.995%, BOC, New Zealand) delivered at a flow rate of 2 l/min, measured by an electronic volumetric flowmeter (Omega, FDP 10). A radio frequency (RF) voltage was applied to the needle at 13.56 MHz. The signal was produced by a custom-built power generator and a matching network. The network consisted of a 4.4 µH induction coil network placed in series with the plasma, and a 50 Ω shunt resistor placed in parallel with the inductance and the plasma, in order to match the load impedance to the internal impedance of the power generator (50 Ω). The consumed power was monitored using a P6103 Tectonics probe (Amplifier Research, Souderton, United States of America) connected via a dual-directional coupler to a power meter (Amplifier Research, model PM 2002). The power consumed by the plasma during the treatments was 50 or 100 mW.
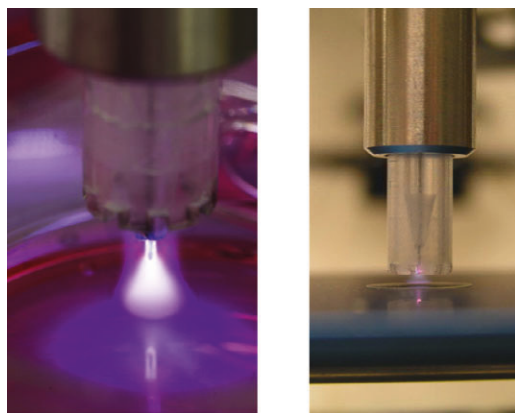

Figure 1. The plasma needle (Left photo by courtesy of Bart van Overbeeke, *Matrix* magazine, the Netherlands)

2.2. EXPERIMENTAL PROTOCOL

The experiments were carried out twice on a 1 day old biofilm. Each experiment had a different saliva sample (same donor). The effect of a 'single' treatment on a 1 day old microplate plaque biofilm was investigated. The treatments were performed in triplicate.

2.3. PREPARATION OF THE MICROPLATE BIOFILM
MICROCOSMS (MBM)

Approximately 20 ml of stimulated saliva was collected from a donor who had refrained from oral hygiene for 24 h. Ethical approval was granted from the Wellington Ethics Committee, New Zealand (Ref. Number 04/07/051). Dithiothreitol was added (0.5 mM final concentration) and the saliva was filtered through sterile glass wool and collected in a sterile glass beaker and mixed [14]. The prepared saliva (100 µl) was inoculated onto 9 mm diameter sterile Thermanox™ coverslips (Nunc Inc., Naperville, IL, USA) that had been placed in each well of the 24-well microplates (Sarstedt, Sarstedt Australia Pty Ltd., Ingle Farm, Australia) for 1 h. After 1 h the saliva was gently aspirated from the coverslips and the base of the wells, and 1.8 ml of growth media (defined medium mucin, DMM) [14] was added. The influence of sucrose supplementation was studied by adding sucrose to the media at a final concentration of 0%, 0.15% and 0.30% by weight. The plates were then incubated in an anaerobic hood in an atmosphere of 80% N_2, 10% CO_2 and 10% H_2 (Coy^{TM}, Laboratory Products Inc., Grass Lake, MI, USA) at 35ºC without shaking.

2.4. APPLICATION OF THE ANTIMICROBIAL AGENTS

The antimicrobial agents were applied at the same time as the growth media was replenished. The liquid chemical agents were applied to the plaque biofilms on the Thermanox™ coverslips directly in the wells. For plasma treatment, the slips were removed and treated outside the wells. The biofilms were harvested for analysis 24 h after the treatments.

2.5. PLASMA NEEDLE APPLICATION

Plaque biofilms were treated with plasma for 1 min or for 5 min, at a distance approximately 1 mm from the biofilm surface, to guarantee the optimum performance [7]. The plasma control sample was prepared by exposing the plaque biofilms to a helium flow of 2 L/min, for 1 and 5 min. For the negative control, plaque biofilms were also exposed to air for 1 and 5 min. After treatment the plaque biofilms were placed in new sterile microplates with fresh media.

2.6. CHLORHEXIDINE DIGLUCONATE APPLICATION

Chlorhexidine digluconate (CHX) was used as a positive antimicrobial reference. After complete removal of the supernatant, 1 ml CHX (0.2%) (Sigma-Aldrich Inc, New Zealand) was added to the 24 h biofilms for 10 min. The CHX was removed and the biofilms were rinsed twice with 1 ml of sterile water for 1 min. The coverslips with adherent biofilm were placed into a new sterile plate; fresh media were added and the samples were incubated for a further 24 h. For the CHX control, biofilms were treated with sterile water for 10 min.

2.7. MICROBIOTA PROFILING BY CHECKERBOARD DNA-DNA (CKA) ANALYSIS

Plaque suspensions were prepared for Checkerboard DNA-DNA (CKB) analysis by placing the coverslip and adherent biofilm in sterile water and mixing vigorously to remove the adherent biofilm. Aliquots of the samples were dispensed, the cells harvested and the pellets stored at $-80°C$ until analyzed.

For the CKB analysis, cells were resuspended in 0.25 M NaOH/0.5 x TE buffer to a final concentration of 2 mg/ml per sample. A 100 µL aliquot of each suspension was heated at 96°C for 5 min to lyse the cells and extract the DNA. Samples were neutralised with 800 µL 5M NH4 acetate and deposited onto a 15 x 15 cm positively charged nylon membrane (Roche) using the 30 parallel lanes of a multi-channel immunoblotter (Minislot 30, Immunetics). A UV-Crosslinker (Hoefer) set at 70,000 $µJ/cm^2$ was used to cross-link the DNA to the membrane. Two sets of DNA standards (equivalent to 10^5 and 10^6 cells of the target species), and one positive (plaque) and one negative (*E. coli*) control were also cross-linked to each membrane.

The plaque and standard DNA on the membranes were cross-hybridized with 40 unique DIG-labelled probes (prepared from whole cell chromosomal DNA) using a 45 channel miniblotter (Immunetics), and left overnight with gentle shaking at 42°C. Any unbound probe was removed using a high stringency wash (68°C) in phosphate buffer. Membranes were blocked and then incubated with anti-DIG:AP antibody (Roche) for 1 h at room temperature. Excess antibody was washed off and the probe-DNA hybrids were detected via chemi-luminescence using CDP-Star (Roche) in detection buffer. Hybrids were visualised using chemi-luminescent film and recorded digitally using the Chemigenius II and GeneSnap v. 6 software (SynGene).

To quantify the CKB data, the spot intensities of each sample in the digital image were compared to those of the internal. The resultant values were converted to absolute and total percentage of probe counts. The mean percentage of the DNA probe count was reported.

2.8.   PHOTOGRAPHY AND TRANSMISSION ELECTRON MICROSCOPY

Photographs of the individual biofilms were taken using an Olympus Camedia (C-5050 Zoom) digital camera (Olympus America Inc., Pty Ltd., New York USA).

    The coverslips with the plaques for transmission electron microscopy (TEM) analysis were fixed in half strength Karnovsky fixative, post-fixed in osmium tetroxide (Sigma Aldrich) with added potassium ferrocyanide (Sigma Aldrich), dehydrated in graded ethanol series and embedded in Procure 812 (Epon substitute). Sections were cut with a Reichert-Jung Ultracut E microtome, stained with uranyl acetate and lead citrate, and examined with a Philips CM100 microscope.

3.   Results

3.1.   MICROBIOTA COMPOSITION: EFFECT OF SUCROSE

The microbiota composition of the microplate plaques was analysed by CKB analysis. Individual species responded differentially to sucrose supplementation, which yielded substantial variations in the microbial profiles (Fig. 2). Note that in absence of sucrose, *H. parainfluenzae* was the dominant species, comprising more than 50% of the total population.

Figure 2. Effect of sucrose on species composition of 1 day old MBM plaque. The screened species are split in four groups. Upper left: Gram positive aerobes and streptococci (facultative), upper right: Gram negative aerobes, lower left: Gram positive anaerobes (facultative), lower right: Gram negative anaerobes. Black bar: 0% sucrose, gray bar: 0.15%, and white bar: 0.30%. Standard deviation is 10–15%

3.2. MICROBIOTA COMPOSITION AFTER PLASMA AND CHX TREATMENT

The MBMs for treatment were grown for 1 day in 0.15% sucrose; the composition for 0.15% sucrose in Fig. 2 was taken as a baseline. Figure 3 shows the composition of the 1-day old film after treatments and another 1 day of incubation. The percentage of screened Gram negatives and anaerobes decreased in the biofilm composition after the treatments, both with plasma and with CHX. Interestingly, plasma reduced the actinomyces, while the percentage of streptococci (except *S. mutans*) was increased.
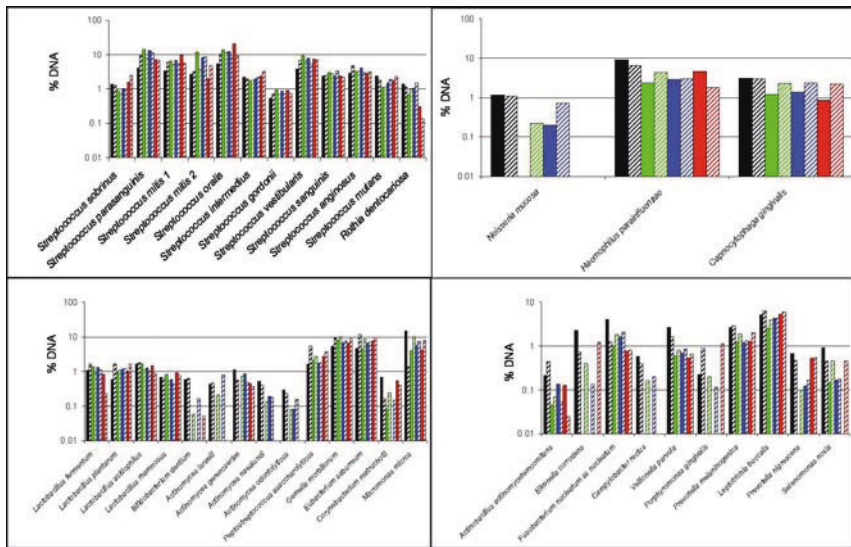

Figure 3. The baseline composition and the composition 1 day after the treatments of the MBMs. The MBMs were 1 day old (grown in 0.15% sucrose) prior to treatment. In order of appearance from left: black bar: baseline, black/white bar: untreated, green bar: plasma 100 mW, 1 min, green/white bar: plasma 1 min control, blue bar: plasma 100 mW, 5 min, blue/white bar: plasma 5 min control, red bar: CHX, red/white bar: CHX control. The standard deviation is 20%

The most remarkable compositional changes are summarized in Table 1:

TABLE 1. Percentage of total DNA. The affected species of the MBMs 1 day after the treatments. The MBMs were 1 day old, grown in 0.15% sucrose and then treated. Plasma power was 100 mW. Standard deviation: 20%

Species	Plasma 1 min (N = 5)	Plasma 5 min (N = 4)	CHX (N = 5)	Untreated (N = 6)
Streptococci:				
mutans	1.1	1.5	1.8	2.0
sobrinus	0.9	1.0	1.6	1.3
mitis 2	11.7	8.1	2.0	3.3
oralis	13.9	12.3	20.5	10.4
Gram+ aerobes:				
R. dentocariosa	0.7	1.1	0.3	1.2
Gram+ (fac.) anaerobes:				
L. plantarum	0.9	1.2	1.0	1.6
B. dentium	0.0	0.0	0.0	0.3
A. israelii	0.0	0.0	0.0	0.6
Gram- aerobes:				
H. parainfluenzae	2.4	2.8	4.7	6.5
N. mucosa	0.0	0.2	0.0	1.0
C. gingivalis	1.2	1.4	0.9	3.0
Gram- anaerobes:				
E. corrodens	0.0	0.0	0.0	0.7
C. rectus	0.0	0.0	0.0	0.4
P. gingivalis	0.0	0.0	0.0	0.9
S. noxia	0.2	0.2	0.0	0.5

3.3.   APPEARANCE AND STRUCTURE OF THE MICROPLATE PLAQUES

Immediately after treatment, there were no visible changes to the MBMs after plasma treatment, but the film treated with CHX was broken and clearly disturbed. Individual cells within the biofilm were affected by both plasma and CHX treatments, cell lysis was particularly evident after plasma treatment (Fig. 4), but also observed after CHX treatment. Morphological differences in responses to treatments were observed. Plasma-treated cells had unstructured membranes as compared to CHX-treated or untreated bacteria.

4.   Discussions

Microplate biofilm microcosm is an advanced model system for oral flora, cultured under conditions that are optimal for the growth of a bacterial community. Large variety of species comprises the biofilm; their coexistence may be symbiotic or competitive. Thus, this is an intrinsically complex system and its response to various external factors is also complex and not easy to predict. In principle, MBM is a reliable model; the only source of uncertainty may be introduced by a non-constant film thickness. This thickness can vary, unless the films are grown in a CDFF [10]. In our experiments, the approximate thickness of the MBM plaques was 1 mm, which is rather large as compared to a real situation in the mouth.
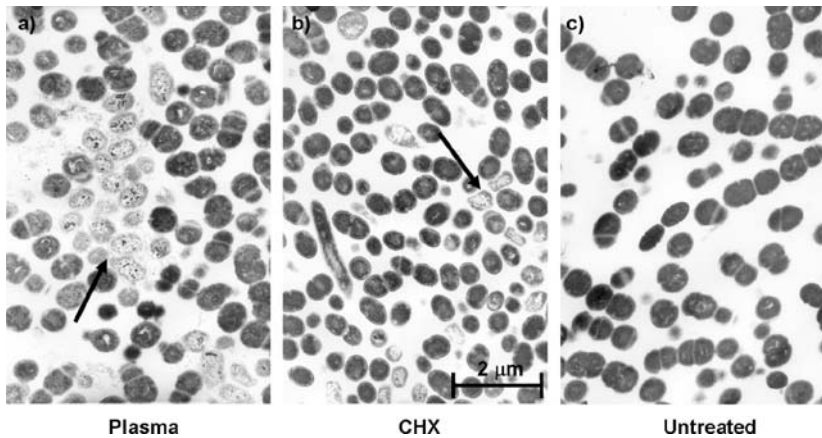
Figure 4. Effects of plasma (5 min at 100 mW) and chlorhexidine digluconate on the ultra-structure of the microplate plaques immediately after treatment. The microplate plaques were grown in 0.15% sucrose for 24 h prior to treatment

It should be mentioned that the MBM model does not entirely reflect the *in vivo* situation. The MBMs grown *in vitro* were only 1 day old and grown in an anaerobic environment. The biofilms encountered *in vivo* can be more mature, and they are not grown in a completely anaerobic environment. In mature biofilms the matrix is better developed, and if the bacteria grow aerobically, as in the mouth, the aerobic species might be located at the top or surface layer and the anaerobic bacteria at the bottom of the biofilm. In case of MBMs, the distribution of various species is probably random. Besides, the MBM model is not exposed to exactly the same chemical environment as the oral biofilms. The latter have to survive in a more hostile environment, which is created by the immune system of the organism. The oral defence system consists of both non-specific factors, such as saliva flow, lysozyme protease (causing cell lysis) and apo-lactoferrin (causing cell death), and specific immune factors (lymphocytes, macrophages, IgG, sIgA, IgM secretion). In presence of these factors, bacteria may be easier to kill by additional (externally administered) antimicrobial agents.

Keeping in mind advantages as well as shortcomings of this model, we shall attempt to analyse the complex behaviour of the biofilm. From the above-presented data, we can draw some general conclusions. Firstly, the behaviour of MBM is greatly affected by the sucrose concentration of the DMM. Sucrose is a very important nutrient for the oral flora; it is transformed into lactic acid. Thus, an increase of the sucrose concentration leads to an increased acidity (decrease of the pH) and to an increase of the biomass due to bacterial growth. The resulting low pH selects for aciduric organisms, such as most streptococci (e.g. *S. mutans*) and lactobacilli. Furthermore, it is shown that sucrose concentration has a significant influence on the species composition: it promotes the growth of several anaerobic species and reduces the growth of Gram negative bacteria (Fig. 2). Sucrose concentration is probably the primary factor that determines the composition and time development of the MBMs. The effect of anti-plaque treatment seems to be of a lower order, and treatment results manifest themselves only after a certain time following the treatment.

In treated samples, at a given sucrose concentration, both CHX and plasma show bactericidal or bacteriostatic action (growth reduction) on the biofilm, but the effects of these agents are different.

CHX changes the MBM structure visibly, the biofilm appears partly broken and dissolved. There are no such drastic changes in macroscopic appearance of plasma-treated samples. However, at the microscopic level (Fig. 4) one can see that both plasma and CHX lead to cell lysis. The effect of plasma on the cell morphology is puzzling: most cells appear swollen and their membranes seem damaged, yet there is no complete cell disintegration.

CKB analysis shows several compositional shifts after treatments. The selectivity of plasma and CHX towards various species is different. Both treatments are not completely lethal to all bacteria: in fact, some species are enhanced while others are reduced. Apparently, plasma treatment of 1 day old films has a fairly strong bacteriostatic influence on *S. mutans*, which is a major pathogen causing caries. This is in agreement with our previous studies of a single-species *S. mutans* film, where we observed significant growth reduction [9]. Both plasma and CHX seem to target the anaerobes; the plasma is reduces the relative population of Gram negatives (mainly associated with periodontitis). The actinomyces (pathogens associated with oral abscesses, especially *A. israelii*) are suppressed. In conclusion, the most affected group by plasma are the Gram negative anaerobes; CHX seems to be more effective against Gram positives (with several exceptions, such as lactobacilli).

Interestingly, plasma increases the percentage of several streptococci (other than *S. mutans*), and plasma as well as CHX enhance several lactobacilli. This effect may be attributed to mutual interactions of species in a complex biofilm. Treatments cause certain imbalances in the population, such as selective suppression of Gram negative and/or anaerobic species. This in turn will to a new composition, because reduction of one species may promote the growth of another one. Especially lactobacilli are known to have antagonistic relations with several other (pathogenic) species [15]. Suppression of these pathogens would cause lactobacilli to thrive.

The mechanisms of plasma and CHX interactions with bacteria are completely different. CHX is a non-specific cell-killing chemical, which attacks all cell membranes and causes cell lysis: the membrane is practically dissolved, and the cytoplasm leaks out. In contrast, plasma can affect many cell constituents, and the effects may be sub-lethal as well. The action of plasma is based on active radicals, in particular on the reactive oxygen species family (ROS). This family comprises short-living O and OH, as well as ozone, peroxide anion etc. Plasma needle operated in helium and air is a good source of atomic oxygen and hydroxyl radicals [2]. These species are capable of bacterial inactivation; however, their penetration into organic samples is limited by their lifetime. Therefore, the effect of treatment duration on the efficacy is not apparent. Most likely the 1 min treatment is sufficient and further prolongation does not improve the results [7].

Membrane damage in plasma interactions with cells is one of the important killing mechanisms: the ROS generated by the plasma can cause lipid peroxidation and lysis (often referred to as "bacteria etching" in physical literature, see Moisan et al. [5]). This could explain swelling of plasma-treated bacteria: when the membrane

damage is not very extensive (no complete destruction), Na, Ca and water enter the cell and cause swelling; this is usually followed by cell death. Previous tests on eukaryotic cells showed that lethal membrane damage (necrosis) could occur, especially after long plasma treatment times and at high power levels [6]. However, under low-power conditions such as applied in this paper, necrosis in eukaryotic cells did not occur, but sub-lethal responses were found. Plasma effects on bacteria can be also delayed-lethal, or sub-lethal, when the membrane is not severely compromised. One of the possible mechanisms is the radical-induced damage to intracellular components (e.g. DNA damage). The affected bacteria would have to repair the damage, and in this way they would deplete their energy resources; this effect also leads to swelling, necrosis and lysis (in analogy to lytic necrosis that follows ischemic stress). In case of less severe damage, no necrosis but cell cycle can occur. In fact, delay of bacterial growth, observed in plasma treatment of single-species biofilms (*S. mutans*) was most likely due to cell cycle arrest [9]. In a biofilm, such arrest in one group of species will cause further shifts in the composition, as seen in the CKB data.

5. Concluding Remarks

In summary, we can state that plasma effects on bacteria are of more complex nature than mere killing. Additional complication arises from the limited penetration depth of short-living radicals into an organic biofilm. Species present in the top layer will be destroyed, but the underlying layers may undergo sub-lethal transformations. Since the microcosm is a quasi-independent system, where various bacteria compete with each other, death of one species can result in enhancement of another one. Treatment with antimicrobials, be it plasma or chlorhexidine, does not inactivate all species, but it definitely does disturb the plaque.

We should keep in mind that the used plaque models were much thicker than in a realistic situation. In the oral cavity the biofilm is usually much thinner, and after treatments, disturbed plaque with weakened bacteria would be easier to destroy by the natural defence system of the body. The current results on plasma treatment in combination with previously established cell cycle arrest of *S. mutans* [9] give a reasonable indication that plasma treatment would contribute to oral hygiene. Naturally, the ultimate proof of effectiveness of plasma treatment must be supplied by an *in vivo* study.

References

[1]   Sladek REJ, Stoffels E, Walraven R, Tielbeek PJA, Koolhoven RA, Plasma treament of caries: a new method in dentistry. IEEE Trans. Plasma Sci. 32(4): 1540–1543 2004.
[2]   Stoffels E, Gonzalvo YA, Whitmore TD, Seymour DL, Rees JA, Mass spectrometric detection of short-living radicals produced by a plasma needle. Plasma Sources Sci. Technol. 16(3): 549–556 2007.

[3] Laroussi M, Non-thermal decontamination of biological media by atmospheric pressure plasmas: review, analysis and prospects. IEEE Trans. Plasma Sci. 30: 1409–1415 2002.

[4] Laroussi M, Leipold F, Evaluation of the roles of reactive species, heat, and UV radiation in the inactivation of bacterial cells by air plasmas at atmospheric pressure. Int. J. Mass Spectrom. 233: 81–86 2004.

[5] Moisan M, Barbeau J, Moreau S, Pelletier J, Tabrizian M, Yahia L'H, Low-temperature sterilization using gas plasmas: a review of the experiments and an analysis of the inactivation mechanisms. Intl. J. Pharm. 226: 1–21 2001.

[6] Stoffels E, Kieft IE, Sladek REJ, Van den Bedem LJM, Van der Laan EP, Steinbuch M, Plasma needle for *in vivo* medical treatment: recent developments and perspectives. Plasma Sources Sci. Technol. 15(4): S169–S180 2006.

[7] Sladek REJ, Stoffels E, Deactivation of Escherichia coli by the plasma needle. J. Phys. D: Appl. Phys. 38: 1716–1721 2005.

[8] Bin Liu, Goree J, Drake D, Stoffels E, Killing of S. Mutans Bacteria using a plasma-needle at atmospheric pressure. IEEE Trans. Plasma Sci. 34(4): 1317–1324 2006.

[9] Sladek REJ, Filoche SK, Sissons CH, Stoffels E, Treatment of Streptococcus mutans biofilms with a nonthermal atmospheric plasma. Lett. Appl. Microbiol. 45(3): 318–323 2007.

[10] Sissons CH, Artificial dental plaque biofilm model systems. Adv. Dental Res. 11: 110–126 1997.

[11] Wimpenny JWT, The validity of models. Adv. Dental Res. 11: 150–159 1997.

[12] Wall-Manning GM, Sissons CH, Anderson SA, Lee M, Checkerboard DNA-DNA hybridization technology focused on the analysis of Gram positive bacteria. J. Microbiol. Methods. 51: 301–311 2002.

[13] Vleugels M, Shama G, Deng XT, Greenacre E, Brocklehurst T, Kong MG, Atmospheric plasma inactivation of biofilm-forming bacteria for food safety control. IEEE Trans. Plasma Sci. 33: 824–828 2005.

[14] Sissons CH, Cutress TW, Hoffman MP, Wakefield JStJ, A multi-station dental plaque microcosm (Artificial Mouth) for the study of plaque growth, metabolism, pH and mineralization. J. Dental Res. 70: 1409–1416 1991.

[15] Servin AL, Antagonistic activities of lactobacilli and bifidobacteria against microbial pathogens. FEMS Microbiol. Rev. 28: 405–440 2004.

APPLICATIONS OF NON THERMAL ATMOSPHERIC PRESSURE PLASMA IN MEDICINE

S. KALGHATGI[1], D. DOBRYNIN[2], G. FRIDMAN[3],
M. COOPER[2], G. NAGARAJ[4], L. PEDDINGHAUS[5],
M. BALASUBRAMANIAN[5], K. BARBEE[3], A. BROOKS[6],
V. VASILETS[2], A. GUTSOL[2], A. FRIDMAN[2],
AND G. FRIEDMAN[1]
*[1]Department of Electrical and Computer Engineering,
Drexel University, Philadelphia, USA*
*[2]Department of Mechanical Engineering, Drexel University,
Philadelphia, USA*
*[3]School of Biomedical Engineering, Drexel University,
Philadelphia, USA*
*[4]Department of Internal Medicine, College of Medicine,
Drexel University, Philadelphia, USA*
*[5]Department of Pathology and Laboratory Medicine,
College of Medicine, Drexel University, Philadelphia, USA*
*[6]Department of Surgery, College of Medicine, Drexel University,
Philadelphia, USA*

Abstract: Non-thermal atmospheric pressure plasma is now being developed for use in various medical applications. Over the past few years a lot of clinical applications of non-thermal plasma have been tested and the results show promising potential for Plasma Medicine. In this paper we present a review of various applications of non-thermal plasma in medicine like non-thermal plasma assisted blood coagulation and skin sterilization, melanoma skin cancer treatment and treatment of cornea lesions.

Keywords: Non-thermal plasma, dielectric barrier discharges (DBDs), sterilization, disinfection, blood coagulation, wound healing, tissue regeneration, plasma medicine

1. Introduction

Recently non-thermal atmospheric pressure plasma has emerged as a promising new tool in medicine. Compared to conventional thermal plasma [1–5], non-thermal plasma is selective in its treatment and is safe since it does not burn tissue. Non-thermal plasmas generate active species, radicals, or ultraviolet which are used for targeted chemical modification and catalysis [6–8,9–16] unlike thermal plasmas [1–5] which employ high temperature that causes significant thermal tissue desiccation, burning, and eschar formation. One good example of this is the Argon Beam or Argon Plasma

Coagulator (APC) developed mainly to cauterize wounds [17]. The medical community is now shifting its preference toward non-thermal room temperature plasma's where thermal damage is minimized or eliminated. This potentially leads to many new applications including sterilization of living tissue without damage [18], blood coagulation [18,24], apoptosis [19,20] and modulation of cell attachment [20,21,22].

Two different approaches to the use of non-thermal plasma effects in medicine have been pursued. In one approach, plasma is created remotely and its afterglow is delivered by a jet to the desired location. In this indirect approach relatively long living active plasma species do most of the desired work, while most of the charged particles do not survive outside the plasma generation region. Alternatively, non-thermal atmospheric pressure plasma has been generated in direct contact with living tissue. This treatment produces various effects much faster due to direct contact with charged species [23]. This allows for treatment of biological samples without thermal damage while biological processes are initiated and/or enhanced with the help of electrical charges [23]. In this paper we report medical applications of direct non-thermal, room temperature atmospheric plasma discharge which is safe for treatment of living animal or human tissue (Fig. 1) [18]. The applications discussed are blood coagulation, skin sterilization, tissue regeneration and treatment of skin diseases like Melanoma cancer.
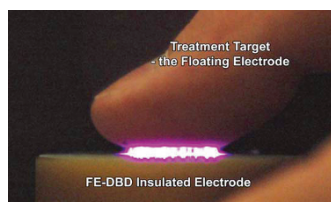
Figure 1. Electrically safe non-thermal e-plasma for treatment of living tissue without causing damage [18]

2. Non Thermal Plasma Assisted Blood Coagulation

Blood coagulation is an important issue in medicine, particularly with regards to wound treatment and wound healing. Thermal plasma has been traditionally used for this application in form of the so-called cauterization devices: argon plasma coagulators (APC), argon beam coagulators etc. [4,17]. In these devices, plasma is just a source of local high temperature heating, which cauterizes the blood. Recently developed new non-thermal plasma-medical systems achieve effective blood coagulation without any thermal effects [18,24]. In such systems, rapid clotting is achieved through non-thermal plasma enhancement of specific physiological mechanisms of blood coagulation without any damage to the surrounding tissue [18].

Non-thermal plasma was experimentally confirmed to significantly hasten blood coagulation [18,24]. Visually, a drop of blood drawn from a healthy donor and left on a stainless steel surface coagulates on its own in about 15 min, while a similar drop treated for 15 s by e-plasma coagulates in under 1 min (Fig. 2a).
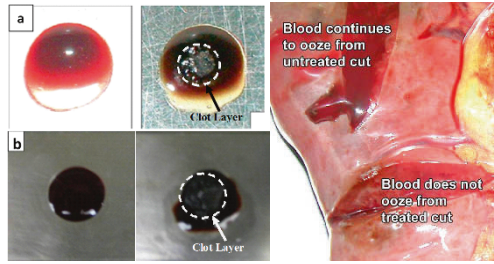
Figure 2. Coagulation of the e-plasma-treated non anticoagulated whole blood and citrated whole blood. (a) Non anticoagulated donor blood treated with e-plasma for 15 s exhibits an immediate clot layer formation. (b) Citrated whole blood treated with e-plasma for 15 s exhibits an immediate clot layer formation [25]. (c) 30 s of non-thermal plasma treatment of human spleen: blood coagulates without tissue damage. Top cut: blood continues to ooze from an untreated area; bottom cut: blood coagulates while the wound remains wet [25]

Similarly, 0.5 ml of citrated (anticoagulated) whole blood left in a well does not coagulate on its own even when left in the open air for well over 15 min, while the same sample treated with DBD-plasma for 15 s exhibits immediate clot layer formation on the surface exposed to plasma discharge as shown in Fig. 2b. Non-thermal plasma treatment of cuts on organs leads to similar results where blood is coagulated without any visible or microscopic tissue damage. Figure 2c shows a human spleen treated by non-thermal plasma for 30 s – blood is coagulated and without any thermal damage to the tissue surrounding the cut and the temperature of the cut remains at room temperature (even after non-thermal plasma treatment for as long as 5 min) and the wound remains wet, which will, in turn, decrease healing time [18].

Effective plasma stimulation of the in-vivo blood coagulation has been demonstrated by Fridman et al. in experiments with live SKH1 mice [25]. Fifteen seconds of non-thermal plasma treatment is able to coagulate blood at the surface of a cut Saphenous vein (Fig. 3) as well as tail vein of a mouse. In these experiments only ability of direct non-thermal plasma treatment to coagulate blood was tested and the animal was not left alive to test improvement in healing times. Full in vivo investigation of ability of plasma to hasten wound healing through wound sterilization

Figure 3. Blood coagulation in a live animal

and blood coagulation is discussed in Fridman et al. [25]. and Balasubramanian et al. [26,27]. The above discussion indicates that non-thermal plasma is capable of coagulating blood and it does so by initiating/enhancing natural coagulation processes [24].

3. Non Thermal Plasma Treatment of Melanoma Skin Cancer

Initiation of apoptosis, or programmed cell death, is an important issue in cancer treatment as cancer cells acquired the ability to switch off the apoptosis pathway and multiply faster than they die and thus are more resistant to chemotherapeutic drugs.

Non-thermal plasma treatment is shown to initiate apoptosis in Melanoma cancer cell lines – a threshold at which plasma treatment does not cause immediate necrosis but initiates complex cascade of biochemical processes leading to cell death many hours and even days following the treatment [19]. Melanoma cells, treated by plasma at doses significantly below those required for cell destruction, survive the plasma treatment but develop apoptosis many hours post treatment and die (disintegrate) by themselves. This could potentially be an interesting approach for cancer treatment, especially if by manipulation of plasma parameters the treatment could be made selective to cancerous cells over healthy cells, as was demonstrated before for bacteria vs. healthy cells [18,25]. A way to target apoptosis development only in specific areas of the body is needed, and can be achieved by the non-thermal plasma treatment.

Melanoma cells, treated by plasma, immediately show evidence of cell necrosis – an expected outcome in the tradition of the recent trend of surface sterilization by plasma (see [6,28–32] for example). However, the remaining cells that survived the treatment do not behave as the untreated cells do. The general trend observed in treated cells is that they continue to die for days after the treatment. Figure 4 shows the percentage of inactivated (dead) cells among treated and untreated populations. Thus, it was observed that 5 s of plasma
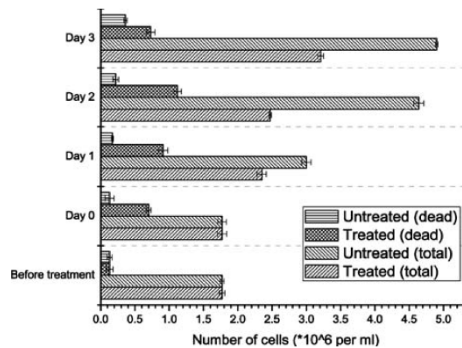

Figure 4. Results of observation of treated and untreated cells for a 3-day period: percent of dead cells before and after FEDBD treatment. Treatment time: 5 s

treatment does not inactivate cells immediately; however, cell growth slows down significantly, and the number of dead cells increases 24 h after treatment, which is indicative of cell death occurring long after the treatment.

Thus, non-thermal plasma can kill Melanoma skin cancer cells. Very low doses of non-thermal plasma (5 s at 0.8 W/cm^2 of plasma treatment) where no cell necrosis was observed were shown to initiate apoptotic behavior, or programmed cell death in Melanoma cancer cells. Apoptotic behavior was deduced from the fact that treated cells do not initially die but stop growth and die en masse 12–24 h following treatment, while untreated cells continue to grow and proliferate. Apoptotic behavior was confirmed through DeadEnd™ Fluorometric TUNEL System (Fig. 5) apoptosis staining with subsequent flow-Cytometry.
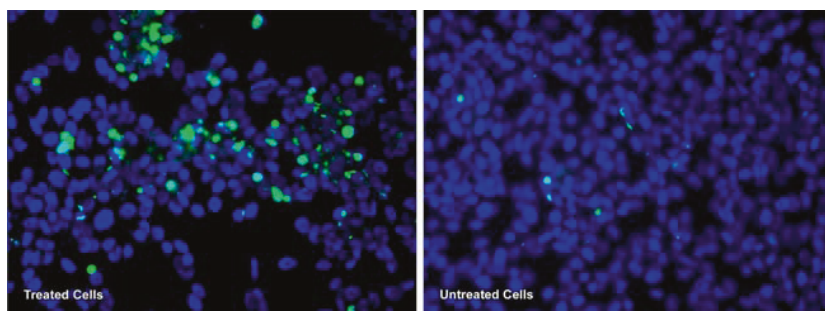

Figure 5. Images of treated and untreated Melanoma cancer cells stained following TUNEL assay protocol. All cells are stained blue (darker circles) and apoptotic cells are also stained green (bright spots). Treatment time: 5 s; assay performed 24 h following treatment

4. Non Thermal Plasma Treatment of Skin

A great care must be taken in killing of micro-organisms on living tissue in order to avoid damage to the tissue itself. In many situations, including civilian hospitals, the use of chemicals such as alcohol or Betadine is simply not feasible for tissue sterilization during an operation. Chemical burns, for example, can result from sterilization by wiping an area around an injection site. For similar reasons, chemical sterilizers are hardly ever used on open wounds. Non-thermal plasma treatment systems address this unmet need. Conventional electric discharges (both high and low pressure and temperature) are well-known for their ability to sterilize various surfaces. The advantage of non-thermal atmospheric pressure plasma system is its ability to sterilize living animal or human tissue without any damage to the treated tissue.

The results from the previous rodent model provided strong evidence for the ability to sterilize the surface of the skin [18], but to evaluate the effects on the underlying skin cells and tissue, it is necessary to test the safety of the treatment in a model that more closely resembles human skin. We developed a realistic animal (pig) model for evaluating the safety of this approach to skin sterilization. This

model was chosen because of the similarity between porcine skin and human skin. The pig was anesthetized and skin on the back was shaved and prepped. Skin was treated with FE-DBD plasma for 30 s, 2 and 5 min (Fig. 6a) while complete hospital-grade sterilization is achieved in less than 5 s of plasma treatment. Right after the plasma processing there were no visible damage or inflammation of the skin even after 5 min of treatment (Fig. 6b).

(a)   (b)
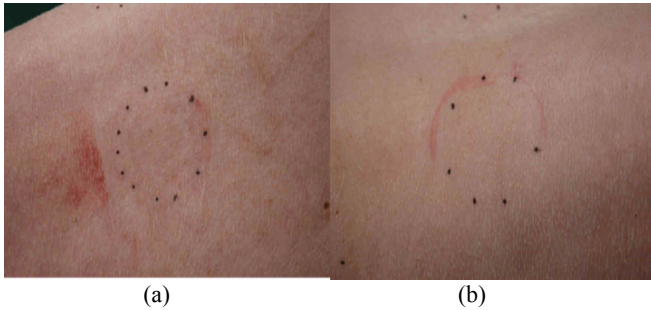
Figure 6. (a) Non-thermal atmospheric pressure plasma treatment of a pig's skin. (b) Skin right after 2 min (left) and 5 min (right) of plasma treatment: no visible changes

5. Non Thermal Plasma Treatment of Cornea Lesions

Another plasma generating system was developed in Petrozavodsk State University [33]. This device allows to produce plasma with average mass temperature not exceeding 30–40°C. It consists of a coaxial cathode and needle-like anode, which is fixed in metal capillary (Fig. 7). The plasma generating substance is fed through the capillary to the discharge gap. The anode is connected with the positive lead of the power source and the cathode is grounded. The discharge appears on the nozzle output if the pressure on the nozzle input is higher than the atmospheric pressure. The discharge is a specific plasma sphere with the diameter ~4 mm, the discharge voltage is 1–3 kV, the pulse duration is about 50 μs, and the total power was kept on the order of 1–2 W.
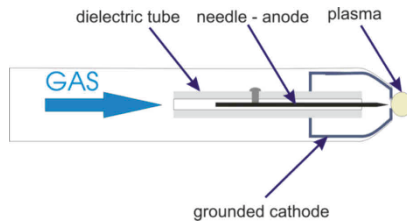
Figure 7. Schematic of the medical microplasmatrone

Noble gases, air and water can be used as a plasma generating matter. The flow of plasma generated by the device contains electrons, ions, excited atoms of

hydrogen and oxygen, and excited molecules of water. Plasma radiates intensively electromagnetic waves in UV, visible, infrared, sub-millimeter, and millimeter ranges. Plasma parameters allow to treat living tissue without destruction and any damaging. Ability of the medical micro-plasma system to sterilize has been demonstrated [34]. Staphylococcus culture in liquid media ($\sim 2 \cdot 10^6$ CFU/ml) have been treated by the air plasma of 3 mm diameter, incubated for 24 h, and counted (Table 1).

TABLE 1. Results of Staphylococcus inactivation by air plasma [36]

Culture volume, ml	Plasma exposure time, s			
	0 (control)	25	50	100
1	$2 \cdot 10^6$ cfu	0 cfu	0 cfu	0 cfu
2	$4 \cdot 10^6$ cfu	25 cfu	0 cfu	0 cfu
3	$6 \cdot 10^6$ cfu	$1 \cdot 10^6$ cfu	680 cfu	460 cfu

A 6-log reduction in viable bacteria is achieved in 25 s of treatment; however the sterilization efficiency drops off with increasing volume of liquid which inhibits UV penetration and diffusion of active species generated in plasma. Nevertheless, the micro-plasma system should be a good solution for treatment of living human and animal skin as the bacteria are normally at much lower concentrations on skin ($<10^5$ cfu/cm^2).

A series of experiments on plasma treatment of rabbit eyes were carried out. In a first set of experiments healthy eyes of rabbits were exposed to plasma [34]. It was affirmed that cornea changes after cold plasma treatment have no destructive character and completely disappear in 3 days. No iris and lens changes were revealed. The aim of the second set of investigations was to study cold plasma influence on pathogenic staphylococcus culture under experimental ulcerous bacterial keratitis [35] which is the most dangerous and rapidly passing cornea affection. Four eyes of 4 rabbits were infected with 0.1 ml of pathogenic staphylococcus culture containing $2 \cdot 10^9$ bacteria per 1 ml. Three days later when lesion developed eyes were treated with plasma. Exposition amounted 5 s. A strong bactericidal effect right after the plasma treatment was found. After the 5th day of infection (the second plasma treatment) ulcer surface was purified of pus completely, active dissolving of exudation "train" in front tube started, pupil area opened. From these results the following important conclusion was made: plasma processing interrupts experimental ulcerous keratitis progress.

These results offered a strong ground for application of the medical micro-plasma system for treatment of human patients with ulcerous eyelid wounds (Fig. 8a), which is shown in [36]. Necrotic phlegmon on the surface of the upper eyelid was treated by air plasma plume of 3 mm diameter for 5 s once every few days (Fig. 8b). By the 5th day of treatment (two plasma treatment sessions) the eyelid edema and inflammation were reduced; and by the 6th day (third session)

the treated area was free of edema and inflammation and a rose granular tissue appeared. Bacteriological tests showed absence of pathogenic flora. A week later three more plasma treatments were made. Six days after the last treatment the patient was discharged from the hospital without any infiltration and necrosis symptoms.

Figure 8. Cold plasma treatment of phlegmonous eyelid defeat. (a) patient's eyelids before plasma treatment. (b) patient's eyelids after plasma treatment sessions

These experimental results show that low temperature plasma treatment has the following properties; "soft" nondestructive affection on tissue; has strong bactericidal effect; a stimulation effect is revealed during plasma treatment. Therefore it can be applied for wound surfaces sterilization, and also for stimulation reparation processes at treatment of wounds, trophic ulcers, sharp and chronic inflammatory processes, other defeats of external covers of soft tissues, mucous membranes, sterilization of the medical tools and dressing means.

Conclusion

A variety of medical applications of Non-Thermal Atmospheric Pressure plasma were discussed in this review. We reported applications of non-thermal plasmas in medicine for rapid blood coagulation by enhancing natural coagulation processes, initiation of apoptosis in melanoma skin cancer, safe and rapid sterilization of living tissue, tissue regeneration and enhanced wound healing in necrotic tissue. These are not the only applications in medicine where non-thermal atmospheric pressure plasma can be applied but non-thermal atmospheric pressure plasma is a promising new tool in medicine.

References

[1]   Watson JP et al. (1997) Gut 40:Th156
[2]   Vargo JJ (2004) Gastrointest Endosc 59(1):81
[3]   Puhlev I et al. (2001) Cryobiology 42(3):207
[4]   Colt HG, Crawford SW (2006) Respirology 11(5):643
[5]   Raiser J, Zenker M (2006) J Phys D: Appl Phys 39(16):3520
[6]   Stoffels E (2006) J Phy D: Appl Phys 39(16)
[7]   Bogaerts A et al. (2002) Spectrochim Acta Part B 57(8):609
[8]   Fridman A, Chirokov A, Gutsol A (2005) J Phys D: Appl Phys 38(2):R1
[9]   Anderson KM et al. (1999) Med Hypotheses 52(5):451
[10]   Eliasson B, Egli W, Kogelschatz U (1994) Pure Appl Chem 66(6):1275

[11] Baydarovtsev YP, Vasilets VN, Ponomarev AN (1985) Russ J Chem Phys 4(N1):89
[12] Yalin AP et al. (2002) Plasma Source Sci Technol 11(3):248
[13] Stoffels E et al. (2002) Plasma Source Sci Technol 11(4):383
[14] Stoffels E (2000) High Temp Mater Process 5(2):191
[15] Sosnin EA et al. (2004) Plasma Sci IEEE Trans 32(4):1544
[16] Sosnin EA et al. (2004) Technol Phys Lett 30(7):615
[17] Ginsberg GG et al. (2002) Gastrointest Endosc 55(7):807
[18] Fridman G et al. (2006) Plasma Chem Plasma Process, 26(4): 425–442
[19] Fridman G et al. (2007) Plasma Chem Plasma Process 27(2): 163–176
[20] Kieft I E et al. (2006) IEEE Trans Plasma Sci., 34(4): 1331–1336
[21] Stoffels E et al. (2003) J Phys D, Appl Phys 36(23): 2908–2913
[22] Kieft I.E et al. (2005) IEEE Trans Plasma Sci 33(2): 771–775
[23] Fridman G et al. (2007) Plasma Process Polym 4: 370–375
[24] Kalghatgi S et al. (2007) IEEE Trans Plasma Sci 35(5): 1559–1566
[25] Fridman G, Shereshevsky A, Peddinghaus M, Gutsol A, Vasilets V, Brooks A, Balasubramanian M, Friedman G, Fridman A (2006) *Bio-Medical applications of non-thermal atmospheric pressure plasma*. In *37th AIAA Plasmadynamics and Lasers Conference*. San Francisco, California
[26] Balasubramanian M et al. (2007) Transfusion 47(2): 6A-6A
[27] Balasubramanian M et al. (2006) Blood (ASH Annual Meeting Abstracts), 108(ab. 4043)
[28] Zhang R et al. (2006) Plasma Sci IEEE Trans 34(4):1370
[29] Tarasenko O et al. (2006) Plasma Sci IEEE Trans 34(4):1281
[30] Sladek REJ, Baede TA, Stoffels E (2006) Plasma Sci IEEE Trans 34(4):1325
[31] Sharma A et al. (2006) Plasma Sci IEEE Trans 34(4):1290
[32] Laroussi M et al. (2006) Plasma Process Polym 3(6–7):470
[33] Gostev V, Dobrynin D (2006) *Medical microplasmatron*. In *3rd International Workshop on Microplasmas (IWM-2006)*. Greifswald, Germany
[34] Misyn FA, Besedin EV, Komkova OP, Gostev VA (2000) *Experimental investigation of bactericidal influence of "cold" plasma and its interaction with cornea*. In *Diagnostics and treatment of infectious diseases*. Petrozavodsk, Russia
[35] Misyn FA et al. (2000) *Experimental curing of bacterial ulcerous keratitis with "cold" plasma*. In *Diagnostics and treatment of infectious diseases*. Petrozavodsk, Russia
[36] Misyn FA, Gostev VA (2000) "Cold" plasma application in eyelid phlegmon curing. In *Diagnostics and treatment of infectious diseases*. Petrozavodsk, Russia

PENETRATION OF DIELECTRIC BARRIER DISCHARGE TREATMENT INTO FLUID FOR BIOMEDICAL APPLICATIONS

G. FRIDMAN[1,*], A. SHERESHEVSKY[2], A. D. BROOKS[2], A. FRIDMAN[3], A. GUTSOL[3], AND G. FRIEDMAN[4]

[1]*School of Biomedical Engineering, Science, and Health Sciences, Drexel University*
[2]*Department of Surgery, Drexel University College of Medicine*
[3]*Department of Mechanical Engineering and Mechanics, Drexel University*
[4]*Department of Electrical and Computer Engineering, Drexel University*

Abstract: Treatment of melanoma cell cultures submerged into a typical cell growth buffer solution by room-temperature atmospheric pressure air plasma generated through the Dielectric Barrier Discharge above the surface of the fluid is investigated. It is shown that the plasma discharge can inactivate or permeabilize the cytoplasmic membrane of Melanoma cells at depths of about half a millimeter of the fluid within a few tenths of seconds. It is also demonstrated that the observed effects occur only when the cells are present in the solution during the plasma treatment and, therefore, cannot be attributed to chemical changes in the solution alone.

Keywords: Non-equilibrium plasma, non-thermal plasma, dielectric barrier discharge, melanoma cells, cancer cells

Thermal ablation and cauterization of tissue by Atmospheric Pressure Plasma (APP) is a well-established method for treatment of certain medical problems. Non-thermal APPs often referred to as 'cold', however, can be much more tunable and selective in their treatment because they do not burn and could achieve various useful sublethal results. Several types of cold APP treatment approaches have been developed recently. In general, they can be classified as indirect or direct. Indirect APP treatment bathes the tissue or biological sample only by plasma discharge afterglow consisting mainly of a visible and ultraviolet (UV) radiation, stream of radicals and

---

*Corresponding author: School of Biomedical Engineering, Science, and Health Sciences, Drexel University, 3141 Chestnut Street, Philadelphia, PA 19104, tel: +1-215-895-0576, fax: +1-215-895-1633, email: greg.fridman@drexel.edu.

other relatively long-living chemically active species generated remotely in the APP discharge. Vacuum UV radiation (wavelength <200 nm), charged particles and other short-living species (like non-metastable electronically excited molecules) do not participate in the indirect APP treatment due to high absorption coefficient of atmospheric air for the former, and short life time of the latter. In contrast, direct room-temperature APP treatment maintains the discharge in the direct contact with the surface of the biological sample by transferring some current to the sample, and employs not only chemically active plasma species, but also charged particles, short-living radicals, excited molecules as well as vacuum UV radiation. As a result, direct treatment by cold APP discharge has the potential to be much more tunable, selective, and efficient than the indirect treatment. It has been shown recently, for example, that direct cold APP treatment can kill bacteria on the mammalian tissue surface within seconds without any damage to tissue itself [1]. This treatment can also trigger natural coagulation of blood [1–3], a reversible detachment of cells from a substrate [4], apoptosis in cells, and other biological effects.

Previous work has investigated effects of non-thermal APP treatment of cells placed on exposed surfaces [5, 6] or indirect APP treatment of mammalian cells submerged into a culture medium [7, 8]. The detachment of mammalian vascular cells was observed after indirect APP treatment by the "plasma needle" when the thickness of the liquid layer covering the cells was less than 0.1 mm [8]. Here we present investigation of the direct treatment of cells that are covered by up to a half a millimeter of cell culture fluid. We demonstrate that this treatment does not occur only due to chemical modifications of the buffered culture medium, providing evidence of penetrating effects of direct cold plasma treatment.

The specific discharge we employ for generation of cold APP is the Floating Electrode Dielectric Barrier Discharge (FE-DBD). Similar to conventional DBD, FE-DBD employs one powered dielectric-covered electrode and another floating electrode, like a surface of a human or animal tissue, which remains at plasma floating potential during treatment and is disconnected from ground. It has been recently demonstrated that this discharge is safe and effective in direct treatment of tissue and blood [1]. Experimental set-up employed with submerged Melanoma cell culture is schematically illustrated in Fig. 1. The following discharge parameters were employed in the reported experiments. The discharge gap between the bottom of the 1 mm thick quartz plate covering the copper electrode and top surface of the fluid was set to 1.5 mm. The diameter of the copper electrode employed was 2.5 cm. Alternating polarity voltage of 35 kV magnitude (peak to peak) and 12 kHz frequency was applied to the copper electrode, while the aluminum Petri dish remained at a floating potential to mimic the conditions that exists when this discharge is used to treat living tissue. The power delivered into the plasma discharge was estimated via direct electrical measurements and confirmed calorimetrically (data not shown). Both electrical and calorimetric measurements indicated the power level of 4 ± 1 W (corresponding to surface power density of 0.8 ± 0.2 W/cm^2).
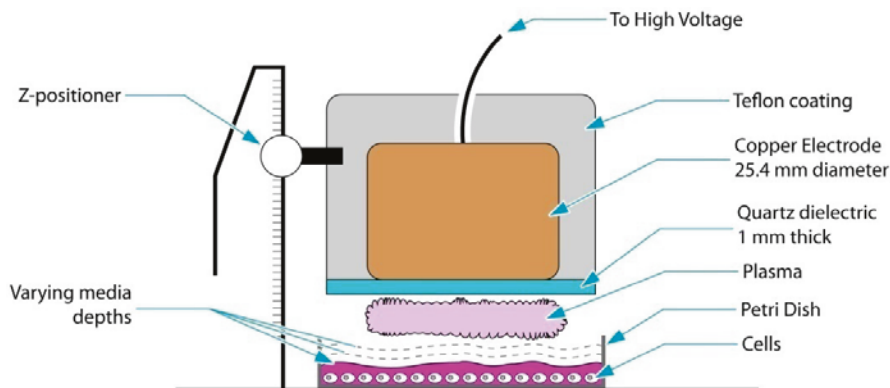
Figure 1. Schematic of FE-DBD treatment of Melanoma cells

It should be emphasized that DBD discharges are normally employed in dry conditions (extremely dry for ozone production, for example). Despite the fact that one of the DBD electrodes was fluid, the observed discharge had a typical filamentary structure of dry DBD discharges [1, 9]. Temperature of the excited and/or charged species present within these filaments is generally higher than that of the surrounding gas. To measure the temperature of the DBD filaments we employed emission spectroscopy (TriVista Spectrometer System with Princeton Instruments PIMAX intensified CCD camera) to obtain spectra of plasma in air over the liquid surface. Specifically, micro-discharge (filament) temperature was obtained from a fitting of simulated spectra to that of the second positive system of N_2 [10, 11]. For these types of measurements it is assumed that the vibrational temperature is an approximation of the electronic temperature, while the rotational temperature is a good approximation for the temperature of heavier species (ions, metastables, and neutral atoms and molecules). Using this methodology, the filament temperature was found to be around 500 K ($\pm$50 K).

Melanoma cells (ATCC A2058) were cultured on the surface of an aluminum dish. Cells were allowed to grow while the dish was kept within an incubator (CO_2 auto flow incubator at 37°C) for 72 h. After this, the original growth medium was removed and a measured volume of fresh culture medium was added to the dish while the cells remain attached to the bottom surface. The volume of the culture medium was measured to obtain the desired depth which is varied in these experiments from 0 to 0.33 mm (Fig. 1). The submerged cells were placed into the DBD treatment set-up and treated by plasma for periods of time ranging from 0 to 30 s. Immediately after the plasma treatment the culture medium used during the treatment was replaced with a fresh medium. The cells were then analyzed by Trypan Blue exclusion test to determine their viability through the cellular membrane integrity. Trypan Blue only enters cells through permeabilized cytoplasmic membranes. Fig. 2 reports the results in terms of percentages of affected cells and treatment times. No effect on the cells is observed in control experiments where plasma treatment does not occur.
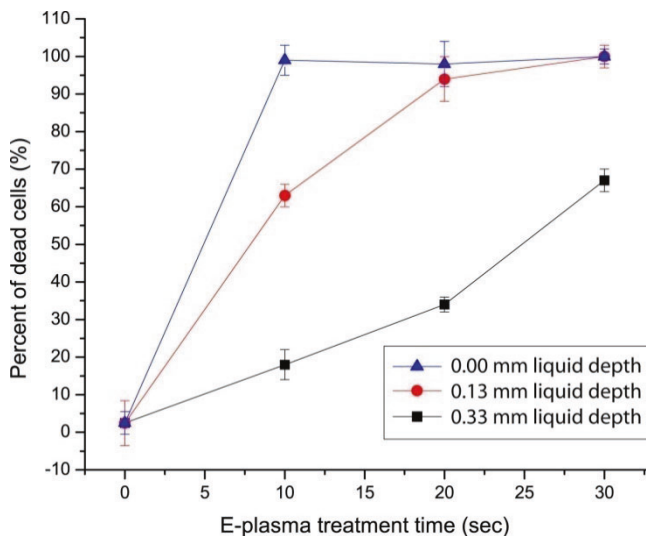
Figure 2. Percent of dead cells (cells that uptake Trypan blue) after treatment at different liquid depths. The thickness of the cell layer at the bottom of the dish is about 30 μm

As is evident from Fig. 2, direct exposure of the surface of the fluid culture medium has a substantial effect on the submerged melanoma cells. Without the medium protecting the cells, cell wall fracture is achieved within 10 s of treatment and all of the cells uptake the ink (Trypan Blue), indicating that the cell wall has been compromised and the cell is dead. Interestingly, even though the DBD plasma at room temperature and pressure in air exhibits a high degree of non-uniformity, all the cells are affected by the treatment in as little as 10 s; indeed, we observe similar behavior of cells coming in direct contact with plasma even at shorter treatment times down to 2 s where we have previously shown sterilization of high concentration of bacteria from a surface of a hydrogel [1]. When a layer of media is introduced which covers these cells, the number of compromised cells decreases but it is clear that the plasma treatment is permeabilizing these cells somehow, even through a layer of liquid cell growth medium. A question naturally arises if these effects are simply due to chemical changes in the growth medium. Indeed, measurement of the pH of the culture medium showed substantial changes with the treatment time (Fig. 3).

We have carried out additional control experiments to understand the role of the changing chemistry of the culture medium. In these experiments, grown cell culture was transferred into the culture medium pre-treated by the DBD discharge in manner identical to the one used to treat submerged cell culture. Changes of the pH of the culture medium were identical to the ones found in experiments with the submerged cells. As before, the cells were placed into fresh culture medium after remaining in the pre-treated culture medium for the amount of time equal to the

plasma pre-treatment time. Similarly to the control (untreated) cells, cells transferred into the culture medium pre-treated by the plasma in this fashion and then placed into the fresh medium did no uptake Trypan Blue.
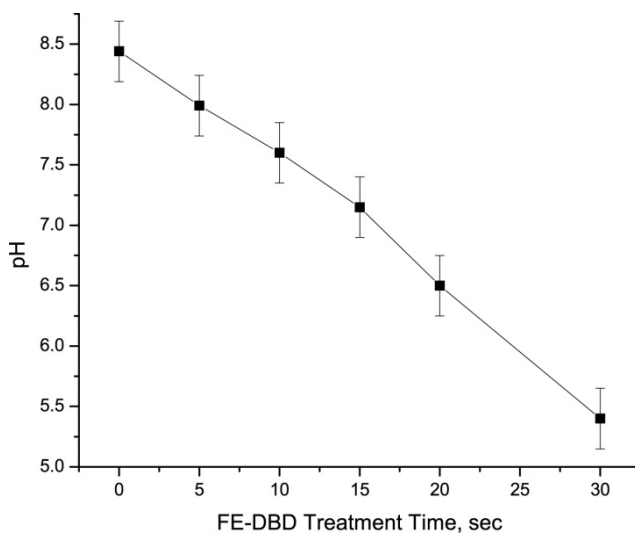

Figure 3. pH change of the buffer medium under FE-DBD treatment

The results of placing cells in acidified media temporarily indicate that the DBD plasma does not affect the cells simply through changes in the chemical composition of the culture medium. Several possibilities exist that might explain why cell inactivation, disruption of cellular membrane's normal functions, or disruption of cell metabolism occurs only in the presence of the DBD discharge. One possibility is that UV radiation (probably in the UV-C band) works in synergy with chemically active species produced by direct plasma in the culture medium to break the integrity of cellular membranes (Fig. 4 – emission spectra from plasma in UV range). Photon energy of the UV-C radiation (about 4–6 eV) is sufficient to break some chemical bonds in bio-molecules [12]. More energetic VUV-photons, however, are unable to penetrate deep through the layer of liquid cell culture media protecting the cells. The UV-C radiation can be effectively delivered to the cell membranes, but its energy can be sufficient also for structural reorganization of the bio-molecules (including, fatal but slow DNA changes), and disruption of hydrogen bonds responsible for the integrity of the membrane's lipid bi-layer. Such disruption of the lipid bi-layer may open the membrane to penetration of multiple active plasma species, particularly such strong oxidants as atomic oxygen, peroxide radicals, singlet oxygen, NO, and positive ions [9]. Thus, deep penetration of the strong plasma treatment effect can possibly be attributed to synergy of UV-C radiation with plasma-generated active chemical oxidants.
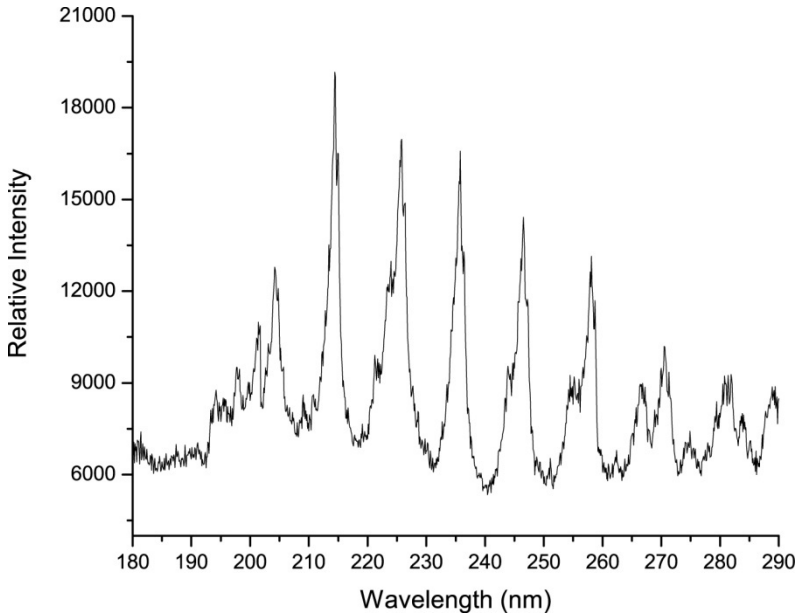
Figure 4. Emission from DBD plasma over the cell surface in UV range

Another possibility is that DBD streamers actually create plasma or highly conductive channels reaching the bottom of the dish and cells. The DBD micro-discharges have sufficient energy to remove the water protective film covering the cells either by electrical effect (such as the streamer electric field) or by localized thermal effect (as their temperature was shown to be on the level of 500 K, see above). When the cells are open to direct contact with plasma, their intensive deactivation may take place due to multiple factors, and particularly to positive ions inducing strong catalytic, mechanical and electric field effects at the cell surface.

Acknowledgement

References

[1]   Fridman, G., et al., *Blood Coagulation and Living Tissue Sterilization by Floating-Electrode Dielectric Barrier Discharge in Air.* Plasma Chemistry and Plasma Processing, 2006. **26**(4): pp. 425–442.
[2]   Ginsberg, G.G., et al., *The Argon Plasma Coagulator.* Gastrointestinal Endoscopy, 2002. **55**(7): pp. 807–810.

[3]   Vargo, J.J., *Clinical Applications of the Argon Plasma Coagulator.* Gastrointestinal Endoscopy, 2004. **59**(1): pp. 81–88.

[4]   Stoffels, E., et al., *Plasma Needle: A Non-Destructive Atmospheric Plasma Source for Fine Surface Treatment of (Bio)Materials.* Plasma Sources Science and Technology, 2002. **11**(4): pp. 383–388.

[5]   Laroussi, M., *Nonthermal Decontamination of Biological Media by Atmospheric-Pressure Plasmas: Review, Analysis, and Prospects.* Plasma Science, IEEE Transactions on, 2002. **30**(4): pp. 1409–1415.

[6]   Laroussi, M. and Leipold, F., *Evaluation of the Roles of Reactive Species, Heat, and Uv Radiation in the Inactivation of Bacterial Cells by Air Plasmas at Atmospheric Pressure.* International Journal of Mass Spectrometry, 2004. **233**(1–3): pp. 81–86.

[7]   Kieft, I.E., et al., *Electric Discharge Plasmas Influence Attachment of Cultured Cho K1 Cells.* Bioelectromagnetics, 2004. **25**(5): pp. 362–368.

[8]   Kieft, I.E., et al., *Plasma Treatment of Mammalian Vascular Cells: A Quantitative Description.* Plasma Science, IEEE Transactions on, 2005. **33**(2): pp. 771–775.

[9]   Fridman, A., Chirokov, A. and Gutsol, A., *Non-Thermal Atmospheric Pressure Discharges.* Journal of Physics D: Applied Physics, 2005. **38**(2): pp. R1–R24.

[10]   Laux, C.O., et al., *Optical Diagnostics of Atmospheric Pressure Air Plasmas.* Plasma Sources Science and Technology, 2003. **12**(2): p. 125.

[11]   Yalin, A.P., et al., *Spatial Profiles of N2+ Concentration in an Atmospheric Pressure Nitrogen Glow Discharge.* Plasma Sources Science and Technology, 2002. **11**(3): p. 248.

[12]   Lin, C.K., et al., *Vibrational Predissociation Spectra and Hydrogen-Bond Topologies of H+ (H2o)(9–11).* Physical Chemistry Chemical Physics, 2005. **7**(5): pp. 938–944.

PLASMA SURFACE MODIFICATION OF THREE DIMENSIONAL POLY (ε-CAPROLACTONE) SCAFFOLDS FOR TISSUE ENGINEERING APPLICATION

E. D. YILDIRIM[1], M. GANDHI[1], A. FRIDMAN[2], S. GÜÇERI [1], AND W. SUN[1]

[1]*Laboratory for Computer-Aided Tissue Engineering, Department of Mechanical Engineering and Mechanics, Drexel University, Philadelphia, PA 19104, USA*
[2]*Drexel Plasma Institute, Department of Mechanical Engineering and Mechanics, Drexel University, Philadelphia, PA 19104, USA*

Abstract: In the present study, the effect of oxygen-based plasma treatment on the three dimensional poly (ε-caprolactone) (PCL) was analyzed in terms of surface wettability, surface energy, and surface biocompatibility. The surface treatment was carried out for 1, 3, and 5-min durations on three dimensional PCL scaffolds at atmospheric pressure using a radio frequency (RF) plasma treatment system. The solid surface energies of the modified and unmodified PCL scaffolds were calculated by using the Owens-Wendt's method. To examine the effect of oxygen plasma treatment on cell-scaffold interaction, mouse osteoblast cell line (7F2) was used. Oxygen plasma treatment contributed in decreasing the hydrophobicity of PCL for the 1-min treatment. A change in the surface energy from 39.98 mN/m for untreated to 52.54 mN/m for 1-min treated was observed by the increment in the polar component of surface energy. However, with the extended treatment times (3-min, and 5-min), the hydrophilicity, and the surface energy remained unaffected. The highest mouse osteoblast cells proliferation rate was observed for the 1-min treated sample.

Keywords: Plasma treatment, tissue engineering, scaffolds, poly (ε-caprolactone), mouse osteoblast cell, cell proliferation, surface modification

1. Introduction

Favorable cell-substrate interaction during early stage of the cell seeding is one of the most desirable features of tissue engineering. The ability of bone cells to produce an osteoid matrix on the scaffold can be affected by the quality of the cell-scaffold interaction, and the scaffold structure. The surface treatment of scaffolds with a variety of agents have been tried to improve cell-substrate

interaction. Among the established scaffold manufacturing techiques such as solvent casting, membrane lamination, freeze drying, phase seperation, 3D printing, the fused deposition modeling (FDM), the precision extrusion deposition (PED) system introduced in literature by Computer Aided Tissue Engineering Laboratory (CATE), Drexel University [1] seem the most versatile of techniques. From a manufacturing standpoint, PED processes advantages over FDM. PED has an ability to build scaffolds with controlled and defined architectures without using chemical solvents [1–3]. In addition, unlike FDM, the PED material is in the pellet form, therefore it does not require a precursor filament preparation [1,4].

Poly-ε-caprolactone (PCL) is an ideal material in tissue engineering and drug delivery applications due to it's biodegradable, biocompatible properties [1,5–9]. The cell adhesion determines the successful formation of tissue constructs leading to subsequent cell proliferation, differentiation and new tissue ingrowth. However, the surface hydrophobicity works against PCL when it comes to cell attachment [10]. The chemical inertness and low surface energy of the PCL causing an inadequate interaction with the biological surfaces can be modified by various surface treatment processes such as chemical treatment, thin film deposition, blending, ion beam radiation and plasma treatment [11,13–16]. For the biocompatible polymers, preserving the surface functionalization of the bulk properties is particularly crucial [17,18]. Therefore plasma can modify the surface without changing the bulk properties [17]. Another advantage conferred offered by plasma treatment is the absence of residual solvent or swelling of the substrate unlike wet chemical surface modification techniques. In addition, plasma treatment can be carried out at near-ambient temperature, thereby minimizing the risk of damage to heat-sensitive materials [17,19]. Radio-frequency (RF) plasma has been used to functionalize the surface of the biomaterial in order to increase the protein deposition, cell proliferation, and attachment [13,16,20–22].

In plasma surface modification, the surface is bombarded with the plasma generated radicals and ions which are reacting with surface species and functional groups [17,18]. The ion and radical bombardment introduces the different functional groups onto the polymer surface. It is possible to manipulate these groups and surface properties of polymer by carefully choosing the working gas or gases like argon, oxygen, nitrogen, flourine, carbon dioxide and water. Oxygen plasma treatment is particularly used in biological application to improve the biocompatibility of the material by introducing polar hydroxyl (-C-OH), carbonyl (-C=O), carboxyl (-OH-C=O) oxygen containing functional groups on polymer surface and cleaving the C-C and C-H bond in the polymer backbone. These polar functional groups not only increase the wettability and solid surface energy of the polymer surface but also improve the early cell attachment and protein adsorption [12,13,16,18,21–26].

The first cell-material interaction starts with the formation of a cell adhesive protein layer from serum containing media. The cells attach to these absorbed proteins via cell surface adhesion receptors like integrins and extra-cellular matrix (ECM) proteins including fibronectin, vitronectin, fibrinogen and those containing the arginine-glycine-aspartate (RGD) sequence. At this point, surface energy, chemistry and topography of substrate may influence which proteins adhere to the

surface [12,23,27]. Since mouse osteoblast cells are anchorage-dependent cells, the attachment and proliferation of these cells can be controlled by oxygen plasma treatment which increases the cell affinity of the material by binding the cell adhesion proteins [12,21,27].

In this study, we report a study about the influence of physicochemical properties of oxygen-based RF plasma treated 3D PCL scaffold on mouse osteoblast cell proliferation. For this purpose, PCL scaffold were treated with oxygen based RF plasma with different exposure times. Then mouse osteoblast cells (7F2) were cultured on treated PCL scaffolds for 7 days. The plasma treated PCL surfaces were characterized in terms of the hydrophilicity and surface energy via contact angle measurements and the Owens-Wendt method, respectively. The mouse osteoblast cell proliferation were characterized by the alamarBlue™ assay.

2. Material and Methods

2.1. SCAFFOLD FABRICATION VIA PRECISION EXTRUSION DEPOSITION

The three dimensional square prism PCL scaffolds were fabricated with the precision extrusion deposition (PED) system which is one of the solid freeform fabrication techniques. The PED system consists of a XYZ positioning component, material extruder component, and a temperature control component. The fabrication of 3D scaffolds is conducted by two software systems. The data processing software generates the process toolpath and the system software controls the material deposition according to the designed toolpath. The designed CAD model of the scaffold converted into STL format and sliced for toolpath generation. In-house developed systems control software was used to define and control the fabrication process parameters and XYZ positioning of material extruder. In the present study, the scaffolds were designed with dimensions of $15 \times 15 \times 2.5$ mm (length × width × height). The pore size was 300 μm and the strut width was 250 μm. The scaffolds were extruded as 0/90° laid-down pattern with fully interconnected channel networks. Each scaffold consisted of 17 layers with a slice thickness of 150 μm. During the fabrication process, the nozzle tip temperature was maintained at 110°C. The fabrication was done at room temperature.

2.2. PLASMA TREATMENT

The surfaces of scaffolds were modified with a plasma reactor (PDC 32G, Harrick Scientific Inc., New York) for 1, 3, and 5-min. The system included a radiofrequency generator capable of 0–18 W at a frequency range of 8–12 MHz, a vacuum pump, a helical internal electrode around the reactor, and instrumentation for pressures. RF plasma was initiated and maintained by external electrodes outside the reactor vessel. PCL scaffolds were placed inside the chamber and exposed to the plasma for 1, 3, and 5-min and a pressure of 10 psi maintaining a

pure oxygen gas flow rate of 1 standard liter/min and power of 18 W at room temperature. The untreated samples were used as controls. After the plasma treatment, the samples were returned to the laminar hood for cell seeding.

3.   Characterization of Surface Properties

3.1. CONTACT ANGLE

The measurement of contact angles with different probe liquids is a common method to assess the hydrophilicity and wettability of a surface [28]. In the present study, to assess the improvement in hydrophilicity and wettability of the PCL surface, contact angle measurements were conducted with polar and apolar probe liquids. The contact angle (θ) of probe liquids on treated and untreated PCL sample surfaces were measured immediately after plasma treatment, by sessile drop technique using a video-camera (Hitachi VKC360) to record the drop image. The glycerol and diiodomethane were supplied from Fisher Scientific (Pittsburg, PA) and ultrapure water was provided by Agilent Technologies (Germany). A drop of probe liquid (5 μL) was placed onto the plasma-treated and control PCL sample surface. When the liquid settled (become sessile), contact angle measurements were taken at least three times and an average value was calculated.

3.2. SOLID SURFACE ENERGY

Measuring contact angle using probe liquids with known surface tension properties on the polymer is the most practical way to determine the solid surface energy of the polymer [29–31]. The surface energy of a liquid, σ_l, in equilibrium with its vapor, γ_{sl}, and the contact angle of a liquid drop resting on a solid surface, θ, was formulated through Young's Equation in 1805 [29–34]:

$$\sigma_s = \gamma_{sl} + \sigma_l \cdot \cos\theta \qquad (1)$$

where σ_s is the surface energy of the solid and γ_{sl} is the solid/liquid interfacial energy. σ_l is the experimentally determined surface energy of the probe liquids, and θ stands for the contact angle corresponding to the angle between vectors σ_l and γ_{sl}. So far, in the literature there are five main models used to determine the solid surface energy (σ_s) and solid/liquid interfacial energy (γ_{sl}) from the contact angle measurements [35,36]. Common target of these methods is to eliminate the interfacial energy (γ_{sl}) from the Young Equation [29,37] for calculating the solid surface energy. In the present study, we used Owens-Wendt method to evaluate the solid surface energy (σ_s) of poly-ε-caproloctane scaffold surfaces. In Owens-Wendt's method, the surface tension of liquid and solid phase can be separated into a dispersive component σ^D and a polar component σ^P. The solid surface energy is the summation of its polar and dispersive components.

$$\sigma_l = \sigma_l^P + \sigma_l^D \quad \sigma_s = \sigma_s^P + \sigma_s^D \tag{2}$$

where superscripts D and P represent the dispersive and polar components, respectively where subscripts s and l denote solid and liquid phases, respectively. To calculate the solid/liquid interfacial energy (γ_{sl}), especially for low energy surfaces such as polymers, Wu [36,38] claimed that harmonic mean equation is better suited instead of the geometric mean. In the present study, the harmonic mean equation was used in calculations to determine (γ_{sl}).

$$\gamma_{sl} = \sigma_s + \sigma_l - \left(\frac{4\sigma_l^D \sigma_s^D}{\sigma_l^D + \sigma_s^D} + \frac{4\sigma_l^P \sigma_s^P}{\sigma_l^P + \sigma_s^P} \right) \tag{3}$$

It is possible to calculate the polar and dispersive fractions of the surface energy with the aid of a single linear regression from the contact angle data of various liquids [28,35]. This approach is useful when doing measurements with three or more probe liquids [35].

4. Characterization of Cell-Surface Interaction

4.1. CELL PREPARATION

To evaluate the effect of plasma treatment on 3D PCL scaffolds for bone tissue applications, the mouse osteoblast cell line (7F2) (American Type Culture Collection) was used. The 7F2 osteoblast cells were cultured with Alpha minimum essential medium with 2 mM L-glutamine and 1 mM sodium pyruvate without ribonucleosides and deoxyribonucleosides, and 10% fetal bovine serum (FBS; Hyclone). Cells were maintained in an incubator equilibrated with 5% CO_2 at 37°C. Upon confluency, cells were digested by 3 mL trypsin and cell suspension was prepared. Then, the cell suspension was centrifuged (3,300 rpm, 2-min, Fisher, PA) and the supernatant was discarded. The cell pellet was diluted with culture medium and counted by hemocytometer (Hausser Scientific Company) to prepare cell suspension with a concentration of 5.6×10^5 cells/mL. Immediately after oxygen plasma treatment, the mouse osteoblast cells with passage number 26 were seeded on oxgen plasma treated and untreated samples with an initial cell density of 5.6×10^5 cells per sample. Then, the samples inside the 12-well plate were incubated at 37°C up to 7 days for further examination.

4.2. CELL PROLIFERATION

Mouse osteoblast cell proliferation on oxygen plasma treated and control samples at various time points after seeding was evaluated by the non-toxic alamarBlue™ assay (Biosource International, USA). The alamarBlue™ (aB) assay incorporates a fluorometric indicator based on the detection of metabolic activity. The amount

of fluorescence is directly proportional to the number of living cells. 10% (v/v) of aB assay solution was added to each well and mixed several times with the medium to make a homogenized solution. The well-plate was placed in the incubator for 4 h at 37°C in a 5% CO_2 condition. Then, 800 μL solution was taken out of each well and put into a new well-plate in order to measure the fluorescence intensity by multi-well plate reader (Genius, TECAN, USA). The fluorescence intensity was measured at 0, 3 and 5 days after seeding.

5. Results

5.1. EFFECT OF OXYGEN PLASMA TREATMENT ON SURFACE HYDROPHILICITY AND SURFACE ENERGY OF PCL

In Table 1, the variation of contact angles data of ultrapure water, diiodomethane, glycerol on untreated and varying duration oxygen plasma treated PCL surfaces were given. The contact angle of probe liquids on PCL scaffold decreased with oxygen plasma treatment.

TABLE 1. Measured static contact angle data and drop profiles of probe liquids on oxygen plasma treated and untreated pcl scaffold surface

Treatment duration	Static contact angle (°)		
	Ultrapure water	Diiodomethane	Glycerol
Untreated	57.55	34.45	70.79
1-min	34.49	26.60	37.99
3-min	40.65	31.49	38.13
5-min	43.55	30.37	43.35

The ultrapure water contact angle data of untreated PCL scaffold decreased from 57.55° to 34.49° in 1-min (Table 1) with oxygen plasma treatment. However, after 1 min there was no significant difference in the probe liquids contact angle data with the prolonged treatment time. The glycerol contact angle on PCL scaffold decreased from 70.79° for the untreated sample to 37.99° for the 1-min treated samples. After plasma treatment time of 1min, the ultrapure water contact and glycerol contact angles were increased for 3- and 5-min treated samples. The diiodomethane contact angle data, after 1-min treatment, vary only slightly for 3-min and 5-min treated samples. Table 1 indicates that the hydrophilicity of PCL scaffolds improved after 1-min oxygen plasma treatment time, then decreased again with the prolonged treatment time.

The total surface energy (σ_s) of PCL and its polar (σ_s^P) and dispersive (σ_s^D) components before and after oxygen plasma treatment, were calculated by Owens-Wendt's method. As an input in this method, the measured contact angle data (Table 1) and liquid surface tension components of three probe liquids taken from literature were used. The effect of oxygen plasma treatment on total solid surface

of PCL is given in Fig. 1. The variation in the polar and dispersive components of solid surface energy of PCL with oxygen plasma treatment is given in Fig. 2.
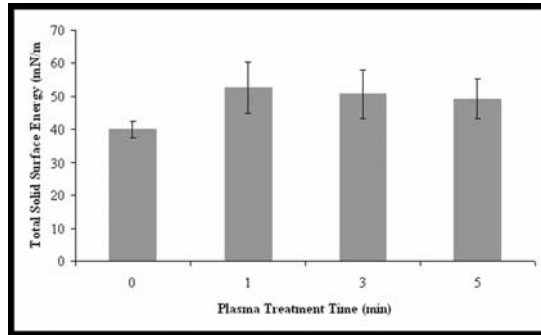
Figure 1. Variation in total solid surface energy of PCL with oxygen plasma treatment time. Error bars represent the standard deviations
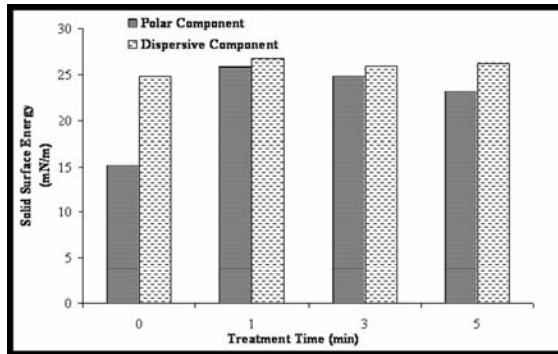

Figure 2. Variation in dispersive and polar component of solid surface energy of pcl with oxygen plasma treatment time

In Fig. 1 shows that the total surface energy (σ_s) of PCL increased with the oxygen plasma treatment time from 39.98 mN/m for untreated to 52.54 mN/m for 1-min oxygen plasma treated scaffold. However, prolonged treatment time (3-min and 5-min) does not affect the total surface energy significantly. In Fig. 2, the effect of oxygen plasma treatment on polar and dispersive component of PCL solid surface energy is given. The polar components of the surface energy of PCL scaffold is affected greatly with oxygen plasma treatment compared to the dispersive component. Since there was not a significant change in the dispersive components, the polar components first increased with 1-min treatment and decreased again with the prolonged treatment time which was observed in the variation of total surface energy with treatment time. This indicates that polar makes the primary contribution in the change of solid surface energy. From Fig. 2 we can also say that polar chemical functional groups had been introduced to the PCL surface by oxygen plasma treatment.

5.2. EFFECT OF OXYGEN PLASMA TREATMENT
  ON PROLIFERATION OF MOUSE OSTEOBLAST
  CELLS ON PCL SCAFFOLDS

The metabolic activity of mouse osteoblast cells on plasma treated and untreated PCL scaffold were examined by the alamarBlue™ assay. The proliferation rate of mouse osteoblast cells for the 7 day culture period on treated and untreated (control) PCL scaffolds is given in Fig. 3.
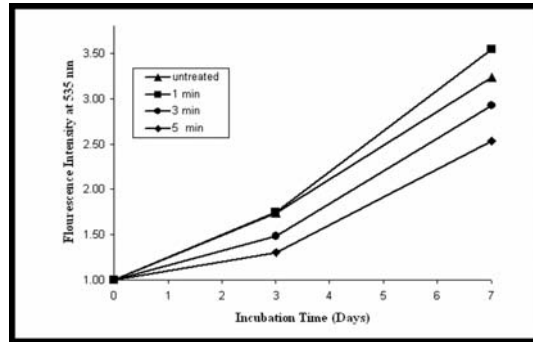
Figure 3. Normalized fluorescence intensity of mouse osteoblast cells according to day 0 values for various different plasma treatment durations

The highest proliferation rate was observed for the 1-min treated sample. The cell number on 1-min treated sample was higher than the untreated, 3-min, and 5-min treated PCL scaffold. After 1-min treatment, the plasma affected the cell proliferation adversely. From here, we can conclude that although plasma treatment increased proliferation of mouse osteoblast cells on 1-min treated PCL scaffold, there was an optimum treatment time for cell proliferation.

6. Discussion

The diameter of the cells used in vitro study dictates the minimum pore size, which varies from one cell type to another. Depending on the applications, pore size of the scaffold must be carefully controlled. Pore sizes between 100–350 μm are the optimum pore size for the regeneration of bone. In the present study, in order to fabricate fully interconnected, well defined 3D scaffolds, the PED system was used to build scaffold with 300 μm pore size. The hydrophilicity of a polymer is a factor affecting the solid surface energy which is directly related to the degree of cell adhesion. Therefore, in this study the surface of the PCL scaffolds were treated with oxygen-based RF plasma treatment in order to increase the hydrophilicity and surface energy of naturally hydrophobic PCL surface. Before and after plasma treatment hydrophilicity, polar and dispersive components of surface energy were calculated for different treatment time. The polar components of

the surface energy of PCL scaffold were affected greatly with oxygen plasma treatment as compared to the dispersive components. This indicates that polar components show the main contribution in the change of solid surface energy. The positive correlation of cell proliferation with the increase of surface energy PCL scaffold is clear but detailed analyzing of optimum treatment time has to be done. There is an optimum treatment time for the surface of PCL to enhance the mouse osteoblast cell attachment and proliferation between 0-min and 1-min.

Conclusion

In order to enhance the osteoblastic cell proliferation and adhesion on PCL scaffolds, surface were modified by oxygen-based RF plasma treament for 1-min, 3-min and 5-min. The effect of treatment was evaluated by means of contact angle, surface energy, and mouse osteoblast cell affinity. The total solid surface energy of PCL and its polar and dispersive components were calculated by the Owens-Wendt method. Oxygen plasma treatment contributed in decreasing the hydrophobicity of PCL for 1-min treatment and in changing the surface energy from 39.98 mN/m for untreated to 52.54 mN/m for 1-min treated by the increment in polar component of surface energy. However with the extended treatment time (3-min and 5-min), the hydrophilicity and surface energy did not change and the rate of mouse osteoblast cell proliferation was relatively low compared to the untreated PCL scaffold. Further examinations should be done to evaluate effect of overdose plasma treatment on PCL scaffolds.

Acknowledgment

References

[1] Wang, F., et al., *Precision extruding deposition and characterization of cellular poly-epsilon-caprolactone tissue scaffolds.* Rapid Prototyping Journal, 2004. **10**(1): 42–49.

[2] Hutmacher, D.W., M. Sittinger, and M.V. Risbud, *Scaffold-based tissue engineering: rationale for computer-aided design and solid free-form fabrication systems.* Trends in Biotechnology, 2004. **22**(7): 354–362.

[3] Liu, X.H. and P.X. Ma, *Polymeric scaffolds for bone tissue engineering.* Annals of Biomedical Engineering, 2004. **32**(3): 477–486.

[4] Yeong, W.Y., et al., *Rapid prototyping in tissue engineering: challenges and potential.* Trends in Biotechnology, 2004. **22**(12): 643–652.

[5] Engelberg, I. and J. Kohn, *Physicomechanical properties of degradable polymers used in medical applications: a comparative study.* Biomaterials, 1991. **12**(3): 292–304.

[6]   Pitt, C.G. and A. Schindler, *Biodegradation of polymers*, in *Controlled drug delivery*, Bruck, S.D. (Ed) 1983, CRC Press: Boca Raton, FL. p. 55–80.

[7]   Hutmacher, D.W., et al., *Mechanical properties and cell cultural response of poly-caprolactone scaffolds designed and fabricated via fused deposition modeling.* Journal of Biomedical Materials Research, 2001. **55**(203–216).

[8]   Darling, A. and W. Sun, *3D Microtomographic characterization of precision extruded poly-e-caprolactone tissue scaffolds.* Journal of Biomedical Materials Research Part B: Applied Biomaterials, 2004. **70B**(2): 311–317.

[9]   Zein, I., et al., *Fused deposition modeling of novel scaffold architectures for tissue-engineering applications.* Biomaterials, 2001. **23**: 1169–1185.

[10]   Chen, G., et al., *Silk fibroin modified porous poly-epsilon-caprolactone scaffold for human fibroblast culture in vitro.* Journal of Materials Science:Materials in Medicine, 2004. **15**: 671–677.

[11]   Britland, S.T., et al., *Micropatterned substratum adhesiveness: a model for morphogenetic cues controlling cell behavior.* Experimental Cell Research, 1992. **1998**: 124–129.

[12]   Anselme, K., *Osteoblast adhesion on biomaterials.* Biomaterials, 2000. **21**(7): 667–681.

[13]   Oyane, A., et al., *Simple surface modification of poly (epsilon-caprolactone) to induce its apatite-forming ability.* Journal of Biomedical Materials Research Part A, 2005. **75A**(1): 138–145.

[14]   Liu, H.Z., et al., *Effects of DBD plasma operating parameters on the polymer surface modification.* Surface & Coatings Technology, 2004. **185**(2–3): 311–320.

[15]   Safinia, L., et al., *Towards a methodology for the effective surface modification of porous polymer scaffolds.* Biomaterials, 2005. **26**(36): 7537–7547.

[16]   Yang, J., J.Z. Bei, and S.G. Wang, *Enhanced cell affinity of poly (D,L-lactide) by combining plasma treatment with collagen anchorage.* Biomaterials, 2002. **23**(12): 2607–2614.

[17]   Vasilets, V.N., A.V. Kuznetsov, and V.I. Sevast'yanov, *Regulation of the biological properties of medical polymer materials with the use of a gas-discharge plasma and vacuum ultraviolet radiation.* High Energy Chemistry, 2006. **40**(2): 79–85.

[18]   Chan, C.M., T.M. Ko, and H. Hiraoka, *Polymer surface modification by plasmas and photons.* Surface Science Reports, 1996. **24**(1–2): 3–54.

[19]   Cioffi, M.O.H., H.J.C. Voorwald, and R.P. Mota, *Surface energy increase of oxygen-plasma-treated PET.* Materials Characterization, 2003. **50**(2–3): 209–215.

[20]   Zhu, X., et al., *Effect of argon-plasma treatment on proliferation of human-skin-derived fibroblast on chitosan membrane in vitro.* Journal of Biomedical Materials Research Part A, 2005. **73A**(3): 264–274.

[21]   Qu, X., et al., *The effect of oxygen plasma pretreatment and incubation in modified simulated body fluids on the formation of bone-like apatite on poly (lactide-co-glycolide) (70/30).* Biomaterials, 2007. **28**: 9–18.

[22]   Gugala, Z. and S. Gogolewski, *Attachment, growth, and activity of rat osteoblasts on polylactide membranes treated with various lowtemperature radiofrequency plasmas.* Journal of Biomedical Materials Research Part A, 2006. **76A**(2): 288–299.

[23]   Kaibara, M., et al., *Proliferation of endothelial cells on the plasma-treated segmented-polyurethane surface: attempt of construction of a small caliber hybrid vascular graft and antithrombogenicity.* Colloids and Surfaces B-Biointerfaces, 2000. **19**(3): 209–217.

[24]   Chim, H., et al., *Efficacy of glow discharge gas plasma treatment as a surface modification process for three-dimensional poly (D,L-lactide) scaffolds.* Journal of Biomedical Materials Research Part A, 2003. **65A**(3): 327–335.

[25] Kim, Y.J., et al., *Surface characterization and in vitro blood compatibility of poly (ethylene terephthalate) immobilized with insulin and/or heparin using plasma glow discharge.* Biomaterials, 2000. **21**: 121–130.

[26] Alves, C.M., et al., *Modulating bone cells response onto starch-based biomaterials by surface plasma treatment and protein adsorption.* Biomaterials, 2007. **28**: 307–315.

[27] Marxer, C.G., *Protein and cell absorption: Topographical dependency and adlayer viscoelastic properties determined with oscillation amplitude of quartz resonator*, in *Depatment of Physhics*. 2002. Universite de Fribourg: Fribourg, Switzerland.

[28] M. Gindl, G. Sinn, W. Gindl, A. Reiterer, S. Tschegg, *Colloids and Surfaces a-Physicochemical and Engineering Aspects*, 2001. **181**(1–3):279.

[29] Lopes, M.A., et al., *Hydrophobicity, surface tension, and zeta potential measurements of glass-reinforced hydroxyapatite composites.* Journal of Biomedical Materials Research, 1999. **45**(4): 370–375.

[30] Brant, J. and A. Childress, *Assessing short-range membrane-colloid interactions using surface energetics.* Journal of Membrane Science, 2002. **203**: 257–273.

[31] Volpe, C.D., et al., *The determination of a 'stable-equilibrium' contact angle on heterogeneous and rough surfaces.* Colloids and Surfaces a-Physicochemical and Engineering Aspects, 2002. **206**: 47–67.

[32] Wu, S., *Calculation of interfacial tension in polymer systems.* Journal of Polymer Science Part C, 1971. **34**(19).

[33] Wu, S., *Polymer interface and adhesion.* 1982, New York: Marcell Dekker.

[34] Hansen, F.K., *The Interfacial Tension between Acrylic Monomers and Polymers and Non-ionic Surfactants Investigated by the Automatic Sessile Drop Method.* Journal of Colloid and Interface Science, 1999. **210**(1): 144–151.

[35] Zhuang, Y.X. and A. Menon, *Wettability and thermal stability of fluorocarbon films deposited by deep reactive ion etching.* Journal of Vacuum Science and Technology, 2005. **A23(3)**: 434–439.

[36] Owens, D.K. and R.C. Wendt, *Estimation of the surface free energy of polymers.* Journal of Applied Polymer Science, 1969. **13**(8): 1741.

[37] Gindl, M., et al., *A comparison of different methods to calculate the surface free energy of wood using contact angle measurements.* Colloids and Surfaces a-Physicochemical and Engineering Aspects, 2001. **181**(1–3): 279–287.

[38] Hansen, F.K. and J. Hveem, *The Interfacial Tension between Acrylic Monomers and Polymers and Non-ionic Surfactants Investigated by the Automatic Sessile Drop Method*. Journal of Colloid and Interface Science, 1999. **210**(1): 144–151.

PLASMA ASSISTED SURFACE MODIFICATION PROCESSES FOR BIOMEDICAL MATERIALS AND DEVICES

P. FAVIA[1,2,3,*], E. SARDELLA[1,2], L. C. LOPEZ[1], S. LAERA[1],
A. MILELLA[1], B. PISTILLO[1], F. INTRANUOVO[1],
M. NARDULLI[1], R. GRISTINA[2], AND R. D'AGOSTINO[1,2,3]
[1]*Department of Chemistry, University of Bari, via Orabona 4,
70126, Bari, Italy*
[2]*CNR Institute of Inorganic Methods and Plasmas, IMIP-Bari, Italy*
[3]*Plasma Solution Srl, Spin off of the University of Bari, Italy*

Abstract: This contribution reviews cold plasma processes that are investigated and utilized in academic and technological fields related to Life Sciences, in particular for tailoring surface composition and morphology of materials of different utilization in Medicine and Biology for implants, prostheses, biosensors, devices and scaffolds for tissue engineering. The final goal of the research in this field is, in general, to achieve the capability of driving at will the behaviour (adhesion, growth, morphology, physiology, etc.) of cells and biological tissues *in vitro* and *in vivo* at the surface of modified materials.

Recent advances on different plasma-processes for biomedical applications, developed in radiofrequency (RF, 13.56 MHz) Glow Discharges at the group of the authors are reported in this review, including: the synthesis of functional surfaces for direct cell growth and biomolecule immobilization; the deposition of non-fouling coatings; the deposition of nano-composite bacterial resistant coatings; the synthesis of nano-structured surfaces. *In vitro* biological tests for plasma-processed surfaces are also described.

Keywords: Plasma enhanced chemical vapor deposition, plasma treatment, antibacterial coatings, teflon-like coating, micro-nano structured surfaces, biomolecule immobilization, cytocompatibility tests

1. Plasma and Life Sciences

Plasma Chemistry and Life Sciences met probably the first time in the 1950s, when S. L. Miller ignited an electrical discharge in a gas mixture of the presumed components (methane, ammonia, hydrogen and water vapour) of the primordial

---

atmosphere on Earth. Aminoacids were found after the experiment in the glass vessel reactor, and a consistent hypothesis on how Life could start on our planet was confirmed [1–2].

When scientists realized that non equilibrium (cold) plasmas could alter surface composition and properties of materials by means of dry etching, thin film deposition (PE-CVD, Plasma Enhanced Chemical Vapor Deposition) and treatment/ grafting processes, wide, deep and fertile research fields were opened, both from the academic and economical point of view. Plasma technologies matured scientifically and technologically in the 1970s, boosting the powerful development of Microelectronics and Solar Cells that is still going on nowadays. In this framework, glow discharges started to be tested also for biomedical applications; one of the first paper in this field [3], published in 1969, described plasma treatments of polyolefins aimed to graft $-NH_2$ groups that, in proper pH conditions, could ionize to $-NH_3^+$ and immobilize non-thrombogenic negatively-charged heparin molecules, to provide non-thrombogenicity and blood compatibility to polymer surfaces. Since then the idea of adapting the surface of biomedical materials, devices, wares, Tissue Engineering scaffolds, sensors and prostheses to the best interaction with biological molecules, cells, fluids and tissues *in vitro* and *in vivo* has produced a huge quantity of scientific literature and patents through the years, were non equilibrium plasmas play a main role.

After the burst in Microelectronics and Semiconductors, plasma processes have permeated so many different areas of Science and Technology in the last 30 years: Polymers, Packaging, Optics, Automobile, Textiles, Paper, Membranes and Sensors, just to mention a few, were all impacted by Plasma Science and Technology, sooner or later. The versatility of low pressure glow discharges in modifying the surface of materials without altering their bulk, at room temperature, with a dry solvent-free technology; the extremely large variety of chemistry and properties virtually offered on any solid surface; and, very important, the possibility of scaling-up processes to industrial sizes and throughput with "real" substrates (webs, inside of tubes, fabrics, non woven materials, granules, lenses etc.), open continuously new fields to this technology [4].

In addition to the properties listed above, the intrinsic sterility of surface-modification plasma processes is also appealing for applications in Biology and Medicine. In the last 20 years also atmospheric pressure plasma processes (Atmospheric Pressure Glow Discharges, APGD; Dielectric Barrier Discharges, DBD) have reached an important level of development in many more fields (e.g., TV Displays), including surface-processing of materials [5], even though the process versatility of low pressure systems is still far to be reached.

Today Plasma Science and Technology impacts three different large areas of Life Science, namely: surface modification of materials for biomedical applications, sterilization/decontamination of biomedical surfaces, and treatments of living biological tissues. The first topic is the subject of this short review, the other two are largely discussed in other contributions to this book.

Non equilibrium plasma processes can easily tune the hydrophilic/hydrophobic character of polymer surfaces, thus their wettability. At a more sophisticated level

of surface engineering, plasma processes can tailor the adsorption of proteins and adhesion of cells to materials, for *in vitro* biomedical applications, by carefully using functional coatings or grafted surfaces; such surfaces, characterized by proper chemical groups, can also immobilize peptides and carbohydrates to mimic the functions of ligand proteins involved in driving specific responses from the adhering cells, or enzymes for specific molecule recognition applications and bio-sensors. Surfaces with improved cell-adhesive properties respect to the substrate can be synthesized, as well as surfaces characterized by non-fouling properties (i.e., the ability to completely discourage the adhesion of organic and biological entities). In the fields of Tissue Engineering and Bioreactors, cold plasmas are investigated for adapting the surface of biodegradable and permanent scaffolds and of membranes to the best interaction with specific cell types, to allow them to function as they were *in vivo*.

After the understanding that not only the chemical composition, but also the morphology of a surface can drive the behavior of cells in contact with it [6], plasma etching, deposition and grafting processes became often part of procedures optimized to sculpt micro- or nano-features (e.g., 3D random relieves or geo-metrical, ordered features) on biomedical materials and devices to drive selected cell responses like adhesion, growth, physiological behavior, etc. Plasma chemistry can provide also functional surfaces where anti-bacterial molecules are immobilized, as well as nano-composite coatings capable of releasing anti-bacterial silver ions in wet environments.

It is worth to mention, in this context, that also thermal plasma technologies are utilized for biomedical applications; plasma-spray techniques, for example, are utilized in production to coat the metal surface of orthopaedic prosthesis and devices with hydroxy-apatite, the mineral moiety of human bones. Such coatings are designed to improve the osteoconductivity and the osteointegration of the implant, thus allowing a solid and faster healing at the bone-prosthesis interface after the surgery [7].

The reader is warmly suggested to give a look to ref. [8] for a complete and updated overview of the use of materials and surfaces in Biomedical Sciences, and to ref. [9] for a complete recent review of many different applications of non equilibrium plasmas in Life Science.

The next sections describe different plasma-processed surfaces of biomedical interest under investigation at the group of the authors, as well as *in vitro* bio-logical tests for their characterization. All plasma processes described have been performed in parallel-plate RF (13.56 MHz) glow discharges.

2. Synthesis of Functional Surfaces for Cell Growth and Biomolecule Immobilization

Plasma modification processes have been extensively used to modify materials for bio-medical purposes [9–11] since they allow to obtain surfaces with a tuneable density of surface functional groups without altering their mechanical features.

In particular, plasma treating polymers with non-polymerizable gases (H_2, O_2, NH_3, N_2/H_2, etc.) lead to surfaces rich of N-and O-containing functional groups, such as amino, carboxylic and hydroxyl; similar functionalized surfaces can also be obtained from PE-CVD processes with organic compounds (allylamine, acroleyn, acrylic acid, etc.). Substrates displaying surface chemical functionalities can alternatively be obtained by means of plasma-induced graft polymerization of organic monomers, which is a plasma treatment process, necessary to activate the surface, soon followed by a chemical interaction of the treated surface with an organic monomer [12].

Whatever is the plasma process employed, substrates displaying surface polar chemical groups (e.g., $-NH_2$, COOH, OH, etc.) might *per se* confer an adhesive "biological activity" to the material and may improve the spreading and growth of cells [13]; it has been, in fact, diffusely documented that both oxygen- and nitrogen-containing groups promote cell adhesion and growth [14–16].

Just to mention a few representative examples of functionalizing PE-CVD processes, glow discharges fed with vapors of acrylic acid (AA) deposit thin functional organic films (plasma deposited Acrylic Acid, pdAA), which are characterized by –COOH and other O-bearing groups and have been largely used as cell-adhesive surfaces [17–19]. The distribution of the different oxygen-containing functional groups on the coatings, which at last drive its stability in water media (no leach of low weight molecules, no delamination from the substrate) and its ability to drive the response of proteins and cells in biological environment, can be tuned by properly driving, by means of the experimental discharge parameters, the relative density of the fragments of the monomer in the discharge. These functional coatings can be utilized in engineering biomedical surfaces to improve the spreading and growth of certain cells [20].

Amine containing surfaces, obtained by plasma-grafting processes in NH_3 discharges or by PE-CVD from aminated organic monomers, have been also employed to successfully promote cell colonization [21]. Lastly, plasma-synthesized surfaces displaying -OH surface groups have been used to promote cell culture [22], but this strategy has been less exploited for biomedical purposes, if compared with -COOH and N-bearing substrates. On the other hand, many immobilization and deposition methods that use plasma processes have been also employed for producing surfaces which prevent protein and cell adsorption [23] as well as bacterial adhesion [24], as it will be shown in the next sections.

In order to trigger specific cell-surface interactions, an helpful approach is represented by the immobilization of biomolecules on plasma-modified materials displaying properly selected "anchor" surface functional groups. In particular, many functionalization methods offered by plasma deposition and treatment (grafting) modification processes can produce surfaces functionalized with chemical groups suitable for immobilization of enzymes, peptides, proteins, polysaccharides, and others biomolecules.

Plasma treatment and deposition processes can build functional surfaces for immobilization reactions to be performed in water solutions at mild conditions. Very often biomolecules are immobilized at the surface of functionalized materials

by means of "spacer arm" molecules [25], that keep them tethered at the surface. The use of a spacer arm allows tethered biomolecules to assume their active conformation and keep their natural biological activity unaltered. The idea, in this research, is to hide artificial surfaces with properly selected molecules and imitate, in this way, the natural environment were cells live and function, to allow cells to "recognize" such new environment.

The literature is full of examples of immobilization reactions performed onto plasma-modified materials for various biomedical applications [21]. We have performed the immobilization of different kind of biomolecules ranging from short peptides such as RGD (Arginine – Glycine – Aspartic acid), to galactose derivatives.

RGD is the minimum adhesion domain contained in proteins part of the extracellular matrix (ECM, i.e., the natural scaffold where cells live *in vivo*), such as fibronectin and vitronectin [26]; RGD is certainly the most common peptide molecule that has been investigated to be immobilized for enhancing adhesion and growth of different cell lines on materials. We have reported the immobilization of RGD molecules onto COOH groups obtained on polymer surfaces, polyethylene-terephtalate (PET) [27] and polyethersulfone (PES) membranes [28], among others, by using pdAA functional coatings. For applications of (bio)materials in water, from the immobilization reactions to the final use as cell-growth substrates, plasma deposited functional coatings must result stable in water media. For pdAA coatings it was found, for example, that a surface density of –COOH groups exceeding 8–10% respect all surface carbons (XPS data) result in changes of surface composition after prolonged immersion in water [18], likely due to the leach of low weight compounds in water and/or to delamination of the coating from the substrate.

The immobilization of RGD has been accomplished trough a bis-amino spacer arm molecule (O,O'-Bis(2-aminopropyl)-polyethylene glycol 500) immobilized at the surface of the pdAA layer by using a water soluble carbodiimide (EDC) activation step (scheme shown in Fig. 1). A peptide bond can be formed between the pdAA layer and the spacer molecule, as well as between the spacer and RGD afterwords. 3T3 fibroblasts were cultured onto PET substrates surface-modified with immobilized RGD, and cell adhesion and growth was found enhanced, on these substrates, with respect to native PET and to pdAA surfaces; furthermore cells displayed a different morphology on each tested surface, revealing their sensibility to differences in chemical surface compositions.

We have also reported the immobilization of galactose derivatives at the surface of pdAA-coated PES membranes, also in this case by means of a linear bis-amine spacer arm [30], for controlling adhesion, proliferation and differentiation of primary pig and human liver cells [29]. Surface-immobilized galactose moieties were shown to trigger specific performances of hepatocytes, as attested after having evaluated the expression of liver specific functions; in particular, human hepatocytes cultured on galactose-immobilized modified membranes displayed higher levels of albumin production and of urea synthesis when compared with the same cells cultured on untreated membranes.
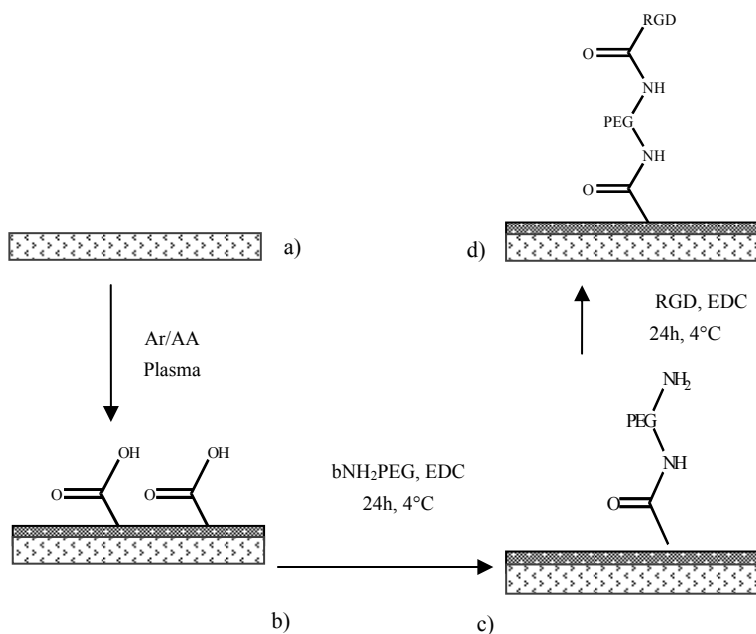
Figure 1. Immobilization scheme employed for RGD. (a) native substrate; (b) plasma modification with Ar/AA PE-CVD to obtain a surface rich of COOH groups; (c) immobilization of the spacer molecule; and (d) immobilization of RGD

3. Deposition of PEO-like Non-Fouling Coatings

Conventional polyethyleneoxide (PEO) and polyethyleneglycol (PEG) polymers are known for their hydrogel behaviour in water media, which is most likely at the base of their non fouling behaviour against the adhesion of cells, bacteria, proteins and other biological entities [31,32]. For this reason, continuous [33,34] and modulated [35,36] PE-CVD processes fed with volatile monomers characterized by -CH_2CH_2O- ethylene oxide (EO) units in their structure, such as glycols (e.g., DEGDME, Di-Ethyl Glycol Di-Methyl Ether, $CH_3O(CH_2CH_2O)_2CH_3$, or homologous molecules with n = 3 or 4) or crown ethers, are studied extensively to impart durable non fouling properties to biomedical surfaces.

Mild fragmentation conditions (e.g., low power input, modulated rather than continuous discharges, and others) are generally utilized to plasma-deposit PEO-like coatings in order to keep as high as possible the fraction of intact EO moieties (PEO character) in their structure, a feature that is correlated to the non fouling properties. PEO character and non fouling properties are associated to the relative contribution of the ether peak component (~286.5 eV of Binding Energy) of the C1s XPS (X-rays Photoelectron Spectroscopy) signal, and can be quantified easily. The fragmentation extent of the monomer in the glow discharge can be

revealed by actinometric optical emission spectroscopy (AOES) measurements of CO and other emitting fragments (e.g., CH) of the monomer, whose relative density in the plasma was found inversely correlated with the PEO character of the coatings [34] deposited in different discharge conditions: the more CO is revealed in the plasma, the higher is the monomer fragmentation, the lower is the PEO character of the coating, and *viceversa*.

When the PEO character is high (70–80% or more) the coatings are hydrophilic, show low (40 ± 2) advancing water contact angle (WCA) values, and display non fouling properties. The recovery of the methyl groups of the films toward the atmosphere was hypothesized to lower the surface tension of the coating; in fact hydrocarbon fragments have been detected on the top most layer of the films by means of ToF-SIMS (Time of Flight Secondary Ions Mass Spectrometry). Also peaks deriving from the DEGDME monomer were detected (M^+ ions, where $M = CH_2CH_2O$), as well M_2^+, M_3^+ and $(MH)^+$, $(M_2H)^+$ and $(M_3H)^+$ ions. The relative intensity of the peaks changes as function of the RF power input of the PE-CVD process. In particular, a clear decrease in relative amount of M_2^+ and M_3^+ ions was observed as the power increases [37], confirming that the retention of the EO monomer structure (and of the related non fouling character) is loss when the fragmentation is increased in the plasma.

As reported earlier in this contribution, the adsorption of proteins on a biomaterial is of primary importance for cell-biomaterial interactions, since this adsorbed protein layer rather than the substrate itself mediates all following events; the recognition of the proteins adsorbed at the surface of a material would promote cell adhesion and growth and would initiate wound healing and new tissue growth.

We have used the QCM-D (Quartz crystal Microbalance with Dissipation monitoring) technique to quantify the non fouling effect of coatings plasma-deposited from DEGDME. We have exposed 3 mm thick quartz crystals coated with 60 nm films of different PEO character to a fibronectin solution. A 50 μg/ml solution of fibronectin (0.05 M Tris buffered saline, pH 7.5, Sigma Aldrich) was injected, in contact with the QCM crystal, at 37°C in the QCM-D analytical chamber, and the frequency shift of the crystals was converted in mass changes of the electrode. None or poor fibronectin adsorption was observed on coatings with a PEO-character higher than 70%, while an adsorption of 0.15 μg/cm^2 (saturation value) was observed on coatings with 30% PEO-character. The saturation of the substrate was reached after 2 h of exposure to fibronectin. These results were confirmed by XPS and ToF-SIMS: no nitrogen from fibronectin was detected on coatings with a PEO-character higher than 70%. Although testing the non fouling character with only a protein could be reductive, the resulting data are in agreement with those obtained from 3T3 murine fibroblast culture tests on surfaces with different PEO characters: higher amount of adsorbed cell adhesive proteins like fibronectin corresponded to larger sample area covered by the adhering cells.

In Fig. 2 the area covered by cells on coatings with a PEO-character ranging from 20% to 40% is shown as a function of culture time (3–96 h). CCPS (cell culture PS) and PET substrates were included in the experiment as reference.

In this experiment also coatings with PEO character higher than 70% (the only ones, in effect, that could be labeled as "PEO-like" and non fouling) were utilized. It was found that such coatings remained always free of cells within the time scale of this experiment, and no adhering cells could ever be observed on them; rather than adhere to the PEO-like surface, cells were floating in the culture medium. Cell adhesion data relative to covered areas were always zero, therefore they are not reported in Fig. 2. In effect we have always measured the non fouling effect on such coatings in many similar experiments, in our lab, with several cell lines, and on several kind of substrates, up to several weeks.
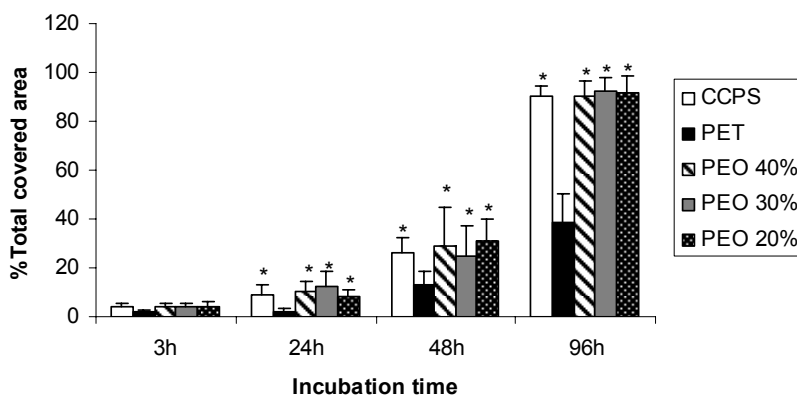
Figure 2. Total area covered by cells on different PEO-like coatings with 20% (PEO20%), 30% (PEO30%) and 40% (PEO40%) of PEO-character. CCPS and native PET were used as references. The Student's t-test (for three samples, assuming unequal variances) was used to compare statistically differences of adhesion on each PEO-like sample and CCPS against native PET. $*p < 0.01$

The area coverage by fibroblasts on all coatings with PEO-character lower than 70%, instead, was found quite similar, always larger respect to native PET, and comparable to CCPS reference substrates. CCPS Petri dishes are well known commercial substrates for cell growth protocols; they are used often as substrate of reference because they is able to promote cell adhesion. CCPS commercial substrates are obtained by means of customized corona treatments in air that allow the grafting of O-containing functionalities, including ether groups, on PS.

To complete this section it must be reported that plasma-deposited non fouling PEO-like coatings are becoming very popular and reliable nowadays for many different plasma-aided micro- and nano-patterning protocols [38–42] aiming to transfer micro- and nano-metric domains with different properties (e.g., protein adhesive and non fouling; biomolecule functionalized and non fouling, etc.) at the surface of biosensors and biochips intended to function in water media. During the development of such devices, that often use soft lithography [43,44] procedures, it was clearly tested that the non fouling effect of PEO and PEO-like surfaces holds very well in water, while it does not occur at all in dry conditions. Proteins, in fact,

can be easily transferred by micro-contact printing at these surfaces with dry procedures [45].

Another important piece of information on plasma-deposited PEO-like coatings deals with their behaviour *in vivo*: the non fouling effect, in fact, was not confirmed on PEO-like coated materials implanted in animals [46] where, clearly, the immune system of the host is triggered and the events occurring at the surface of the coating are much more complex than in a cell culture medium.

4.   Plasma-Deposited Nano-Composite Bacterial Resistant Coatings

The presence of implants and devices in the body is known to increase the susceptibility to infections, major risk factors in hospitals, and to activate the biological defences and the immune system of the host [47]. Proteins from ECM and blood, host cells (fibroblasts, osteoblasts, endothelial) and bacteria decide the fate of a biomaterial surface *in vivo* [48,49]. The adhesion of bacteria at the interface between the material and the physiological medium can seriously compromise the correct functioning of a biomedical device, as well as the health of the host. When bacteria adhere at the surface of a material, they may proliferate and develop in a biofilm shield layer, that prevents drugs to reach them at a therapeutic concentration to defeat the infection [50]. Biofilms are generally described as surface-associated bacterial communities consisting of exopolysaccharide-surrounded micro-colonies. The removal of the device from the host is required in many cases.

Research is heavily funded world-wide to develop materials for use as implantable devices where the growth of infectious biofilms is inhibited; bio-materials coated with silver oxide or alloys have been investigated in this context, but in many cases controversial or disappointing clinical results were produced concerning the use of silver. For thousands years the inhibitory effect of silver against a broad spectrum of bacterial strains has been known, which is mainly due to silver ions released in water media [51]. Biomaterials including silver in their structure have been developed with the aim of retarding bacterial adhesion and biofilm formation during the healing processes. As an example, heart valves made with silver-impregnated materials have been developed [52], and polyethylene or fabric sheets coated with silver nano-particles for wound healing [53].

Materials with sustained-release of silver ions may soon be viable options in the medical industry for complete antibacterial protection of devices. Despite the variety of applications being developed and investigated for nano-silver materials, very little is still known of the effects of silver nano-particles on the environment and on the human health. In 1975 the *United States Pharmacopeia* and *National Formulary* guidebooks officially removed all products containing colloidal silver when it was discovered that long-term use of silver preparations lead to argyria, a pathologic condition due to the uncontrolled high amount of silver circulating in the host body [54], which turns skin to a bluish-grey colour for the accumulation of silver salts in the skin and in internal organs. A close control of the structure of silver-based antibacterial coatings should be achieved, as well as how directing the

toxicity of silver only against bacteria, and a deeper knowledge of the correlations between the structure/composition of the material and its properties of cytotoxicity and bactericidal/bacteriostatic effect.

All advantages of plasma processes can be utilized to produce a drug delivery system with carefully customized structure and controlled Ag^+ release properties in biological media. Nano-composite plasma deposited coatings have been extensively studied since the early 1980s, with pioneering articles published by Kay et al. [55] and by Biedermann et al. [56], including their potential application as antibacterial coatings [57–59]. The word nano-composite refers to thin coatings with nano-metric clusters of a certain compound (metal, ceramic, polymer, etc.) embedded in a matrix of different nature. The PEO-like coatings described in the previous section can embed silver nano-clusters; if a properly configured plasma reactor is utilized (asymmetric parallel plate geometry, silver RF cathode) and enough energy is delivered to the discharge, it is possible to couple the deposition of PEO-like coatings from a proper EO monomer with the sputtering of silver from the cathode [59]. Ag/PEO-like (i.e., PEO-like with Ag clusters embedded) nano-composite coatings can be deposited in this way, where the antibacterial agent is entrapped in the PEO-like matrix. When the matrix swells in water, the coating leaches the drug, Ag^+ ions, at controlled rate. Changing the nature of the monomer and the nature of the RF cathode, other kinds of nano-composite coatings could be deposited. Generally, since the RF power drives both the sputtering of silver and the fragmentation of the monomer, the cross-linking and the $C_xH_yO_k$ composition of the matrix is far from that needed to obtain non fouling coatings. The cross-linking degree of the organic matrix, the overall density of silver (1–24 atom %), and the dimension (5–90 nm) of the clusters increase with the RF power. A detailed description of the deposition mechanism of Ag/PEO-like coatings is reported in ref. [59].

The composition of Ag/PEO-like coatings can be easily controlled *in situ* during the deposition by means of AOES. As for the PEO-like, the PEO character of Ag/PEO-like coatings is correlated with the AOES density of CO in the discharge: the lower the I_{CO}/I_{Ar} emission ratio in the plasma phase, the higher the amount of ether groups in the coatings (high PEO-character). The Ag content of the coatings can also be controlled, and it results proportional to the AOES density of Ag atoms sputtered in the plasma [57].

Ag/PEO-like coatings exhibit high WCA hysteresis (i.e., high difference between advancing and receding WCA values) due to the presence of Ag clusters. Force vs distance Atomic Force Microscopy (AFM) curves attest for a chemical homogeneous surface, with no silver in the outermost layer. The roughness (R_{RMS}) AFM values of different Ag/PEO-like coatings were found to increase with the silver content in the 1–10 nm range, with maximum height of the nano-bumps in the 5–70 nm range. TEM (Transmission Electron Microscopy) micrographs attest the presence of the silver clusters, so these bumps should be due to Ag clusters partially protruding from the surface of the coatings. Figure 3 shows Ag clusters of nanometric dimensions embedded in two Ag/PEO-like coatings plasma-deposited in different experimental conditions.

(a)   (b)
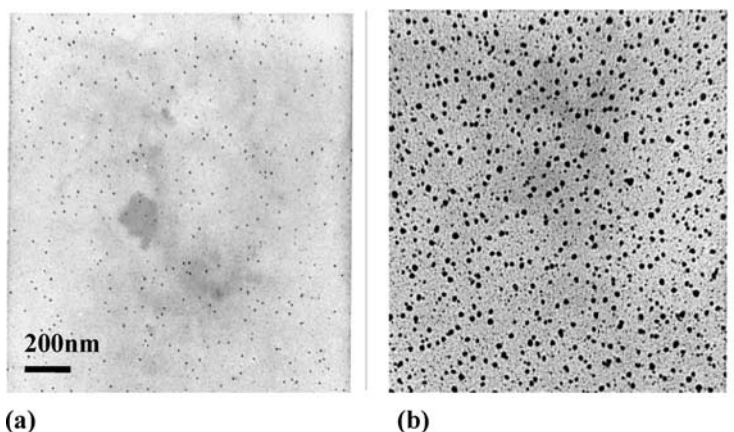
Figure 3. TEM pictures of a Ag/PEO-like coating containing 1% (a) and 5% (b) of silver (XPS determined)

Ag/PEO-like coatings show a good stability in water: no evidence of the underlying substrate after water soaking was observed by XPS attesting for no dissolution of the PEO-like matrix; the density of silver in the coating, instead, decreases with the increase of the soaking time, due to the leach of Ag^+ ions in wet conditions, as shown in Fig. 4, where ICP-AAS (Inductively Coupled Plasma Atomic Absorption Spectroscopy) data are reported. The trend suggests that a reservoir-type release mechanism occurs [60], similar to that of other drug delivery systems, where the therapeutic agent is uniformly dispersed/dissolved in an inert (i.e., non-degrading) polymer matrix, and its release appear to be controlled by the diffusion from the matrix. For the case shown in Fig. 4 the rate
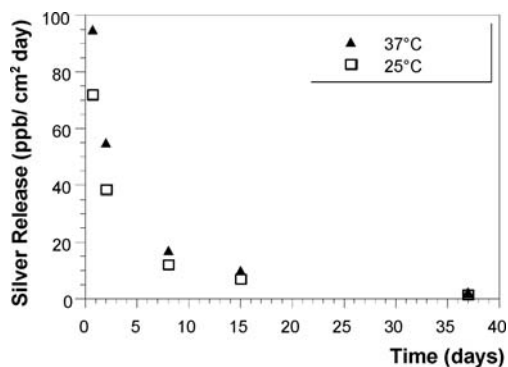
Figure 4. Rate of Ag^+ release in water (ICP-AAS data), of plasma deposited Ag/PEO-like coatings containing 8% of silver (XPS). Values acquired at 25°C and 37°C are reported

of Ag$^+$ release was found higher at 37°C within the first 15 days; after it appeared not influenced by the temperature. Similar trends were found for different (Ag content, PEO character) Ag/PEO-like coatings. In general, the leach rate in water increases with the temperature and with the Ag content of the coating (not shown).

Ag/PEOlike coatings were found very effective in reducing the proliferation of bacteria at surfaces, at any loading of silver, for example against different kind of bacteria, including *Psaeudomonas aeuruginosa* [61], a very dangerous opportunistic pathogen of humans that causes infections of the urinary tract, of the respiratory system, and of the gastrointestinal system.

Plasma deposited nano-composite Ag/PEO-like coatings could be utilized, in principle, in several biomedical devices and wares to be temporary used *in vivo*, such as wound dressings and bandages and catheters, but their use could be also tested for permanent *in vivo* applications such as implants and prosthesis, to test whether they can be effective in inhibiting post-surgery bacterial infections.

5. Plasma-Aided Synthesis of Nano-Structured Surfaces

As shown in the previous sections, it was demonstrated that substrate topography could play a major role in promoting certain cell behaviours. Patterning and immobilization strategies techniques are utilized, for example, to mimic onto artificial surfaces cellular and extra-cellular organization that exists in nature [62]. Artificial materials with surface micro- and nano-features can imitate some of the mechanical and chemical constraints of natural 3D architectures, and activate specific biological recognition pathways that could determine the success of a biomaterial [63,64]. Soft lithography [43,65,66] and other approaches have been developed in the 1990s for this purpose. Micro-lithography can be used to obtain patterns where the contemporary presence of chemical and topographical cues produces predetermined effects on cell adhesion.

A combination of different PE-CVD processes through proper "physical masks" can be successfully utilized to produce micro-metric domains of different biologically relevant properties (i.e., hydrophilic/hydrophobic, acid/base, polar/apolar, smooth/rough, etc.) at surfaces, such as cell-adhesive tracks surrounded by cell-repulsive domains; cells can be aligned in the micro-metric tracks where a cell-adhesive coating was deposited, confined in the tracks by non fouling domains. In our laboratory cell-adhesive pdAA coatings were deposited on PS substrates followed by the plasma deposition of PEO-like non fouling coatings (PEO character >70%) through TEM copper grids with different patterns [38]. Human hTERT fibroblasts seeded on such patterned substrates aligned along the cell-adhesive pdAA tracks [37].

The combination of chemical and topographical constraints at the micron scale level clearly influences cell morphology: cells were found stretched and aligned along pdAA tracks with width comparable with the size of the cells (tens of micron), while they adhered in a random way, on the same pdAA surface, when the dimension of the domain was much larger. Cells could not adhere on the non

fouling domains; time-lapse movies show a few cells "slipping" on the PEO-like domains while "moving" from one pdAA domain to another, and keeping unaltered their round shape. Moreover, cells were observed to migrate along the pdAA tracks, an important hint of cell viability, fundamental for potential applications in tissue engineering and applications were cell sorting is needed like in case of analytical devices.

Investigations completed on cells cultured on micro- and nano-textured surfaces of different materials have clearly shown that cells react to material topography very likely because of stretch reactions to any form of unevenness at the surface of the substrate such as bumps, roughness, relieves, pores, holes and other structures, either random or regularly arranged. Beside producing regular micro-arrays of different domains when combined with physical masks, plasma processes can also be combined with Colloidal Lithography (CL), a well-known surface patterning technique [39], to texture surfaces with regularly spaced nano-relieves [67].

In CL procedures a monolayer of metal or polymer spheres of proper nano-metric dimensions is assembled in a hexagonally packed 2D lattice monolayer, and is utilized as nano-metric physical mask to develop a regular pattern of relieves (bumps, cones, pillars, etc.) at the surface of interest [68]. In spite of the fact that this technique is still far to guarantee coverage of large areas, nevertheless it allows to prepare well defined surfaces for investigating the fundamental principles that drive cell-surface interactions, and for biosensor applications [69,70].

PE-CVD, plasma treatment and dry etching processes can be applied in different moments of CL surface-modification protocols [71,72]; both PE-CVD and plasma etching processes can be used, for example, to transfer the pattern of the assembled CL layer to the substrate. When nano-structured surfaces are obtained, a further surface chemical modification could be performed, e.g., the deposition of a highly conformal PE-CVD coating characterized by proper functional groups and properties, in order to obtain different samples with the same topographic features and different chemical composition, or *viceversa*, to disentangle the effect of surface chemistry from that of topography in protein adsorption and cell adhesion studies [39].

Certain PE-CVD processes can provide surfaces directly with coatings characterized by random relieves, with no need of physical mask or of any other means. Fluorocarbon coatings plasma-deposited in continuous (CW) discharges are known for their smoothness, hydrophobic character, variable F/C ratio, cross-linking, and high chemical inertness [73 and ref. there in]; modulated (MW, i.e., the discharge is pulsed on/off at defined time intervals) PE-CVD processes, instead, can deposit fluorocarbon coatings characterized by surface nano-/micro-metric relieves, variable roughness, high F/C ratio and low cross-linking, that confer them low dielectric (low k) constant, extremely high hydro- and oleo-phobic (stain resistance) character, and low friction coefficient [73 and ref. there in]. The deposition mechanism of such nano-structured coatings has been recently described by Milella et al. [74–76].

"Teflon-like" nano-structured coatings deposited from RF glow discharges fed with different fluorocarbon gases have been produced in our laboratory, with roughness depending on plasma parameters (e.g., duty cycle, monomer flow rate and deposition time) [73]. Such highly fluorinated coatings are characterized by crystalline poly-tetrafluoroethylene (PTFE) ribbon-shaped nanostructures randomly distributed within an amorphous less fluorinated fluorocarbon background. Nano-structured fluorocarbon coatings have been obtained also in the afterglow (AG, downstream respect to the glow) of RF glow discharges fed with hexafluoro-propylene oxide (HFPO). The coatings were characterized by a F/C ratio very close to 2, by a teflon-like (mainly CF_2 component) C1s signal, and by nano-structures shaped like petals. Roughness and hydrophobic character of such coatings were found to increase with the distance from the glow, up to more than 500 nm (R_{RMS}) and 165° (WCA), respectively; smooth coatings with F/C ratio of 1.5–1.6 were found, instead, in the glow zone of the corresponding discharge, characterized by WCA values of about 110°.

In Fig. 5 two SEM (Scanning Electron Microscopy) pictures are shown of two micro-structured coatings plasma-deposited from TFE (MW, ribbon-like structures) and HFPO (AG, petal structure), respectively.
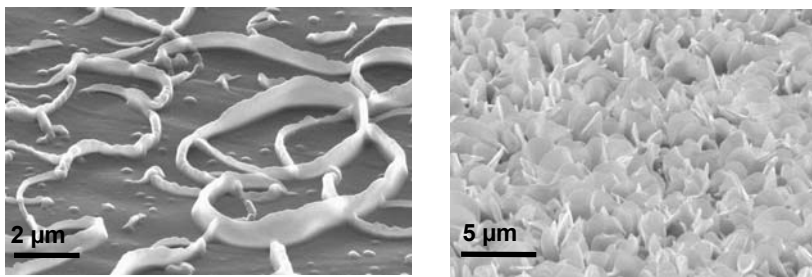
Figure 5. SEM pictures of two nanostructured fluorocarbon coatings plasma-deposited from TFE (MW, ribbon-like structures) and HFPO (AG, petal structure) monomers, respectively

The effect of roughness on adhesion and growth of many cell lines (MG63, 3T3 fibroblasts [77], Saos-2 [78] has been investigated on plasma-deposited fluorocarbon nano-structured coatings characterized by different roughness and identical surface composition. To eliminate the slight difference in chemical composition between substrates of different roughness, which is due to the different composition of the nanostructures (CF_2) with respect to the amorphous back-ground (CFx, x < 2), all substrates were conformally coated with same CW coating deposited from TFE in defined CW conditions. In this way cell-growth experiments could be done on substrates characterized by variable roughness and identical F/C chemical composition, as confirmed by SEM, AFM, XPS and WCA measurements. This research, that still is going on, and will include also cell-growth

experiments on other plasma-deposited surfaces beside fluorocarbon, reveals clearly that cells feel the differences of surface roughness, chemical composition, density, height and shape of the nano-structures.

Figure 6 clearly show how 3T3 fibroblast cells grow faster on fluorocarbon surfaces characterized by the highest roughness within the particular set of flat, rough (RRMS~ 40 ± 5 nm) and very rough (RRMS~ 233 ± 21 nm) fluorocarbon nano-structured plasma-deposited surfaces chosen. For this particular experiment coatings deposired from modulated C_2F_4 glow disharges were utilized [81]. Other effects related to the nature of the nano-structured surfaces were observed on adhering cells as a function of roughness, depending on the cells utilized. It was found that the presence of fluorinated nano-structures influence the spreading of the cells, protrusion of filopodia and/or lamellae, as well as the density of focal sites and stress fibers on the membrane of the cells [80,81].
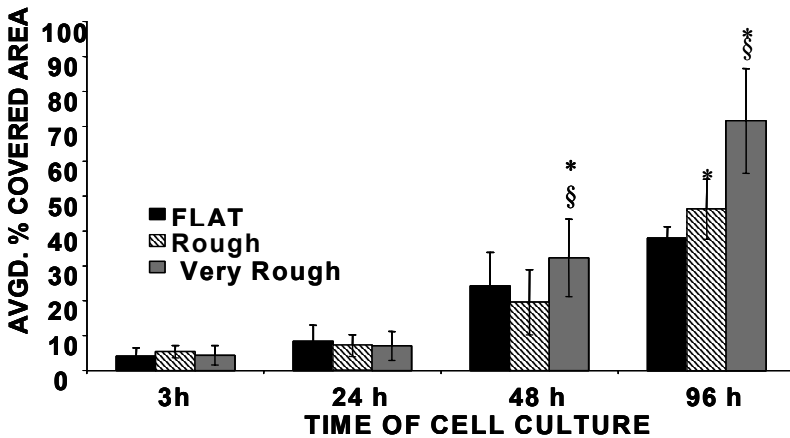
Figure 6. Average percentages of sample areas covered by 3T3 fibroblast cellsgrown on FLAT, Rough (RRMS~ 40 ± 5 nm) and Very Rough (RRMS~ 233 ± 21 nm) fluorocarbon nano-structured surfaces plasma-deposited from modulated C_2F_4 glow discharges [79]. The unpaired Student's T-test was used to evaluate statistical significant differences among samples. *p < 0.01 vs. FLAT; § p < 0.01 vs. Rough

6. Biological Tests of Plasma-Processed Surfaces

Biomaterials must be tested in many different ways to determine whether they are compatible with biological entities and can function appropriately *in vivo*. Testing biomaterials, particularly in living systems, is very complicated due to the high number of variables to consider *in vivo*, and to the high number of experiments that have to be performed to achieve statistically valid indications, with animals first, then with humans. *In vitro* tests, at least at the beginning of the investigation, can provide rapid and inexpensive data on cytotoxicity, cell compatibility and

other biological interactions, but their results cannot be used to built a complete model of the physiological functions, since it is not possible to completely reproduce the entire range of cellular responses occurring *in vivo*; cell–cell and cell–matrix interactions occurring *in vitro* are much less complicated than in living systems.

As a rationale, new materials and surfaces to be possibly used in the biomedical field have to be previously tested *in vitro* to establish whether they go further toward *in vivo* evaluation with animals and humans. *In vitro* tests, also, are extremely useful to "look" how cells respond to chemical composition and morphology of surfaces, in order to plan carefully production processes of biomedical devices, membranes and sensors.

In vitro cell culture studies allow one to fully control the culture environment, to limit the interactive nature of the biological medium, to isolate and quantify molecules relevant to biological responses, to achieve rapid and reproducible results and, last but not least, to limit the sacrifice of animals. Cell culture experiments, extensively used since more than two decades, are the more obvious and reproducible methods to evaluate *in vitro* the compatibility of materials, as it and surface-modified [82].

The best approach for planning *in vitro* tests on biomaterials depends strongly on the particular case, and generally it relies on cell culture experiments with primary or with immortalized cells. Primary cells are originated directly from a living tissue, after isolation of the tissue itself, mechanical or enzymatic disgregation, and seeding of the resulting cells in proper culture vessels. All different cell types part of the particular living tissue enter, thus, in a primary cell culture. Primary cells are highly functional, but their reproductive capacity is low; they grow *in vitro* until all the substrate surface available is occupied by cells, i.e., till the culture becomes confluent. At this stage it becomes necessary to subculture cells into new vessels.

Primary cells usually retain their specific functions, and are a very useful tool to investigate a specific cell type in a controlled environment. After a certain number of growth passages, though, depending on the particular cell type, primary cells do not proliferate anymore [83]; further, since they derive directly from a living biological host, their behaviour can change strongly from donor to donor. Although primary cultures offer, in principle, the best tool for a complete simulation of *in vivo* systems, as seen above, limitations to their use exist; furthermore, most of the primary cells type are not commercially available and are quite expensive.

In order to avoid these drawbacks, "immortalized" cell lines could be used. Such highly proliferative cells can be derived from tumors, or from primary cells immortalized in some chemical or biological way [84]. The phenotype of immortalized cells is often different from that presented from the same cell *in vivo*. In spite of this, the uniformity of cell population (due to their clonal origin), the high proliferation rate and the possibility of long term storage allow to use immortal cell lines in a wider range of cases, and to perform highly reproducible experiments.

At present, a variety of different tests are validated to evaluate the biological compatibility of materials with cells; they can assess morphology, membrane integrity, proliferation, and specific cell functions.

An important concept in evaluating the biocompatibility of materials is "cytotoxicity", defined as the ability of a material in inhibiting the viability of the cells, i.e., the health of the cells in terms of survival and normal metabolism. Evaluating the cytotoxicity of a material should include counting dead and alive cells as a function of the time of contact with the surface of the material under scrutiny, as well as monitoring their physiological status and their morphological changes. Many different cheap, reproducible, and easy quantitative assays exist to test the cytotoxicity of surfaces; the choice depends mainly on the particular kind of cells, and on the particular drug/material under study.

Viability tests measure quickly the proportion of viable cells among all those adhering at a substrate [85]; most viability tests are performed under the microscope, by using a dye/stain molecule to which cells are normally impermeable (e.g., trypan blue or naphthalene black), or dye/stain molecules (e.g., diacetyl fluorescein or neutral red) taken up only by living cells [86].

Alternatively, metabolic assays can be used to probe the survival of the cell population, defined as the retention of the metabolic or/and proliferative abilities of the cells. The MTT test is probably the most common metabolic assay; in this test the yellow water-soluble 3-(4,5-dimethylthiazol-2-yl)-2,5-diphenyl tetrazolium bromide (MTT) molecule, given to the cells through their culture medium, is reduced by dehydrogenase enzymes present in the active mitochondria of living cells into a dark blue compound, formazan, that can be spectrophotometrically quantified at 570 nm [87]. The resulting optical density can be correlated with the viability of the cells.

In order to visualize precisely the contour, the shape and the external details of cells (i.e., lamellae, fillopodia, etc.) adhering at materials after different growth time intervals, cells must be first fixed at the surface of the substrates before being observed. Paraformaldehyde or gluteraldehyde are used to preserve the external morphology presented by the cells at the moment of the fixation; methanol, instead, is used to permeabilize the membrane of the cell to fluorescent dies and/or to antibodies that bind specifically to molecules of the internal cell structures and allow their recognition [88]. Fixed cells can be stained (e.g., with Coomassie Blue), then observed with an optical microscope and described/classified in term of cell shape, contour, protrusions. For most cells observed at the surface of substrates, for example, a spheroidal shape is considered sign of no cell-substrate interactions, while complicated contours (e.g., spindle- and star-like) generally indicate strong cell-substrate interactions and stressed cytoskeleton structure. A very good knowledge of the behaviour of cells in biological systems is required to properly evaluate such morphological data, since it is well known that cells don't behave all in the same way.

Digital images can be acquired at different magnifications and then used to evaluate the distribution of the many possible single cell morphologies with some software for image analysis (e.g., Image J, downloadable from rsb.info.nih.gov/ij/,

the website of the National Institute of Health, US). This approach, for example, has been used by our group for analyzing neuronal differentiation by studying the related sprouting of neurites from cells grown on functionalized PET. In this case the substrates were coated with PE-CVD RF glow discharges of acrylic acid and allylamine vapours [89].

Immunofluorescence microscopy can allow detailed observation of the cytoskeleton of the cells, and can provide thorough clues on the adaptation of cells to different surfaces. The distribution of actin and tubulin, two main cytoskeletal proteins, is usually investigated; other cytoskeleton proteins can be labeled and observed to achieve more specific hints on the formation of specific cell-substrate complexes. Vinculin, for example, can highlight in detail the density of the focal contacts at the membrane of the cells, i.e., of those nano-metric structures of the cellular membrane specialized in the cell-substrate attachment [90]. This kind of observation becomes particularly interesting when cells are in contact with topo-graphically structured surfaces, and can help also in understanding the reaction of the cytoskeleton to the stress induced by the interactions with the substrates.

The study of actin conformation can clearly show how the cytoskeleton of certain cells react to smooth surfaces characterized by a slightly different chemical composition. The cytoplasmatic distributions of actin proteins of HepG2 (hepatoma cell lines) seeded on untreated PS and on two PS surfaces plasma-treated in two different NH_3 RF glow discharges are shown in Fig. 7. Such surfaces are grafted with different densities of N-containing chemical groups (different N/C surface ratio, different distribution of grafted groups). HepG2 cells seeded on untreated PS (Fig. 7a), where no polar groups are grafted and a relevant hydrophobic character (WCA ~ 90°) is present, show a round shape and a clear tendency to cell-cell aggregation rather than cell-surface interactions, as attested also by the accumulation of actin at the cell-cell interfaces. Such cells clearly "don't like" the untreated PS surface where they are seeded. Cells seeded on NH_3-plasma treated PS (Fig. 7b and c) surfaces, instead, where polar N-groups are grafted and the hydrophilic character is increased (WCA 40–50°), clearly show a stronger inclination to interact with the surface rather than with other cells. In Fig. 7b (PSA, N/C XPS ratio 0.28 ± 0.01; C-N/C-OR XPS C1s component 9%) cells assume a spread morphology, retain their individuality, and exhibit actin quite evenly distributed in small spots all over the cytoskeleton. In Fig. 7c (PSF, N/C XPS ratio 0.23 ± 0.02; C-N/C-OR XPS C1s component 23%) the spreading and the individuality of the cells is also evident, but actin appears distributed much less evenly, instead, concentrated in localized stress fibers. The formation of stress fibers in cells seeded on the PSF sample is probably due to the fact that these cells adhere much more tightly to the PSF surface, where the density of N-groups is slightly lower respect to the PSA surface, and the distribution of the grafted groups is different, as attested by the difference in the XPS C1s components.

Many other tests can be performed to probe the behaviour of cells at artificial surfaces; in particular, tests able to investigate the physiological behaviour of the cells can provide relevant biological data. Such tests are highly cell-dependent

(e.g., the production of urea and albumin for liver cells; that of alkaline phosphatase for osteoblast cells, etc.), and allow to check how the functions of the cell are altered by the surface under scrutinity.
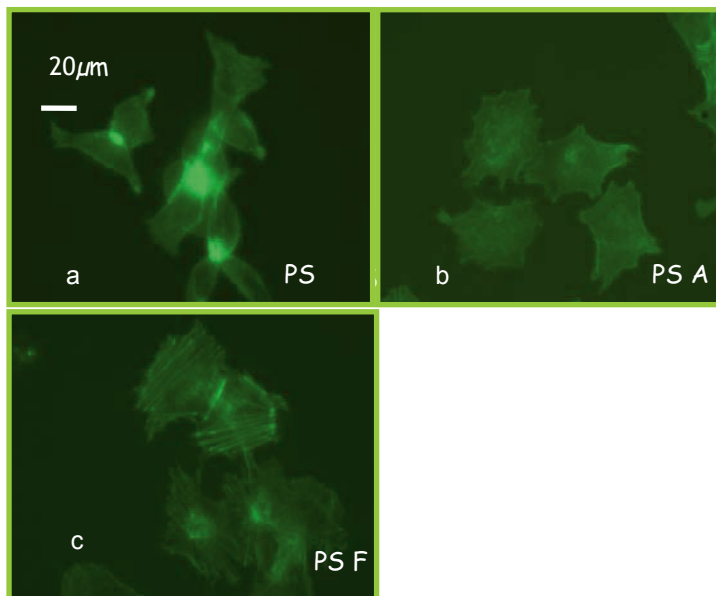
Figure 7. Fluorescence microscopy pictures of HepG2 cell seeded on: (a) untreated PS; (b) PSA: NH3 plasma-grafted PS (N/C = 0.28 ± 0.01, XPS data) (c) PSF: NH3 plasma-grafted PS (N/C = 0.23 ± 0.02, XPS data). The distribution of F-actin was revealed with Alexa Fluor® 488 phalloidin (Molecular Probes)

At the end of this section it must also be stressed that *in vitro* tests are necessary, but often not sufficient, to establish whether a certain surface can be used in biomedical devices to go toward *in vivo* use. It is in fact necessary *in vivo* evaluation test in animals and humans; in order to achieve a complete under-standing of how a modified surface can interact with the human organism.

Conclusions

Different non equilibrium plasma-processed surfaces of interest in Life Science have been described, as well as biological tests to be performed *in vitro* on sur-faces of biomedical interest for their characterization.

To conclude this contribution, it has to be reported that plasma processes have produced so much research and potential applications so far, but still they are considered as promising techniques in Life Science, still to be fully developed rather than well established. Certainly, though, they attract interest and efforts from researchers, as well as attention and investments from companies and

funding bodies. Moreover, commercial biomedical products that make use or are fabricated with cold plasma processes are already present on the market, such as tissue-culture polystyrene Petri dishes, plasma-sterilizers, long wear (up to 30 days) contact lenses, pacemakers with plasma-coated wires, and wound-healing bandages with cell adhesive/releasing plasma-deposited coatings.

A boom of commercial plasma processed biomaterials and devices is thus expected in the next future, and a deeper and wider penetration of Plasma Technologies in Life Science.

Acknowledgments

References

[1]   S. L. Miller, Science, 117(3046), 528–529, 1953
[2]   S. L. Miller, J. Am. Chem. Soc. 2351, 77–79, 1955
[3]   J. R. Hollahan, B. B. Stafford, R. D. Falb, S. T. Payne, J. Appl. Polym. Sci. 13, 807, 1969
[4]   M. R Wertheimer, R. d'Agostino, P. Favia, C. Oehr, Plasma Process. Polym. 2, 7–15, 2005
[5]   U. Kogelschatz, Plasma Process Polym. 4, 678–681, 2007
[6]   P. Clark, P. Connolly, A. S. G. Curtis, J. A. T. Dow, C. D. W. Wilkinson, Development 108, 635–644, 1990
[7]   X. Shuyan, L. Jidong; L. Sim, H. D. Cheong, K. Ostrikov, Plasma Process. Polym. 2(5), 373–390, 2005
[8]   B. D. Ratner, A. S. Hoffman, F. Schoen, J. Lemons (eds). Biomaterials Science: An Introduction to Materials in Medicine, 2nd edn, San Francisco, Elsevier, 2004
[9]   Special issue devoted to "Plasma Processes for Biomedical Applications", P. Favia (ed), Plasma Process. Polym. 3(6/7), 2006
[10] S. Ben Rejeb, M. Tatoulian, F. A. Khonsari, F. A. Durand, A. Martel, J. F. Lawrence et al., Anal. Chim. Acta. 376, 133, 1998
[11] D. A. Puleo, R. A. Kissling, M. S. Sheu, Biomaterials, 23, 2079–2087, 2002
[12] C. Baquey, F. Palumbo, M. C. Portedurrieu, G. Legeay, A. Tressaud, R. d'Agostino, Nucl. Instr. Meth. Phys. Res. Sec. B–Beam Interact. Mater. Atoms, 151, 255, 1999

[13] R. Daw, T. O'Leary, J. Kelly, R. D. Short, M. Cambray-Deakin, A. J. Devlin, I. M. Brook, A. Scutt, S. Kothari, Plasmas Polym. 4, 113, 1999

[14] G. H. Hsiue, S. D. Lee, C. C. Wang, M. H. I. Shiue, P. C. T. Chang, Biomaterials, 14(8), 591, 1993

[15] R. Sipheia, G. Martucci, M. Barbarosie, C. Wu, Biomater. Artif. Cell. Im. 21(4), 455, 1993

[16] K. S. Siow, L. Brichter, S. Kumar, H. J. Griesser, Plasma Process. Polym. 3, 392, 2006

[17] R. Daw, S. Candan, A. J. Beck, et al., Biomaterials, 19, 1717, 1998

[18] L. Detomaso, R. Gristina, G. S. Senesi, R. d'Agostino, P. Favia, Biomaterials, 26, 3831, 2005

[19] R. Daw, I. M. Brook, A. J. Devlin, R. D. Short, E. Cooper, G. J. Leggett, J. Mater. Chem. 8, 258, 1998

[20] R. Daw, T. O'Leary, J. Kelly, R. D. Short, M. Cambray-Deakin, A. J. Devlin, I. M. Brook, A. Scutt, S. Kothari, Plasmas Polym. 4, 113, 1999

[21] H. J. Griesser, R. C. Chatelier, T. R. Gengenbach, G. Johnson, J. G. Steele, J. Biomater. Sci. Polym. Ed. 5, 531, 1994

[22] S. I. Ertel, B. D. Ratner, T. A. Horbett, J. Biomed. Mater. Res. 24, 1637, 1990

[23] J. D. Andrade, S. Nagaoka, S. Cooper, T. Okano, S. W. Kim, Trans ASAIO 33, 75, 1987

[24] W. R. Gombotz, W. Guanghui, T. A. Horbett, A. S. Hoffman, J. Biomed. Mater. Res. 25, 1547, 1991

[25] P. Favia, F. Palumbo, R. d'Agostino, S. Lamponi, A. Magnani, R. Barbucci, Plasmas Polym. 3, 77, 1998

[26] M. D. Pierschbacher, E. Ruoslahti, Nature, 309, 30, 1984

[27] L. C. Lopez, R. Gristina, G. Ceccone, F. Rossi, P. Favia, R. d'Agostino, Surf. Coat. Technol. 200(1–4), 1000, 2005

[28] L. De Bartolo, S. Morelli, L. C. Lopez, L. Giorno, C. Campana, S. Salerno, M. Rende, P. Favia, L. Detomaso, R. Gristina, R. d'Agostino, E. Drioli, Biomaterials, 26, 4432, 2005

[29] L. De Bartolo, S. Morelli, M. Rende, S. Salerno, L. Giorno, L. C. Lopez, P. Favia, E. Drioli, J. Nanosci. Nanotechnol. 6, 2344, 2006

[30] L. C. Lopez, R. Gristina, L. De Bartolo, S. Morelli, P. Favia, R. d'Agostino, JABB, 2, 211, 2004

[31] K. L. Prime, G. M. Whitesides, J. Am. Chem. Soc. 115, 10714, 1993.

[32] E. E. Johnston, B. D. Ratner, J. D. Bryers, in: Plasma-Processing of Polymers, R. d'Agostino, P. Favia, F. Fracassi (eds); Kluwer Acad. Publ., NATO ASI Series, E: Appl. Sci., 346, 1997

[33] G. P. Lopez, B. D. Ratner, C. D. Tidwell, C. L. Haycox, R. J. Rapoza, T. A. Horbett, J. Biomed. Mat. Res. 26, 415, 1992

[34] F. Palumbo, P. Favia, M. Vulpio, R. d'Agostino, Plasmas Polym. 6, 163, 2001

[35] Y. J. Wu, A. J. Griggs, J. Jen, S. Manolache, F. Denes, R. B. Timmons, Plasmas Polym. 6(123), 2001

[36] Y. J. Wu, R. B. Timmons, J. S. Jen, F. E. Molock, Coll. and Surf. B: Bioint. 18, 235, 2000

[37] E. Sardella, R. Gristina, G. Ceccone, D. Gilliland, A. Papadopoulo Bouraoui, F. Rossi, G. S. Senesi, L. Detomaso, P. Favia, R. d'Agostino, Surf. Coat. Technol. 200, 51, 2005

[38] E. Sardella, R. Gristina, G. S. Senesi, R. d'Agostino, P. Favia, Plasma Process. Polym. 1(1), 63, 2004

[39] E. Sardella, P. Favia, R. Gristina, M. Nardulli, R. d'Agostino, Plasma Process Polym. 3, 456–469, 2006

[40] F. Bretagnol, A. Valsesia, G. Ceccone, P. Colpo, D. Gilliland, L. Cerotti, M. Hasiwa,
      F. Rossi, Plasma Process Polym. 3, 443, 2006
[41] J. Clemmens, H. Hess, J. Howard, V. Vogel, Langmuir, 19, 1738, 2003
[42] J. Clemmens, H. Hess, R. Lipscomb, Y. Hanein, K. F. Böringer, C. M. Matzke,
      G. D. Bachand, B. C. Bunker, V. Vogel, Langmuir, 19(26), 10967, 2003
[43] Y. Xia, G. Whitesides, Soft Lithography, Angew. Chem. Int. Ed. 37, 550, 1998
[44] G. Geissler, Y. Xia, Adv. Mater. 16, 1249, 2004
[45] Y. Vickie Pan, T. C. McDevitt, T. K. Kim, D. Leach-Scampavia, P. S. Stayton,
      D. D. Denton, B. D. Ratner, Plasma Polym. 72, 171, 2002
[46] M. Shen, L. Martinson, M. S. Wagner, D. G. Castner, B. D. Ratner, T. A. Horbett,
      J. Biomater. Sci. Polym. 13/4, 359–499, 2002
[47] L. G. Harris, R. G. Richards, Int. J. Care Injured, 2006(37), S3–S14
[48] A. Gristina, Science, 237(4822), 1987
[49] R. E. Baier, A. E. Meyer, J. R. Natiella, R. R. Natiella, J. M. Carter, J. Biomed.
      Mater. Res. 18(4), 327, 1984
[50] D. G. Allison, P. Gilbert, J. Ind. Microbiol. 15, 311, 1995
[51] J. L. Clement, P. S. Jarrett, Metal-Based Drugs, 1, 467–482, 1994
[52] G. Cook, J. W. Costerton, et al., Int. J. Antimicrobial Agents, 13, 169–173, 2000
[53] S. Silver, FEMS Microbiol. Rev. 27(2–3), 341–353, 2003
[54] S. Barrett, Retrieved November 28, 2006, from http://www.quackwatch.org/
      01QuackeryRelatedTopics/PhonyAds/silverad.html. 2005
[55] E. Kay, Z. Phys. D, 3, 252,1986
[56] H. Biederman, L. Martinu, Plasma Deposition, Treatment and Etching of Polymers,
      R. d'Agostino (ed), Academic Press, New York, 1990
[57] P. Favia, M. Creatore, F. Palumbo, V. Colaprico, R. d'Agostino, Surf. Coat. Technol.
      142, 1–6, 2001
[58] P. Favia, R. d'Agostino, Vide, 57, 40, 2002
[59] P. Favia, R. Pinto Mota, M. Vulpio, R. Marino, R. D'Agostino, M. Catalano, Plasmas
      Polym. 5, 1, 2000
[60] J. Heller, A. S. Hoffman, Biomater. Sci. 7, 628, 2004
[61] D. J. Balazs, K. Triandafillu, E. Sardella, G. Iacoviello, P. Favia, R. d'Agostino,
      H. Harms, H. J. Mathieun, Plasma Process. Polym. 2, 351, 2005
[62] G. A. Abrams, S. L. Goodman, P. F. Nealey, M. Franco, C. J. Murphy, Cell Tissue
      Res. 299, 39, 2000
[63] J. A. Jansen, A. F. von Recum, Biomater. Sci. 2, 218, 2004
[64] T. A. Desai, Med. Eng. Phys. 22, 595, 2000
[65] Y. Xia, G. M. Whitesides, Angew. Chem. Int. Ed. 37, 550, 1998
[66] R. S. Kane, S. Takayama, E. Ostuni, D. E. Ingber, G. M. Whitesides, Biomaterials,
      2363, 23–24, 2004
[67] P. Hanarp, D. S. Sutherland, J. Gold, B. Kasemo, Coll. Surf., A, 214, 23, 2003
[68] Y. Xia, B. Gates, Y. Yin, Y. Lu, Adv. Mater. 12, 693, 2000
[69] A. Valsesia, M. M. Silvan, G. Ceccone, D. Gilliland, P. Colpo, F. Rossi, Plasma
      Process. Polym. 2, 334, 2005
[70] A. Valsesia, P. Colpo, M. Manso, T. Meziani, G. Ceccone, F. Rossi, Nanoletters, 4,
      1047, 2004
[71] E. Sardella, S. Lovascio, P. Favia, R. d'Agostino, Polymer 4–3, S887–S890, 2007
[72] E. Sardella, R. Gristina, R. d'Agostino, P. Favia, Adv Plasma Technol; 13, 243–268,
      R. d'Agostino, P. Favia, Y. Kawai, H. Ikegami, N. Sato, F. Arefi-Khonsari (eds);
      2007
[73] P. Favia, in: "Plasma Polymers and Related Materials", H. Biederman (ed); Imperial
      College, London, 25, 2004

[74] A. Milella, F. Palumbo, P. Favia, G. Cicala, R. d'Agostino, Plasma Process. Polym. 1, 164, 2004

[75] A. Milella, F. Palumbo, P. Favia, R. d'Agostino, Special issue of Pure Appl. Chem., 77, 2, 2005

[76] A. Milella, F. Palumbo, R. d'Agostino, Fundamental on plasma deposition of Fluorocarbon Coatings in: Advanced Plasma Technology; 9, 175–196 R. d'Agostino, P. Favia, Y. Kawai, H. Ikegami, N. Sato, F. Arefi-Khonsari (eds); 2007

[77] F. Rosso, G. Marino, L. Muscariello, G. Calfiero, P. Favia, E. D'Aloia, R. d'Agostino, A. Barbarisi, J. Cell Physiol. 207(3), 636, 2006

[78] R. Gristina, P. Rossini, F. Intranuovo, E. Sardella, M.Nardulli, P. Favia, R. d'Agostino, Plasma processed Nanostructured surfaces for Biomedical purposes; Proceeding of 21st European conference on Biomaterials (ESB) Brighton, UK, 2007

[79] G. S. Senesi, E. D'Aloia, R. Gristina, P. Favia, R. d'Agostino, Surface Science, 601, 1019, 2007

[80] M. J. Dalby, M. O. Riehle, D. S. Sutherland, H. Agheli, A. S. Curtis, Biomaterials, 25, 77, 2004

[81] M. J. Dalby, S. Childs, M. O. Riehle, H. J. Johnstone, S. Affrossman, A. S Curtis, Biomaterials, 24(6), 927, 2003

[82] M. Nardulli, R. Gristina, R. d'Agostino, P. Favia, in: Advanced Plasma Technology, Riccardo d'Agostino, Pietro Favia, Yoshinobu Kawai Hideo Ikeagami Noriyoshi Sato and Farzaneh Arefi-Khonsari (eds); Wiley Verlag, Berlin, 2008

[83] B. Alberts, A. Johnson, J. Lewis, M. Raff, K. Roberts, P. Walter, Molecular biology of the Cell, 4th edn, Garland Science, New York, 2002

[84] M. Obinata, Cancer Sci. 98(275), 2007

[85] R. I. Freshney, Culture of Animal Cells, A manual of basic technique, 4th edn, Wiley-Liss, New York, Chichester, Weinheim, Brisbane, Singapore, Toronto, 2000

[86] A. Castañoa, M. J. Gómez-Lechónb, Toxicol In Vitro. 19(5), 695, 2005

[87] T. J. Mossman, Immunol. Methods, 65, 55, 1983

[88] L. L. Lanier, N. L Warner, J. Immunol. Meth. 47, 25, 1981

[89] M. Buttiglione F. Vitiello, E. Sardella, L. Petrone, M. Nardulli, P. Favia, R. d'Agostino, R. Gristina, Biomaterials, 28(19), 2932, 2007

[90] M. J. Dalby, Int. J. Nanomed. 2(3), 373, 2007

4. ELECTRIC DISCHARGES FOR PLASMA DECONTAMINATION

NANO-SECOND DIELECTRIC BARRIER DISCHARGE FOR DIRECT MEDICAL APPLICATIONS

H. AYAN[1], G. FRIDMAN[2], A. F. GUTSOL[1], A. A. FRIDMAN[1], AND G. FRIEDMAN[3]

[1]*Department of Mechanical Engineering and Mechanics, College of Engineering, Drexel University, Philadelphia, PA 19104 USA*
[2]*School of Biomedical Engineering, Science, and Health Systems, Drexel University, Philadelphia, PA 19104 USA*
[3]*Department of Electrical and Computer Engineering, College of Engineering, Drexel University, Philadelphia, PA 19104 USA*

Abstract: Dielectric Barrier Discharge (DBD) is being adapted to medical applications, including those requiring sterilization of surfaces of living tissue. This paper is focused on operation of such systems near living tissue and on a novel discharge where tissue acts as one of the electrodes.

Typical DBD is non-uniform on microscopic scale displaying filamentary structure. When surfaces being treated are flat and the discharge gap is uniform, the discharge filaments are distributed relatively uniformly over the surface. Moreover, the filaments are often mobile in this case and surface sterilization is relatively uniform over sufficient exposure times. The situation changes when surface non-uniformities are present. Such surface non-uniformities can be due to inherent skin topology or due to contamination, for example. In the presence of surface non-uniformities, discharge filaments may become pinned. Filament will also tent to accumulate on large non-uniformities near the smallest discharge gap making surface sterilization highly non-uniform.

In this study, the authors discussed a methodology for creating highly uniform DBD on non-uniform surfaces using high voltage pulses with few nanosecond rise and fall times. It is demonstrated that such pulses can be created using standard spark-gap circuits. It is also demonstrated that the uniform DBD discharge is more effective in sterilization than DBD with standard sinusoidal or microsecond pulse excitation. Lastly, the extent of uniformity of the new nanosecond DBD discharge was measured by using fast moving photosensitive films and it was demonstrated that no filaments are present in this discharge.

Keywords: Atmospheric pressure discharges, dielectric barrier discharges, direct treatment, nonthermal plasma, plasma medicine

1. Background and Introduction

Several variations of Dielectric Barrier Discharge (DBD) have been developed for non-damaging living tissue sterilization and many more medical applications [1–3]. Along with that, DBD has been shown by histology as not damaging to the treated tissue. However, preliminary experiments show that a person who touches the DBD can feel the discharge action. Some of these unpleasant sensations are related to the non-uniformity and thermal effects of the plasma. These non-uniformity and thermal effects of the discharge are strongly dependent on the electrical properties of the discharge, i.e. driving voltage, and waveform shape.

DBDs are mostly applied at atmospheric pressure, generally in air and are an uncomplicated way to generate low temperature atmospheric pressure plasma. However, in most cases, breakdown of an atmospheric pressure gas with the presence of at least one dielectric barrier in the gap, results in multi-streamer mode of operation with formation of microdischarges [4] and subsequent filaments, that are visible to naked eye.

In this study we first employed a conventional microsecond-pulsed waveform system with a few µs pulse durations. After that we have developed a double spark gap external circuit and generated a new discharge with short pulses on the order of tens of nanosecond pulse duration. Both plasma systems have been analyzed and compared for thermal effects and temperature of the discharge and uniformity in order to determine the possibilities to control the uniformity and heating effect with driving waveform.

2. Materials and Methods

The DBD was generated by sphere-to-plane discharge configuration of two electrodes. The high voltage electrode (Fig. 1) is borosilicate glass (Pyrex®) test tube (cat. # 60825-902, VWR Scientific, San Francisco, CA) with conductive silver paste (SPI West Chester, PA) filling. Thickness of the glass test tube was approximately 0.75 mm and glass test tubes' radii of curvature were 5 mm. This test tube electrode was in contact near its tip with the grounded plane metal electrode.

An external circuit shown in Fig. 2 has been developed with a double spark gap configuration to obtain short pulses. When the bigger (main) spark gap breaks down, charge initially stored in the main capacitor is transferred to the discharge as the voltage across the plasma electrodes rises rapidly. The smaller (secondary) spark gap starts to charge and eventually short outs the DBD resulting in a rapid decay of the voltage across the DBD electrodes.

Electrical analyses have been done by measuring instantaneous current and voltage across the electrodes. These measurements were performed using a high frequency high voltage probe (#PVM-4, 1000:1, North Star High Voltage,

Marana, AZ) connected in parallel with the discharge and a high frequency current probe on the high voltage electrode wire (#CM-10-L, Ion Physics Corporation, 0.1 V/Amp, 45 MHz bandwidth). The probe signals were acquired and recorded using a high speed oscilloscope (500 MHz bandwidth, 5 Gsample/s, TDS5052B Digital Phosphor Oscilloscope, Tektronix, Inc., Richardson, TX). Recorded data was processed using customized MATLAB code which integrates the instantaneous power ($V*I$) over many cycles to determine an average energy per cycle and average power.
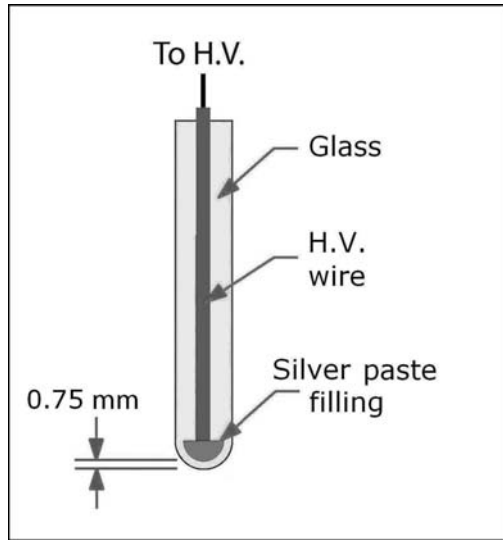
Figure 1. Glass test tube high voltage electrode
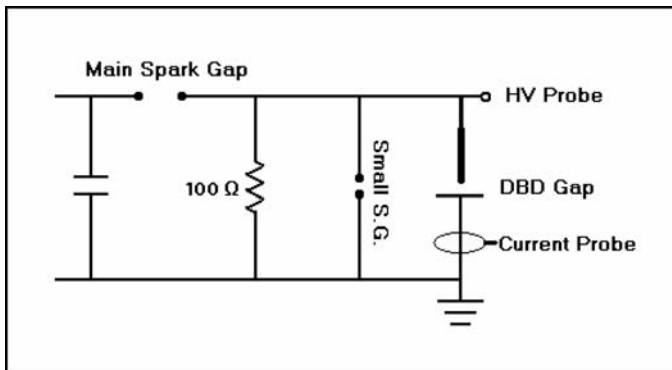
Figure 2. Schematic of double spark gap configuration external circuit

Electrical measurements for average power were verified with custom made calorimeter set-up (Fig. 3). Calorimeter was composed of a peristaltic pump (model # 3386, Control Company, TX), two manual thermometers (model # 112C, −1–51°C, 1/10°C div., Palmer Instruments, Inc., NC), copper tubing welded to plane ground electrode, thermally insulated copper housing for DBD. Water was pumped with controllable flow rate through the copper tube that surrounds chamber. One thermometer was placed before the chamber to measure the inlet temperature of the water. A second thermometer was located after the chamber to measure the outlet temperature of the water. Electrodes were placed in the copper chamber that was embedded in the heat insulation casing to prevent heat loss to ambient. As plasma ignited, dissipated energy in the chamber was taken away by copper chamber and copper tube surrounding the chamber and transferred to the running water. Steady heat transfer from discharge to the water through copper plate and tubing was measured at the inlet and outlet water ports. Temperature differences between inlet and outlet were recorded periodically and this data was fitted to two-term-exponential-formation curve with 95% confidence for time goes to infinity. Average power dissipation in the discharge gap could be calculated by using flow rate and temperature increase of the water. Typical water flow rate was from a few to 100 mL/min and measurement durations were up to for 200 min.
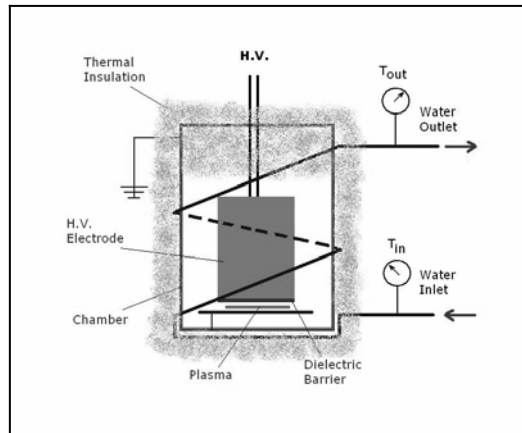
Figure 3. Schematic calorimeter set-up

Optical emission spectroscopy was employed to measure the vibrational T_{vib} and rotational T_{rot} temperatures of the nanosecond pulsed uniform DBD at 375.4 nm and 380.4 nm lines of the Second Positive System of N_2. A fiber optic bundle (Princeton Instruments-Acton, 10 fibers – 200 μm core) was utilized to acquire the optical emission from the discharge and to transmit it to the spectrometer (Princeton Instruments – Acton Research, TriVista TR555 spectrometer system with PIMAX digital ICCD camera, Trenton, NJ). The spectrum of the background noise obtained for the same exposure time was subtracted from the discharge emission spectrum prior to the temperature estimation. A low pressure mercury

lamp was used to determine the slit function of the spectrometer. The room temperature was 22°C throughout the spectroscopic measurements. Experimental spectrum was compared to simulated spectrum with T_{vib} and T_{rot} determined by the best fit (minimum RMSE) between the modeled and experimental spectrum described in detail elsewhere [5,6].

Uniformity of the new discharge was measured qualitatively by exposing a commercial photofilm to the plasma [4] (Fig. 4). The photofilm was placed between the insulated test tube electrode and the grounded metal electrode. A roll-to-roll set-up driven by an electric motor was employed to advance the photofilm at the rate of about 1 m/s, while pulses of DBD plasma where produced. Color and black & white (b&w) photofilms were used to acquire Lichtenberg figures.
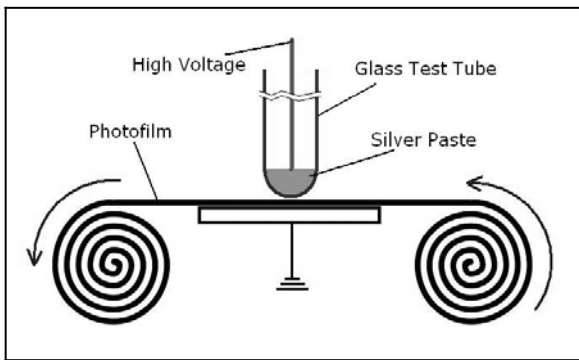
Figure 4. Schematic of experimental setup to acquire the Lichtenberg figures on photofilm

3.   Results and Discussion

In the external circuit, the size of the main spark gap determines the voltage that appears across the discharge electrodes after the spark breakdown. The frequency of voltage pulses is determined by the magnitude of the current used to charge the main capacitor. Secondary spark gap affects mainly the length of the voltage pulse that is maintained across the DBD electrodes. For the current source used here to charge the main capacitor, changing the main spark gap from 15 to 24 mm with 3 mm intervals, resulted in repetition rates between 250 and 100 Hz, respectively, for secondary spark gap between 2.5 to 4.5 mm. Pulse duration is linearly dependent on secondary spark gap length. For 2.5 and 4.5 mm gap distances pulse durations are approximately 15 and 30 ns, respectively. Peak voltage across the DBD is linearly dependant on main spark gap distance with approximately 1 kV per 1 mm for the above mentioned range. As gap increases from 15 to 27 mm, peak voltage increases from 15 to 27 kV. The rise time of approximately 3 kV/ns is obtained on the front end of the voltage pulse.

The details of the conventional (microsecond-pulsed) DBD can be summarized as follows. It is obtained using a peak of approximately 10 kV which rises maximally at the rate of 10 kV/μs. Voltage in this conventional DBD is

maintained for about 2–5 µs. Thus, both voltage rise and pulse duration are at least two orders of magnitude longer for the conventional DBD compared to the nanosecond DBD. Microsecond pulsed DBD was operated at 100 Hz repetition rate, its lowest repetition rate, in order to be able to capture consecutive pulses. The Lichtenberg figures for the conventional microsecond DBD are shown in Fig. 8c and d. Both plasma systems were operated with the same electrode. Typical waveforms of two discharges are given below in Fig. 5.
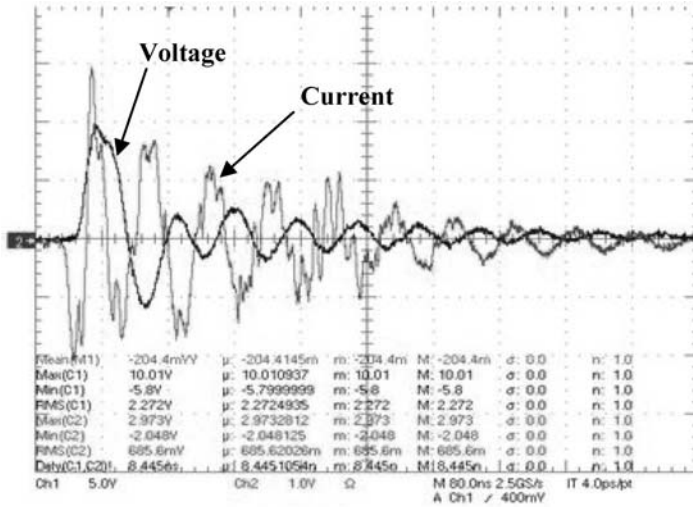
(a)
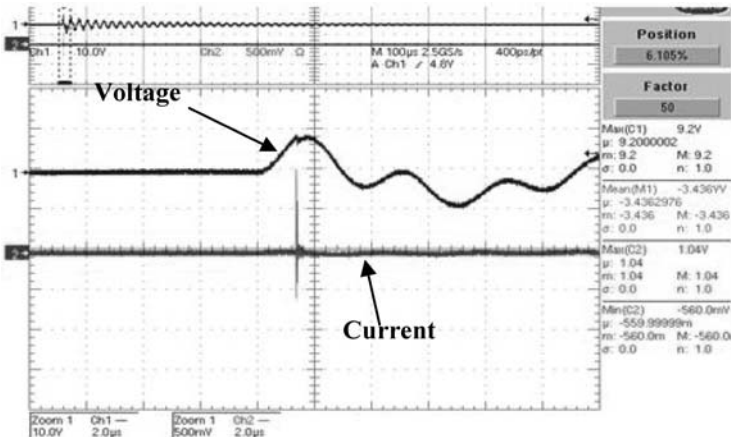
(b)

Figure 5. Typical waveforms of two discharges (a) Nanosecond-pulsed (b) Microsecond-pulsed

The discharge at the glass test tube electrode is shown in Fig. 6. The discharge typically appears dim. Nevertheless, it can be seen in Fig. 6a and b that plasma is spread all over the spherical tip of the electrode. Figure 6a was taken in light room and Fig. 6b was taken in completely dark room. Both images were taken at the same conditions, i.e. repetition rate was approximately 190 Hz and exposure time of the photography was 0.62 s.
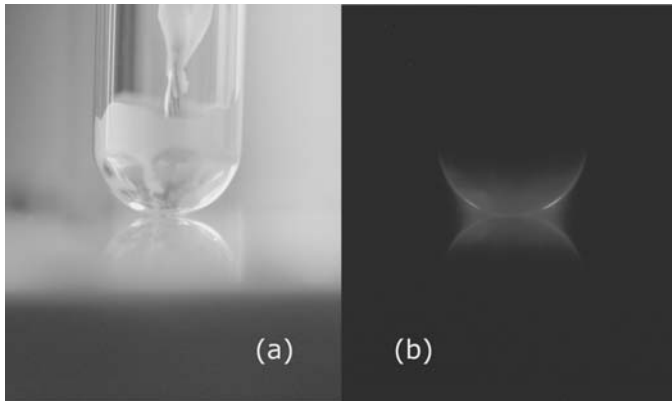
Figure 6. Side view of nanosecond pulsed DBD between glass covered electrode and ground metal electrode (a) in light room and (b) in complete dark room for same exposure time (bottom halves of the images are due to reflection from the ground plate electrode surface)

Curve fitting [5,6] of model spectra to experimental data for average of 5 measurements gave rotational temperature of 313.5 ± 7.5 K and vibrational temperature of $3,360 \pm 50$ K. Additionally, measurement of the surface temperature of the grounded electrode in the presence of the discharges was done using a reversible liquid crystal temperature indicator (model 4002B, Accuracy: $\pm 1°C$, LCR Hallcrest L.L.C., IL). A sheet of the temperature indicator was placed over the grounded copper electrode and acted as the secondary electrode in the discharge. In the presence of the discharge the surface temperature was around $25°C$, while the temperature of the ground electrode surface without the discharge was measured to be $22°C$. With those low temperatures it is possible to treat living tissue prolonged durations (Fig. 7).

Figure 8 shows the Lichtenberg figure [4,7] of a single nanosecond pulse of DBD plasma on b&w (a) and color (b) photofilms. To demonstrate the uniformity of the nanosecond pulse DBD developed here, the authors compare its Lichtenberg figures with those of a more conventional microsecond DBD.

As evident from the Fig. 8, Lichtenberg figures show significant difference between the two discharges. The nanosecond pulsed discharge appears in round pattern that is approximately equal size of diameter of the high voltage electrode without any bright spot or irregular pattern distribution. The contact point of the electrode appears as the dark point at the center of Fig. 8a. Rays-type pattern at

the edge of the spot appeared apparently because of the secondary surface discharge. Fig. 8a, b also verifies that nanosecond pulsed DBD ignites uniformly over a relatively large range of electrode gap distances (0.1–4 mm, due to the curvature of the glass covered high voltage electrode). On the other hand, discharge patterns of microsecond pulsed DBD in Figs. 8c, d clearly show the filamentary structure (microdischarges) when used with the same electrode for the same characterization.
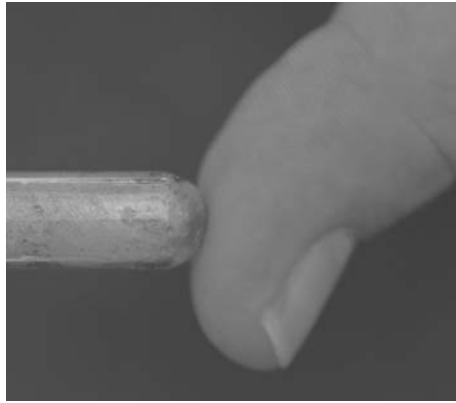
Figure 7. Appearance of nanosecond DBD igniting on finger (Exposure time: 1 s)
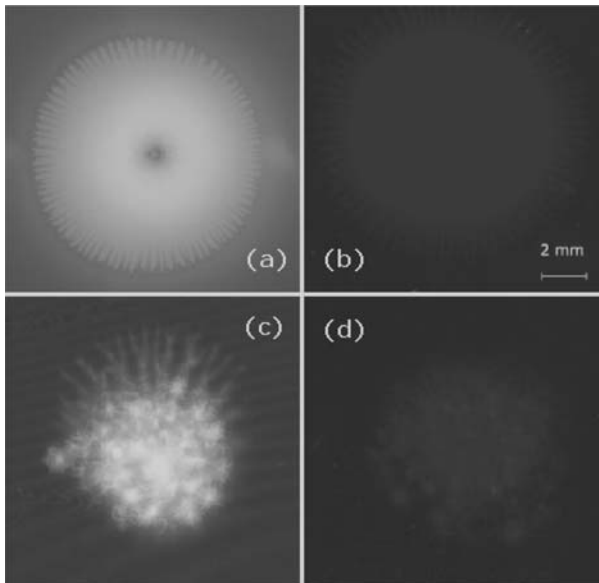
Figure 8. Lichtenberg figures of two different DBD systems on the emulsion of the photofilms: (a) nanosecond pulsed DBD – b&w, (b) nanosecond pulsed DBD – color, (c) microsecond pulsed DBD – b&w, and (d) microsecond pulsed DBD – color

For power measurement main spark gap was adjusted to 21 mm and secondary spark gap was 3 mm. Average power of the nanosecond pulsed DBD was found 62 ± 3 mW for these conditions. Repetition rate has been measured as 192 Hz (+20/–25 Hz) giving 0.323 ± 0.03 mJ average energy dissipation per period. Since all of the energy dissipates during the pulse, with average 20 ns pulse duration, power of one single pulse can be calculated as much as ~16 kW.

Finally, nanosecond pulsed DBD has been tested for demonstration of sterilization by treating bacteria culture on agar. Bacteria for sterilization demonstration were skin flora transferred [3] onto a blood agar plate (Trypticase Soy Agar with 5% Sheep Blood; Cardinal Health, Dublin, OH). Figure 9 shows the image of agar surface covered with skin flora (dark red area covering most of the surface) has been sterilized (light red area) with nanosecond pulsed DBD treatment for 15 s. This result does show sterilization ability of the discharge as well as its efficiency. Treatment with power as low as few tens of mW for 15 s, with average power density approximately 1 mW/mm^2 (discharge diameter equals to electrode diameter) can sterilize. This power density is one order of magnitude lower than typical conventional DBD [8] power density. Sterilization can be attained with nanosecond pulsed DBD with significantly lower power density for the same duration of treatment.
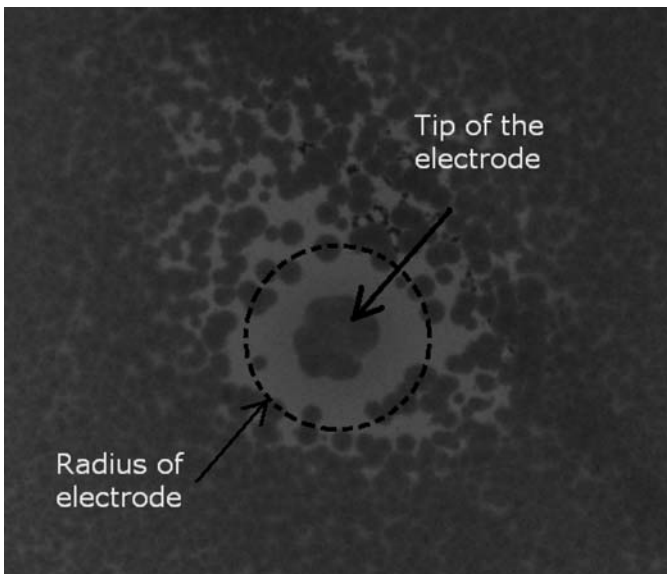
Figure 9. Agar with skin flora treated by nanosecond pulsed DBD

Conclusion

In summary, the authors have developed a new uniform non-thermal plasma system for living tissue sterilization and possible other medical applications.

Experiments reveal that new nanosecond pulsed DBD does not require uniform discharge gaps as it can ignite and sustain over wide ranges of gap for the same substrate, it means it does not require smooth surface of the electrode. This feature gives an important advantage to new discharge over others, for compatibility to real tissue operations that are dominated with irregular surfaces. The discharge uniformity is demonstrated qualitatively with a new technique for such high frequency discharge. Lichtenberg figures of nanosecond pulsed DBD show clearly that few tens of nanosecond pulse duration avoids streamer formation and generates uniform discharge working in atmospheric pressure air. Additionally, the authors have demonstrated the ability of the discharge to sterilize. Finally, it should be emphasized that the technique was employed to generate a few tens of nanosecond long pulses is easy and cheap. This method would be easily used for variety of further applications.

Acknowledgment

References

[1]   M. Laroussi, et al., IEEE Trans. Plasma Sci. 28 (2000) 184–188
[2]   E. Stoffels, et al., Plasma Sources Sci. Technol. 11(4) (2002) 383–388
[3]   G. Fridman, et al., Plasma Chem. Plasma Proc. 26(4) (2006) 425–442
[4]   U. Kogelschatz, Plasma Chem. Plasma Proc. 23 (2003) 1
[5]   C.O. Laux, von Karman Institute Lecture Series 2002–07, Physico-Chemical Modeling of High Enthalpy and Plasma Flows, eds. D. Fletcher, J.-M. Charbonnier, G.S.R. Sarma, and T. Magin, Rhode-Saint-Genèse, Belgium, 2002
[6]   D. Staack, et al., Plasma Sources Sci. Technol. 15 (2006) 818–827
[7]   U. Kogelschatz, IEEE Trans. Plasma Sci. 30(4) (2002) 1400
[8]   G. Fridman, et al., Plasma Process. Polym. 2007(4), 370–375

UNIFORM AND FILAMENTARY NATURE
OF CONTINUOUS-WAVE AND PULSED
DIELECTRIC BARRIER DISCHARGE PLASMA

M. COOPER[1], Y. YANG[1], G. FRIDMAN[2], H. AYAN[1],
V. N. VASILETS[1], A. GUTSOL[1], G. FRIEDMAN[3],
AND A. FRIDMAN[1]
[1]Department of Mechanical Engr. and Mechanics,
Drexel University, Philadelphia, USA
[2]School of Biomedical Engineering, Science, and Health Systems,
Drexel University, Philadelphia, USA
[3]Electrical and Computer Engineering Department,
Drexel University, Philadelphia, USA

Abstract: Observations of atmospheric pressure DBD plasma were conducted through the transparent electrode in Air, Argon, Helium, Nitrogen and Oxygen gasses at 1 and 3 standard liters per minute (slpm) flow rates through the discharge gap, utilizing three types of excitation waveforms. Three phenomena were observed: (1) plasma filaments travel with the gas at the same speed as the gas for some but not all gases; (2) propagation of excitation is observed in Nitrogen plasma and the filament motion has no directional preference with gas flow direction; and (3) Oxygen, Nitrogen and Helium plasmas were observed to be rather uniform at least over longer time periods.

1. Introduction

Current applications of atmospheric pressure dielectric barrier discharge (DBD) include ozone production [1,2], treatment of gases [3], industrial surface treatment [4–7], and other applications. DBD's biocidal properties make atmospheric pressure DBD potentially a favorable system for medical applications [8–11]. Uniformity of sterilization should depend on the discharge spatial uniformity. Also, it has been shown experimentally that when exposed to DBD, the patient's discomfort is directly related to the intensity of microdischarges, or filaments, in

this plasma [12]. Furthermore, the number of microdischarges depends upon the excitation waveform, power, and the type of gas [12]. A change in any of these three variables may result in a higher filament temperature, and thus increases the discomfort experienced by the patient. Thus, comfortable and effective treatment requires plasma with little or no filamentation. This stemmed the need to observe and characterize plasma in which the excitation waveform, gas type, and flow rate were varied to obtain the most uniform lowest power plasma with highest bactericidal abilities (bacterial studies are not presented here, please see [9], [10] for further details).

Three plasma excitation waveforms were used for characterization: a sinusoidal waveform, quasi-sinusoidal continuous waveform, and pulsed excitation. The surface power density was kept at a constant value for each particular gas, ranging from 0.4 to 2 W/cm^2 for different gases. Air, Argon, Helium, Nitrogen and Oxygen were chosen for the experiments reported on in this paper. The three excitation waveforms chosen here are due to the power supply availability in our lab and their previous use in medical and biological studies (see [9], [10]). Presented in this paper are the results and highlights of the observed effects that authors deemed of note.

2.   Experimental Setup

The experimental setup (Fig. 1) features a water electrode 25.4 mm in diameter separated from a brushed stainless steel base by a 2 mm perforated aluminum spacer. The water electrode was comprised of a quartz viewing windows at the upper and lower surfaces. Regular tap water was degasified and used as a conducting medium. The Nikon D70 camera was used for digital photography. Photos of the discharge were taken at decreasing shutter speeds from 30 to 1/6,400 s to characterize plasma spatial uniformity at different time scales. The upper (transparent) electrode is water cooled by allowing the water contained within the electrode to circulate to an ice-cooled external container (Fig. 1). Due to the nature
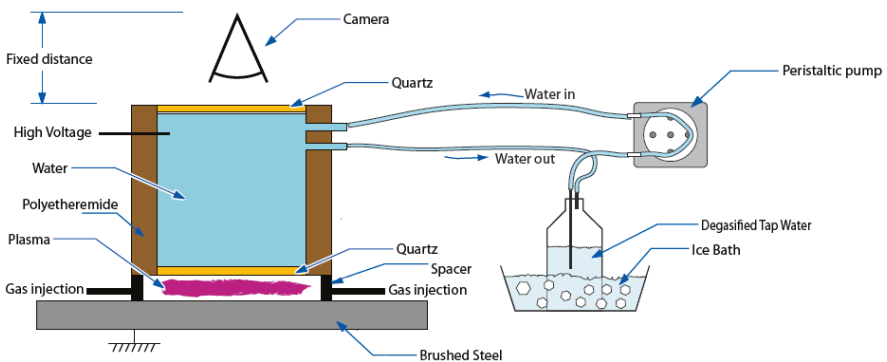
Figure 1. Experimental setup

of the pump and the setup, water recirculation often resulted in bubble formation which is visible in pictures taken at small apertures (less light reaches the camera's Charge Coupled Device (CCD) sensor) and long shutter speeds (the time during which light is collected on the CCD); therefore, approximately 2–3 mm shadows seen in some of the pictures are artifacts of bubbles just below the upper quartz window; these bubbles do not affect the plasma in any way as the lower plasma-contacting quartz is bubble-free. The plasma is formed within a two millimeter gap distance between the brushed steel and the lower quartz face of the electrode. Gas is introduced into the setup through ten out of twelve equidistant tubes which are connected to the perforated spacer in the base of the chamber and exit through the remaining two (Fig. 2).
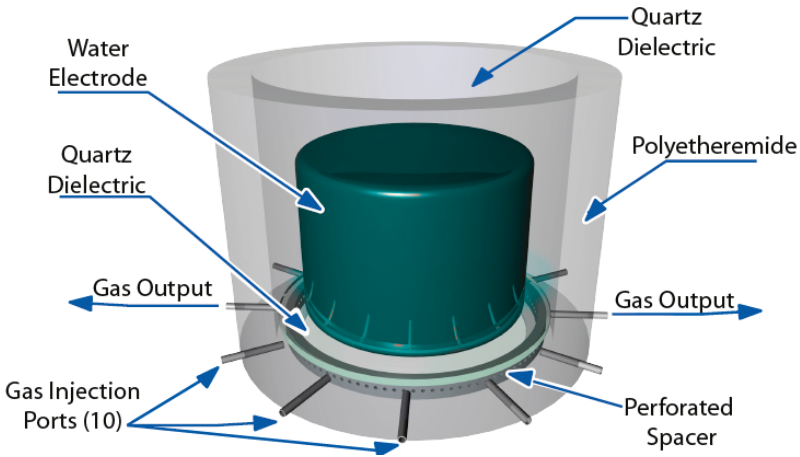
Figure 2. Experimental setup detailing the two gas output ports and the ten gas injection ports

2.1. WAVEFORMS

Sinusoidal, quasi-sinusoidal ('continuous'), and "micro-pulsed" waveforms were applied to the voltage. The pulse duration and characteristics of each waveform are given in Fig. 3.

The pulse durations shown in Fig. 3 are taken to be the full width at half maximum (FWHM). The rise time is time interval for the major pulse to change from 20% to 80% of its maximum amplitude. The typical pulsed waveform has positive or negative polarity pulses at 0.1 to 1 kHz repetition rate, up to 35 kV peak to peak, 1.7 μs pulse duration and 0.75 μs rise time. The continuous waveform generates up to 35 kV peak to peak at 8.7 kHz with a continuous quasi-sinusoidal bipolar wave signal. The sinusoidal waveform is a varying frequency and voltage system where sinusoidal waves were amplified and stepped up to high voltage [19]. For our experiments, the frequency is fixed at 12 kHz.
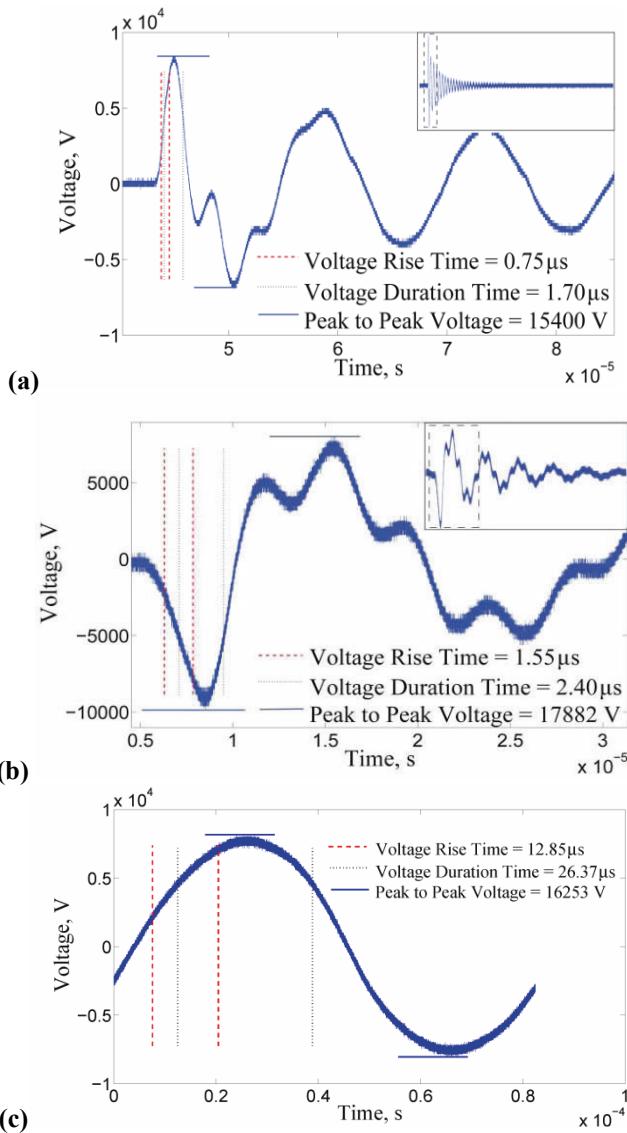
Figure 3. Waveforms generated by the power supplies: (a) pulsed; (b) continuous; and (c) sinusoidal

3. Results and Discussion

3.1. ARGON

When observed at exposition times greater than 0.1 s, Argon plasma is composed of a diffuse background and filaments developing along the direction of flow. At

closer observation with low exposition times, it can be seen that filaments travel in the direction of gas flow and at the velocity close to the estimated velocity of gas flow. This effect is observed only in argon and air plasma. This is due to the memory effect [18] of a filament being bound to the gas and not the surface. Plasma in Argon, for example, is shown in Fig. 4.
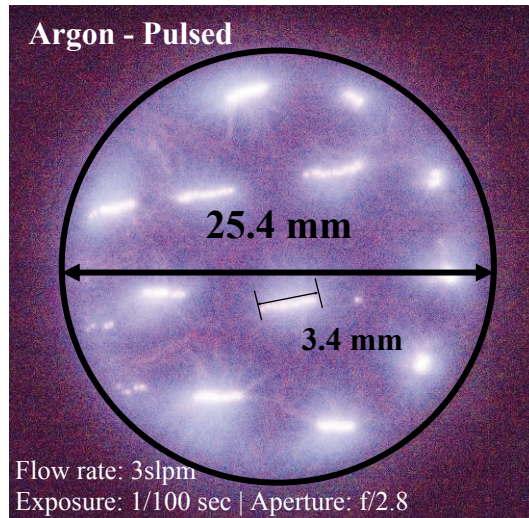
Figure 4. Motion of the filaments with gas flow observed in Argon plasma

A filament travels approximately 3.4 mm in 1/100 s resulting in a velocity of 3.4 m/s. The gas flow rate for this picture is 3 standard liters per minute (slpm) through the volume of a cylinder with height 2 mm and diameter 25.4 mm, meaning that the average residence time of the gas in this volume is about 0.02 s, and in that case the average linear gas velocity will be on the order of 1 m/s, which is comparable with the filament movement velocity. It means that the memory effect in argon or air DBD [16,17] is related not only to charge deposition on the surface but also to the pre-ionization (or high concentration of excited molecules) that exists in the gas after DBD polarity change.

3.2. HELIUM

Previous experiments display the uniform nature of DBD plasma at atmospheric pressure in helium [13]. We also observe uniform plasma in helium at least with long exposition time (but for some cases at short exposure also (see below) and with all three power supplies.

Helium plasma exhibits a uniform background, with some filaments in stationary positions (Fig. 5). We believe that these filaments are artifacts of particulate contamination on the bottom electrode.

Helium - Pulsed

Flow Rate: 1slpm | Aperture: f/5.6

Helium - Sinusoidal

Flow Rate: 3 slpm |Aperture: f/2.8
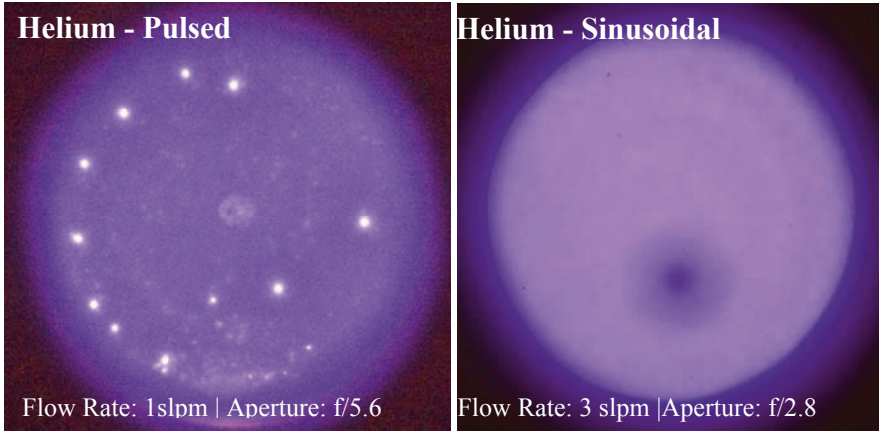
Figure 5. No evidence of excitational propagation observed in Helium. Both pictures are taken at ¼ s exposure time

3.3. OXYGEN

Plasma uniformity was achieved (Fig. 6), as reported for some previous experiments using oxygen plasma [14,15]. The DBD plasma in oxygen is observed to be diffuse and is visible at a minimum exposure time of 1/30 s versus 1/4,000 s for Helium at ~2 W/cm². As the exposure time decreases, filamentary structures which create the appearance of diffuse plasma at longer exposures are revealed (Fig. 6).

Oxygen - Sinusoidal

Exposure: 30 sec | Aperture: f/6.3

Exposure: 1/4 sec | Aperture: f/2.8
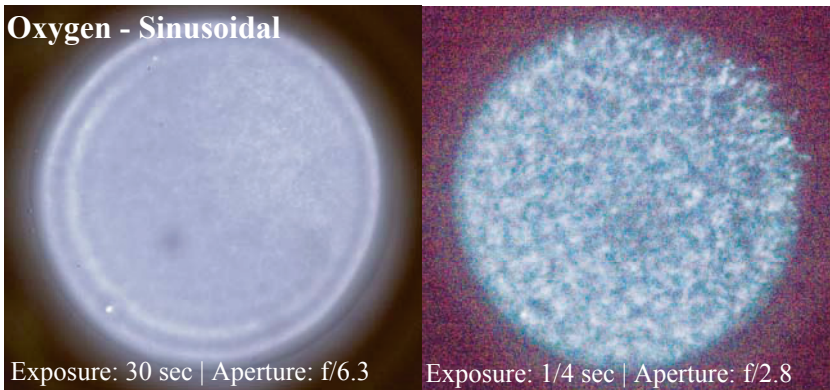
Figure 6. DBD plasma uniformity with sinusoidal waveform in oxygen. Flow rate: 1 slpm

3.4. NITROGEN

Nitrogen DBD plasma uniformity is also observed at long exposures and for all waveforms (Fig. 7). Interesting occurrences are in Nitrogen using sinusoidal waveform. It is possible to see that in plasma generated using the sinusoidal waveform, filaments in Nitrogen have no preferential direction of travel (Fig. 8), contrary to Argon and Air, where streamer channels flows in the direction of gas and at the velocity comparable to the bulk gas velocity.
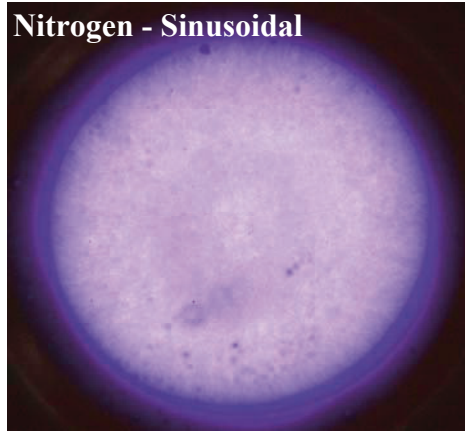
Figure 7. Nitrogen uniformity at 1 slpm flow rate, 30 s exposure time and f/32 aperture

An interesting phenomenon, however, can be observed at short exposures with the sinusoidal voltage waveform at 1.2 W/cm^2. The observed effect in Fig. 9 can be attributed to either the propagation of non-equilibrium vibrational excitation radialy from the filament or to the increase of a reduced electric field, E/n. These probable phenomena results in a cylindrical front of weak breakdown approximately 4 mm from the center of the microdischarge (Fig. 9). So, instead of the whole microdischarge current concentrated in one channel that is typical for standard DBD [16,17], a complex radialy symmetrical distribution of the micro-discharge current appears, and characteristic radial size of this current is about 4 mm in the particular case presented in Fig. 6. Therefore interaction between microdischarges that usually have characteristic distance on the level of 0.5–1 mm now have much larger characteristic distance, and microdischarges form two-dimensional quasi-crystal with the lattice size of about 5–8 mm. It looks like this crystal structure is rather 'rigid' and gas flow cannot move 'nodes' of this lattice (in contrast with the argon case, Fig. 4). On the other hand, stochastic processes in microdischarge formation [16,17] case slow stochastic (random) drift of the 'lattice nodes' (Fig. 8).
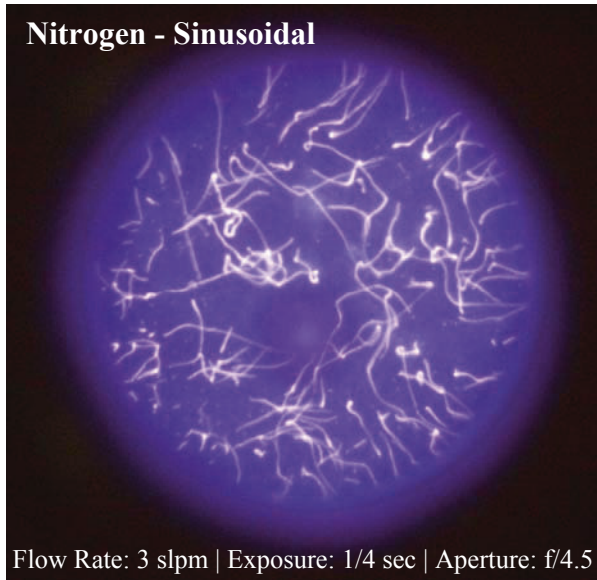
Figure 8. Nitrogen filaments generated using sinusoidal waveform have no preferential motion direction
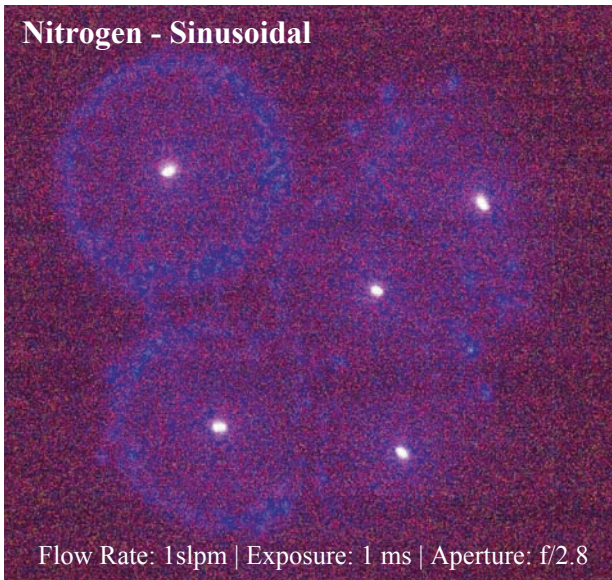
Figure 9. Propagation of excitation observed in Nitrogen at low exposures is exclusive to the sinusoidal waveform

The propagation phenomenon was not observed in the cases of the pulsed and continuous power waveforms for all gasses. A weaker version of the propagation phenomenon may occur, however is not observed.

4. Summary and Future Work

Three phenomena were observed in the discussed experiments: memory effects can be bound to the gas *or* to the surface; a cylindrical front of weak breakdown was observed in Nitrogen plasma where filaments have no directional preference of motion; and there is great uniformity in both Oxygen and Helium plasma without the use of complex electrode structures or special power supplies.

Future work will focus on better understanding and modeling of the mechanisms of excitation propagation observed in Nitrogen plasma.

References

[1] Haverkamp, R.G., Miller, B.B., and Free, K.W. "Ozone production in a high frequency dielectric barrier discharge generator." Ozone: Science & Engineering 24(5) (2002) 321–328.

[2] Samaranayake, W.J.M., Miyahara, Y., Namihira, T., Katsuki, S., Hackam, R., Akiyama, H. "Ozone production using pulsed dielectric barrier discharge in oxygen." IEEE Transactions on Dielectrics and Electrical Insulation, 7(6) (2000) 849–854.

[3] Joseph Shiloh, Avner Rosenberg, and Elhanan Wurzberg. Modular dielectric barrier discharge device for pollution abatement. Patent number: 6245299. Issue date: Jun 12, 2001.

[4] Roth, J.R. Industrial Plasma Engineering: Volume I, Principles. Institute of Physics Publishing, Bristol and Philadelphia 1995, ISBN 0-7503-0318-2.

[5] Roth, J.R., Tsai, P.P.-Y., Liu, C. Steady-State, Glow Discharge Plasma, U.S. Patent a5,387,842, issued February 7, 1995.

[6] Roth, J.R., Tsai, P.P.-Y., Liu, C., Laroussi, M., Spence, P.D. One Atmosphere Uniform Glow Discharge Plasma, U.S. Patent a5,414,324, Issued May 9, 1995.

[7] Roth, J.R. Method and Apparatus for Cleaning Surfaces with a Glow Discharge Plasma at One Atmosphere of Pressure, U.S. Patent #5,938,854, Issued August 17, 1999.

[8] Fridman, G., Shereshevsky, A., Jost, M.M., Brooks, A.D., Fridman, A., Gutsol, A., Vasilets, V., and Friedman, G. "Floating electrode dielectric barrier discharge plasma in air promoting apoptotic behavior in melanoma skin cancer cell lines." Plasma Chemistry and Plasma Processing 27 (2007) 163–176.

[9] Fridman, G., Peddinghaus, M., Ayan, H., Fridman, A., Balasubramanian, M., Gutsol, A., Brooks, A., and Friedman, G. "Blood coagulation and living tissue sterilization by floating-electrode dielectric barrier discharge in air." Plasma Chemistry Plasma Processing 26 (2006) 425–442.

[10] Fridman, G., Brooks, A.D., Balasubramanian, M., Fridman, A., Gutsol, A., Vasilets, V.N., Ayan, H., and Friedman, G. "Comparison of Direct and Indirect Effects of Non-Thermal Atmospheric Pressure Plasma on Bacteria." Plasma Processing of Polymers, 2006, 10.1002/ppap.200600217, accepted.

[11] Gadri, R.B. et al. "Sterilization and plasma processing of room temperature surfaces with a one atmosphere uniform glow discharge plasma (OAUGDP)." Surface Coatings Technology 131 (2000) 528–542.

[12] Ayan, H., Fridman, G., Gutsol, A., Vasilets, V., Fridman, A., and Friedman, G. "Heating
      effect of dielectric barrier discharges in sterilization," presented at the 34th IEEE Int.
      Conf. Plasma Science, Albuquerque, NM, Jun. 17–22, 2007.

[13] XMangolini, V., Anderson, C., Heberlein, J., and Kortshagen, U. "Effects of current
      limitation through the dielectric in atmospheric pressure glows in helium." Journal of
      Physics D: Applied Physics. 37 (2004) 1021–1030.

[14] Abolmasov, S. N., Shirafuji, T., and Tachibana, K. "Submillimeter Dielectric Barrier
      Discharges at Atmospheric Pressure: Edge Effect." IEEE Transactions on Plasma Sci.
      33(2) (2005) 941– 948.

[15] Battey, J.F. "Design criteria for uniform reaction rates in an oxygen plasma." IEEE
      Transactions on Electron Devices. 24(2) (1977) 140–146.

[16] Chirokov, A., Gutsol, A., Fridman, A., Sieber, K. D., Grace, J. M., and Robinson, K. S.
      "Analysis of two-dimensional microdischarge distribution in dielectric-barrier discharges."
      Plasma Sources Science and Technology 13 (2004) 623–635.

[17] Fridman, A., Chirokov, A., and Gutsol, A. Non-thermal atmospheric pressure discharges.
      Journal of Physics D: Applied Physics 38 (2005) R1–R24.

[18] Massines, F., Rabehi, A., Decomps, Ph., Ben Gadri, R., Segur, P., and Mayoux, C.,
      Mechanisms of a glow discharge at atmospheric pressure controlled by dielectric barrier,
      Journal of Applied Physics 83(6) (1998) 2950–2957.

[19] Blood Coagulation and Living Tissue Sterilization by Floating-Electrode Dielectric Barrier
      Discharge in Air, G. Fridman, M. Peddinghaus, H. Ayan, A. Fridman, M. Balasubramanian,
      A. Gutsol, A. Brooks, G. Friedman, *Plasma Chemistry and Plasma Processing*, 26 (2006)
      425–442.

CONTINUOUS AND PULSE POWER SUPPLIES
FOR DIFFERENT PLASMA APPLICATIONS

N. MEDVEDEVA AND D. MEDVEDEV
STC Quinta LTD, Moscow, Russia

Abstract: New types continuous power supplies for the arc and glow types of discharges were presented. Possibilities of generation of some new moods of these discharges were demonstrated and new applications of these discharges were proposed.

Possibility of generation of new type of pulse DBD discharge by the special power supply was shown. Application of this type of DBD for ozone generators working on air with natural atmospheric humidity was demonstrated.

1. Introduction

Different plasma applications require different plasma parameters. There is no ideal plasma for all cases. For some cases nanosecond pulse discharges are more effective than microsecond for other cases there is opposite situation. The choice is determined by the active particles which we want to generate and processes which we want to stimulate by plasma.

The control of plasma parameters and desirable processes in plasma is possible by the optimization of power supply parameters for given task. In this paper we will show two examples of such optimization for completely different kinds of power supplies.

1.1. CONTINUOUS POWER SUPPLIES FOR ARC AND ARC-LIKE AND GLOW-LIKE DISCHARGES

Arc plasmatrons are suitable simple and reliable plasma source which have wide utilization region, particularly for plasma ignition of engines. Arc plasmatrons have well known set of advantages (simplicity, wide working region of pressure and so on) and disadvantages (electrodes life time). To find other variant of gas discharge for plasma torch generation which can remove problem of electrodes

life time is vitally significant for all applications of plasma which require long operation time (for example for plasma stabilization of combustion). One of possible variant of discharges is transient form of gas discharge which we can obtain by decreasing of arc current and at the same time by modification volt-ampere characteristic and other parameters of power supply to increase discharge voltage. This approach give us possibility to obtain nonstationary form of discharge in gas flow which have characteristic features of gliding arc discharge and glow which we will call high pressure glow like discharge (HPGL) in gas flow to emphasize difference with regular arc discharge. By this way we succeeds in decreasing discharged current more than ten times with the same power of discharge conserving small dimensions and all basic features of arc plasmatron. Erosion of electrodes connected with current was decreased dramatically.

Electric parameters of glow like discharge in gas flow was studied in wide region of gas pressure, discharge current and gas velocities. There was determining regimes when stable discharge existing in pressure region from 0.2 up to 30 atm which have practical interest for plasma assisted combustion applications. Stable plasma torch generated by glow like discharge in gas flow was obtained in all pressure region for the for the discharge current from 20 mA to 1 A. Typical voltage wave form of high pressure glow like discharge ion gas flow is shown below on fig. 1 and fig. 2.

As we can see voltage waveform is close to voltage of gliding arc but there is some difference because instead of almost notched shape which is characteristic for gliding arc there is some base of constant voltage. This base increase with operating current increasing (in this case discharge will transform to regular arc discharge), will decrease with gas flow increasing and will increase with operating pressure increasing. Like in the case of gliding arc plasma filament stretch and rend in gas flow. But in this case plasma filament is restored not by breakdown but by jumping of plasma filament to one of previous points.

So there was found transient nonstationary form of gas discharge which is convenient plasma torch generation with extremely small electrodes erosion. Discharge current was decreased more than ten times (compared with arc) with the same power of discharge conserving small dimensions and all basic features of arc plasmatron.
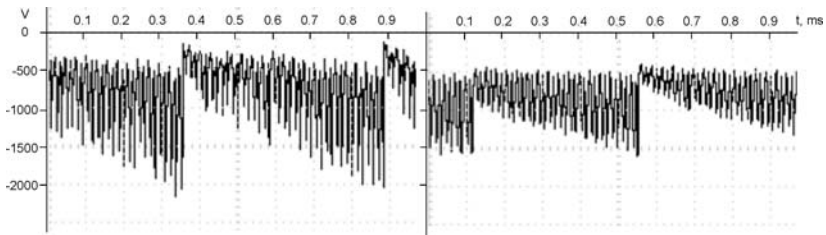
Figure 1. Two different types of breakdowns in plasmatron in HPGL mode of discharge with different current and air flow (left corresponds with low current and high air flow, right corresponds with high current and low air flow)
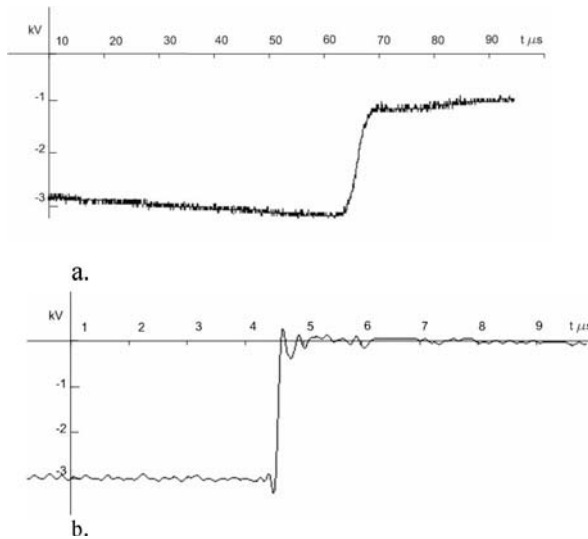
Figure 2. Two different types of breakdowns in plasmatron in HPGL mode of discharge with different current and air flow ((a) corresponds with high current and small air flow, (b) corresponds with low current and high air flow)

Electric parameters of discharge were studied in wide region of gas pressure, discharge current and gas velocities practically interesting for plasma assisted combustion applications.

Figure 3. DC power supplies for different kinds of arc and glow discharge applications

Features:

Volt-ampere characteristic optimized for reaching of maximum load voltage.
Wide region of smooth current regulation.
Absence of any ballast resistors give us high energy efficiency.
Electric scheme parameters give us possibility to operate at the extremely small current region and avoid repetition spark regime.
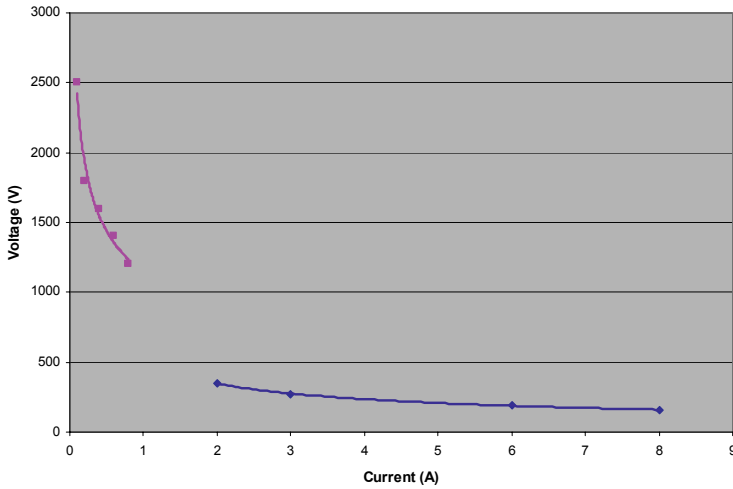
Figure 4. Volt-ampere characteristic of plasmatron with conventional power supply in arc mode and optimized power supply in HPGL mode
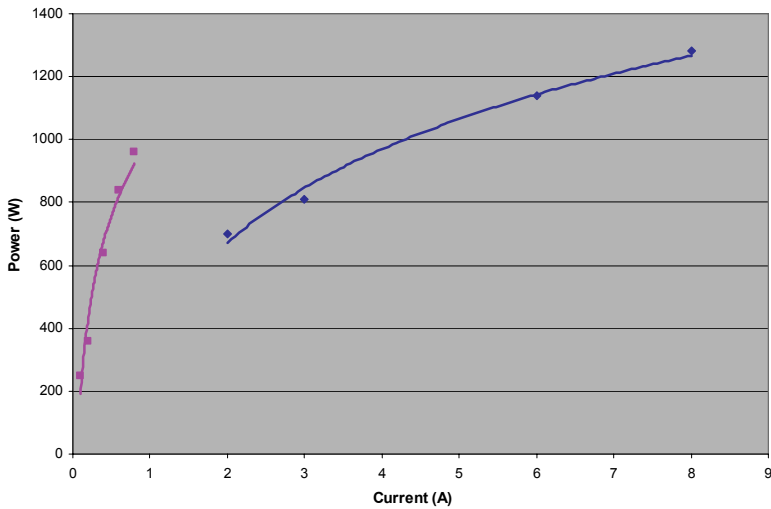
Figure 5. Power-current characteristic of plasmatron with conventional power supply in arc mode and optimized power supply in HPGL mode

Comparison of volt-ampere and power-current characteristic of plasmatron with conventional power supply in arc mode and optimized power supply in HPGL mode give us example of influence of power supply parameters on the behavior and type of discharge in DC plasmatron.

2. Microsecond DBD Optimized for the Long Time Operation on the Atmospheric Air with Natural Humidity

NOX generation and nitric acid deposition on the electrodes is significant problem for long time operation of DBD in air with presence of water vapors.

Selective generation of anomic oxygen with minimization of reaction of dissociation of nitrogen and (in some cases) water is extremely significant task for the wide region of practical application of DBD in atmospheric air- ozone generators without air drying, air purification surface treatment and so on. By this reason most of ozone generators work on dried air or oxygen [1,2].

This task is possible to solve by optimization of DBD parameters via DBD power supply modification.
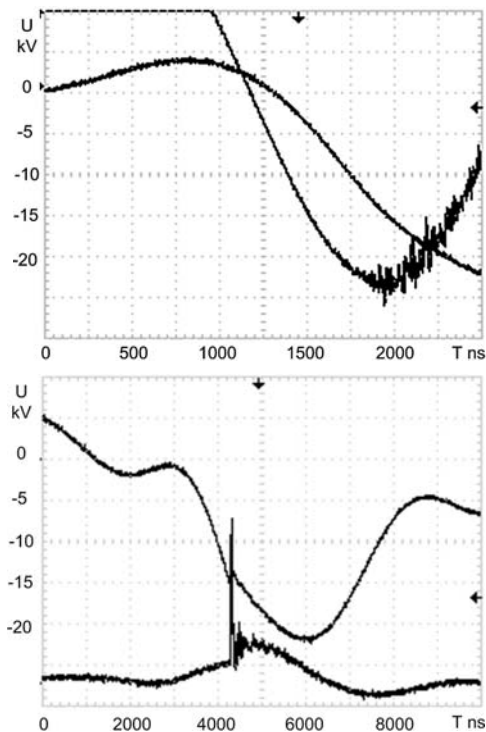
Figure 6. Voltage and current wave forms of conventional pulse DBD (top) and DBD optimized for long time operation on atmospheric air with natural humidity (bottom)

As a result of this optimization we obtain changing of characteristic of discharge and reach perfect characteristic of ozone generators based on such kind of DBD and working on atmospheric air with natural humidity. Other result is possibility of long time operation of such ozone generators working on atmospheric air with natural humidity without any acid deposition on electrodes.
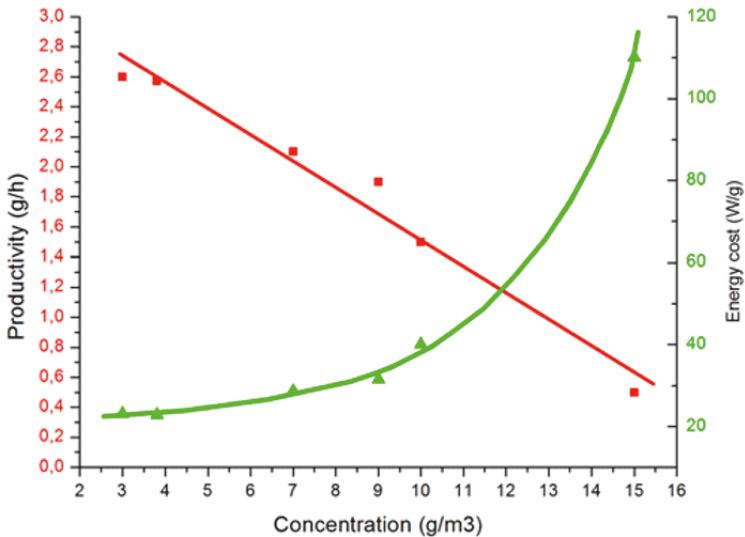
Figure 7. Dependence of ozone productivity and ozone generation energy cost on ozone concentration for DBD ozonizer optimized for air with natural humidity

Figure 8. Commercial ozone generators line based on the pulse DBD optimized for air with natural humidity

Figure 9. Electrodes condition of DBD optimized for air with natural humidity after 1 year nonstop operation. We can see no deposition of acid on the surface of electrodes

References

[1]   Abolentsev V., Korobtsev S., Medvedev D., Shiryaevskyi V. Ozone generation in pulse corona discharge. PROCEEDINGS of 17th Symposium on Plasma Physics and Technology, Prague 1995, June 13–16, p. 155–157.

[2]   Korobtsev S., Medvedev D., Shiryaevsky V. Ozone generators based on pulse corona discharge. ECWATECH 96 Second International congress "Water: Ecology and Technology", Moscow, 17–21 Sept. 1996, Abstracts, p. 165–166.

PLASMA AND GAS DISCHARGE METHODS OF AIR AND GAS PURIFICATION

D. MEDVEDEV, M. DEMINSKY, V. JIVOTOV, A. KNIJNIK,
S. KOROBTSEV, B. POTAPKIN, G. KONOVALOV,
M. KROTOV, AND R. SMIRNOV
RRC "Kurchatov Institute", Moscow, Russia

Abstract: Two different approaches to the problem of gas purification by plasma methods treatment are presented: removing of pollutions by oxidation reactions and by reduction reactions. Different practical examples of both approaches utilization are presented. Several pilot gas cleaning I systems installed on different plants are presented. Several types of reactor geometers for heterogeneous reactors were considered with practical examples of utilization. Some theoretical models of homogeneous and heterogeneous plasma chemical processes of pollutions removing have been proposed.

1. Introduction

Kurchatov Research Center have long time experience of development and commercialization of the plasma technologies for different air and gas cleaning applications. This technologies based on nonequilibrium and transient kinds of discharges can be utilized for industrial waste gases treatment and exhaust of engines. There are several approaches to these tasks based on completely different active particles and molecules generated by plasma.

1.1. APPROACHES

- Direct treatment of gas mixture or air by plasma
- Admixing of the gas treated by plasma to main gas flow

1.2. PROCESSES

- Gas phase reactions
- Reactions in water aerosol and droplets particles
- Reactions on catalyst surface stimulated by the active particles generated by plasma

1.3. REACTIONS

- Oxidation of admixtures by active particles generated by plasma up to substances removable by physical methods
- Reduction of admixtures by active particles generated by plasma

2. Example of Oxidation Approach Utilization

One of the most interesting examples of p gas discharge purification of waste air from small admixture of CS_2 – one of the main atmospheric pollutant in viscose fiber industry. Non-thermal plasma application for pollution control is the subject of widespread research now [1,2]. Several examples of this technology implementation can be mention at present and pulse corona discharge process is one of the most promising cases [2]. However the experience gained to date clearly indicates that process energy cost is one of the main problem need to be solved to provide extensive utilization of non-thermal plasma technologies in the modern industry. One of the ways to reduce plasma energy consumption is to apply heterogeneous discharge where chain reaction or quenching effects can take place. This paper is devoted to the theoretical and experimental studies of mechanisms and kinetics of CS_2 oxidation in air under corona discharge conditions.

3. Experiment

3.1. DESCRIPTION OF THE EXPERIMENTAL SETUP

Experiments on the removal of carbon disulfide from an air flow have been carried out on a specially designed laboratory setup. This experimental set-up consists of the following main units:

- High voltage pulse power supply unit and control block
- Discharge reactor
- Gas preparation and distribution system with the apparatus for gas sampling

The experimental setup includes a special system to measure gas flow rate and gas sampling system in different points of the experimental setup (Point 1 – before discharge reactor, Point 2 – at the output). The general gas scheme of the experimental corona discharge reactor is shown in Fig. 1.
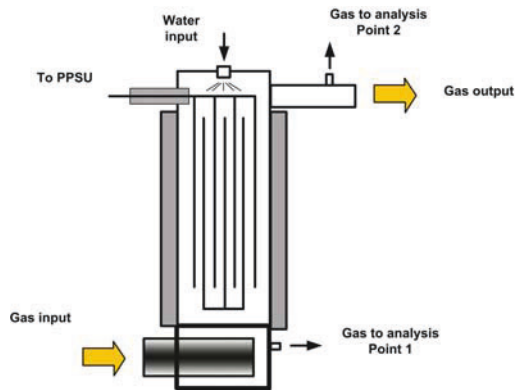
Figure 1. Scheme gas cleaning installation based on the heterogeneous impulse corona discharge

The pulse power supply unit (generated periodic high voltage pulses for electrodes of the discharge chamber) is based on an uncontrolled spark gap that used as a switch element.

The main technical parameters of the pulse power supply unit are the following:

Pulse voltage	Up to 30 kV
Average power	Up to 1,500 W
Pulse repetition frequency	From 100 to 1,000 Hz
Current pulse duration	Up to 200 ns
Pulse polarity	Positive

Changing of working frequency of the spark gap varies the average power of the pulse power supply unit.

The power measurements of the power supply unit (and consequently – corona discharge power) are carried out by measuring devices (voltmeter and ammeter) placed in primary (power) and in high voltage circuits of the power supply unit, and also directly by wattmeter installed in the primary power circuit.

The case of a discharge reactor for pulse corona discharge was made from stainless steel in the form of a parallelepiped, its dimensions being 270*310*1380 mm*mm*mm. The case of this reactor has heat insulation. The working temperature in the discharge zone is up to 100°C.

The electrode system of this discharge chamber represents alternating wire rows. High voltage wire rows alternate with grounded rows. The length of the working zone (coronning) of each wire is 1,000 mm, and the diameter is 0.6 mm.

To quench and remove from the discharge chamber the reaction products a system of water (or water solutions) input to the discharge zone is included into the experimental system. This system consists of a water buster vessel, water pipeline and injector for water input into the discharge chamber. The injector is placed on the upper cap of the discharge chamber.

3.2.   REMOVAL CS$_2$ FROM AN AIR FLOW

Test conditions: air flow varied from 100 to 300 m^3/h, CS$_2$ concentration was in the range from 300 to 1,000 mg/m^3. Concentration of the carbon disulfide was measured by an analytical chemical method. Energy cost of the process did not depend on the input pollutants concentration (in the mentioned range). The experimental result for carbon disulfide treatment at different gas temperatures is shown in Fig. 2.
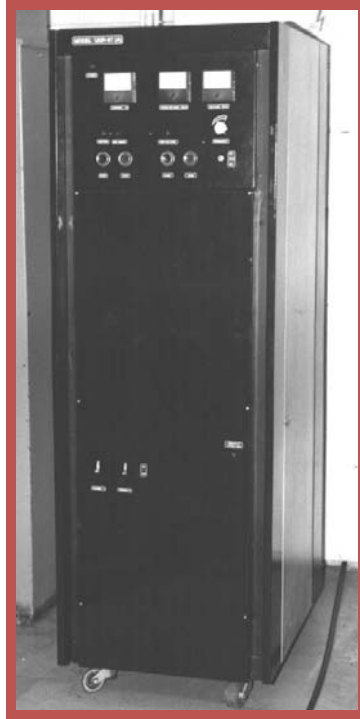
Figure 2. Ten kilowatt power supply for pulse corona discharge

These results are in a good agreement with preliminary laboratory tests [2]. The main oxidation products (in a liquid phase) were sulfuric and sulfurous acids (the ratio between them depends on the process conditions). We did not see the gaseous sulfur oxides in the products. In the experiments we also studied the influence of alkali components on the efficiency of the process. When the alkali (NaOH) is added to water sprayed the main reaction products became the salts (sodium sulphite and sodium sulphate) and the energy cost of CS$_2$ removal decreased about three times.

4. Modeling

4.1. PRODUCTION OF CHEMICAL ACTIVE SPECIES

The rate coefficients of electron induced gas phase reactions were obtained from solution of kinetic Boltzmann equation for electron energy distribution function. This equation was solved with use of two spherical harmonic expansion [3]. This approximation gives accurate rate coefficients for moderate reduced field intensities. The elastic and rotational collisional integrals are written in so-called diffusion approximation. Inelastic collisional integral, in turn, contains vibrational, electronic and ionization collisional integrals (according to [4]). Without super-elastic collisions Boltzmann equation is solved by direct integration with Sherman boundary condition. Accuracy of solution was controlled by the balance of dissipated and consumed energy and was less than 0.5%.

The set of the cross-section square data for N_2 (elastic, vibration, rotational and electronic excitation cross sections) was taken from report [5]. Cross-sections for O_2 were obtained from reviews [6] and [7]. Recent Yousfi [8] set of the cross-section dates for H_2O after fitting procedure was used, because it supplied quite good agreement with experimental values of transport coefficients.

5. CS$_2$ Oxidation Mechanism

The primary reactions generated by streamer electrons were described in the frame of approach considered above. Specific energy input in the streamer was varied in the range 10^{-4}–10^{-1} eV/mol. by means of changing the electrons concentration and the pulse duration. Diffusion processes were treated in the preposition of the quick mixing at the diffusion time scale. Calculations were performed both in the regime of the single pulse and multi pulses variant. CS_2 concentration has varied in the range 300 – 2,000 ppm. Based on the literature data the chemical mechanism of the CS_2 oxidation processes occurring in the air under corona discharge condition was developed. It includes about 50 reactions. The whole set of processes with significant difference in the time scale were taken into account – the processes of active species production in streamer and subsequent chemical reactions of these species; ion-molecular reactions of ions generated in the streamer channel and their recombination; chemical reactions of active radicals.

Calculations were carried out with help of software package Chemical Workbench Ver 2.1. A O-D model was used to describe parameters evolution in the discharge chamber. This model with active species production describes the kinetics of chemical reactions in the confined volume under constant pressure and temperature. To simulate the effect of single corona pulse a chain of two 0-D reactors was used (Fig. 3). So that an outlet composition of the first reactor was at the same time an inlet one for the second model. Fist of them was intended for the modeling of active species production processes at the time scale up to 200 ns and the second one for reactions simulation in streamer afterglow.

In the case of multi pulse regime each odd reactor is intended for modeling of active species production in the streamer channel and next even – to simulate CS_2 cleaning process in the post discharge phase.
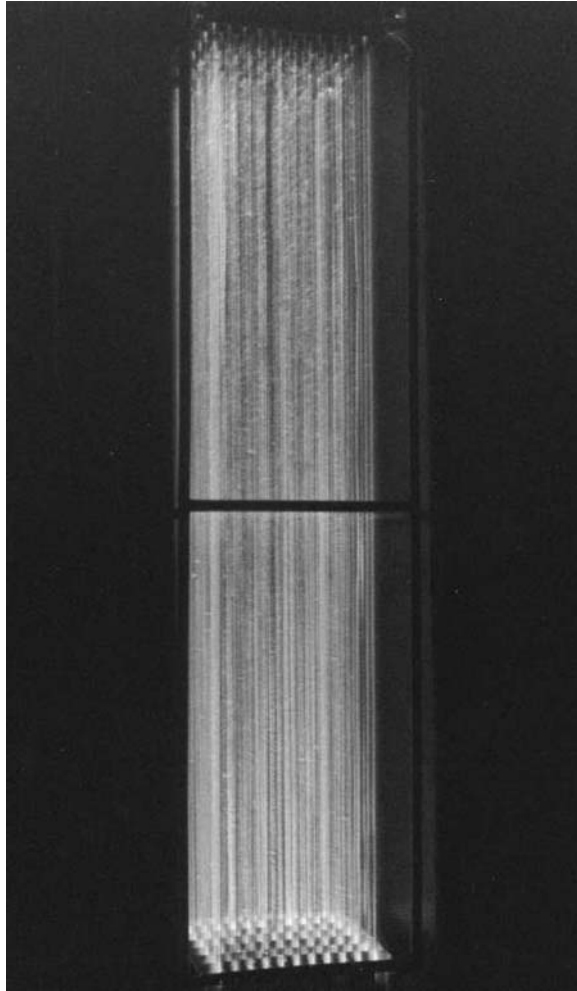
Figure 3. Luminescence of high power wire to wire pulse corona discharge

Sensitivity analysis has shown that mechanism of CS_2 oxidation we can present as follows:

$$CS_2 + O \rightarrow CS + SO, k = 3.2 \times 10^{-11} \exp(-650 \text{ K/T}) \text{ cm}^3\text{molecule}^{-1}\text{s}^{-1} \qquad (1) [9]$$

$$CS_2 + O \rightarrow COS + S, k = 3.65 \times 10^{-12} \exp(-701/T) \text{ cm}^3\text{molecule}^{-1}\text{s}^{-1} \qquad (2) [10]$$

$$CS_2 + O \rightarrow CO + S_2, k = 1.0 \times 10^{-13} \text{ cm}^3\text{molecule}^{-1}\text{s}^{-1} \qquad (3) [11]$$
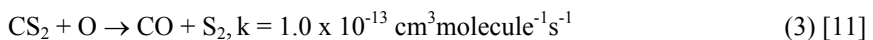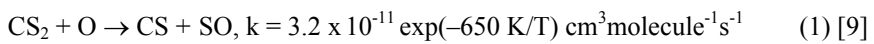
Formed CS radicals (product of reactions CS_2 and O) takes part in the reactions with atomic oxygen:

$$CS + O \rightarrow CO + S, k = 2.7 \text{ x } 10^{-10} \exp(-760/T) \text{ cm}^3\text{molecule}^{-1}\text{s}^{-1} \qquad (4) [9]$$

$$S + O_2 \rightarrow SO + O, k = 2.3 \text{ x } 10^{-12}\text{cm}^3\text{molecule}^{-1}\text{s}^{-1} \qquad (5) [9]$$

$$SO + O + M \rightarrow SO_2 + M, k = 5.31 \text{ x } 10^{-11}\text{cm}^3\text{molecule}^{-1}\text{s}^{-1} \qquad (6) [9]$$
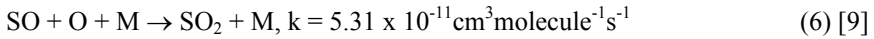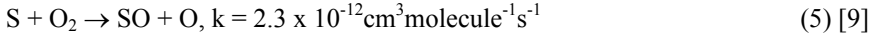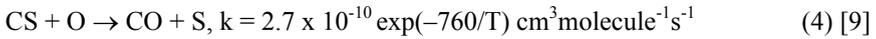
Here one can see chain process formed by reactions (1–5). Unfortunately O-atom is reacting with molecular oxygen as well and this is the main chain termination channel:

$$O + O_2 + M \rightarrow O_3 + M, k = 6.0 \text{ x } 10^{-34}(T/300)^{-2.3} \text{ cm}^3\text{molecule}^{-1}\text{s}^{-1} \qquad (7) [12]$$
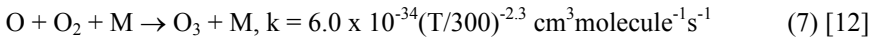
It was shown that for oxygenated systems (especially when O_2 concentration is high about 20% and above) O-atom reacts with O_2 forming ozone, which in turn practically doesn't react with CS_2 and very slowly reacts with CS in gas phase. It was found also that a competition between limiting channels of chain propagation (1) and chain termination (7) is strongly controlled by temperature. One can see (Fig. 4, initial composition was $CS_2 - 0.1\%$, $O_2 - 20\%$, $H_2O - 2\%$, $N_2 - 77.9\%$) that relatively small temperature increase can lead to the significant increase of CS_2 removal efficiency. This conclusion is in a good agreement with appropriate experimental results.
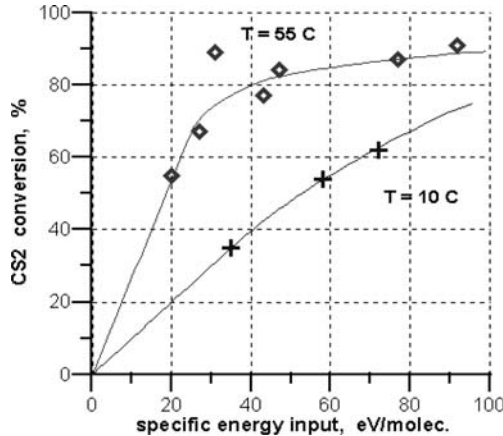
Figure 4. Dependences of CS_2 purification rate on the specific energy input per molecule for two different temperatures

An effect of streamer intensity on CS_2 removal efficiency via chain mechanism described above was examined as well. Streamer intensity in this case was varied by mean of pulse duration changing. The results of these calculations for the same initial composition are presented at Fig. 4. It was found that a decrease of streamer intensity leads to an increase of CS_2 removal efficiency. So

that barrier discharge or short pulse corona might be more effective in terms of CS_2 treatment via gas phase oxidation mechanism.

However calculations results have shown also that in case of pure gas mechanism the main products of CS_2 oxidation are not only carbon dioxide but sulfur dioxide and carbon oxide-sulfide (Fig. 5, Fig. 6, Fig. 7). At the same time ozone at the rather high concentration level is present in the outlet gas. In addition it was shown that further energy deposition does not change situation. That is why water spay was used in the experiments to illuminate disadvantage of plasma system in this specific case. Analysis has shown that ozone in this case can react with intermediate products in the alkali water droplets forming relatively stable sulfites and sulfates.
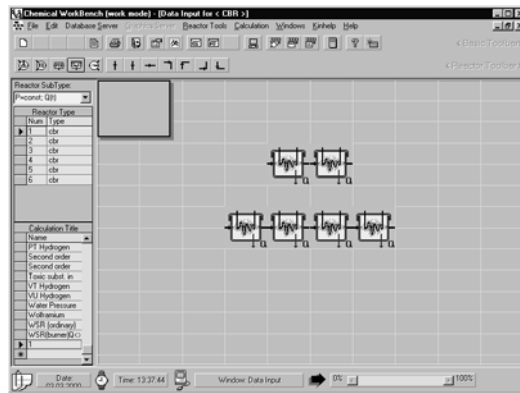
Figure 5. The main products of the gas phase CS_2 oxidation reaction
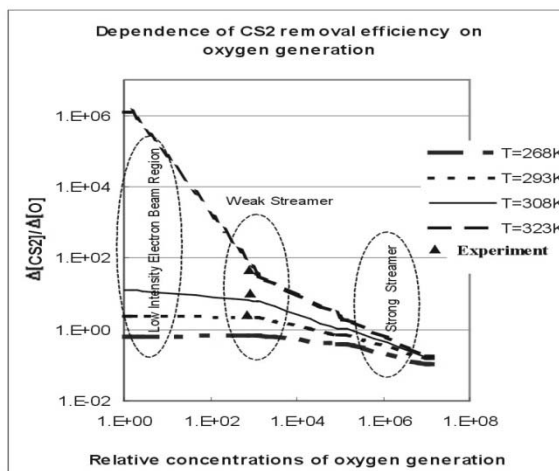
Figure 6. Dependence of the CS_2 removal efficiency on the oxygen generation
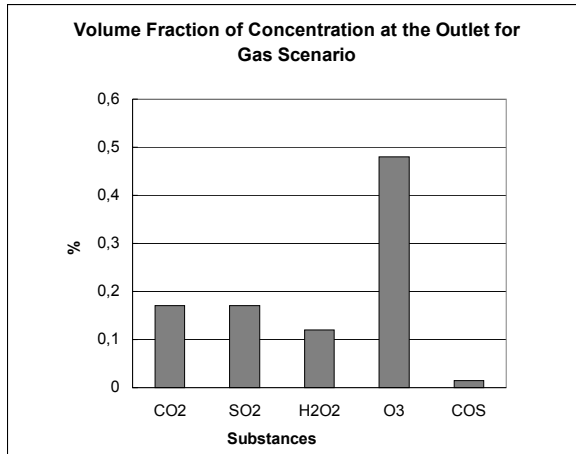
Figure 7. Volume fraction of the concentration at the outlet for the gas scenario

Both experimental and theoretical analysis has shown that pulse corona discharge can be rather effective in terms of CS_2 removal when processes parameters are selected to provide chain character of oxidation reactions. It was found that for initial CS_2 concentration about 0.1% the removal efficiency is increasing with an increase of the gas temperature and decrease of streamer intensity. However it was found that one of the main products of CS_2 oxidation under corona discharge in gas phase is toxic carbon oxide-sulfide and at the same time ozone is intensively generated by corona streamer. Water injection into discharge can help to solve this problem and to increase significantly the efficiency of CS_2 removal. At addition the alkali (NaOH) to water sprayed the main reaction products became the salts (sodium sulfite and sodium sulfate) and the energy cost of CS_2 removal decreased about 3 times.

5.1. EXAMPLE OF OXIDATION APPROACH UTILIZATION

Elimination of hazardous admixtures from air is extremely hopeful technology which have real advantages in the cases when it can be use. One of the most evident utilization for this technology is deNOX task for the exhaust of engines. Utilization of this technology based on the reactions of NO with syngas determined by the development of reliable, compact and effisient syngas production technology. Conventional catalytic technology, essentially if we are speaking about small and moderate scale portable applications, has certain problems because of relatively low specific productivity, high metal capacity and equipment size. Even thermal plasma, being very high energy density media, is giving an attractive alternative for the hydrogen and syngas production [13]. In this approach plasma

replaces catalysis and accelerates chemical reactions mainly because of high temperature effect. The advantages of plasma chemical method are extremely high specific productivity of apparatus, low investment and operation costs. However relatively high electric energy consumption, related with gas heating applies certain restrictions on possible applications of thermal plasma approach. Non-thermal plasma can accelerate chemical reactions at the low temperature as well because of active species generation by fast electrons. If active species, generated by non-thermal plasma, are capable to promote many cycles of chemical transformation when high specific productivity of plasma can be combined with low energy consumption of traditional catalyst. That is why this so-called plasma catalysis approach is the subject of permanent, strong interest of several last decades [14–17].

One of the examples of plasma catalysis in case of exothermal reaction is SO_2 oxidation under pulse electron beam effect $SO_2 + \frac{1}{2} O_2 = SO_3$. The results of experiments [16], confirmed later by independent works, clearly demonstrated that a number of oxidation reactions per one active species generated by plasma can be several hundreds that is why someone can speak about plasma catalytic activity. It was shown also that the most probable catalysis mechanism under experimental conditions is ion-molecular chain oxidation with negative ions as a chain carrier.

Hydrocarbon conversion processes and in particular methane decomposition into hydrogen and carbon black, which are a subject of our current interest, are endothermic reactions and to cover process enthalpy and to shift chemical equilibrium to hydrogen and carbon, methane should be heated in any case. Nevertheless temperature level required to shift chemical equilibrium is relatively low (600 – 1,000 K) and one can use for the process relatively low potential heat while plasma will be applied only as a catalytic agent for active species generation.

However, the basic obstacle in a way of wide introduction of the energy installations on the basis of Fuel Cells, which will use hydrogen (or syn-gas as a fuel), is absence of an effective and safe way of storage of hydrogen and absence of the infrastructure for its distribution. One of approaches at the decision of these problems is manufacture of hydrogen on a place of consumption from hydrocarbons in the special converter and use existing infrastructure of the hydrocarbons distribution. In [18] it is shown, that for onboard hydrogen production the most preferable way is manufacture syn-gas (a H_2 and CO mixture) in the partial oxidation process of the hydrocarbons (gasoline for mobile applications [18]). Due to kinetic limitations of this process it is necessary to find a way for its acceleration. Plasma of the gas discharge can be used for acceleration of the process and, correspondingly, for the increase of syn-gas output. Research of the plasma-assisted partial oxidation of hydrocarbon fuels (kerosene (brutto $C_{11}H_{21,7}$) and methane (CH_4)) with the air as oxidant: $C_mH_n + m/2\ O_2 + (N_2) = n/2\ H_2 + mCO + (N_2)$ was conducted. Otherwise the utilisation of such converters produced NOx free exhaust.

6. Experiment

6.1. EXPERIMENTAL INSTALLATION

6.1.1. *Plasmatron and Mixing-Reactor*

Plasma of the microwave discharge can be the source of the active particles (ions, radicals) that can accelerate the partial oxidation process that have radical-chain mechanism [19]. On the other hand active particles of plasma have small life-time at atmospheric pressure. In order to that particles may affect the partial oxidation process fast mixing reactor combined with coaxial microwave plasmatron was designed. Schematically plasmatron and mixing reactor are shown on Fig. 8. In the mixing reactor plasma jet (with the composition corresponding with type of plasma-forming gas and power of discharge) mixed with the preliminary heated reagent.
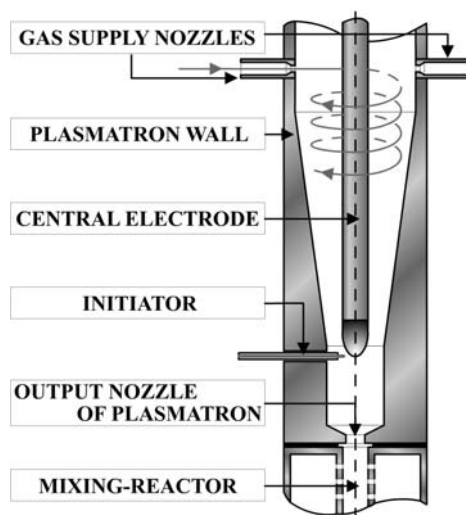
Figure 8. Plasmatron and mixing-reactor

Significant work was performed on optimization of the inner geometry of the plasmatron and optimization of the mixing channel. As a result, plasmatron efficiency was higher than 90%, and time of full mixing of plasma jet with reagents (as a result of diagnostic experiments) was $1 \div 1,5 \bullet 10^{-4}$ s. Plasmatron can work on different types of plasma-forming gases.

6.1.2. *Experimental Stand*

General scheme of the experimental stand is shown on Fig. 9.
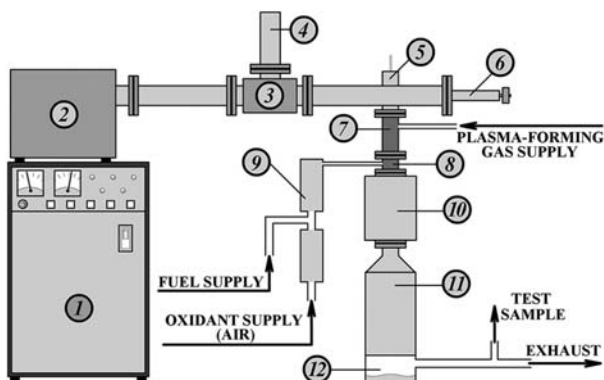
Figure 9. Experimental stand (general view)

Stand consists of the power supply (1), microwave-radiation generator (2), ferrite circulator (3) with the concerted load (4), waveguide-coaxial transition (5) with adjusting waveguide piston (6), plasmatron (7), a mixing-reactor (8), a heater-evaporator of the fuel-air mixture (9), heat-isolated reaction volume (10), heat-exchanger (11) and moisture-accumulator (12).

Parameters of the experimental stand: output microwave power – $1 \div 5$ kW, temperature of preliminary heating of reagents 300–800°C, total oxidant (air) supply – 3.75 l/s., as plasma-forming gas in experiments argon, air, a mix of the fuel and air in full combustion stochiometry were used.

6.2. EXPERIMENTS

The main task of experiments was to investigate plasma effect on the acceleration of partial oxidation process in comparison to other types of energy input in system. Various plasma forming gases were used to modelling different types of plasma jet influence on the process. Thermal effect of plasma (an energy input to the preheated reagents) was modelled by using argon as plasma-forming gas. When plasmatron worked on air or on fuel and air mixture besides thermal effect it is possible to observe effect of different radicals and ions influence on the process.

For the comparison, experiments with the other energy inputs in the system were carried out. Thermal input in system was changed by the varying the reaction stochiometry (reaction with the air redundancy), in such a case in the system two reactions were proceed at the same time – a partial oxidation and a full combustion of fuel. Thus energy output from a full combustion heat partial oxidation reagents and (by the increasing temperature in the area of intense reaction) accelerate the process.

Experiments were carried out in the following way. Heater-evaporator was preheated to the working temperature (300°C for kerosene and 750°C for methane), after that, discharge was initiated (by inserting tungsten electrode into discharge camera, Fig. 8, after discharge initiation, initiator was removed from

camera) in air as plasma-forming gas and fuel was feed into heater-evaporator. Then plasma-forming gas was changed (if it was not experiment with the air as plasma-forming gas) and when the stationary conditions was achieved (about 5 min from the beginning of experiment) a test sample for gas analysis were taken.

7. Results and Discussion

7.1. METHOD OF RESULTS PROCESSING

Concentrations of $[H_2]$, $[CO]$, $[N_2]$, $[CO_2]$, $[CH_4]$, $[C_2H_2]$, $[C_2H_4]$, $[C_2H_6]$, $[C_3H_6]$, $[C_3H_8]$, $[Ar]$ in the dry gas test samples was obtained by chromatograph analysis. Concentrations of $[H_2O]$ and $[C]$ (soot) were received from calculations. Experiments were carried out with the different fuel/air ratios (stochiometry coefficient) so in order to compare different working conditions degree of conversion to syngas dependence from energy input in the reagents was analysed. Degree of conversion to syn-gas defined as ratio of measured syn-gas amount to the maximal syn-gas amount can be achieved. Energy inputs (different types) in the system was related to $sm^3(N)$ of reagents of partial oxidation reaction. Plasma energy input was defined as a part of the power of the discharge (measured in experiment) that corresponds to the partial oxidation reagents (a part of energy heat Ar, and can't affect partial oxidation reaction, for example). Thermal energy inputs in the system – energy input from preheating of reagents and energy input from full combustion of the part of fuel (reaction with the air redundancy) also corresponds to the partial oxidation reagents. Brutto-formula of kerosene (mix of different liquid hydrocarbons) $C_{11}H_{21,7}$ was experimentally determined on mass-chromatograph FINNIGAN MAT ITD-800. Thermochemical data, used on calculations achieved from NIST [20].

Experimental results of the plasma-assisted kerosene partial oxidation are shown on Fig. 10. For the methane conversion to syn-gas the same picture can be seen. Points for curves drawing are chosen from big massive of experimental data for the best visual illustration of effect. On each of presented curves only one type of energy input in system is changed. Curve 1 is the base dependence that shows the effect from thermal energy input in system – from the full combustion of the part of fuel. These experimental points were received without discharge and with redundancy of oxidant.

Two groups of curves (2–7) have start point on the base curve 1, at this point fuel/air ratio was fixed then discharge on different types of plasma-forming gases was initiated. Curves 2 and 5 shows increase of the plasma energy input with the Ar as plasma-forming gas. Curves 3 and 6 shows increase of the plasma energy input with the air as plasma-forming gas. Curves 4 and 7 shows increase of the plasma energy input with the fuel/air mixture in full combustion stochiometry as plasma-forming gas. As it can be seen from Fig. 10 with the discharge degree of the conversion to syn-gas is higher than in case of the same amount of the thermal energy input in the system.
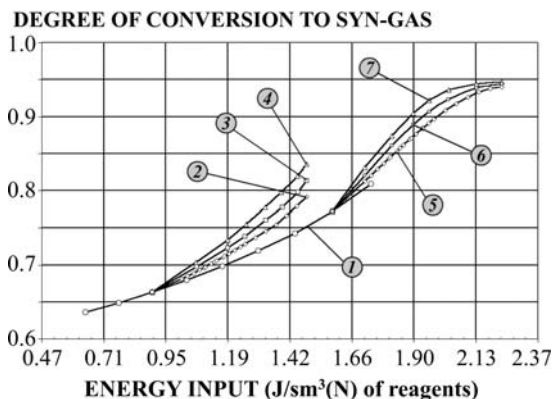
Figure 10. Experimental results of plasma-assisted kerosene reforming

For the numerical description of the effectiveness of the different types of the energy inputs on increment of the degree of conversion to syn-gas were calculated. For this calculation were used all experimental data (not only points on Fig. 10). Results of this calculation for different plasma-forming gases:

Error!= 1.35 ± 0.15 – Ar
Error!= 1.69 ± 0.15 – Air
Error!= 2.03 ± 0.15 – Fuel-air mixture

were α^* – degree of the conversion to syn-gas, $\varepsilon_{dis.}$, ε_{therm} – energy inputs from discharge and from combustion of the part of fuel correspondingly.

In case of Ar as plasma-forming gas thermal effect from plasma was realized. Nevertheless, degree of conversion to syn-gas in case of Ar plasma is higher than in case of thermal energy input by the full combustion of part of fuel. This effect can be explained in the following way. Temperature of preliminary heating of reagents was limited by ignition of reagents into heater-evaporator, so in both cases temperature of preliminary heating were the same. Fast mixing of the Ar plasma jet with the reagents lead to mixture becomes "overheated" so temperature in zone of intense reaction (front of flame) becomes higher in comparison with the case of two parallel reaction (full combustion and partial oxidation) proceed. This effect can lead to the higher degree of conversion to syn-gas.

In case of using "active" gases (air and fuel-air mixture) this thermal plasma effect is also realized. Higher degree of conversion in comparison to Ar plasma demonstrates another, chemical effect on the partial oxidation process from plasma active particles. For complete description of the effect ant the mechanism of the effect additional investigations is required.

8. Design of the Prototype of Plasma Converter

One of the main aspects of the presented work was to develop a prototype of the converter as a result of the experimental work. For the solution of this task experimental work was concentrated not only on investigation of plasma effect but also on optimization of the process and choosing optimal working conditions of the installation.

Working conditions for prototype designing was chosen between curves 4 and 7 on Fig. 10. Mixture of reagents has oxidant (air) redundancy, and power of the discharge was fixed on the level of 1 kW for using industrial magnetrons from domestic microwave ovens. Typical gas compositions in the optimal working conditions in test samples are shown on Table 1 (for kerosene conversion) and Table 2 (for methane conversion).

TABLE 1. Output gas and degree of conversion to syn-gas for kerosene partial oxidation

H_2	CO	N_2	CO_2	CH_4	C_2H_4	C_2H_2	α^*
19.9	23.0	54.6	1.0	0.6	0.1	0.8	0.84

Power of the discharge – 1 kW, syn-gas output – 7.3 m^3 (N) per hour, energy cost of the syn-gas – 0.137 kW*h/m^3

TABLE 2. Output gas and degree of conversion to syn-gas for methane partial oxidation

H_2	CO	N_2	CO_2	CH_4	C_2H_4	C_2H_2	α^*
19.9	23.0	54.6	1.0	0.6	0.1	0.8	0.84

Power of the discharge – 1 kW, syn-gas output – 7.3 m^3 (N) per hour, energy cost of the syn-gas – 0.137 kW*h/m^3

As a result of this work fully operational prototypes of plasma converter of hydrocarbons was developed (Figs. 11 and 12).

Figure 11. Fully operational prototype of plasma converter of hydrocarbons

Figure 12. Plasma converter of hydrocarbons with 0.5–5 kW (2,45 GHz) power. Productivity level about 10 standard meter cubic of syngas per hour

Productivity of the converter up to 10 $m^3(N)$ of syn-gas per hour. In the same converter methane or liquid hydrocarbons can be used as fuel for syn-gas production.

Plasma-assisted process of hydrocarbons (methane and kerosene) conversion into syn-gas was experimentally investigated.

It was shown that energy input from discharge leads to higher increase of degree of conversion to syn-gas in comparison with thermal energy input from full combustion of the part of fuel.

Results of kerosene and methane conversion into syngas in optimal working conditions were presented.

On the basis of the experimental investigations prototype of plasma converter of hydrocarbons was designed.

Conclusion

- Examples of utilization of completely different of air purification technologies are shown
- This approaches based on the different kinds of gas discharges (equilibrium and transient) and types of reactions (oxidation and reduction reactions)
- Practical application fields for these technologies were analyzed

References

[1] E.M. van Veldhuizen (Ed), Electrical discharges for environmental purposes: fundamentals and applications, NOVA Science publishers, Inc, Huntington, New York.

[2] V. Abolentsev, S. Korobtsev, D. Medvedev et al., Proceedings of Advanced Oxidation Technologies for Water and Air Remediation, London, Canada, June 25 1994, p. 70.

[3] L.S. Frost and A.V. Phelps, Phys. Rev. A (1964), Vol. 136, p. 1538.

[4] S. Yoshida, A.V. Phelpsa and L.C. Pitchford, Phys. Rev. A (1983), Vol. 27, p. 2858.

[5] I.V. Kochetov and V.G. Pevgov, in collection '*Plasmokhimicheskie processy*' (in Russian), Nauka (1979), p. 4.

[6] A.V. Phelps and L.C. Pitchford, JILA information Center report, 26 (1985).

[7] L.J. Kieffer, JILA information Center report (1973), Vol. 13, p. 139.

[8] M. Yousfi, A. Poinsignon, et al., in '*Non-thermal plasma techniques for pollution control*', NATO ASI Series, Series G., Vol. 34, Part A, p. 299.

[9] W.B. DeMore, S.P. Sander, D.M. Golden, R.F. Hampson, M.J. Kurylo, C.J. Howard, A.R. Ravishankara, C.E. Kolb, and M.J. Molina, Chemical kinetics and photochemical data for use in stratospheric modeling. Evaluation number 12 JPL Publication, pp. 97–94 (1997).

[10] D.L. Singleton, R.J. Cvetanovic, Evaluated chemical kinetic data for the reactions of atomic oxygen O(3P) with sulfur containing compounds J. Phys. Chem. Ref. Data (1988), Vol. 17, p. 1377.

[11] W.F. Cooper and J.F. Hershberger, An infrared laser study of the O(3P) + CS_2 reaction J. Phys. Chem. (1992), Vol. 96, pp. 5405–5410.

[12] W.B. DeMore, S.P. Sander, R.F. Hampson, Chemical Kinetics and Photochemical Data for Use in Stratospheric Modelling, Eval. N9, 1990. J. Phys. Chem. (1975), Vol. 79, p. 779.

[13] L. Bromberg, D.R. Cohn, and A. Rabinovich, Int. J. Hydrogen Energy (1997), Vol. 22, pp. 83–91.

[14] M. Venugopalan and S. Veprek, *Plasma Chemistry IV*, Berlin: Springer-Verlag (1983), p. 16.

[15] A. Gicquel, S. Cavadias, and J. Amouroux, J. Phys. D: App. Phys. (1986), Vol. 19, pp. 2013–2042.

[16] E. Barachnikov, G. Belensky, V. Denesenco, B. Potapkin, et al., Soviet Acad. Sci., Doklady (1990), Vol. 239, pp. 1081–1087.

[17] A. Czernichowski, T. Czech, and J. Miczeraczyk, Proc. of the First International Conference on Advances in Oxidation Technologies, London, Ontario (1995), p. 246.

[18] A. Docter and A. Lamm, Gasoline fuel cell systems. J. Power Sources (1999), Vol. 84, pp. 194–200.

[19] E.S. Shetinkov, *Physics of Gas Burning*. Moscow, 1965.

[20] NIST, http://webbook.nist.gov/chemistry/

MODEL FOR DEVELOPMENT OF ELECTRIC BREAKDOWN IN LIQUIDS AND STABILITY ANALYSIS

Y. YANG, J. ZHU, Y. CHO, A. GUTSOL, AND A. FRIDMAN
Department of Mechanical Engineering and Mechanics,
Drexel University, Philadelphia, PA, USA

Abstract: A semi-numerical model is presented for the development of electric breakdown in liquids based on nanosecond time scale. In this model, breakdown starts in the pre-existed bubble at the tip of the electrode. Formation of plasma immediately makes the surface of the bubble charged to the potential of the electrode, and the imbalance between the electrostatic force and surface tension makes the bubble elongate at high speed. Numerical estimations made using this model are in good agreement with published experimental data. Linear analysis also shows that the instability of the Rayleigh-Taylor type develops in the plasma-gaseous channel surface points with high curvature.

Keywords: Electric breakdown initiation, nanosecond, electrostatic force, surface tension, stability analysis, capillary wave

1. Introduction

There is increasing interest in the study of electric breakdown in liquids as these processes find more application in industry and academic research. For example, oil filled gaps are used for the insulation of high-voltage devices because of filling oil's higher permittivity [1]; some liquid noble gases are used in nuclear and high-energy physics for radiation detection [2]. More recently, electric breakdown is developed as a physical, non-chemical means of biofoul removal and contaminant reduction in water, with the potential for extension into a wide range of other water treatment applications [3]. In all these applications, it is important to get a better understanding of the key physical mechanisms that take place in the process.

It is generally agreed that the electrical breakdown of liquid involves the generation and growth of a bubble, or more precisely, a cavity at the tip of the electrode in a short time period [4–6]. A number of models for breakdown have been suggested based on microsecond time scale. Some propose that electron avalanche is formed in the liquid phase at the initial stage, and the bubble is generated at the cathode by local heating due to the intense electron emission or perhaps by ion current [4,6]. Others models suggest a bubble dynamic process in which an

electron avalanche develops in the vapor phase following the formation of a pre-existing bubble [5].

With the advances in image recording technique, recent studies using fast Schlieren-photography shows that the essential of electrical breakdown in liquid involves fast initiation and propagation of low-density filaments (bubbles, cavities, cracks). The breakdown starts within nanoseconds after application of high voltage, and the growth rate of the filament is up to several kilometers per second [7]. A physical intuition and some elementary estimations say that during such a short time, heating is probably not the best explanation of channel formation at the initial stage of a discharge.

The objective of this paper is to present a model for initiation and development of breakdown in liquids subjected to high voltage based on nanosecond time scale. The model is consists of two components: explanation and numerical estimations for propagation of filaments during breakdown and a stability analysis of the filaments.

2. Model

According to the bubble nucleation theory in boiling, micro-bubbles appear and disappear at the nucleation sites at the liquid-solid interface. The number of the bubbles and location depend upon the surface roughness, fluid properties and operation conditions. Surface tension that exists on the interface of a bubble crates additional pressure inside the bubble:

$$P_{in} - P_{\infty} = 2\gamma / r$$

where P_{in} is the pressure inside the bubble, P_{∞} is the ambient pressure, γ is surface tension coefficient of the liquid and r is the radius of the bubble. For water at room temperature $\gamma = 0.078$ N/m. To maintain a bubble with radius of 1 micron, the additional pressure inside would be 1.78 atm.

When high voltage is applied to the electrode, breakdown first happens in the gas phase bubbles. The direct ionization rate coefficient k_I of air in the reduced electric field E/n_0 of 10^3 V·cm^2 is in the order of 10^{-10} to 10^{-9} cm^3/s. The molecule density n_0 inside the bubble under previously estimated pressure is in the order of 10^{19} cm^{-3}. The time need for breakdown would be $(k_I n_0)^{-1}$, which is in the order of 0.1 to 1 ns. This process is fast enough to explain the initiation developed within nanoseconds observed in [7]. Electrons, due to their high mobility, will move faster and deposit on the gas-liquid interface. As a result, the interface will be charged negatively to the electrode potential. For a typical breakdown voltage $\Phi_0 = 30$ kV and electrode radius $r = 1$ mm, the electric field at the electrode tip can be estimated as $\Phi_0/r = 3\times10^7$ V/cm. This strong field will push the bubble to form the bush-like structure.

To quantify the process described above, we now define the equations for the formation and propagation of the plasma-filled filaments. Gravity is neglected here because it is very small in comparison with electric forces (see estimations

below). Because of external forcing by the electric field, the isolated system of the forming plasma channel does not conserve energy or momentum. First it is assumed that the filament is an elongated object with a rounded tip. When plasma is produced inside the bubble, the gas-liquid interface can be regarded as equi-potential with the electrode due to high plasma conductivity.
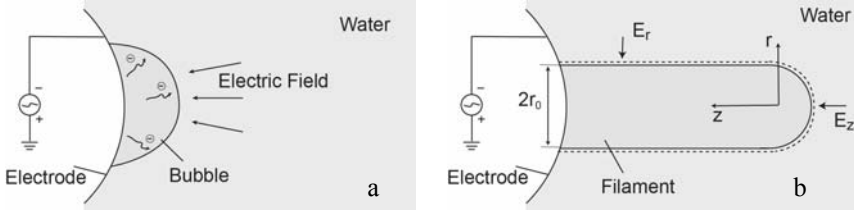
Figure 1. (a) – initial bubble form at the moment of high voltage application; (b) – bubble elongation and gaseous plasma filament formation due to interaction of electrical forces with surface tension and external pressure forces

Assume the charge density both inside and outside the filament surface can be ignored comparing with that on the filament surface. For a slender filament, apply-ing Laplace Equation in the radial direction:

$$\frac{1}{r}\frac{\partial}{\partial r}(r\frac{\partial \Phi}{\partial r}) = 0 \tag{1}$$

with boundary condition: $\Phi\big|_{r=r_0} = \Phi_0$ and $\Phi\big|_{r=R} = 0$. Φ_0 is the potential at the interface, r_0 is the radius of the filament, and R is the radius where the potential can be regarded as zero.

By solving the equation, the radial electric field E_r and local surface charge density σ can be written as:

$$E_r = \frac{\partial \Phi}{\partial r} = -\frac{\Phi_0}{r_0 \ln(R/r_0)} \tag{2}$$

$$\sigma = \varepsilon E_{r_0} = -\varepsilon \frac{\Phi_0}{r_0 \ln(R/r_0)} \tag{3}$$

where ε is permittivity of the liquid. Similarly, we can get the electric field and local charge density in the axial direction near the tip of the filament:

$$E_z = \frac{\partial \Phi}{\partial r} = -\frac{\Phi_0}{r_0} \tag{4}$$

$$\sigma = \varepsilon E_{z_0} = -\varepsilon \frac{\Phi_0}{r_0} \tag{5}$$

Since $R \gg r_0$, it is obvious that the electrostatic pressure in the axial direction is much higher than that at the radial direction, and both of them are inversely proportional to r_0^2. At the initial stage of the filament growth r_0 is usually small, which means the bubble will grow in all directions. At some point the electrostatic force will first reach balance with surface tension and ambient pressure in the

radial direction, thus keeping constant radius, while the bubble continues growing in the axial direction. Considering the force balance in the axial direction:

$$P + E_r\sigma - \gamma/r_0 = P_\infty \tag{6}$$

where P is the liquid vapor pressure inside the filament (growth of the bubble due to electric force reduces the gas pressure and vapor pressure becomes larger that the gas pressure) , γ is the surface tension of the liquid, and P_∞ is the ambient pressure. Since the liquid vapor pressure is usually small compared to P_∞, the force balance equation is reduced to

$$E_r\sigma - \gamma/r_0 = P_\infty \tag{7}$$

At the tip of the filament, the pressure caused by the axially directed electric force is

$$E_z\sigma = [\ln(R/r_0)]^2 E_r\sigma = [\ln(R/r_0)]^2(\gamma/r_0 + P_\infty) \tag{8}$$

Although it is convenient to consider the filament to be a tube with constant radius, a more realistic state for experiments thins due to the stress at the interface from the interaction between the hydrodynamic pressure on the elongating bubble and the electric force (Fig. 2). In such a 'needle' shape filament, the hydrodynamics pressure against the driving force of fast propagation is proportional to the tangent of the angle of attack. Assume the hydrodynamics pressure and surface tension is in balance with the electric pressure when the filament growth reaches maximum:

$$\frac{1}{2}\rho v_0^2 \tan\alpha = E_z\sigma_z = \varepsilon\frac{\Phi^2}{r_0^2} \tag{9}$$

where v_0 is the maximum velocity, α is the angle of attack of the growing filament, which can be estimated as $\alpha \approx r_0/L$ (L is the length of the filament). Then the maximum velocity can be written as:

$$v_0 = \frac{\Phi}{r_0}\sqrt{\frac{2\varepsilon_{water}}{\rho\tan\alpha}} \approx \frac{\Phi}{r_0}\sqrt{\frac{2\varepsilon_{water}L}{\rho r_0}} \tag{10}$$
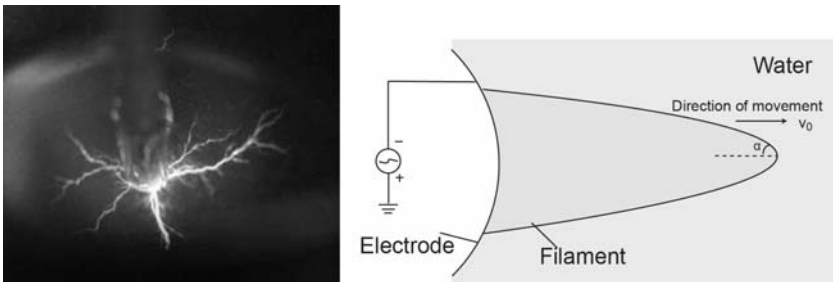
Figure 2. (a) Photo of corona discharge in water; (b) schematic diagram of needle shape filament

At the initiation state of a typical breakdown of water, the radius of the filament is in the order of 1 μ and the length is in the order of 1 mm. As shown in Fig. 3, the relation between growth rate and applied voltage can be calculated, which is in good agreement with experiment results [7] (about 3 km/s at 12 kV).
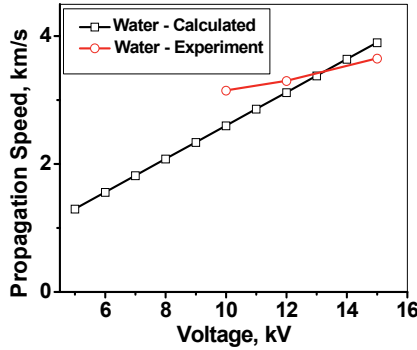
Figure 3. Comparison of calculated and measured propagation speed of filament during breakdown of water

3. Stability Analysis

Now we discuss the linear stability analysis of axisymmetric perturbation of a filament surface that is based on the method used in the papers [8]. Assume a small wave-like disturbance occurred at the surface of cylindrical bubble with initial radius r_0, as shown in Fig. 4. The peak-to-peak amplitude and wave number
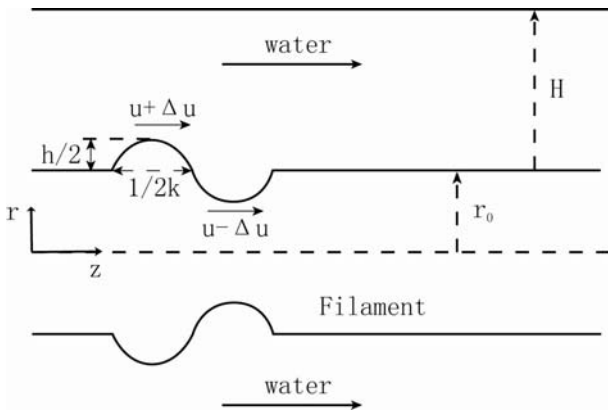
Figure 4. Schematic diagram of disturbance at the surface of filament

of the disturbance is h and k, respectively. H is the depth of wave influence [9], u is the velocity of liquid relative to the disturbance. Then surface of the perturbation is represented by

$$r = r_0 + \frac{h}{2}\exp(ikz + iwt) \tag{11}$$

With the perturbation, the local electrostatic force, surface tension and hydrodynamic pressure will be changed. Generally, the surface tension tends to minimize the surface area and subsequently stabilize the disturbance, while the electrostatic force tends to push the disturbance to grow. In the reference frame that moves together with the disturbance, the effects of these three forces are considered separately, and summed up when it comes to pressure balance between the crest and trough along the stream line.

3.1. ELECTROSTATIC PRESSURE

According to the Equations (2) and (3) from part II, the electrostatic pressure is proportional to the square of local curvature of the interface, which is different at the crest and trough of the perturbation:

$$p_{E,c} = \varepsilon\phi_0^2 \frac{M_c^2}{4} \tag{12}$$

$$p_{E,t} = \varepsilon\phi_0^2 \frac{M_t^2}{4} \tag{13}$$

where $p_{E,c}$ and $p_{E,t}$ is the electrostatic pressure at crest and trough respectively, M_c and M_t is the mean curvature at the crest and trough respectively. The mathematical expression for the mean curvature can be written as [10]:

$$M = \left(\frac{1}{r\sqrt{1+(\partial_z r)^2}} - \frac{\partial_z(\partial_z r)}{(1+(\partial_z r)^2)^{1.5}}\right) = \frac{1}{r} - \partial_z \partial_z r \tag{14}$$

Plug Equation (11) into Equation (14), we can get expressions for M_c and M_t:

$$M_c = \frac{1}{r_0 + \dfrac{h}{2}} + \frac{h}{2}k^2 \tag{15}$$

$$M_t = \frac{1}{r_0 - \dfrac{h}{2}} - \frac{h}{2}k^2 \tag{16}$$

Subsequently, $p_{E,c}$ and $p_{E,t}$ can be written as:

$$p_{E,c} = \varepsilon\phi_0^2 \frac{M_c^2}{4} = \varepsilon\phi_0^2 \frac{1}{4}\left(\frac{1}{(r_0 + \frac{h}{2})^2} + \frac{hk^2}{r_0 + \frac{h}{2}}\right) \qquad (17)$$

$$p_{E,t} = \varepsilon\phi_0^2 \frac{M_t^2}{4} = \varepsilon\phi_0^2 \frac{1}{4}\left(\frac{1}{(r_0 - \frac{h}{2})^2} - \frac{hk^2}{r_0 - \frac{h}{2}}\right) \qquad (18)$$

So the electrostatic pressure difference between the crest and trough is:

$$\Delta p_E = -\frac{\varepsilon\phi_0^2 h}{2r_0^3} + \frac{\varepsilon\phi_0^2 hk^2}{2r_0} \qquad (19)$$

3.2. STATIC PRESSURE – SURFACE TENSION

Similarly, the surface tension across the interface at the crest and trough can be written as:

$$p_{T,t} = \gamma M_t = \frac{\gamma}{r_0 - \frac{h}{2}} - \frac{h\gamma}{2}k^2 \qquad (20)$$

$$p_{T,c} = \gamma M_c = \frac{\gamma}{r_0 + \frac{h}{2}} + \frac{h\gamma}{2}k^2 \qquad (21)$$

Then the surface tension difference between the cress and trough is:

$$\Delta p_T = \frac{\gamma h}{r_0^2} - \gamma hk^2 \qquad (22)$$

3.3. HYDRODYNAMIC PRESSURE

When there is disturbance on the interface of the filament, the flow speed of liquid will be perturbed in the depth of wave influence, inducing a dynamic pressure difference between the crest and trough:

$$\Delta p_3 = \frac{1}{2}\rho(u + \frac{\Delta u}{2})^2 - \frac{1}{2}\rho(u - \frac{\Delta u}{2})^2 = \rho u\Delta u \qquad (23)$$

The dynamic pressure is related to the flow speed through Bernoulli's equation. The pressure difference from the electrostatic force and dynamic effect of the flow has the opposite sign from that due to surface tension. For a balance between two kinds of oppositely directed pressure differences we have:

$$\rho u \Delta u + (-\frac{\varepsilon \phi_0^2 h}{2r_0^3} + \frac{\varepsilon \phi_0^2 hk^2}{2r_0} + \frac{\gamma h}{r_0^2} - \gamma hk^2) = 0 \qquad (24)$$

Following the steps described in [8] to eliminate Δu, it is easy to get:

$$\rho w^2 = (\gamma - \frac{\varepsilon \phi_0^2}{2r_0})(k^2 - \frac{1}{r_0^2})k \qquad (25)$$

As we described previously, w is the oscillation frequency of the disturbance and it is complex. From Equation (11) it is clear that if the imaginary part of the complex w is not zero, the disturbance will grow exponentially with time. Since the difference between static pressure due to surface tension at the crest is less than that at the trough, it is possible to conclude that $1/k \ll r_0$. The same conclusion can be reached from the small perturbation assumption, and therefore the second factor in the Equation (25) will always be positive. Once the liquid is fixed, the surface tension γ and permittivity ε are constant, so the stability will depend on the applied voltage and radius of the filament. When the voltage exceeds some critical value, w^2 will be negative and the disturbance becomes instable. Another possibility is when the filament radius reduces to certain value, which happens during the propagation, the instability becomes the dominant process and the single filament begins to grow into the bush-like pattern. When the radius goes to infinity, the equation reduces to $\rho w^2 = \gamma k$, which is the formula for classic capillary wave.

Conclusion

The electric breakdown of liquids involves the generation and propagation of vapor-plasma channels through the liquids. The Semi-numerical model described in this paper explains the dynamics of initiation of pulsed electric breakdown in liquids based on nanosecond time scale. Assuming there are pre-existing bubbles at the tip of the electrode, breakdown will first occur inside the bubble in gaseous phase and make the gas-liquid interface equipotential to the electrode. Then the plasma bubble (streamer) will elongate in the axial direction because of imbalance of electrostatic force and surface tension. The estimated streamer velocity is in a good agreement with published experimental results. Linear stability analysis showed that the branching of the filaments can be attributed to the Rayleigh-Taylor type instability, which develops in the plasma-gaseous channel surface points with high curvature.

References

[1] M. Zahn, Y. Ohki and D. B. Fenneman et al., "Dielectric properties of water and water/ethylene glycol mixtures for use in pulsed power system design", Proceedings of the IEEE, Vol. 74, 1986, pp. 1182–221

[2] E. Aprile, W. H-M. Ku and I. Park, "Delta electron production and the ultimate energy resolution of liquid argon ionization detectors", IEEE Transactions on Nuclear Science, Vol. 35, 1988, pp. 37–41

[3] M. Laroussi, "Nonthermal decontamination of biological media by atmospheric-pressure plasmas: review, analysis, and prospects", IEEE Transactions on Plasma Science, Vol. 30(4), 2002, pp. 1409–1415

[4] A. Beroual, "Electronic and Gaseous Processes in the Prebreakdown Phenomena of Dielectric Liquids", Journal of Applied Physics, Vol. 73, 1993, pp. 4528–4533

[5] H. M. Jones and E. S. Kunhardt, "Development of Pulsed Dielectric Breakdown in Liquids", Journal of Physics D.: Applied Physics, Vol. 28, 1995, pp. 178–188

[6] H. Yamashita, K. Yamazawa, W. Machidori and Y. S. Wang, "The effect of tip curvature on the prebreakdown density change streamer in cyclo-hexane", 1996 IEEE 12th International Conference on Conduction and Breakdown in Dielectric Liquids, 1996, pp. 226–229

[7] W. An, K. Baumung and H. Bluhm, "Investigation of pulsed corona discharges in water by fast imaging diagnostics", presented at 32nd International Conference on Plasma Science Conference, Monterey, CA, June 20–23, 2005

[8] K. E. Kenyon, "Capillary Waves Understood by an Elementary Method", Journal of Oceanography, Vol. 54, 1997, p. 343

[9] K. E. Kenyon, "On the Depth of Wave Influence", Journal of Physical Oceanography, Vol. 13, 1983, pp. 1968–1970

[10] J. Eggers, "Nonlinear Dynamics and Breakup of Free-Surface Flows", Reviews of Modern Physics, Vol. 69, 1997, pp. 865–930

SIMULATION OF ATMOSPHERIC PRESSURE NON-THERMAL PLASMA DISCHARGES FOR SURFACE DECONTAMINATION APPLICATIONS

T. FAROUK, B. FAROUK, A. GUTSOL, AND A. FRIDMAN
Department of Mechanical Engineering and Mechanics
Drexel University, Philadelphia PA 19104, USA

Abstract: Numerical simulations are conducted to characterize atmospheric pressure plasma discharges for surface decontamination applications. A self consistent two-dimensional hybrid model is developed to simulate the atmospheric pressure radio frequency (RF) plasma discharges in helium-oxygen mixtures. Numerical simulations are carried out for the plasma generated between an annulus electrode configuration with gas flow in between the electrodes and a surface to be decontaminated in front of the plasma afterglow. Basic plasma properties such as electron number density, radical, ion and excited species number densities, gas temperature, electric field and electron temperature are studied. The simulations indicated the discharge to operate in the α mode at low power. In the α mode the discharge was found to be uniform and volume dominated. At high power the discharge was found to transition to γ mode, with peak ionic species near the electrode surfaces. The discharge was also found to constrict in the axial direction. In both the modes He_2^*, O, O_2 ($^1\Delta_g$) and O_3 were the dominant species in the after glow of the discharge. O, O_2 ($^1\Delta_g$) and O_3 are key species for surface decontamination. Peak gas temperature predictions indicate the discharge to be a non-thermal non-equilibrium discharge. However the peak temperature of the discharge while in the γ mode was ~150 K higher than that at the α mode.

Keywords: Atmospheric pressure, plasma jet, decontamination, hybrid model

1. Introduction

Over the past two decades, there has been considerable interest in applying non-thermal plasmas to hazardous, chemical destruction, pollution control, surface decontamination and sterilization [1–8]. Several different kinds of atmospheric pressure plasma sources have been employed for this purpose which include gliding arc [1], pulsed negative and positive corona [2], pulsed dielectric barrier discharges (DBD) [7], resistive barrier discharges [5] and atmospheric pressure plasma jet [4]. Operating in atmospheric pressure provides operation flexibility

due to the removal of the vacuum systems. Furthermore, higher reaction rate and continuous process makes it more advantageous than its low pressure counter part.

Experimental studies of decontamination using atmospheric pressure non-thermal plasmas have been conducted by several researchers [2,4,5,7,9]. The experimental studies involved in identifying the key dominant species in the plasma discharge and hypothesizing the mechanism responsible for decontamination. Thiyagrajan et al. [5] developed an atmospheric pressure resistive barrier discharge and used for biological decontamination. They carried out detailed electrical, chemical, optical and biological studies of the discharge. Their experimental studies indicated overwhelming amount of ozone and negligible amount of NO_2 and ultra violet (UV) light present in the discharge. A pulsed DBD with coaxial electrode configuration was developed by Laroussi and Lu [7]. Copper ring electrodes attached to a cylindrical glass tube was used as their electrode configuration and helium was used as the carrier gas. Their measurements identified the presence of excited nitrogen and helium, nitrogen ions, atomic oxygen and hydroxyl radicals. Hermann et al. [4] used an atmospheric pressure plasma jet (APPJ) and conducted experiments on decontamination of chemical and biological warfare agents. They used helium-oxygen mixture as the carrier gas and treated *Bacillus globigii* as a surrogate for *Bacillus anthracis*. Their experiments showed a 4.5 s decimal reduction value of the spore population with plasma exposure. They drew a comparison of the decontamination efficiency of APPJ with other plasma sources and concluded that APPJ was more efficient because of its high power. Despite all the experimental works there has not been any detailed modeling of plasma surface decontamination. Numerical simulations can provide insight into the physico-chemical processes occurring in the discharge and thereby help identify the dominant species responsible for the decontamination.

In this work we present preliminary results from a hybrid model to simulate a RF atmospheric pressure plasma jet in helium-oxygen mixture. The model contains detailed volume chemistry and would provide insight into the parameters that affect the decontamination process.

2.   Mathematical Model

The model developed consists of the momentum and energy conservation for the multi-component gas mixture, and continuity equations for each component of the mixture (electrons, ions, radicals and neutrals). The species considered include 4 neutral species (He, O_2, O and O_3), 6 ionic species (He^+, He_2^+, O^+, O_2^+, O^- and O_2^-), 3 electronically excited species (He^*, He_2^* and $O_2(^1\Delta_g)$) and electrons. These species were identified from the dominant reaction chemistry of helium – oxygen plasma in atmospheric pressure and the reaction rates were obtained from the literature [10–12]. The electron transport coefficients (mobility μ_e and diffusion D_e) and rates of the electron induced reactions, are calculated using the electron energy distribution function (EEDF) obtained as a solution of the Boltzmann equation using the two-term spherical harmonic expansion (SHE). In order to simplify the

numerical efforts, a modified local-field approximation was employed in the present work. In this approximation, the EEDF is calculated for different values of the reduced electric field (E/N) and electron number density (n_e). Two-dimensional look-up tables for electron transport coefficients and reaction rates are produced this way. These look-up tables are prepared first and used for the present plasma calculations instead of running the numerically expensive Boltzmann solver simultaneously with the discharge simulation model. In the present model the electron energy balance equation is solved to accurately resolve the sheath region and take into account the non-local effects induced by electron thermal conduction. In this work, the plasma is simulated using an advanced version of the CFD-ACE+ [13] code and the external circuit is simulated using a general purpose circuit simulator, SPICE [14]. The transport of the charged and neutral particles and the electric field are solved by the CFD-ACE+ solving the PDE's. This solver provides currents to electrodes for a given potential at the electrodes. This current data is used to run the SPICE code and the voltage at the electrodes is recalculated by solving the ordinary differential equations for the external circuit. For each step, the overall solution is iterated until the convergence of current/voltage is reached.

3. Schematic of the Problem Geometry

Schematic of the atmospheric pressure plasma jet is shown in Fig. 1(a). The computational domain has an annulus electrode configuration. The inner and outer electrode have a radius of 0.5 and 0.6 cm respectively; an inter-electrode separation of 0.1 cm. The substrate to be treated is located 0.5 cm away from the electrodes. The length of the substrate was chosen to be 2.0 cm. The inner electrode was powered and the outer electrode was grounded and they were coupled to an external circuit (Fig. 1b). The external circuit contains a ballast resistance R and a capacitance C_P. The ballast resistance and the capacitance are connected to the power supply in series and in parallel respectively. The ballast resistance is necessary to limit the discharge current. The capacitance C_P is present intrinsically due to the external cables, which is known as the parasitic capacitance.
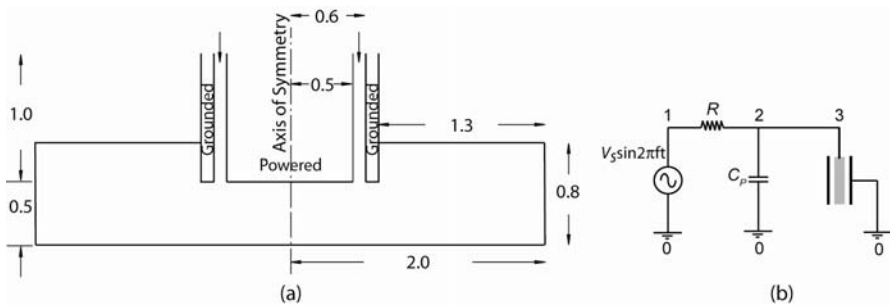
Figure 1. Schematic of the (a) computational domain (all dimensions are in cm) and (b) external circuit (the numbers denote the different nodes in the circuit)

4. Results and Discussion

In the simulations the supply voltage amplitude was fixed at 1,000 V, the driving frequency was held constant at 13.56 MHz, the capacitance was fixed at 0.1 pF and the ballast resistance was varied from 5 to 2 kΩ. For the gas mixture the inlet velocity was fixed at 5.0 m s^{-1} and the oxygen mass fraction was varied from 1–4%. We report results from two of our cases, ballast resistance 5 kΩ and 2 kΩ with 1% oxygen mass fraction. For a ballast resistance of 5 kΩ a rms discharge voltage 221.91 V, rms discharge current of 96.89 mA and rms power of 17.79 W was obtained. Figure 2 shows the velocity vector plot in the entire domain for a ballast resistance of 5 kΩ. It can be seen that the gas mixture attains a fully developed flow within a very short distance. Once fully developed the velocity has a Poiseuille like profile, with a maximum velocity at the center. The gas flow attains a peak gas velocity of ~8 m s^{-1} once it leaves the inter-electrode spacing. The Reynolds number is ~60, satisfying the assumption of laminar flow. The gas mixture leaves the domain through the sides, which is much clear in the streamline patterns (Fig. 3). In Fig. 3 it is shown that the flow creates two counter rotating vortices. One vortex is found to form at the end of inner powered electrode, creating a recirculation zone. This would result in a decrease in the effluent species in that region, creating a non-uniform distribution of the active species. The other vortex is formed near the top exit. These vortices are formed due to the annulus inter-electrode configuration.
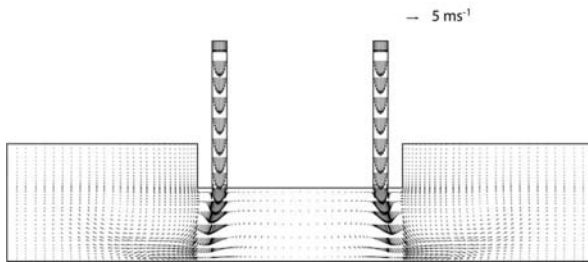
Figure 2. Velocity vector plot (5 kΩ ballast resistance, 1% O_2. $V_{d\ rms}$ = 221.91 V, $I_{d\ rms}$ = 96.89 mA, P_{rms} = 17.79 W, Current density = 30.84 mA cm^{-2} (rms), Power density = 5.66 W cm^{-2} (rms))
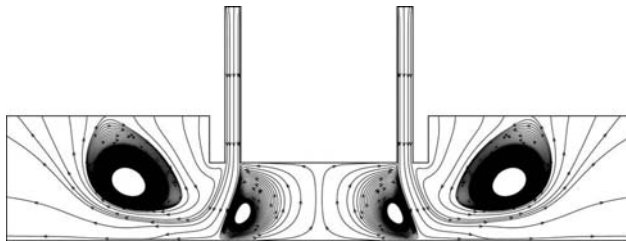
Figure 3. Streamline patterns (5 kΩ ballast resistance, 1% O_2. $V_{d\ rms}$ = 221.91 V, $I_{d\ rms}$ = 96.89 mA, P_{rms} = 17.79 W, Current density = 30.84 mA cm^{-2} (rms), Power density = 5.66 W cm^{-2} (rms))

Neutral gas temperature for the same case is shown in Fig. 4. A peak gas temperature of 352 K was obtained, an increase of 52 K from the ambient. The presence of helium and gas flow provides cooling of the discharge. The predicted gas temperature indicates the discharge to be non-thermal. Near the substrate a peak gas temperature of ~318 K was found. This cancels out the possibility of having thermal damage to the substrate. The rise in the gas temperature also explains the fact of increased gas velocity at the end of the inter-electrode spacing.

Figures 5, and 6 show the time averaged O and O_3 number density contour for a 5 kΩ ballast resistance. A peak O number density of ~9 × 10^{20} m^{-3} and ~2 × 10^{20} is predicted in the plasma volume and in the plasma after glow respectively. Similar trends were observed for O_3. In the after glow of the discharge a peak O_3 of ~1.1 × 10^{19} m^{-3} is predicted. The decrease of O at the substrate is due to the surface quenching reactions. An artificial destruction term of O having a sticking coefficient of unity was provided at the substrate. This would simulate an idealized case of O being used for surface decontamination purpose. This was necessary since no surface reaction rate constant for atomic oxygen O and surface interaction was available in the literature. For the O_3 species an insulated boundary condition was provided. These long lived active species (O and O_3) are the key components for surface decontamination [5,7]. The predicted number density indicated sufficient amount of these species available for surface decontamination purpose. It is
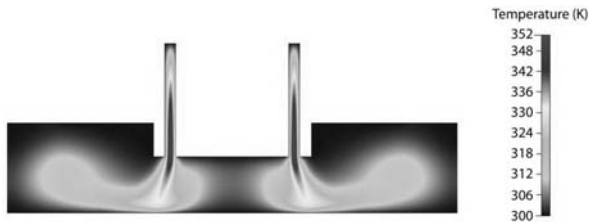
Figure 4. Neutral gas temperature contours (5 kΩ ballast resistance, 1% O_2. $V_{d\ rms}$ = 221.91 V, $I_{d\ rms}$ = 96.89 mA, P_{rms} = 17.79 W, Current density = 30.84 mA cm^{-2} (rms), Power density = 5.66 W cm^{-2} (rms))
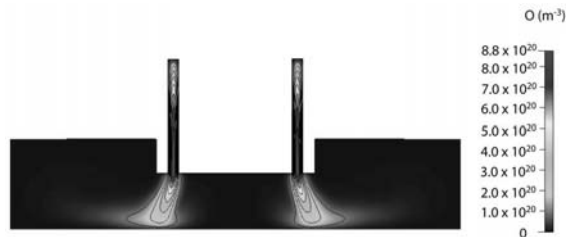

Figure 5. Time averaged O number density contours (5 kΩ ballast resistance, 1% O_2. $V_{d\ rms}$ = 221.91 V, $I_{d\ rms}$ = 96.89 mA, P_{rms} = 17.79 W, Current density = 30.84 mA cm^{-2} (rms), Power density = 5.66 W cm^{-2} (rms))
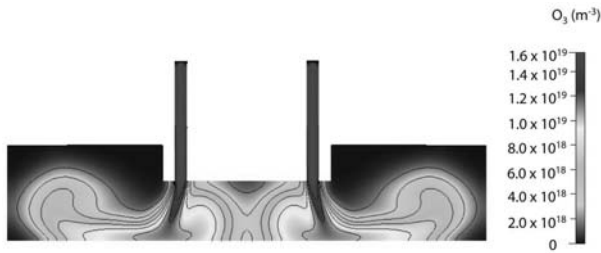
Figure 6. Time averaged O_3 number density contours (5 kΩ ballast resistance, 1% O_2. $V_{d\ rms}$ = 221.91 V, $I_{d\ rms}$ = 96.89 mA, P_{rms} = 17.79 W, Current density = 30.84 mA cm^{-2} (rms), Power density = 5.66 W cm^{-2} (rms))

clearly evident that the central region of the substrate (opposite to the powered electrode) has very little active species present this is due to the recirculation zone present there. This is more clearly depicted in Fig. 8a where the distribution of these long lived active species along the substrate length is shown.

Time averaged ion and electron number density profiles along the radial distance at x = 5.5 mm is represented in Fig. 7. It was found that of the different ionic species O_2^+ is the dominant positive ion with a peak number density of ~4 × 10^{17} m^{-3}. The dominant negative ion was found to be O_2^- with a peak number density of ~3 × 10^{17} m^{-3}. The predicted peak He_2^+ and He^+ number density were ~3 × 10^{16} m^{-3} and 4 × 10^{12} m^{-3} respectively. These are smaller by one and five orders of magnitude than that of O_2^+. The smaller He^+ and He_2^+ number density is because of the high ionization potential of helium compared to that of oxygen. All the ionic species density profile show a dome like shape with the peaks located in the central region of the discharge, indicating a volume dominated discharge phenomenon. This characteristics is typical of a α mode discharge [15]. However the profiles show a shift in the peak towards the inner electrode because of the self bias initiated due to size difference in the electrode surfaces. The total
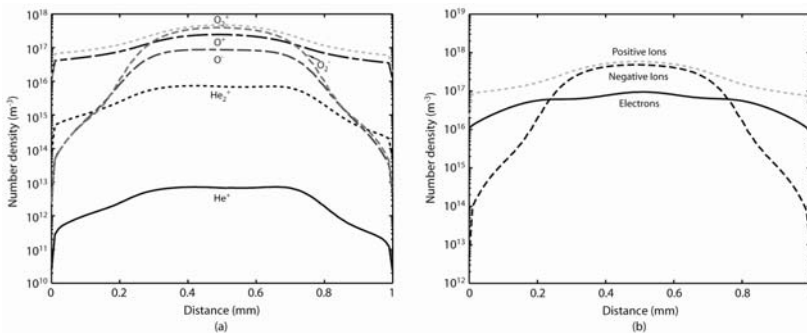
Figure 7. Time averaged (a) ion number density (b) positive ions ($He^+ + He_2^+ + O^+ + O_2^+$), negative ions ($O^- + O_2^-$) and electron number density along the radial distance at x = 5.5 mm. (5 kΩ ballast resistance, 1% O_2. $V_{d\ rms}$ = 221.91 V, $I_{d\ rms}$ = 96.89 mA, P_{rms} = 17.79 W, Current density = 30.84 mA cm^{-2} (rms), Power density = 5.66 W cm^{-2} (rms))

positive ions, negative ions and electron number density profile are shown in Fig. 7b. The discharge is found to be dominated by negative ions instead of electrons. The peak electron number density is smaller by an order of magnitude than that of the negative ions. The existence of higher negative ions is due to higher attachment rates of electrons with O_2 and O.

Figure 8a represents the long lived active species He_2^*, O_2 ($^1\Delta_g$) and O along the length of the substrate. The central region of the substrate is found to have significantly less amount of active species. This is due to the presence of the vortex in that region. The species have a peak number density at a distance of 6 mm from the center which is the location of the jet impingement. He_2^*, O_2 ($^1\Delta_g$) and O number density profile along the axial distance at a fixed radial distance of 5.5 mm is shown in Fig. 8b. All the long lived active species are observed to reach a peak value at 10 mm (end of the plasma domain). In the afterglow the species number density are found to decrease. A sharp decrease near the surface is due to the surface quenching reactions.

Neutral gas temperature contours for a 2 kΩ ballast resistance and 1% oxygen mass fraction is presented in Fig. 9. For a ballast resistance of 2 kΩ, the simulation predicted a rms voltage, current and power of 272.1 V, 234.2 mA and 52.1 W
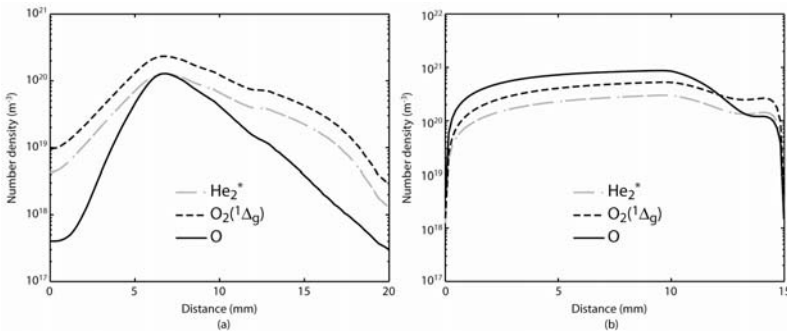
Figure 8. (a) Time averaged He_2^*, O_2 ($^1\Delta_g$) and O number density along the radial distance at x = 15 mm. (b) Time averaged He_2^*, O_2 ($^1\Delta_g$) and O number density along the axial distance at r = 5.5 mm. (5 kΩ ballast resistance, 1% O_2. $V_{d\,rms}$ = 221.91 V, $I_{d\,rms}$ = 96.89 mA, P_{rms} = 17.79 W, Current density = 30.84 mA cm^{-2} (rms), Power density = 5.66 W cm^{-2} (rms))
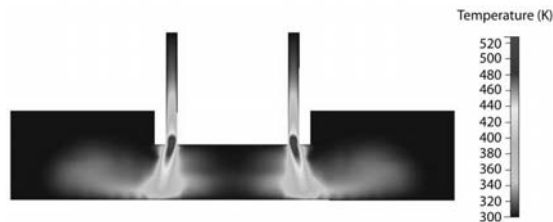
Figure 9. Neutral gas temperature contours (2 kΩ ballast resistance, 1% O_2. $V_{d\,rms}$ = 272.1 V, $I_{d\,rms}$ = 234.32 mA, P_{rms} = 52.1 W, Current density = 74.58 mA cm^{-2} (rms), Power density = 16.58 W cm^{-2} (rms))

respectively. The peak neutral gas temperature for this high power was predicted to ~524 K, higher by 224 K from the ambient. This indicates significant gas heating even with the presence of helium and fast gas flow. The peak gas temperature was located near the edge of the electrodes. Compared to the low power α mode discharge the peak gas temperature was higher by 172 K. Near the substrate surface the gas temperature was observed to be ~410 K.

Comparing with the low power α mode discharge the time averaged peak O number density at high power was found to be ~9.5×10^{21} m^{-3}. The peak O was larger by an order of magnitude than that of the α mode discharge. However the peak O_3 was found to be ~2.7×10^{17} m^{-3}, which is smaller by two orders of magnitude. The decrease in the O_3 number density is due to high gas temperature observed. Since the high power discharge is significantly hotter and the major O_3 production mechanism ($O + 2O_2 \rightarrow O_3 + O_2$) having a very sensitivity on gas temperature [11], the O_3 concentration is found to decrease. The time averaged He* monomer number density for both the cases (5 and 2 kΩ ballast resistance) is shown in Fig. 10. Since the electronically excited He* monomer is responsible for the brightness of the discharge, the He* number density contours describe the visual appearance of the discharge. At low power He* number density contours indicate a luminous zone in the central region of the discharge. This appearance is similar to an α mode discharge [15], where the discharge is volume dominated. At high power a constriction of the discharge is observed. The distribution of He* further predicts two bright luminous regions near the electrode surface and a lesser bright region in the center. The bright region near the electrode surfaces is typical of a γ mode discharge [15].
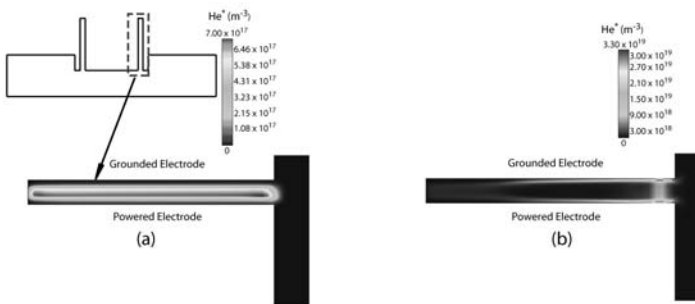
Figure 10. Time averaged He* number density contours (a) 5 kΩ ballast resistance (V$_{d\,rms}$ = 221.91 V, I$_{d\,rms}$ = 96.89 mA, P$_{rms}$ = 17.79 W), (b) 2 kΩ (V$_{d\,rms}$ = 272.1 V, I$_{d\,rms}$ = 234.32 mA, P$_{rms}$ = 52.1 W)

The ion density profiles (Fig. 11a) show high production rates of the ions near the electrode surfaces in the sheath region. The dominant positive ion was found to be O_2^+ with a peak number density of ~10^{19} m^{-3}, larger by two orders of magnitude than the α mode discharge. A significant increase in the He$_2^+$ and He$^+$ number density were also observed. The peak He$_2^+$ and He$^+$ number density were larger by

3 and 4 orders of magnitude than that of the α mode. The higher He_2^+ and He^+ number density is a result of the high electric field. The peak electric field in the γ mode was found to be ~25 kV cm^{-1}. The ion density profiles also indicates a transition from a volume dominated (α mode) to a sheath dominated discharge (γ mode). In the γ mode the electron number density was found to be significantly higher than that of the negative ions. Smaller sheath sizes (68 μm) and higher current density (74.58 mA cm^{-2} (rms)) in the γ mode makes secondary electron emission due to ion bombardment important. The electron number density increase in the γ mode is an effect of the secondary electron emission.
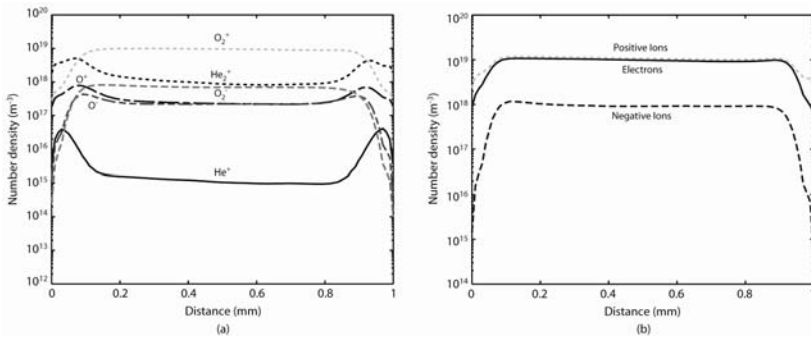
Figure 11. (a) Time averaged ion number density (b) Time averaged positive ions (He^+ + He_2^+ + O^+ + O_2^+), negative ions (O^- + O_2^-) and electron number density along the radial distance at x = 9.4 mm. (2 kΩ ballast resistance, 1% O_2. $V_{d\,rms}$ = 272.1 V, $I_{d\,rms}$ = 234.32 mA, P_{rms} = 52.1 W, Current density = 74.58 mA cm^{-2} (rms), Power density = 16.58 W cm^{-2} (rms))

Conclusion

A hybrid model has been developed to simulate an atmospheric pressure plasma jet for surface decontamination applications. The model has an extensive volume chemistry involving 47 reaction step and 14 species. The predicted dominant species in the after glow of the discharge were O, O_2 ($^1\Delta_g$), O_3 and He_2^* which are the key species responsible for surface decontamination. A non uniform distribution of the active species on the substrate surface was predicted. It was identified that the vortex formed due to the gas flow created this non uniformity. At low power the simulations indicated the discharge to operate in the α mode (volume dominated). At high power a transition was observed in the operation mode. The discharge was found to transition from $\alpha - \gamma$ mode. While operating in the γ mode the discharge constricted in the axial direction and lost its uniformity. The He^* monomer number density distribution depicted the discharge to have bright luminous regions near the electrode surfaces. The gas temperature in the γ mode was also found to be sufficiently higher, making it unsuitable for bio-sterilization and bio-decontamination applications.

References

[1]   Indarto, A.; Yang, D.; Azhari, C.; Mohtar, W.; Choi, J.; Lee, H.; Song, H., Advanced VOCs decomposition methode by gliding arc plasma. *Chemical Engineering Journal* **2007**, *131*, 337–341.

[2]   Masuda, S.; Nakao, H., Control of NOx by positive and negative pulsed corona discharges. *IEEE Trans. Ind. Appl.* **1990**, *36*, 374–383.

[3]   Rosocha, L.; Korzekwa, R., Advances oxidation and reduction processes in the gas phase using nonthermal plasmas. *Journal Advances Oxidation Technologies* **1999**, *4*, 247–264.

[4]   Herrmann, H. W.; Henins, I.; Park, J.; Selwyn, G. S., Decontamination of chemical and biological warfare (CBW) agents using an atmospheric pressure plasma jet (APPJ). *Physics of Plasmas* **1999**, *6*, 2284–2289.

[5]   Thiyagarajan, M.; Alexeff, I.; Parameswaran, S.; Beebe, S., Atmospheric pressure resistive barrier cold plasma for biological decontamination. *IEEE Transactions on Plasma Science* **2005**, *33*, 322–323.

[6]   Laroussi, M., Nonthermal decontamination of biological media by atmospheric pressure plasmas: Review, Analysis and Prospects. *IEEE Transactions on Plasma Science* **2002**, *30*, 1409–1415.

[7]   Laroussi, M.; Lu, X., Room-temperature atmospheric pressure plasma plume for biomedical applications. *Applied Physics Letters* **2005**, *87*, 113901–113903.

[8]   Birimingham, J.; Hammerstrom, D., Bacterial decontamination using ambient pressure nonthermal discharges. *IEEE Transactions on Plasma Science* **2000**, *28*, 51–55.

[9]   Vaze, N.; Gallagher, M.; Vasilets, V.; Anandan, S.; Gutsol, A.; Miovanova, T.; Fridman, A., In *18th International Conference on Plasma Chemistry*: Kyoto, Japan, 2007.

[10] Stadler, K.; Vidmar, R.; Nersisyan, G.; Graham, W., Modeling the chemical kinetics of high pressure glow discharges in mixtures of helium with real air. *Journal of Applied Physics* **2006**, *99*, 1–8.

[11] Herron, T.; Green, D., Chemical kinetics database and predictive schemes for non-thermal humid air plasma chemistry. Part II Neutral species reactions. *Plasma Chemistry and Plasma Processing* **2001**, *21*, 459–481.

[12] Jeong, J.; Park, J.; Henins, I.; Babayan, S.; Tu, V.; Selwyn, G.; Ding, G.; Hicks, R., Reaction chemistry in the afterglow of an oxygen-helium atmospheric pressure plasma. *Journal of Physical Chemistry A* **2000**, *104*, 8027–8032.

[13] CFDResearchCorporation.; ESI US R&D Inc: Huntsville, **2003**.

[14] Johnson, B.; Quarles, T.; Newton, A.; Pederson, D.; Sangiovanni - Vincentelli, A.; Wayne, C., University of Califronia Press: Berkeley, **1991**.

[15] Yang, X.; Moravej, M.; Nowling, G. R.; Babayan, S. E.; Panelon, J.; Chang, J. P.; Hicks, R. F., Comparison of an atmospheric pressure, radio-frequency discharge operating in the a and g modes. *Plasma Sources Science and Technology* **2005**, *14*, 314–320.

DETECTION OF SOLAR PLASMA INFLUENCE ON THE SATELLITE CHANNEL OF COMMUNICATION

K. A. KARIMOV AND R. D. GAINUTDINOVA
Institute of Physics of National Academy of Sciences
Chui Prosp., 265-A, Bishkek, 720071 Kyrgyz Republic

Abstract: Some applications on use of the solar plasma data and solar flare activity for investigation of their influence on the quality of telecommunication are discussed. The practical result of the above-stated researches is reduced to development of warning measures from negative consequences of high levels of solar activity for telecommunication.

The researches are carried out with the purpose of definition of correlation between solar flare activity and signal in the satellite channel of communication in academic Internet network Aknet. The results of joint analysis of changes of solar and geomagnetic activity, and also data on conditions of passage of telecommunication satellite signal are presented. For the analysis the interval of measurements of noise in the telecommunication channel and level of solar flare activity and X-ray radiation was used.

Is shown, that during solar flares accompanying with emission solar coronal substance and X-ray radiation, occurs the short increase of mistakes level of a signal connected with sharp increase of noise of the satellite channel of communication. Short-term increase of mistakes level of signal from the satellite channel is connected with sharp increase of noise level of the satellite channel of communication after solar flares accompanied with emission of coronal matters and result in increase of geomagnetic activity.

The received data can be used in the diagnosis and forecast of noise level in the satellite channel of communication.

Keywords: Solar plasma, solar flare, satellite, telecommunication, magnetosphere, radiowaves, heliogeophysical activity, geomagnetic storm, noise level

1. Introduction

In the satellite channel of communication there is a number of mistakes in reception of a signal from the satellite caused by the various reasons. These mistakes connected with instrument errors, passage of signal in space, ionosphere and atmosphere, solar interference, etc. During solar interference, which is observed close to the periods of spring and autumn equinoxes, the Sun, satellite of

communication and the reception aerials on the Earth are on one line. In these periods power of the direct intensive solar radiation is considerably higher than power of signals from the satellite and the reception of useful signal on the Earth becomes impossible. In this period it is necessary to use communication with another satellite which has been not located on one line with the Sun and reception aerials on the Earth.

The purpose of this investigations development of measures of warning negative consequences for telecommunication from influence of high levels of solar activity.

The data on solar activity and geomagnetic disturbances are used for researches of their influence on quality of telecommunication connection: parameters of solar flare activity; index of geomagnetic activity; characteristic of a signal in the satellite channel of communication.

2.   The Main Results

The mistakes at reception of signal from the satellite are as follows: instrumental errors, conditions of signal propagation in space and terrestrial atmosphere, solar interference, heliogeophysical activity. Among of existing mistakes in transfer of information signal in the satellite channel we shall analyze only one class of mistakes connected with solar flair activity.

Let's consider its influence on conditions of passage of signal in a centimetric range from the geostationary communication satellite [1, 2]. Monitoring of variations of conditions of satellite signal propagation was carried out for the period since May till August, 2004 and in April, 2006. These data were analyzed together with solar radiation parameters with the purpose of definition of correlation between solar flair activity and signal in the satellite channel.

The academic Internet network (Aknet) in Bishkek used the satellite "Express-6" for transfer and reception of signal from the satellite in a centimetric range, which orbit is located on distance 36,000 km from the Earth. The transfer of signal from the Earth on the satellite realizes on frequencies 4.0–6.0 gigahertz ($\lambda = 5.0$–7.5 cm), and back signal is relayed on frequency 3.6 gigahertz ($\lambda = 8.5$ cm).

It is known that for range of radiowaves from 2 up to 10 cm conditions of radiowaves propagation practically do not depend on weather conditions in atmosphere. Ionosphere up to heights of 300 km is completely transparent for propagation of radiowaves in centimetric range. Nevertheless, in signals from the satellite periodically up to 2–3 times per 1 month it is marked a short-term increase of noise level and reduction of relation of signal to noise. In these periods the relation of useful signal to noise is sharply decreased from the level 14–15 decibels up to a level 9–10 decibels, and in the separate periods this relation reaches 3–4 decibels. Let's notice that in these periods the power of solar X-ray radiation reaches 10^{-4}–10^{-5} W/m^2 at noise level 10^{-7} W/m^2. In these periods there is an increase

of a level of mistakes or noise of a telecommunication signal. The limited level noise corresponds to power of X-ray radiation more than 10^{-8}–10^{-7} W/m^2.

At digital coding of a signal it is important to know a level of its mistakes for correct decoding. At increase of noise level it is necessary to raise power of useful signal and repeatedly to send a signal. By repeated transfer of a signal its power a little grows, but is not boundless and with the certain probability this signal is accepted more authentically, with smaller losses. On the other hand it is possible to reduce of passband of the radio receiver in the satellite channel. At existing passband of 1.6 megabits/s in Internet network Aknet the further reduction of passband will result the reduction of throughput of communication channels.

The analysis of a number of large mistakes exceeding number of mistakes equal 50, which means failures in passage of a signal, shows, that their most part corresponds to the periods with high solar flair activity and high level of X-ray radiation more than 10^{-5} W/m^2. In these periods the level of the index of geomagnetic activity K on a 9-mark scale exceeds 5–7 units. It is necessary to have in view of, that K = 5–6 corresponds to magnetic storm and K = 7 correspond to the large magnetic storm.

The most evident representation of influence of the Sun on quality of Internet communication are the periods of spring and autumn equinox. In this periods the Sun, communication satellite and antennas on the Earth are on one line. This phenomenon refers as solar interference and reflects limiting case of the considered phenomenon. Solar interference is observed near to the periods of spring and autumn equinoxes. In these periods the direct intensive solar radiation considerably blocks on power of signals from the satellite and the reception of useful signal on the Earth becomes impossible. For the analysis of the above-stated influence the summer and spring periods were chosen, when the activity of solar processes was maximal and the high level of correlation between mistakes in the satellite channel of communication and level of solar activity was marked [2].

Let's consider particularly two periods of the observations, which have been carried out in July, 2004 and in April, 2006. In Fig. 1a the data of mistakes statistics of the satellite channel from July 13 till August 12, 2004 are given. For the given interval of observations 5 mistakes exceeding 40 standard units are registered.

The first interval with the large mistakes having values more than 80 units, is marked from July 14 till July 16. The second interval is marked from July 27 till July 29 with mistakes from 50 up to 70 units. In other periods mistakes did not exceed an average level of noise equal to 2–8 units.

Let's analyze processes on the Sun and in magnetosphere of the Earth in July as a whole and separately for the above-stated periods. Processes on the Sun in July were rather quiet. The activity of solar spots was rather low and it was marked mainly in optical range.

(a)
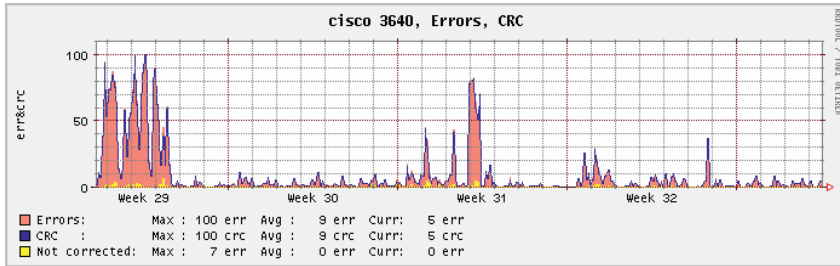
(b)
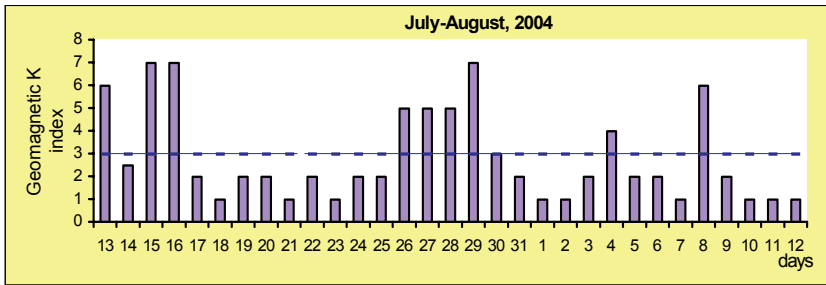
Figure 1. Statistics of mistakes of the satellite channel of communication − (a), and variations of *K* index of geomagnetic activity – (b), in July 13 – August 12, 2004

In a Fig. 1b the variations of the geomagnetic activity index K are presented. Data on geomagnetic activity evidently shows the solar activity and they can qualitatively be used for the analysis as a parameter of solar activity level.

In the above-stated period the increase of solar flair of activity with two maximums was marked. The first maximum was observed on July 15–16, 2004. So, from July 13 till July 17 in a solar coronal there was a new flare near to equators at latitude ~20°N. This flare was accompanied by emission of solar matter from a coronal with speed up to 1,000 km/s (high-speed flow), electron emission, increased X-ray radiation in limits $\gamma = 10^{-3}$–10^{-4} W/m^2 (at background values 10^{-8}–10^{-7} W/m^2).

It is necessary to note that the solar X-ray and ultra-violet radiation reaches the Earth in 7 min. The flows of the charged particles or plasma connected with processes on the Sun, reach the Earth for 2–3 days.

In the period from July 13 till July 17 magnetosphere was he strongly disturbed, and large magnetic storm was observed. In the satellite channel of communication in this period the high level of noise reached 90–100 units was marked.

The orbit of the satellite of communication "Express-6" is on distance 36,000 km, i.e. outside of magnetosphere border, corresponds to 5–6 Earth radiuses. Probably, that at such situation of the satellite the grab of particles in the field of receiver-transmitting antennas on the satellite does not occur.

The second period of disturbances on the Sun was observed from July 26 till July 29, 2004 and was characterized also by high level of flare activity and X-ray radiation. In this period in subequatorial area of the Sun there was a second flare accompanying with emission of coronal substance and increased gamma-radiation, reaching 10^{-4} W/m^2. In this case flow of X-ray radiation reaches heights of first Shuman's resonator at height 100 kms for 7 min, and the flows of a solar wind (coronal substance) achieve the Earth in 2–3 days. Let's note, that in Shuman's resonator the frequencies from 4 up to 60 Hertz are generated which influence on human nervous system and head brain.

It is necessary to note, that besides of Shuman's resonator in the upper atmosphere at heights from 100 up to 500 km there exists the Alfven's resonator. In this resonator Alfven's waves are generated, which impact on the rhythms of human heart and vessel systems, that results in turn for worse its diseases /3/.

In the period from July 28 till July 29 the high-speed flow of a solar wind accompanying with powerful X-ray radiation has intensified. In these days the geomagnetic storm was observed.

The similar processes were observed and in other intervals of time since May till June, 2004.

In the winter period of 2005 two powerful flares by flows of x-ray radiation and with emission coronal substance again were registered in January month on the Sun. The failures in work of the telecommunication channel in this period were very great. For example, the satellite channel of communication to Moscow in this period was filled up on 10% at usual norm 80%.

These phenomena were aggravated by rainy weather with falling of snow, which has covered with layer satellite antennas on ground. It has resulted in reduction of mirror reflective ability of the receiver-transmitting antenna in a centimetric range of waves because of presence of a layer of friable snow on a surface of antenna plate. Practically it was expressed in reduction of speed of transfer of the information in Internet system, that everywhere was observed in Bishkek city by all users of the Internet.

The data on geomagnetic activity submitted on Fig. 2 can be used for the qualitative analysis and estimation of influence of solar flares on a noise level in the satellite channel of communication. For the more detailed analysis of interrelation of the above-stated processes both revealing of mechanisms and physical reasons we shall consider probability of occurrence of failures in the channel of communication depending on the following factors. Accuracy of definition of time and probability of occurrence of failures in the satellite channel of communication depends on a spatial and temporary situation of system "Sun – satellite – receiver antennas on the Earth".

The probability of failures frequency occurrence in the satellite channel of communication on the Earth depends on time passage of receiving-transmitting point along an orbit of the Earth. The level of noise in the channel of communication completely is absent when the reception antennas are in the field of shadow. In this period the occurrence of mistakes is connected only to the technical reasons.

Thus two noises peaks (maximum of failures) in the morning and evening time and third one, rather smaller, in midday are observed. The peaks in morning and evening time are connected with spatial orientation of reception-transmitting antennas relatively the Sun and geostationary satellite. It is necessary to notice, that in a daily variations of failures of communication the basic periods of the maximal deviations or noising at presence disturbances in a solar coronal coincide with these peaks especially typical for morning and evening hours.

Further for the more detailed analysis of failures in communication with accuracy within several minutes the daily data of gamma-radiation of solar flares and time of occurrence of failures in the reception channel were analyzed.

In the period of 5–6 April 2004 the solar flare with emission of substance and x-ray radiation was observed. In this period the failures are registered in the satellite channel of communication. These failures caused by solar X-ray emissions coincide with temporary peaks in distribution of mistakes of reception antennas along the orbit of the Earth.

The analysis shows, that at first on time there is sharp increase of gamma-radiation, and then after 10–20 min (April 5) and 7–10 min (April 6) the failures in work of the channel of communication were registered. As it is visible from figure, the failures in the channel of communication vary from 7 about 20 min after peaks in gamma-radiation. These results prove to be true also by data on other periods of solar flare activity.

In daily variations of geomagnetic activity index K given on Fig. 4b vertical dashed lines draw these mistakes. As it is visible, the given data show in more detail connection of failures in the satellite channel with solar flare activity.

The emissions of coronal substance of the Sun in the flare periods are accompanied by gamma-radiation, which reaches the Earth atmosphere in 7–10 min. In this period disturbances occur in ionosphere in Shuman's and Alfven resonators. These disturbances as powerful electromagnetic pulses reach the reception-transmitting antennas on the geostationary satellite communication and can modulate a high-frequency signal in the satellite channel.

Conclusions

The connection between conditions of passage of signal in the satellite channel of communication and solar flare activity exists. I was registered only in the periods for those solar flares, which were accompanied by emission of powerful X-ray radiation up to values 10^{-4} W/m^2, emission of solar coronal substance consisting of protons, electrons and other particles. In these periods the noise in the satellite channel of communication is registered within several minutes.

The most part of large mistakes exceeding 50 (failures in passage of a signal) is observed in the periods with high solar flare activity and appropriate high level of geomagnetic activity. In this periods index of geomagnetic activity exceeded 5–7 units on a 9–mark scale.

The high level of correlation between mistakes of the satellite channel of communication and level of solar activity is received. The connection between solar flare both geomagnetic activity and conditions of passage of signal in the satellite channel of communication is established.

Such connection is marked after solar flares causing geomagnetic storms. The flares influencing the satellite channel of communication are accompanied by emission of solar plasma as a coronal matter (protons, electrons and other particles) and powerful X-ray radiation up to 10^{-3} W/m^2.

The conclusions, received in the given work, are preliminary and require confirmation on the results of more longer monitoring and analysis of experimental material with the data on other satellite channels and another frequency ranges.

References

[1]   Karimov, K.A. and Gainutdinova, R.D. (2003) On a problem of forecast of geo-magnetic disturbances and its application. – Proceedings of International Conference "Modern Problems of Physics and High Technologies", Russia, Tomsk, pp. 383–388.

[2]   Karimov, K.A. and Gainutdinova, R.D. (2005) Increase of mistake level of satellite signal in periods of high solar and geomagnetic activity. Proceedings of International Meeting "Information-communication technologies in information society". – Bishkek, pp. 270–273.

[3]   Karimov, K.A. and Gainutdinova, R.D. (1999) Environmental changes within Kyrgyzstan. – Proceedings of the NATO ARW on Environmental Change, Adaptation and Security. Dordrecht, The Netherlands: Kluwer Academic Publishers, NATO ASI Series 2: Environment, Vol. 65, pp. 201–204.

"SIMPLE" DIAGNOSTICS OF THE LOW PRESSURE PLASMAS IN CHEMICALLY-ACTIVE MEDIA

D. K. OTORBAEV
Kyrgyz National Academy of Sciences, Chui prospect 265A, Bishkek, 720071, Kyrgyz Republic

Abstract: The "simple" diagnostics for characterisation of non-equilibrium chemically active plasmas are discussed. As to experimental methods the emphasis has been made to the "simple" non-invasive spectroscopic methods of ionising and recombining plasma characterisation. The word "simple" in the title is presented between the quotes, which mean that the methods assumed to be simple only conditionally. In order to be sure that the measurements indeed provide correct information on the plasma parameters, a detailed understanding of kinetics of each particular plasma source is required. Moreover the validity of spectroscopic methods should be checked by independent diagnostic techniques.

Keywords: Ionizing plasmas, recombining plasmas, low pressure plasmas, plasma diagnostics, spectroscopy, optical actinometry, density of atoms and molecules

1.   Introduction

Understanding of chemistry of non-equilibrium plasmas, optimisation of the plasma sources including those used for the decontamination of biological and chemical agents requires determination of densities of the species presented: atoms, molecules, radicals, ions and electrons, preferably spatially defined, with their energy distributions – velocities and internal states.

With appearance of sophisticated experimental techniques for characterisation of non-equilibrium plasmas, the quality of diagnostic methods, and as a consequence the quality of the experimental results, improves very rapidly. Quite often new discoveries in plasma applications are based on sophisticated diagnostic methods. Equipment based on newly opened phenomena, for example the methods used various laser spectroscopy techniques, clearly brings new in-depth knowledge on the internal parameters of plasmas [1,2]. However everything has the price. Invention and following application of new diagnostic techniques require quite significant investments. Not all university and application-oriented research laboratories can afford implementation of newest state-of-the-art experimental technologies. Traditional plasma diagnostic techniques are still very actively used [1]. With that not always on a correct way.

In this paper the "simple" non-invasive spectroscopic methods for the characterisation of low-pressure chemically active plasmas are discussed. Illustrations are given on an example of the diagnostics of two main types of laboratory plasmas – ionizing and recombining.

2. Ionizing Plasmas

One of the most complicated problems in diagnostics of chemically active plasmas is knowledge of its real chemical composition. Glow discharges at reduced pressures in molecular gases represent typical examples of non-equilibrium plasma with a complex chemical composition [3]. High energy inputs to such discharges results in fast reactions in the plasma, and unpredictable distribution of their components on various degrees of freedom [1,3]. Chemical composition of the dc capillary glow discharge in CO_2–N_2–He gas mixture, used as an active media for the waveguide CO_2 lasers, have been determined by three different methods.

2.1. METHODS

In a number of cases the method of optical actinometry permits determination of radical densities in the ground states from the emission spectra of these particles [1,4]. In classical case small quantities of the actinometer are added to the gas under investigation. If the radiative states of radical and actinometer are excited by a direct electron impact from their ground states, and have close to each other excitation potentials, the same group of electrons taking part in their excitation. On the basis of known experimental data one can assume that the electron excitation cross sections of vibronic states of electronically excited molecules proportional to the Frank-Condon factors for the relevant transitions [1]. If respective radiative states are de-populated by the radiative decay, which is reasonable assumption for the reduced pressure plasmas, than for the relative intensities of molecular bands (or atomic lines) of actinometer and radical, one can derive the following ratio [5]:

$$\frac{I_1}{I_2} = \frac{N_{01}}{N_{02}} \cdot \frac{\sigma_{01}^{max}}{\sigma_{02}^{max}} \cdot \frac{\int\limits_{E_1}^{\infty} \varphi_{01}(\epsilon) f(\epsilon) \epsilon^{1/2} \, d\epsilon}{\int\limits_{E_2}^{\infty} \varphi_{02}(\epsilon) f(\epsilon) \epsilon^{1/2} \, d\epsilon} \cdot \frac{\sum\limits_{v^0=0}^{\infty} q_{v^0_{v'}}^{(1)} \psi\left(v^0\right)}{\sum\limits_{v^0=0}^{\infty} q_{v^0_{v'}}^{(2)} \psi^2\left(v^0\right)} \cdot \frac{A_1 \tau_1 \upsilon_1}{A_2 \tau_2 \upsilon_2}, \tag{1}$$

where σ_{0i}^{max} is the excitation cross section of radiative states in maximum, E_i is the excitation threshold, $\varphi_{0i}(\varepsilon)$ is the energy dependence of the excitation cross section, $f(\varepsilon)$ is the electron energy distribution function, $q_{v^0_{v'}}$ are the Frank-Condon factors, $\psi(v^0)$ is the relative vibrational population of molecules in the ground state, A_i, τ_i and ν_i are the radiative transition probability, lifetime and frequency of radiation, N_{0i} is the particles absolute density in ground electronic states.

In case of $E_1 \sim E_2$ and $\varphi_{01}(\varepsilon) \sim \varphi_{02}(\varepsilon)$ via selection of radiative states, from (1) the absolute density of radicals can be derived in respect to the absolute density of actinometer, relative intensities of molecular bands (or atomic lines), and combination of various rate coefficients [4,5]:

$$N_{02} = k\left(\frac{I_1}{I_2}\right)N_{01}.$$ (2)

2.2. EXPERIMENT

Gas discharge has been studied in two different types of cylindrical capillary discharge tubes – of molybdenum glass and beryllium oxide. Tubes have the same length of 48 mm, and radius of 1 mm. The gas mixture was CO_2–N_2–He (1:1:8), pressure range $p = 20$–100 Torr, current strength of $i = 2$–12 mA, voltage between electrodes $U = 2$–6 kV. Spatial distribution of plasma parameters have been measured with use of a rotating quartz cube. Next to the spectroscopy, the mass spectrometry and gas chromatography have been used to measure the stable product densities in the discharges.

2.3. RESULTS AND DISCUSSION

The results of measurements of oxygen atoms and carbon oxide molecules, based on (1) and (2), show that the capillary dc discharges at medium pressures are characterized by a strong dissociation of carbon dioxide molecules. Much stronger than in the discharges of classical CO_2 lasers in wide ($R \sim 10$ mm) tubes. It is important to underline that molecular nitrogen, presented in the initial gas mixture, has been used as a natural actinometer. With increase of power input, and decrease of pressure, the dissociation degree increases monotonically. At pressure of $p = 20$ Torr, and power input of $W = 3$ W/cm, in sealed-off regime of the discharge, the dissociation degree reaches maximum values of ~80% in the molybdenum glass tube, and ~60% in the beryllium oxide tube. The same tendencies were observed for the density of oxygen atoms in the discharges.

It is important to underline that the CO and O densities in the beryllium oxide tube were approximately as twice as lower of the respective densities in the molybdenum glass tube (with other parameters remaining constant). This we put down to different catalytic properties of surfaces in respect of radicals recombination on the tube walls with generation of carbon dioxide molecules.

3. Recombining Plasmas

Typical example of the recombining plasmas is a flowing post-discharge. These types of plasmas are actively used nowadays for active treatment of the surfaces (cleaning, etching, deposition) [6,7]. In recombining plasmas, the excited states of

atoms and molecules are populated by the flux directed from the recombination of ions and electrons to the ground state of stable atoms and molecules.

3.1. METHODS

A particularly simple kinetic scheme can be realized for the first excited atomic states in the recombining plasmas. For example in the conditions of an expanding cascaded arc plasmas a simple kinetic analysis shows that the density of the first excited state n_2^* can be found from the simple balance between the recombination flux Φ to this level and radiative decay from this level [8]:

$$\Phi - n_2^* A_{21} \Lambda_{21} = 0. \tag{3}$$

Here A_{21} is the resonance radiative transition probability, and $\Lambda_{21}(kR)$ is the escape factor for emission of resonance radiation. The escape factor Λ is a function of the effective optical depth (kR). The functional dependence of $\Lambda_{21}(kR)$ determined by the emission and absorption line profiles [9]:

$$kR = \frac{(\ln 2)^{\frac{1}{2}}}{4\pi\sqrt{\pi}} \frac{\lambda_{pq}^4}{c\Delta\lambda_{pq}} \frac{g_p}{g_q} A_{pq} n_q \mu R \,, \tag{4}$$

where λ_{pq} is the wavelength of the radiative transition, $\Delta\lambda_{pq}$ is the width of the emission profile, c is the velocity of light, g_p and g_q are the statistical weights, n_q is the density of the lower state of the transition, μ is a geometrical factor [9], and R is the mean radius of the plasma beam.

In case of known recombination flux Φ, and absolute density of the first excited state n_2^*, one can determine from (3) the escape factor Λ_{21} and effective optical depth (kR) for the resonance radiative transition [9]. Finally, from (4), the particles absolute density in the ground electronic states can be derived. The method has been applied to determination of the absolute ground state density of atomic hydrogen $H(n = 1)$ and argon $Ar(3p^6)$ in a freely expanding plasma jet [10].

3.2. EXPERIMENT

Experiments have been performed for the conditions of expanded cascaded arc plasma at the Eindhoven University of Technology. Details of the experimental set up and the measurement techniques were described earlier [10]. The hydrogen percentage in the total gas flow of Ar-H_2 mixture was varied in the range 0.7–10%. Background pressure was 40 Pa, gas flow rate 58 $cm^3 s^{-1}$, arc current 45 A, arc voltage 80–115 V. The argon density in the first excited state $Ar(3p^5 4s)$ has been measured in a pure argon plasmas by the absorption of eight argon spectral lines, belonging to the transition $Ar(3p^5 4p \rightarrow 3p^5 4s)$. The hydrogen density in the first excited state $H^*(n = 2)$ has been determined in an argon-hydrogen plasma by hydrogen Balmer-α spectral line absorption.

3.3. RESULTS AND DISCUSSION

The radial dependencies of the $Ar(3p^5 4s)$, summed over the states $3p^5 4s(^3P_0, {}^3P_1,$ $^3P_2, {}^1P_1)$, as well as of the $H^*(n = 2)$ state have been determined by absorption spectroscopy for various axial positions in the expansion both in pure argon, and in the Ar-H_2 gas mixtures. In [11] a similar expanding argon plasma was studied using the technique of Thomson-Rayleigh scattering. It have been shown that the agreement between two methods were quite good [10]. Hence the assumptions upon which the discussed method is based were correct, and for the recombining expanding plasma the method can be applied for determination of ground state density of short-lived radicals. The absolute densities of atomic hydrogen at the distances between 40 and 70 mm from beginning of expansion have been calculated from (3). The densities were in the range $(0.2–9) \times 10^{18}$ m^{-3}.

Conclusions

1. Molecular optical actinometry technique, combined with the mass spectro-metry and gas chromatography methods have been used to determine the absolute densities of the O atoms and CO molecules in the CO_2–N_2–He gas mixture of the waveguide CO_2 laser. Different catalytic properties of the discharge tube materials towards recombination of radicals and association of CO_2 open new possibilities for re-generation of CO_2 molecules in the plasma, and as a consequence, for increase the power of laser generation, and development of sealed-off waveguide CO_2 lasers.
2. The densities of argon and hydrogen atoms in the first excited states determined by the technique of visible light absorption spectroscopy. Simple kinetic scheme have been employed to determine absolute ground state density of Ar and H atoms in expanding recombining plasmas. It is important that the kinetic scheme used does not require information on the shape of the electron energy distribution function in the plasma.
3. The accuracy of presented methods of ground state density determination is limited by the errors in the ionization, recombination and excitation coefficients, and in the experimental signal-to-noise ratios. The proposed techniques can be used for characterization of other kinds of radicals in the chemically active plasma.

References

[1]   V.M. Lelevkin, D.K. Otorbaev, D.C. Schram. *Physics of Non-equilibrium Plasmas*, Elsevier, Amsterdam (1992).
[2]   *Atomic and Laser Spectroscopy*, Oxford Classic Texts in the Physical Sciences (ed) A. Corney, Oxford (2006).
[3]   Yu. P. Raizer. *Gas Discharge Physics*, Springer-Verlag, Berlin (1997).
[4]   Zhou Qing, D.K. Otorbaev, G.J.H. Brussaard, M.C.M. van de Sanden, D.C. Schram. *J. Appl. Phys.* **80**, 1312 (1996).

[5]   A.T. Baiterekov, D.K. Otorbaev. *Proc. X Int. Symp. on Plasma Chemistry*, **2**, 2.1–26 (1991).

[6]   D.C. Schram. *Pure Appl. Chem*. **74**, 369 (2002).

[7]   U. Cvelbar, M. Mozetic, A. Ricard. *IEEE Trans. Plasma Sci.* **33**, 834 (2005).

[8]   D.K. Otorbaev, A.J.M. Buuron, N.T. Guerassimov, M.C.M. van de Sanden, D.C. Schram. *J. Appl. Phys.* **76**, 4499 (1994).

[9]   T. Holstein. *Phys. Rev.* **83**, 1159 (1951).

[10] D.K. Otorbaev, A.J.M. Buuron, M.C.M. van de Sanden, R.F.G. Meulenbroeks, D.C. Schram. *J. Phys. D: Appl. Phys.* **27**, 1362 (1995).

[11] R.F.G. Meulenbroeks, A.J. Beek, A.J.G. van Helvoort, M.C.M. van de Sanden, D.C. Schram. *Phys. Rev. E* **49**, 4397 (1994).

INDEX